Instituto Tecnológico y de Estudios Superiores de Monterrey

Campus Monterrey

School of Engineering and Sciences

Stability analysis by the EMHPM for regular and multivariable cutting tools in milling operations

A thesis presented by

José de la luz Sosa López

Submitted to the
School of Engineering and Sciences
in partial fulfillment of the requirements for the degree of

Master of Science

In

Manufacturing Systems

Monterrey Nuevo León, December 3rd, 2020

Dedication

To my parents. Thanks for all your unconditional confidence, support, patience, and encouragement. You were my main motivation for pushing through this work.

Acknowledgements

First, I thank God for so much love and care.

I am very grateful to my thesis advisor, Daniel Olvera Trejo, for the trust, opportunity, availability, patience, support, and even sleepless nights to help me to carry out this work, as well as its support beyond academic subjects.

I acknowledge doctors Alex E. Zúñiga and Oscar Martínez for their support and the opportunity to belong to the research group in which I had a lot of learning. In the same way, I thank Cintya Soria and Emiliano Reséndiz, for their support during the completion of the master's degree. I also thank my classmates who, with their example, gave impetus to motivation to be better, in addition to making my stay at the Tecnológico de Monterrey a transcendental experience.

Likewise, I would like to express my deepest gratitude to my family, to Neftalí Sosa and María A. López, who have always trusted me, and have supported me to pursue my dreams. To my brothers Erwin and Caleb for always giving me their support. To Edith for her understanding, patience, and unconditional support.

Finally, all of these wouldn't be possible without the sponsorship granted by Tecnológico de Monterrey through the Research Group of Nanotechnology for Devices Design, and by the Consejo Nacional de Ciencia y Tecnología de México (CONACYT), Project Numbers 242269, 255837, 296176, National Lab in Additive Manufacturing, 3D Digitizing and Computed Tomography (MADiT) LN299129 and to the University of the Basque Country for its support in publishing an article. These institutions believed in my potential as a professional and researcher.

Stability analysis by the EMHPM for regular and multivariable cutting tools in milling operations

by

José de la luz Sosa López

Abstract

Machining is a process by which a cutting tool removes material from a workpiece through relative movements between to achieve the desired shape. Milling is a common form of machining using rotary cutters to remove material by advancing a cutter into a work piece. The milling process requires a milling machine, workpiece, fixture, and cutter. When milling vibrations occur, they are usually produced by the impact of the vibration of the previous cut on the current one, this type of vibrations is known as self-excited vibration (chatter) since it occurs between the workpiece and the cutting tool. In this thesis we predict unwanted vibrations during the material removal process in milling using stability lobes.

Since milling can be studied using a dynamic equation, a new method for solving a delay differential equation (DDE) is presented by using second- and third-order polynomials to approximate the delayed term using the Enhanced Homotopy Perturbation Method (EMHPM). Different simulations are performed first with regular and later with multivariable tools. To study the proposed method performance in terms of convergency and computational cost in comparison with the first-order EMHPM, Semi-Discretization and Full-Discretization Methods, a delay differential equation that model cutting milling operation process was used. To further assess the accuracy of the proposed method, a milling process with a multivariable cutter is examined to find the stability boundaries. Then, theoretical predictions are computed from the corresponding DDE finding uncharted stable zones at high axial depths of cut. Time-domain simulations based on Continuous Wavelet Transform (CWT) scalograms, Power Spectral Density (PSD) charts and Poincaré Maps (PM) were employed to validate the stability lobes found by using the third-order EMHPM for the multivariable tool and they were compared with experimental results.

List of Figures

Figure 1.1 Chatter in milling with 2 degrees of freedom (DOF). Adapted from [7] ... 2
Figure 1.2 Chatter publications on milling since 1995. ... 4
Figure 2.1 Schematic of the orthogonal cutting process. Adapted from [26] ... 7
Figure 2.2 a) Up-milling and b) down-milling operation ... 9
Figure 2.3 Helical milling cutter geometry. Adapted from [16] ... 11
Figure 2.4 Multivariable milling tool discretized in disks. Recovered from [28] ... 13
Figure 3.1 Solution comparison between Runge-Kutta and other authors of (3.9) ... 30
Figure 3.2 Solution of (3.9) with Runge Kutta ode45 vs. EMHPM ... 34
Figure 3.3 Solutions of Eq. (3.115) by the EMHPM and the dde23 routine. ... 39
Figure 3.4 Scheme for the approximation of the delayed term by a zeroth-order (solid black line) ... 40
Figure 3.5 a) Scheme for the approximation of the delayed term by a first-order. ... 42
Figure 3.6 a) Scheme for the approximation of the delayed term by a second-order. ... 44
Figure 3.7 a) Scheme for the approximation of the delayed term by a third-order. . 47
Figure 3.8 Solution of Mathieu's equation with delay, $N = 50$ and $m = 4$. ... 50
Figure 3.9 Approximate solution of Eq. (3.189) using the EMHPM, $n = 12000\ rpm$, $ad = 1$, a) stable operation $ap = 1.5\ mm$, b) unstable operation $ap = 3$ mm ... 53
Figure 3.10 Convergence rate of absolute error between zeroth-, first-, second- and third-order EMHPM for down-milling operation. Cutting parameters for a) $ap = 1.5$ mm, $ad = 1$ and n=12000 rpm, b) $ap = 3$ mm, $ad = 1$ and n=12000 rpm. ... 54
Figure 3.11 Absolute error with different discretization for zeroth-, first-, second- and third-order vs solution dde23 ... 55
Figure 3.12 Computation time for different discretization in zeroth-, first-, second- and third-order EMHPM vs solution dde23 of Matlab with a) ad=0.05, b) ad=0.1, c) ad=0.5, d) ad=1. ... 55
Figure 3.13 Influence of the number of discretization N and the order m of solution for the EHPM of a) second and b) third order with constant initial condition. ... 56
Figure 3.14 Influence of the number of discretization N and the order m of solution for the third-order EHPM with a) cuadratic initial condition, b) straigth line initial condition. ... 57
Figure 4.1 Comparison of the order of the solution using the EMHPM with first- order approximation for stability analysis in one degree of freedom ... 65
Figure 4.2 Convergence of the EMHPM, first, second and third column represents the solution for the first-, second- and third-order EMHPM, and the first, second, third and fourth row represents values of ad 0.05, 0.1, 0.5 and 1 respectively. ... 67

Figure 4.3 Convergence of the EMHPM of a) first-, b) second- and c) third-order for a degree of freedom as the order of the solution varies for different values of discretization for full immersion. 68
Figure 4.4 Computation time with different discretization for the first-, second-, and third-order solution of the EMHPM with ad=0.05, m=6 vs the reference with $N = 100$ and $m = 10$..... 68
Figure 4.5 Stability diagrams for down-milling operation. The first (a,b,c) and second (d,e,f) rows of subfigures correspond to N = 60 and N = 100 discrete intervals, respectively. First (a,d), second (b,e) and third (c,f) columns correspond to the first-, second- and third-order EMHPM, respectively. Subfigure (g) shows a comparison between the third-order EMHPM (red line), SDM (dot black line), FDM (dash black line), and Chebyshev (dot blue line) methods with N = 60 discrete intervals. 69
Figure 4.6 Representation of the first-order polynomial approximation for the delay subinterval 73
Figure 4.7 Representation of the second-order polynomial approximation for the delay subinterval..... 76
Figure 4.8 Representation of the third-order polynomial approximation for the delay subinterval. 79
Figure 4.9 Comparison of solution with regular tool algorithm vs multivariate tool algorithm for third-order EMHPM, with values of $n = 12000\ rpm$, $zn = 4$, $ad = 1$, $ap = 1.5\ mm$..... 83
Figure 4.10 Numerical comparison of the EMHPM solutions of milling equation Eq. (4.13) with the dde23 MATLAB routine. For a stable milling operation $ap = 1.5$ mm, $ad = 1$ and $n = 12000$ rpm with 10 disks. 84
Figure 4.11 a) Stability lobes for multivariable tool in approximation of first-, second- and third-order, b) zoom in to observe the difference between methods. 84
Figure 4.12 Third-order EMHPM for multivariable tool vs Semi-Discretization, $ad = 1$, $zn = 2$, $\beta = 1°$ 85
Figure 5.1 Methodology to validate a multivariable milling tool..... 86
Figure 5.2 Scheme of the experimental setup for a) the modal analysis and b) cutting forces characterization..... 87
Figure 5.3 a) Comparison of stability lobes for regular (black solid line) and multivariable (red solid line) cutters by using the third-order EMHPM; b) zoom in on chosen cutting conditions for time-domain simulations. The selected points are marked as follows: unstable (cross mark), stable (circle mark), transition (plus mark) cutting conditions. 88
Figure 5.4 Comparison for the Floquet solution and the solution in time-domain using the mean of the peaks for the first 10 periods. 89

Figure 5.5 Analysis of cutting conditions A, B and C. CWT scalograms: a), d), g); PSD: b), e), h) and PM: c), f), i) corresponds to the cutting conditions A, B and C respectively. 90
Figure 5.6 Analysis of cutting conditions D, E, F and G. CWT scalograms: a), d), g), j); PSD: b), e), h), k) and PM: c), f), i), l) corresponds to the cutting conditions D, E, F and G respectively. 92
Figure 5.7 The number of discrete disks and discrete excitation frequencies as a function of axial depth of cut for the multivariable tool. 93
Figure 5.8 a) Arrangement of the assembly and b) test to obtain the modal parameters 94
Figure 5.9 Experimental test to obtain the cutting forces 95
Figure 5.10 Scheme for the representation of ϕst and ϕex for radial immersion of 25 %. 96
Figure 5.11 Stability lobes of multivariable tool for experimentation with $ae = 3.175$ mm, black line represents the lobes for modal parameters at the beginning of the characterization and red lines for the end of the characterization. Circles represent stable cases; squares represent cases with hopf frequencies, and triangles cases with flip frequencies. 97
Figure 5.12 Stability lobes of multivariable tool for experimentation with $ae = 3.175$ mm, and with specific cutting forces obtained with characterization by edges. Circles represent stable cases; squares represent cases with hopf frequencies, and triangles cases with flip frequencies. 97
Figure 5.13 Experimental arrangement to characterize the milling tool 98
Figure 5.14 Signals obtained with n=2500, 3000, 3500, 4000, 4500 rpm, ap=1 mm, a) tachometer signal, b) zoom in of the tachometer signal, c) velocity signal, d) zoom in of the velocity. 98
Figure 5.15 CWT, PSD and Poincaré diagrams to validate experimental tests. 100
Figure 5.16 Stability lobes of multivariable tool for experimentation with $ae = 1$ mm 101
Figure 5.17 Analysis of cutting at 15 mm, with different spindle speeds. 102

List of Tables

Table 3.1 Computational time required for the solution of Mathieu's equation. 50
Table 4.1 Comparison of convergence for different methods for down-milling operation with $ad = 1$. 70
Table 5.1. Main geometric parameters of multivariable tool according to [94]. 87
Table 5.2. Main geometric parameters of experimental multivariable tool. 95
Table 5.3. Specific cutting coefficients characterized by edges with radial immersion of 25% for multivariable tool. 96

Nomenclature

ζ	Relative damping
ψ	Cutting edge offset angle due to helix angle
κ_β	Angular phase offset constant by axial depth due to helix angle
ϕ_{st}, ϕ_{ex}	Cutting entry and exit angles
β	Helix angle of tool
ϕ_{iz}	Edge position angle iz
ϕ	First edge position angle
ϕ_p	Pitch angle between cutting edges for a regular tool
f_z	Feed per tooth
K_{fc}, K_{fe}	Feed force constants for shear and for friction respectively
K_{xc}, K_{yc}, K_{zc}	Specific shear force coefficients in the forward, normal and axial directions
K_{tc}, K_{rc}, K_{ac}	Specific shear force coefficients in the tangential, radial, and axial directions
K_{xe}, K_{ye}, K_{ze}	Specific friction force coefficients in the forward, normal and axial directions
K_{te}, K_{re}, K_{ae}	Specific friction force coefficients in the tangential, radial, and axial directions
D	Tool diameter
δa_p	Discretization of the tool axially
$\delta\phi$	Discretization of the angular rotation of the tool
Δt	Time discretization
Δa_{dsk}	Thickness of each discretized disk in a multivariable tool
d	Index that identifies the list of delays that appear in the equation for multivariable tool
d_n	Non-repeated discrete time delays
x, y, z	Cartesian axes, x in the forward direction, z in the direction of the axis of rotation, and y normal
f_n	Normalized natural frequency
f_m	Natural frequency
f_h	Spindle frequency
f_e	Excitation frequency
ω_n	Angular natural frequency
h_{xx}, h_{yy}	Specific variational cutting forces in the x,y direction, by the variation in x,y
F_R	Resulting force
F_f	Feed force
F_t, F_r, F_a	Force in tangential, radial, and axial directions
F_γ	Friction force
F_s	Shear force

$F_{\gamma n}$	Normal friction force
F_{ns}	Normal shear force
$\bar{F}_x, \bar{F}_y, \bar{F}_z$	Average cutting forces in cartesian directions
$F_{xx}, F_{xy}, F_{yx}, F_{yy}$	Total variational cutting forces in the x,y direction, by the variation in x,y
g	Window function
$\mathcal{H}$	Homotopy function
a_e	Radial depth of cut
a_p	Axial depth of cut
a_d	Radial immersion of the tool
N	Number of discretization
z_n	Number of edges in the tool
$\boldsymbol{P}_i, \boldsymbol{Q}_i, \boldsymbol{R}_i$	Solution matrices for the sub-interval i
$\boldsymbol{D}$	Differentiation matrix
$\boldsymbol{A}, \boldsymbol{B}$	Coefficient matrix
$\boldsymbol{A}_t, \boldsymbol{B}_t$	Matrix of coefficients evaluated over time t
$\boldsymbol{D}_i$	Mapping matrix i
$\boldsymbol{\Phi}$	Floquet transition or monodromic matrix
k, m	Order of approximation and order of solution
p	Expansion parameter
τ, τ_T	Time delay
m_m	Modal mass
t	Variable of time
T	Normalized variable of time
$\boldsymbol{x}, \boldsymbol{y}, \boldsymbol{z}$	Vector of states that describe dynamics in the time domain
n	Spindle speed

Contents

Chapter 1. Introduction 1

1.1 Background 1

1.2 Work Organization 4

1.3 Objectives 4

1.4 Hypothesis 5

1.5 Problem Statement and Context 5

1.6 Solution overview 6

Chapter 2. Milling operation 7

2.1 Introduction 7

2.2 Mechanics of orthogonal cutting 7

2.3 Milling process 9

2.4 Force Models in the milling process 10

Chapter 3. Mathematical modeling of machining 15

3.1 Differential Equations solved with homotopy perturbation methods 15

3.2 HPM procedure 17

3.3 Delay Differential Equations 34

3.4 Analysis of the EMHPM 49

Chapter 4. Stability in Delay Differential Equations 58

4.1 Introduction to the stability of systems with time delay 58

4.2 Stability for regular tools with EMHPM 60

4.3 Analysis of stability in milling for a regular tool in one degree of freedom 63

4.4 Stability of DDE with multiple delays through the EMHPM 71

4.5 Numerical Analysis of the algorithm for multivariable tool 83

Chapter 5. Validation of the milling tool 86

5.1 Experimental characterization of one degree of freedom milling equation and cutting force model 86

5.2 Experimental validation with new parameters of the tool 93

Conclusions 103
Annexes 104
Bibliography 130
Published papers 137

Chapter 1. Introduction

1.1 Background

In the manufacturing industry, is called machining to the process by which a cutting tool removes material from a workpiece through relative movements between both, to achieve the desired shape. Although the machining initially focused on the manufacture of metallic components such as steel alloys, aluminum, cast iron, among others, this process is also used to manufacture non-metallic materials such as composite materials (polymers reinforced with carbon fibers) [1] with great application and boom in the aeronautical industry, and at the other extreme bio-compatible materials such as titanium alloys [2] and even bones [3,4] for medical applications.
Productivity can be greatly increased when the machine-tool operates at high material removal rates, however, great care must be taken to avoid losing the quality of the manufactured parts. The automotive, aeronautical, chemical, naval, nuclear, missile and structural industries often require engineering parts with excellent accuracy and precision [5]. Some factors that can interfere in the efficiency of the manufacture of parts within the required standards are [6]:

- Assembly and disassembly of the workpiece on the machine-tool.
- Clamping systems, including clamping of the part in the machine-tool.
- Machining parameters such as spindle speed, depth of cut, and feed rate.
- Strategies and trajectories.
- Selection of tools and tool holder.
- Tool wear.
- Change of tools.
- Refrigerant management.
- Chip evacuation.
- Tool and work piece vibration, including self-excited vibrations and errors due to cutting forces.
- Measurement of parts (on machine or in a separate process)
- Machine tool accuracy, including geometric errors in its construction, thermally induced errors by sources associated with the cutting process, and errors in the cutting path caused by control and structural dynamics.

Therefore, in this work, attention is focused on the selection of technological parameters of the cutting process that promote productivity by increasing the material removal rate, but at the same time, minimizing the dimensional error caused by the forces of cutting and bending of the part and/or tool.

In machining processes, vibrations are usually produced by the impact of the vibration of the previous cut on the current one, this type of vibrations is known as self-excited vibration (chatter) since it occurs between the workpiece and the cutting tool as showed in Figure 1.1.

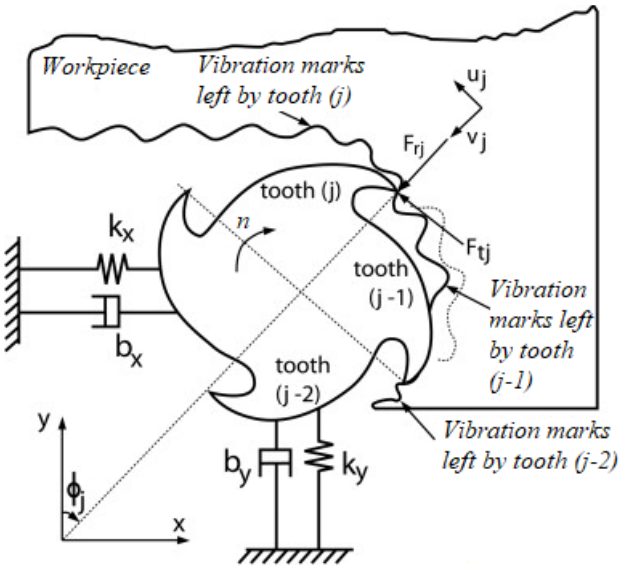

Figure 1.1 Chatter in milling with 2 degrees of freedom (DOF). Adapted from [7]

Chatter effects often have consequences such as poor surface finish, dimensional accuracy out of tolerance, low material removal rate, increased wear on the work tool, etc. [8–10]. Since the precision in the roughness of the part depends on the ability of the machine to position itself in the work area, as well as on the structural deformations during the process, the justification for modeling and analyzing the static and dynamic deformations that arise is observed. in the interaction of the tool-machine and the work piece during the machining operation. Thus, the focus of this document is directed to the analysis of the dynamic process and its modeling, and the extension of the solution of Delay Differential Equations (DDE) which model the dynamics of the process.

Delayed Differential Equations have been studied for more than 200 years [11] as there are many phenomena in different fields of science and engineering in which not only the value at time t but also the response in a previous state $t - \tau$, that is, there is a dependency on the past behavior determined by a delay value. Since solving a DDE is a complicated mathematical task, its solution has been limited, but with the development of computational power, since the last decade interest in them has resumed and new areas of opportunity have emerged.

One of the common examples that can be considered when solving systems with delay is the prey-predator model proposed by Lotka-Volterra where the growth rate of a certain species depends not only on the amount of present food, but also on the previous amount (in the gestation period) [12]. Delay systems appear in many engineering

problems, such as in the shimmy effect (wheel vibration) [13], in vehicle traffic models [14], feedback stabilization problems [15], in the vibration of machine-tools better known as chatter [16], etc.

Although the behavior of systems with periodic delay is not predictable, even for simple linear cases; however, the stability analysis of these systems is of vital importance. According to the theory of Ordinary Differential Equations (ODE), the stability problem is determined by the roots of the characteristic equation: if the real part of all roots is negative or is found on the left side of the complex plane, the system will be asymptotically stable. However, for the analysis of DDEs the approach is different.

In the last decades with the development of high speed machining, there has been a great interest in the offline prediction of the stability of the process, this technique is based on the use of design maps for the optimal selection of cutting parameters, mostly known as stability lobes, which draw the boundary that separates stable oscillations from unstable ones in the face of different combinations of technological parameters of the process. These diagrams allow choosing the value of the parameters or cutting conditions under which the process can be carried out without the presence of chatter vibrations, which cause unwanted effects such as premature wear of the tool, waste of materials, consumables and energy; in addition, in the presence of the chatter, it becomes critical to machine materials that are difficult to cut due that, some advanced materials of cutting tools such as ceramic, silicon nitride and CBN require strict control of vibration to avoid brittle breakage. In recent years there has been further development in high-performance machining operations using tools with variable geometry or multivariable tools, since these help to suppress vibration, even at low cutting speeds, eliminating the vibration phases between adjacent teeth, so multivariable tools can offer high productivity and better surface finishes if designed correctly.

That is why it remains a challenge to develop a fast and accurate computational-analytical methodology capable of determining the stability properties of the delay equation used to model the process.

In recent years, several researchers have been studying the effects of chatter, to mention some are Tlusty [17], Altintas [18], Stépán [19], Park [20], Urbikain [21], Olvera [22], Sosa [23], etc., thus, the number of publications regarding "chatter-milling" has had a growing trend; to get an idea, Figure 1.2 gives a glimpse of how publications on milling chatter have increased until 2020 recovered from Scopus Journal. According to Zhu and Liu [24], the different chatter mechanisms can be classified into regenerative chatter, mode coupling chatter, frictional chatter and force-thermal chatter. In this work we will refer to regenerative chatter, which occurs at frequencies close to, but not equal to, the dominant frequencies of the machine tool.

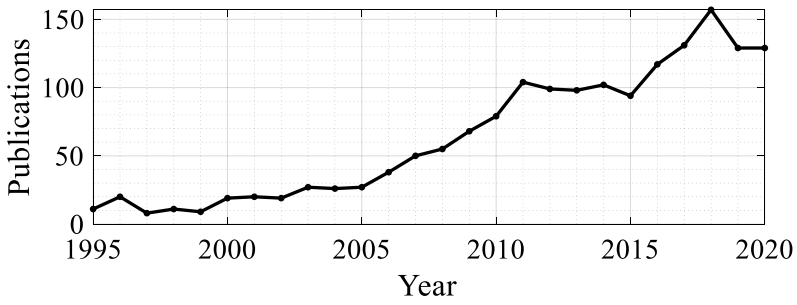

Figure 1.2 Chatter publications on milling since 1995.

1.2 Work Organization

This work is summarized as follows. Chapter 2 focuses on the description of the Homotopy Perturbation Method (HPM) which is the basis from which we start developing the analysis for the study of milling tools. Chapter 3 presents the mathematical expressions to solve DDE's using the homotopy procedure and the development of the Enhanced Multistage Homotopy Perturbation Method (EMHPM) to observe the solution in time domain for milling operations using the first-second and third-order approximation of the method. Chapter 4 studies the application of the first-, second- and third-order EMHPM on the milling equation to demonstrate its improvement in the convergence rate. Also, the stability lobes analysis in milling for regular and multivariable tools are presented. Chapter 5 focuses on theoretical predictions with time-domain simulations and experimental validation for a multivariable tool. Finally, some conclusions are drawn.

1.3 Objectives

Use the methodology based on the homotopy perturbation method to solve the EMHPM with second and third order approximations and apply it in delay differential equations.

Use the EMHPM with second and third order polynomial approximations to solve milling equations and predict the stability zone for milling operations through the stability lobes in regular and multivariable tools.

Compare the solution of the EMHPM with the solution of the SDM and FDM in terms of convergence and computational time.

Perform mechanical test in milling operations using the stability lobes to validate them with the Continuous Wavelet Transform (CWT), the Power Spectral Density (PSD) and Poincaré Maps (PM) and then observe the dominant frequencies in the process and detect when chatter is present.

1.4 Hypothesis

By solving the EMHPM with second and third order approximations, there will be greater convergence in the solution of the differential equations with delay since a quadratic polynomial approximation to the delay term will be used in comparison to the first order solution that uses a linear approximation,

The second and third order EMHPM can be used in the solution of milling problems for both regular and multivariable tools.

Continuous Wavelet Transform (CWT) scalograms, Power Spectral Density (PSD) charts and Poincaré Maps (PM) of the vibration signal on time when milling, will allow to validate the stability lobes generated with the solution of the second and third order EMHPM.

1.5 Problem Statement and Context

During a milling process, unstable vibrations also known as self-excited vibration or chatter may occur. Chatter reduces the machining efficiency due to low material removal rate by reducing the workload and affects surface quality, shortens tool life and accelerates tool wear.

A common technique offline to predict unstable vibrations is the so-called stability lobes of the DDE based on Floquet theory, in which a curve describes the limit of stable vibration under feasible range values of cutting parameters.

Different from the uniform pitch cutter, when a variable pitch cutter is used, the dynamics model of cutting vibration changes from DDEs with a single delay to DDEs with multiple delays. The use of variable pitch cutters has demonstrated to improve productivity.

The stability analysis of the milling process with multiple delays has been studied through different methods, therefore, in the present work, the EMHPM is used to solve the dynamics of the machining process in milling in which the approximation to the delay is performed with polynomials of degree two and three.

Through this work we try to find a competitive solution method in terms of convergency and computational cost, able to solve the DDE present during the milling process to obtain the vibration in time domain when milling, and to predict stability lobes for regular and multivariable tools.

1.6 Solution overview

A new method for solving differential equations with delay is presented by applying the homotopy perturbation method and using a second and third order polynomial as an approximation to the delay term. This method allows finding an analytical-numerical solution that confers advantages of precision and low computational cost. To evaluate the advantages of the proposed method, the solution of the milling equation has been studied and compared with Matlab's dde23 routine, as well as with the zero order and first order approximation. The proposed method shows a rapidly convergence, allowing improvement in computational time; also, is important to point out that the method is applicable for both regular and irregular tools.

Chapter 2. Milling operation

2.1 Introduction

Throughout the 20th century, an attempt has been made to create a suitable model that explains the phenomena that occur during the material removal process in order to predict the shape of the chip, the existing forces and the temperatures in the cut. Some researchers have used traditional methods such as statistical regression methods and response surface methodology to model the processes, others have chosen to apply artificial neural networks to model non-linear problems such as machining processes [25]; however, there is no fully accepted model that describes the phenomenon in its entirety. The material removal process is one of the most important manufacturing techniques to obtain a part with the desired shape and dimensions through the removal of material in the form of chips. Today there are different metal cutting operations such as turning, drilling, boring, grinding, milling, carving, brushing, etc., which are used depending on parameters such as geometry and the application that is going to be given to the final piece.

2.2 Mechanics of orthogonal cutting

Most of the cutting operations generate forces in three dimensions so that the modeling is geometrically complex, that is why the explanation of the material removal mechanism is started using the orthogonal cutting model. In orthogonal cutting the material is removed by the cutting edge of the tool that is perpendicular to the relative feed direction between the tool and the workpiece Figure 2.1.

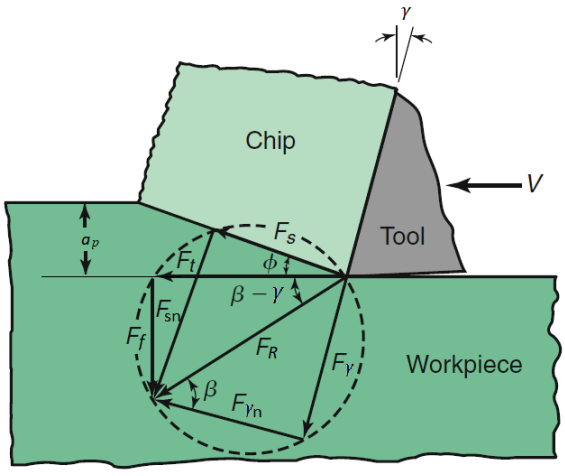

Figure 2.1 Schematic of the orthogonal cutting process. Adapted from [26]

This basic model of chip formation (known as the Merchant model) considers that the material shear occurs in the so-called shear plane, which is usually a very narrow area. The force on the process material F_R is decomposed into F_t (tangential force) which has the same direction as the cutting speed and the feed force F_f which is in the direction of the depth of cut a_p. The force F_R can be decomposed in the direction of the rake face F_γ (friction force) and its normal $F_{\gamma n}$ or in the plane of shear F_s (shear force) and its normal F_{ns}.

Although this model is not unequivocal, it allows qualitative judgments and calculations, as well as an approximate calculation of thermal fields. Thanks to the rise of computation and more sophisticated models, simulation has become a natural tool to deal with the non-linearities involved.

Orthogonal cutting is not directly applicable to many use cases of corner radius, chamfer, or chip breaker geometries. It is practical to carry out a series of experiments to identify certain parameters that relate the shear forces of a specific geometry and the work material to have a model of forces close to reality. Therefore, it is common to define the cutting forces mechanistically as a function of the cutting parameters (feed per tooth (f_z) and axial depth (a_p)) and coefficients of shear and friction cuts for each of the tangential and forward directions.

$$\begin{aligned} F_t &= K_{tc} f_z a_p + K_{te} a_p \\ F_f &= K_{fc} f_z a_p + K_{fe} a_p \end{aligned} \tag{2.1}$$

Constants K_{tc} and K_{fc} as well as the non-contributing coefficients in shear K_{te}, K_{fe} are directly calibrated with experiments for a specific tool-material combination. It must be taken into consideration that when there is wear on the edges of the tool, the shear coefficients are affected. To consider the effect of chip thickness on friction and shear angles, the specific shear pressure (K_t, K_f) is occasionally expressed as a non-linear function of chip thickness.

$$\begin{aligned} K_t &= K_T h^{-p_c} \\ K_f &= K_F h^{-q_c} \end{aligned} \tag{2.2}$$

where p_c and q_c are cutting force constants that must be determined with experiments at different linear advances. Because some metals exhibit different shear coefficients at different speeds, it is necessary to consider this phenomenon in certain applications.

2.3 Milling process

Milling is a cutting process in which a rotary tool executes relative movements on a part. The rotating action of the tool allows the section of material to be pulled out of the part in interference with the tool (chip) [25]. The milling process is one of the important machining processes besides turning. The movements are powered by the degrees of freedom of the machine, and the geometries that can be manufactured are limited by the degrees of freedom and the geometry of the edges of the tool. In recent years, thanks to the great boom in machine tool technology, milling has evolved to become a method with which it is possible to machine a wide range of products.

Machining centers, being composed of multiple axes, allow different operations to be carried out on the same machine; In addition to specific applications, milling is increasingly used to make holes, cavities, surfaces that were previously turned, threading, etc., which is why milling is a versatile and more efficient machining method.

During milling, each of the edges of the tool removes a certain amount of metal, the geometry of the tool, as well as the direction of advance of the piece also play an important role in the removal of chips. Also, in milling operation it is possible to find two general cases of the interaction tool-workpiece, one in which the piece advances in favor of the direction of rotation of the tool and the second that is opposite to the first, this phenomenon has impact especially at the beginning and to the end of the cut.

In up-milling, the feed direction of the part is opposite to that of the rotation of the tool in the cutting area, the chip thickness starts from zero and increases its value to a maximum towards the end of the cut Figure 2.2. In this case, when an edge of the tool hits the workpiece, there are reaction forces that block the tool from the piece, so the cutting edge is forced to begin its task of removing material, there is a great friction which causes the temperature of the region where the phenomenon occurs to rise, and therefore, when the temperature increases, greater surface resistance is presented, which causes greater difficulty in removal by the successive edges of the tool.

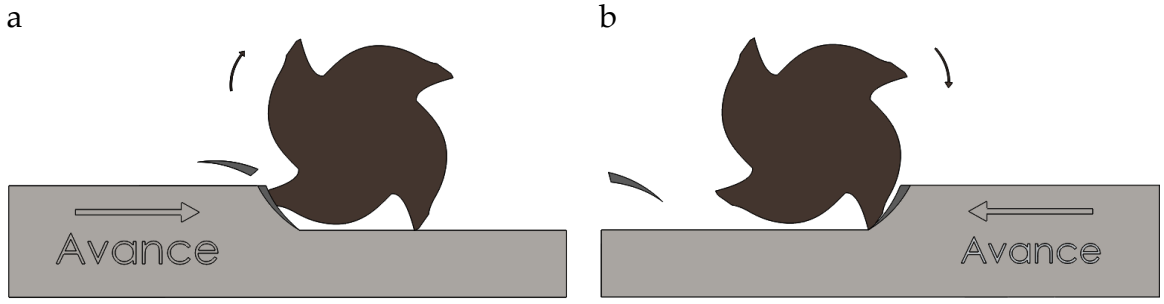

Figure 2.2 a) Up-milling and b) down-milling operation

On the other hand, during down-milling, the forward direction of the work piece is the same as the direction of rotation of the tool in the cutting area, which is why the chip thickness has the maximum value at the beginning of the cut and is reduced to zero when the cut ends; since the edge of the tool begins by cutting a significant thickness of chip, friction and process temperatures are significantly reduced, thus minimizing surface resistance, in addition to the reaction forces resulting from cutting also causing a kind of attraction of the piece of work towards the tool, which is a beneficial effect for the incidence of the following edge.

2.4 Force Models in the milling process

Cutting force models are essential in modeling conventional milling processes used to calculate milling power consumption, prediction of stable machining conditions (without vibration), determination of surface location errors, and design of machine-tools and cutting tools. Machining process models are often generated from rigorous experiments, as they involve the effect of multiple inputs, such as depth of cut, feed rate, speed of cut, tool geometry, work piece geometry, state of wear of the tool, among others [27].

One of the most used tools for roughing and finishing operations are the end mill cutters with helix angle β, diameter D and z_n teeth. To develop analytical expressions of the cutting process, the reference system of the tool is located on the axis of rotation of the tool and the lower plane.

The axial depth a_p is measured in the axial direction and the angle ϕ that describes the orientation of the first tooth is measured from the y-axis, also the angle of the teeth $iz = 1, \dots, z_n$ is described by ϕ_{i_z}.

Due to the helix angle, the position angle of each cutting edge varies with height according to the expression $\psi = k_\beta a_p$, where $k_\beta = 2\tan\beta/2D$. Therefore, the angular position of edge i_z at depth a_p is

$$\phi_{iz}(z) = \phi + \frac{2\pi(iz-1)}{z_n} - k_\beta z \tag{2.3}$$

Forces in the tangential (dF_{tj}), radial (dF_{rj}) and axial (dF_{aj}) directions that act on the differential elements of each cutting edge and with length dz as seen in Figure 2.3,are expressed as:

$$\begin{aligned} dF_{t,iz}\left(\phi_j,z\right) &= \left[K_{tc}h_{iz}\left(\phi_{i_z}\left(z\right)\right)+K_{te}\right]dz, \\ dF_{r,iz}\left(\phi_j,z\right) &= \left[K_{rc}h_{iz}\left(\phi_{i_z}\left(z\right)\right)+K_{re}\right]dz, \\ dF_{a,iz}\left(\phi_j,z\right) &= \left[K_{ac}h_{iz}\left(\phi_{i_z}\left(z\right)\right)+K_{ae}\right]dz \end{aligned} \tag{2.4}$$

where the chip thickness is:

$$h_{iz}\left(\phi,z\right) = f_z \sin\phi_{iz}\left(z\right) \tag{2.5}$$

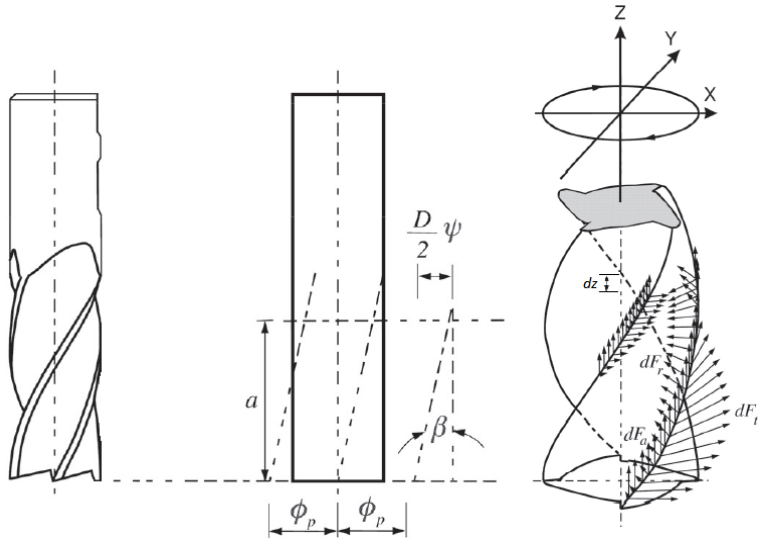

Figure 2.3 Helical milling cutter geometry. Adapted from [16]

In (2.5) f_z is the material removal rate (mm/rev per tooth), the cutting forces are expressed as a function of the variation of the chip area $h_{iz}\left(\phi_{iz}(z)\right)dz$ and the contact length (dz). K_{tc}, K_{rc} and K_{ac} are specific shear force coefficients due to shear in the tangential, radial and axial directions respectively, while K_{te}, K_{re} y K_{ae} are due to friction. The cutting forces are projected onto the tool coordinate system in the feed (x), normal (y), and axial (z) directions using the transformation

$$\begin{aligned} dF_{x,iz}\left(\phi_{iz}(z)\right) &= -dF_{t,iz}\cos\phi_{iz}(z) - dF_{r,iz}\sin\phi_{iz}(z), \\ dF_{y,iz}\left(\phi_{iz}(z)\right) &= dF_{t,iz}\sin\phi_{iz}(z) - dF_{r,iz}\cos\phi_{iz}(z), \\ dF_{z,iz}\left(\phi_{iz}(z)\right) &= dF_{a,iz} \end{aligned} \tag{2.6}$$

Substituting the differential forces from eq. (2.4) and chip thickness from eq. (2.5) in (2.6) we obtain

$$
\begin{aligned}
dF_{x,iz}\left(\phi_{iz}(z)\right) &= \left\{\begin{matrix}\frac{1}{2} f_z\left[-K_{tc}\,sin\,2\phi_{iz}(z) - K_{rc}\left(1-cos\,2\phi_{iz}(z)\right)\right] + \\ \left[-K_{te}\,cos\,\phi_{iz}(z) - K_{re}\,sin\,\phi_{iz}(z)\right]\end{matrix}\right\} dz, \\
dF_{y,iz}\left(\phi_{iz}(z)\right) &= \left\{\begin{matrix}\frac{1}{2} f_z\left[-K_{tc}\left(1-cos\,2\phi_{iz}(z)\right) - K_{rc}\,sin\,2\phi_{iz}(z)\right] + \\ \left[K_{te}\,sin\,\phi_{iz}(z) - K_{re}\,cos\,\phi_{iz}(z)\right]\end{matrix}\right\} dz, \\
dF_{z,iz}\left(\phi_{iz}(z)\right) &= \left[K_{ac} f_z\,sin\,\phi_{iz}(z) + K_{ae}\right] dz
\end{aligned}
\tag{2.7}
$$

To find the coefficients that characterize the tool with the material, it is necessary to carry out a set of experiments at different feed rates per tooth f_z but keeping the radial immersion and the axial depth at a fixed value.

To avoid having the runout effect of the tool in the results, cuts are made with full radial immersion. The average total force per revolution is calculated per tooth, since the material cut by each tooth is the same. The mean is independent of the helix angle, which leads us to replace $dz = a_p$, $\phi_{i_z}(z) = \phi$ y $k_\beta = 0$ in equations (2.7). Integrating and dividing by the pitch angle $\phi_p = 2\pi/z_n$, result the average forces per tooth within the cutting zone $\phi_{st} \le \phi \le \phi_{ex}$:

$$
\begin{aligned}
\bar{F}_x &= \left\{\frac{z_n a_p f_z}{8\pi}\left[K_{tc}\,cos\,2\phi - K_{rc}\left(2\phi - sin\,2\phi\right)\right] + \frac{z_n a_p}{2\pi}\left[-K_{te}\,sin\,\phi + K_{re}\,cos\,\phi\right]\right\}_{\phi_{st}}^{\phi_{ex}} \\
\bar{F}_y &= \left\{\frac{z_n a_p f_z}{8\pi}\left[K_{tc}\left(2\phi - sin\,2\phi\right) + K_{rc}\,cos\,2\phi\right] - \frac{z_n a_p}{2\pi}\left[K_{te}\,cos\,\phi + K_{re}\,sin\,\phi\right]\right\}_{\phi_{st}}^{\phi_{ex}} \\
\bar{F}_z &= \frac{z_n a_p}{2\pi}\left[-K_{ac} f_z\,cos\,\phi + K_{ae}\,\phi\right]_{\phi_{st}}^{\phi_{ex}}
\end{aligned}
\tag{2.8}
$$

Executing cuts in full immersion allows the simplification of Eq. (2.8) since $\phi_{st} = 0$ y $\phi_{ex} = \pi$. Average forces can be expressed by a linear function of feed per tooth as:

$$
\bar{F}_{x,y,z}\left(\phi_{iz}(z)\right) = K_{c_{x,y,z}}\, f_z + K_{e_{x,y,z}} \tag{2.9}
$$

where $K_{c_{x,y,z}}$, f_z and $K_{e_{x,y,z}}$ are calculated by linear regression. In this way, for full immersion the force coefficients are evaluated through (2.8) and (2.9) resulting in the following expressions

$$K_{tc}=\frac{4K_{yc}}{z_n a_p}, K_{te}=\frac{\pi K_{ye}}{z_n a_p}, K_{rc}=-\frac{4K_{xc}}{z_n a_p}, K_{re}=-\frac{\pi K_{xe}}{z_n a_p}, K_{ac}=\frac{\pi K_{zc}}{z_n a_p}, K_{ae}=\frac{2K_{ze}}{z_n a_p} \quad (2.10)$$

Eq. (2.10) can be written as

$$K_{tc}=\frac{4\bar{F}_{yc}}{z_n a_p}, K_{te}=\frac{\pi \bar{F}_{ye}}{z_n a_p}, K_{rc}=-\frac{4\bar{F}_{xc}}{z_n a_p}, K_{re}=-\frac{\pi \bar{F}_{xe}}{z_n a_p}, K_{ac}=\frac{\pi \bar{F}_{zc}}{z_n a_p}, K_{ae}=\frac{2\bar{F}_{ze}}{z_n a_p} \quad (2.11)$$

The procedure is repeated for each cutting geometry; therefore, milling force coefficients cannot be predicted prior to testing for new designs using mechanistic models.

Forces in a multivariable tool

When we have a multivariable tool where the pitch angle and helix angles are not uniform, a way to find the specific cutting coefficients for each tooth is by making experimentation with a radial immersion of 25% of the tool, with this immersion we can obtain by experimentation the forces and observe the effect on each flute. The Eq. (2.8) requires to be evaluated at the entry and exit angle, if the radial immersion is 25 percent, $\phi_{st}=\frac{2\pi}{3}$, and $\phi_{ex}=\pi$.

Figure 2.4 shows a representation of a multivariable tool which is discretized by disks due that when the pitch and helix angles are variables, there are an infinite number of delays, and in order to limit them, a way to solve the problem is by discretizing the tool in a specific amount of disks of thickness Δa, this conceptualization of the tool will be discussed in Section 4.4.

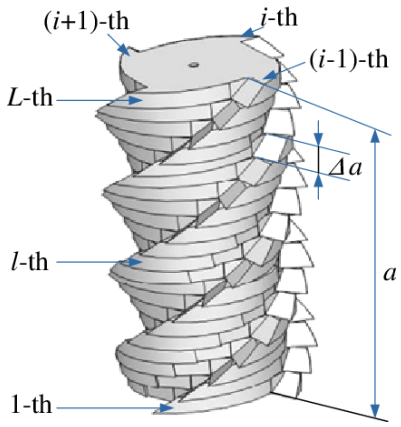

Figure 2.4 Multivariable milling tool discretized in disks. Recovered from [28]

Solving Eq. (2.8) with this consideration we have that

$$\bar{F}_{xc} = \frac{z_n a_p}{8\pi}\left[\frac{3}{2}K_{tc} + \left(\frac{4\pi}{3} - 2\pi + \frac{\sqrt{3}}{2}\right)K_{rc}\right], \qquad \bar{F}_{xe} = \frac{z_n a_p}{2\pi}\left[\frac{\sqrt{3}}{2}K_{te} - \left(\frac{1}{2}\right)K_{re}\right],$$

$$\bar{F}_{yc} = \frac{z_n a_p}{8\pi}\left[\left(2\pi - \frac{4\pi}{3} - \frac{\sqrt{3}}{2}\right)K_{tc} + \frac{1}{2}K_{rc}\right], \qquad \bar{F}_{ye} = \frac{z_n a_p}{2\pi}\left[\left(\frac{1}{2}\right)K_{te} + \left(\frac{\sqrt{3}}{2}\right)K_{re}\right], \tag{2.12}$$

$$\bar{F}_{zc} = \frac{z_n a_p}{4\pi}\left[K_{ac}\right], \qquad \bar{F}_{ze} = \frac{z_n a_p}{6}\left[K_{ae}\right],$$

Like the procedure for a regular tool, to obtain the specific cutting coefficients experimentation is required using different feed rates and evaluating the forces in each flute to obtain the specific cutting coefficients in each edge.

Chapter 3. Mathematical modeling of machining

3.1 Differential Equations solved with homotopy perturbation methods

Dynamic systems can be modeled to describe different systems such as mechanical, biological, or physical. These models allow us to observe, for example, the future rate of change of a variable that depends on the current state of a system. There are many phenomena in different fields of science and engineering that involve not only the value at time t but also the response in an earlier state $t - \tau$, that is, there is a dependency on past behavior determined by the delay value τ. In cases where the net force depends on the current values and some past values (history) such as position and speed, the system is described using a differential delay equation (DDE). The material removal process is one of the most important manufacturing processes to obtain a part with the desired shape and dimensions through the removal of chip material; however, during the process, vibrations may occur due to the repercussion of the vibration of the previous cut on the current one, this type of vibrations is known as self-excited vibration or chatter, since it occurs between the workpiece and the cutting tool. Chatter reduces the machining efficiency (due to low material removal rate by reducing the workload) and surface quality, shortens the tool durability and accelerates the tool wear. Since the regenerative chatter is caused by the phase differences between wavy surfaces left by the adjacent teeth, it can be suppressed by adjusting the pitch angle between the adjacent teeth. The use of variable pitch cutters to improve the stability of the milling process is built on this idea. Different from the uniform pitch cutter, when the variable pitch cutter is used, the dynamics model of cutting vibration changes from DDEs with single delay to DDEs with multiple delays [29]. In the machining of heat-resistant materials such as titanium alloys, which are widely used in the aeronautical sector, there is an increased risk of vibrations due to high cutting forces, to control and suppress chatter vibrations, the use of piezoelectric actuators embedded in the tool holder [30], electromagnetic actuators integrated into the spindle system [31] and tunable clamping table [32] has been analyzed. In the milling process, the use of variable pitch cutters has demonstrated to improve productivity [33]. An alternative to vibration suppression is stability lobes, which try to predict under which parameters or cutting conditions the milling process remains stable or free of vibration.

The milling process can be modeled by nonlinear equations, several perturbation methods have been proposed to find solutions to nonlinear equations, however, most of these are only applied to problems in which the nonlinearity present in the physical system is small, which limits its application. To eliminate this limitation, the Homotopy Perturbation Method (HPM) proposed by Ji-Huan He [34–36] can be used, this method

is a coupling of the traditional perturbation method and homotopy theory used in topology, and consists initially using a simple solution that continually approaches the study problem through a parameter that converges to unity.

The application of HPM has been effective in solving various problems, it has served as the basis for solving epidemic models [37], problems of systems of linear equations [38], up to the solution of non-linear second-order differential equations [39], which usually define the dynamic behavior of mechanical systems.

With the HPM few approximations are required to achieve precise solutions, examples of them are oscillators and non-linear dynamic models, studied in [40–43], however, the HPM is an asymptotic method that relies on some assumptions that limit their convergence as the solution evolves away from the initial conditions.

Liao, author of Homotopy Analysis Method (HAM), states in [44] that HPM is a particular case of HAM when the control parameter takes the value h. Methodologies are susceptible to improvement, as well as to different types of errors in particular applications, so their usefulness should not be disqualified when areas of opportunity are found, but rather modifications should be made to make them more powerful and robust methods. Abbasbandy used the idea of solution by subintervals in the solution of the Ricatti equation [45] and also Chen, Hendi, Bashiri, and Biazar made use of the HPM to analyze models of the Volterra integral equation in [46–49]. Hosein [50] proposed to modify the linear operator proposed by He in such a way that it was stable and called it "Enhanced Homotopy Perturbation Method" (EHPM). On the other hand, Odibat proposed the expansion in the Taylor series of the terms of the independent variable to improve the convergence of the HPM [51]. Hashim and Chowdhury proposed a methodology to obtain the solution of systems of differential equations of first order by means of multiple intervals and called it Multistage Homotopy Perturbation Method (MHPM), in which they obtained good results [52–55]. Ramos in [42], in addition to stating that in the case of ordinary differential equations the HPM and the decomposition technique are identical, which is confirmed in [56], he also sustains that both methods are subject to the same limitation as he calls "noisy" terms, referring to those that appear in successive terms in the solution series and that are canceled when determining the final series of the solution. This makes difficult to prove that the solution converges and does not guarantee that a finite number will achieve a certain approximation. In this sense, he also proposed a methodology by subintervals which he called the Piecewise Homotopy Method. On the other hand, Olvera proposed a method called the Enhanced Multistage Homotopy Perturbation Method (EMHPM), which generalizes the multistage homotopy method to obtain the solution of nonlinear differential equations with variable coefficients, which include time variable terms [57]. In this method, although interval solutions are used, it does not mean that solutions are produced in sections, but rather that a continuous analytical solution is obtained at any instant in time. The results

generated by this method were compared against the results of Hosein [50] and Odibat [51], in order to justify the need for the proposed method.

The EMHPM solves the evolutionary equations by subintervals through the temporary auxiliary transformation, this means that the EMHPM uses a combination of continuous functions over the time domain analyzed, however, it should not be confused with the Finite Element Method which approximates the solution as a linear combination of piecewise functions over small intervals [58–60].

3.2 HPM procedure

HPM rapidly converges on published literature papers where few approximations are necessary to achieve precise solutions. The basic idea of HPM, is illustrated through the following nonlinear differential equation:

$$A(u) - f(r) = 0,\ r \in \Omega \tag{3.1}$$

with the boundary condition:

$$B\left(u, \frac{\partial u}{\partial x}\right) = 0,\ r \in \Gamma \tag{3.2}$$

where A is a differential operator, $f(r)$ is a known analytic function, Ω is the domain, B is a limit operator, Γ is the limit of the domain. The operator A can be divided into a linear part L and a non-linear part N, thus, eq. (1) can be rewritten as

$$L(u) + N(u) = f(r) \tag{3.3}$$

Applying the principles of topology, a homotopy is constructed $v(r,p)\colon \Omega \times [0,1] \rightarrow \mathbb{R}$ that satisfies

$$\mathcal{H}(v,p) = (1-p)\left[L(v) - L(u_0)\right] + p\left[A(v) - f(r)\right] = 0, \quad p \in [0,1],\ r \in \Omega \tag{3.4}$$

That can be expressed as

$$\mathcal{H}(v,p) = L(v) - L(u_0) + pL(u_0) + p\left[N(v) - f(r)\right] = 0 \tag{3.5}$$

where $p \in [0,1]$ is an embedding parameter, u_0 is a proposed initial approximation to Ec. (3.1) that also satisfies the boundary conditions.

Since $p \in [0,1]$, it is observed that

$$\begin{aligned} \mathcal{H}(v,0) &= L(v) - L(u_0) = 0 \\ \mathcal{H}(v,1) &= A(v) - f(r) = 0 \end{aligned} \tag{3.6}$$

The change in p from zero to one cause $v(r,p)$ to change from $u_0(r)$ to $u(r)$. In topology, this is called deformation and in the same context $L(v) - L(u_0)$ and $A(v) - f(r)$ is called homotopy. He in [34] assumed that eq. (3.5) could be expressed as a power series on p.

$$v = v_0 + pv_1 + p^2 v_2 + p^3 v_3 + \ldots \tag{3.7}$$

considering $p = 1$ the approximate solution of eq. (3.1) is

$$u = \lim_{p \to 1} v = v_0 + v_1 + v_2 + v_3 + \ldots \tag{3.8}$$

Application case of HPM

In order to show the precision achieved with the choice of the linear operator, the following non-linear equation was analyzed [50]:

$$\dot{Y} - Y + e^t Y^2 = 0,\ Y(0) = c \tag{3.9}$$

where Y is the independent variable, t is the time, and c is a constant. For this equation, the linear part L and the nonlinear part N can be chosen as:

$$L(Y) = \dot{Y} - Y,\ \ N(Y) = e^t Y^2 \tag{3.10}$$

Therefore, using equation (3.5), the homotopy is as follows:

$$\mathcal{H}(Y,p) = L(Y) - L(y_0) + pL(y_0) + p\left[N(Y)\right] = 0,\ \ y_0(t) = c \tag{3.11}$$

And eq. (3.11) is represented as:

$$\mathcal{H}(Y,p) = \left(\dot{Y} - Y\right) - \left(\dot{y}_0 - y_0\right) + p\left(\dot{y}_0 - y_0\right) + p\left[e^t Y^2\right] = 0 \tag{3.12}$$

Substituting at equation (3.12) the second order expansion $Y = Y_0 + pY_1 + p^2Y_2$, we have:

$$\mathcal{H}(Y,p) = \left(\left(\dot{Y}_0 + p\dot{Y}_1 + p^2\dot{Y}_2\right) - \left(Y_0 + pY_1 + p^2Y_2\right)\right) - \left(\dot{y}_0 - y_0\right) + p\left(\dot{y}_0 - y_0\right) + pe^t\left(Y_0 + pY_1 + p^2Y_2\right)^2 = 0 \tag{3.13}$$

also, we know that

$$pe^t\left(Y_0 + pY_1 + p^2Y_2\right)^2 = pe^t\left(Y_0^2 + 2pY_0Y_1 + 2p^2Y_0Y_2 + 2p^3Y_1Y_2 + p^2Y_1^2 + p^4Y_2^2\right) \tag{3.14}$$

then, developing eq. (3.13),

$$\begin{aligned}\mathcal{H}(Y,p) = \left(\dot{Y}_0 + p\dot{Y}_1 + p^2\dot{Y}_2\right) - \left(Y_0 + pY_1 + p^2Y_2\right) - \dot{y}_0 + y_0 + p\dot{y}_0 - py_0 + \\ e^t\left(pY_0^2 + 2p^2Y_0Y_1 + 2p^3Y_0Y_2 + 2p^4Y_1Y_2 + p^3Y_1^2 + p^5Y_2^2\right)\end{aligned} \tag{3.15}$$

grouping by powers of p, the general solution for the equation (3.9) is obtained:

$$\begin{aligned} p^0 &: \ \dot{Y}_0 - Y_0 - \dot{y}_0 + y_0 = 0 \\ p^1 &: \ \dot{Y}_1 - Y_1 + \dot{y}_0 - y_0 + e^tY_0^2 = 0 \\ p^2 &: \ \dot{Y}_2 - Y_2 + 2e^tY_0Y_1 = 0 \end{aligned} \tag{3.16}$$

The initial approximation is $y_0 = c$, since c is a constant, its derivative $\dot{y}_0 = 0$. Hosein, in [50] considered $y_0 = 0$, so:

$$\begin{aligned} p^0 &: \ \dot{Y}_0 - Y_0 = 0, && Y_0(0) = c \\ p^1 &: \ \dot{Y}_1 - Y_1 + e^tY_0^2 = 0, && Y_1(0) = 0 \\ p^2 &: \ \dot{Y}_2 - Y_2 + 2e^tY_0Y_1 = 0, && Y_2(0) = 0 \end{aligned} \tag{3.17}$$

solving equation (3.17), and using the Laplace transform at p^0:

$$\mathcal{L}\left\{\dot{Y}_0 - Y_0\right\} = \mathcal{L}\{0\} \tag{3.18}$$

by Laplace it is known that $\mathcal{L}\{f'(t)\} = sL\{f(t)\} - f(0),\ \mathcal{L}\{f(t)\} = F(s)$, then:

$$\mathcal{L}\left\{\dot{Y}_0\right\} = s\left(Y_{0(s)} - Y_0(0)\right),\quad \mathcal{L}\left\{Y_0\right\} = Y_{0(s)},\ \mathcal{L}\{0\} = 0 \tag{3.19}$$

Substituting eq. (3.19) in (3.18), and knowing that $Y_0(0) = c$, we have:

$$\begin{aligned} s\left(Y_{0(s)}-c\right)-Y_{0(s)}&=0\\ Y_{0(s)}\left(s-1\right)&=c\\ Y_{0(s)}&=\frac{c}{s-1} \end{aligned} \tag{3.20}$$

now, by using the inverse Laplace transform:

$$\mathcal{L}^{-1}\left\{Y_{0(s)}\right\}=\mathcal{L}^{-1}\left\{\frac{c}{s-1}\right\} \tag{3.21}$$

It is known from Laplace's equations that the transform of e^{at} is

$$e^{at}=\frac{1}{s-a} \tag{3.22}$$

and since c is a constant, and a is equal to one, then the solution at p^0 is:

$$Y_0\left(t\right)=ce^t \tag{3.23}$$

Solving for p^1 from equation (3.17):

$$\mathcal{L}\left\{\dot{Y}_1-Y_1\right\}=-\mathcal{L}\left\{e^tY_0^{\,2}\right\} \tag{3.24}$$

substituting eq. (3.23) in (3.24),

$$\begin{aligned} \mathcal{L}\left\{\dot{Y}_1-Y_1\right\}&=-\mathcal{L}\left\{e^t\left(ce^t\right)^2\right\}\\ \mathcal{L}\left\{\dot{Y}_1-Y_1\right\}&=-\mathcal{L}\left\{c^2e^{3t}\right\} \end{aligned} \tag{3.25}$$

using equation (3.22), we have that $\mathcal{L}\{c^2e^{3t}\}=\frac{c^2}{s-3}$, so:

$$\begin{aligned} s\left(Y_{1(s)}-Y_1\left(0\right)\right)-Y_{1(s)}&=\frac{c^2}{s-3},\ \ Y_1\left(0\right)=0\\ Y_{1(s)}\left(s-1\right)&=-\frac{c^2}{s-3}\\ Y_{1(s)}&=-\frac{c^2}{\left(s-1\right)\left(s-3\right)} \end{aligned} \tag{3.26}$$

Equation (3.26) can be rewritten as

$$\frac{A}{s-1}+\frac{B}{s-3}=-\frac{c^2}{(s-1)(s-3)} \tag{3.27}$$

so, it is necessary to find the values of A and B

$$\frac{A(s-3)+B(s-1)}{(s-1)(s-3)}=-\frac{c^2}{(s-1)(s-3)} \tag{3.28}$$

since the denominator is the same on both sides of the equation, it turns out that:

$$A(s-3)+B(s-1)=-c^2 \tag{3.29}$$

It is observed that to find the solution of A and B, we must substitute in equation (3.29), $s=1$ and $s=3$. So, in the first case: $A(1-3)+B(1-1)=-c^2$, and in the second case with $s=3$, $A(3-3)+B(3-1)=-c^2$, when solving the equations the solution of A and B turns out to be:

$$A=\frac{c^2}{2},\ B=-\frac{c^2}{2} \tag{3.30}$$

therefore, eq. (3.26) is written as follows:

$$Y_{1(s)}=-\frac{c^2/2}{(s-1)}+\frac{-c^2/2}{(s-3)} \tag{3.31}$$

Using the inverse Laplace transform we have $\mathcal{L}^{-1}\{Y_{1(s)}\}=\mathcal{L}^{-1}\left\{\frac{\frac{c^2}{2}}{s-1}+\frac{\frac{-c^2}{2}}{s-3}\right\}$ which is rewritten as: $\mathcal{L}^{-1}\{Y_{1(s)}\}=\frac{c^2}{2}\mathcal{L}^{-1}\left\{\frac{1}{s-1}\right\}-\frac{c^2}{2}\mathcal{L}^{-1}\left\{\frac{1}{s-3}\right\}$. By using equation (3.22) the solution is reached at p^1:

$$Y_1(t)=\frac{c^2}{2}\left(e^t-e^{3t}\right) \tag{3.32}$$

Substituting the eq. (3.23) and (3.32) in (3.17) for p^2, it is obtained:

$$\begin{aligned}&\dot{Y}_2-Y_2+2e^t\left(ce^t\right)\left(\frac{c^2}{2}\left(e^t-e^{3t}\right)\right)=0\\&\mathcal{L}\left\{\dot{Y}_2-Y_2\right\}=\mathcal{L}\left\{c^3\left(e^{5t}-e^{3t}\right)\right\}\end{aligned} \tag{3.33}$$

Following a similar procedure to that developed for the previous solutions:

$$\begin{aligned} & s\left(Y_{2(s)}-Y_2(0)\right)-Y_{2(s)}=c^3\left(\frac{1}{s-5}-\frac{1}{s-3}\right),\ Y_2(0)=0 \\ & Y_{2(s)}(s-1)=c^3\left(\frac{1}{s-5}-\frac{1}{s-3}\right) \\ & Y_{2(s)}=c^3\left(\frac{1}{(s-1)(s-5)}-\frac{1}{(s-1)(s-3)}\right) \end{aligned} \tag{3.34}$$

Equation (3.34) can be written as

$$c^3\left(\left(\frac{A}{(s-1)}+\frac{B}{(s-5)}\right)-\left(\frac{C}{(s-1)}+\frac{D}{(s-3)}\right)\right)=c^3\left(\frac{1}{(s-1)(s-5)}-\frac{1}{(s-1)(s-3)}\right) \tag{3.35}$$

To find the values of A, B, C and D, we will first solve A and B and then we will find the values of C and D. Thus, for A and B we have:

$$\frac{A(s-5)+B(s-1)}{(s-1)(s-5)}=-\frac{c^3}{(s-1)(s-5)} \tag{3.36}$$

since the denominator is the same on both sides of the equation, it turns out that:

$$A(s-5)+B(s-1)=c^3 \tag{3.37}$$

It is observed that to find the solution of A and B, we must substitute in equation (3.37) $s=1$ and $s=5$. So, in the first case: $A(1-5)+B(1-1)=c^3$, and in the second case with $s=5$, $A(5-5)+B(5-1)=c^3$, when solving the equations the solution of A and B turns out to be:

$$A=-\frac{c^3}{4},\ B=\frac{c^3}{4} \tag{3.38}$$

To C and D, we have:

$$\frac{C(s-3)+D(s-1)}{(s-1)(s-3)}=\frac{c^3}{(s-1)(s-3)} \tag{3.39}$$

since the denominator is the same on both sides of the equation, it turns out that:

$$C(s-3)+D(s-1)=c^3 \tag{3.40}$$

It is observed that to find the solution of C and D, we must substitute in equation (3.40) $s=1$ and $s=3$.

In the first case, $C(1-3)+D(1-1)=c^3$, and in the second case with $s=1$, $C(3-3)+D(3-1)=c^3$, when solving the equations the solution of C and D turns out to be:

$$C=-\frac{c^3}{2},\ D=\frac{c^3}{2} \tag{3.41}$$

Equation (3.34) can be written as

$$Y_{2(s)}=\frac{c^3}{4}\left(\frac{-1}{s-1}+\frac{1}{s-5}\right)-\frac{c^3}{2}\left(\frac{-1}{s-1}+\frac{1}{s-3}\right) \tag{3.42}$$

using the inverse Laplace transform we have

$$\mathcal{L}^{-1}\left\{Y_{2(s)}\right\}=\mathcal{L}^{-1}\left\{\frac{c^3}{4}\left(\frac{-1}{s-1}+\frac{1}{s-5}\right)-\frac{c^3}{2}\left(\frac{-1}{s-1}+\frac{1}{s-3}\right)\right\} \tag{3.43}$$

which is rewritten as

$$\mathcal{L}^{-1}\left\{Y_{2(s)}\right\}=\frac{c^3}{4}\mathcal{L}^{-1}\left\{\frac{1}{s-5}-\frac{1}{s-1}\right\}-\frac{c^3}{2}\mathcal{L}^{-1}\left\{\frac{1}{s-3}-\frac{1}{s-1}\right\} \tag{3.44}$$

by using (3.22), $Y_2(t)=\frac{c^3}{4}(e^{5t}-e^t)-\frac{c^3}{2}(e^{3t}-e^t)$ and simplifying, the solution is

$$Y_2(t)=\frac{c^3}{4}\left(e^{5t}+e^t\right)-\frac{c^3}{2}e^{3t} \tag{3.45}$$

so, the solution of (3.17) is:

$$\begin{aligned} Y_0(t)&=ce^t \\ Y_1(t)&=\frac{c^2}{2}\left(e^t-e^{3t}\right) \\ Y_2(t)&=\frac{c^3}{4}\left(e^{5t}+e^t\right)-\frac{c^3}{2}e^{3t} \end{aligned} \tag{3.46}$$

Approximations obtained in (3.46), correspond to the second order solution calculated in [57] when $c = 1$.

Application of the EHPM

After analyzing the HPM, although the non-linear differential equation (3.9) is stable, the linear part suggested in (3.10) generates an undesired behavior, so Hosein et al. in [50] proposed modifying the linear operator to make it stable by adding and subtracting Y in the equation, and named the method "Enhanced Homotopy Perturbation Method" (EHPM). Under this consideration, Eq. (3.9) is rewritten to select a stable operator:

$$\dot{Y} + Y + e^t Y^2 - 2Y = 0,\ Y(0) = c \tag{3.47}$$

The linear and non-linear parts are represented by:

$$L(Y) = \dot{Y} + Y,\ \ N(Y) = e^t Y^2 - 2Y \tag{3.48}$$

The homotopy of Eq. (3.47) is represented by Eq. (3.11), so following the previous procedure we have:

$$\mathcal{H}(Y,p) = (\dot{Y} + Y) - (\dot{y}_0 + y_0) + p(\dot{y}_0 + y_0) + p\left[e^t Y^2 - 2Y\right] = 0 \tag{3.49}$$

Substituting in equation (3.49) the second order expansion $Y = Y_0 + pY_1 + p^2Y_2$, we have:

$$\begin{aligned}\mathcal{H}(Y,p) = &\left((\dot{Y}_0 + p\dot{Y}_1 + p^2\dot{Y}_2) + (Y_0 + pY_1 + p^2Y_2)\right) - (\dot{y}_0 + y_0) + p(\dot{y}_0 + y_0) + \\ &pe^t\left(Y_0 + pY_1 + p^2Y_2\right)^2 - 2\left(Y_0 + pY_1 + p^2Y_2\right)\end{aligned} \tag{3.50}$$

solving equation (3.50):

$$\begin{aligned}\mathcal{H}(Y,p) = &(\dot{Y}_0 + p\dot{Y}_1 + p^2\dot{Y}_2) + (Y_0 + pY_1 + p^2Y_2) - \dot{y}_0 - y_0 + p\dot{y}_0 + py_0 + e^t\left(pY_0^2 + 2p^2Y_0Y_1 + 2p^3Y_0Y_2 + \right. \\ &\left. 2p^4Y_1Y_2 + p^3Y_1^2 + p^5Y_2^2\right) - 2pY_0 - 2p^2Y_1 - 2p^3Y_2\end{aligned} \tag{3.51}$$

grouping by powers of p, we have the general solution for (3.47)

$$\begin{aligned}p^0:&\ \dot{Y}_0 + Y_0 - \dot{y}_0 - y_0 = 0 \\ p^1:&\ \dot{Y}_1 + Y_1 + \dot{y}_0 + y_0 + e^t Y_0^2 - 2Y_0 = 0 \\ p^2:&\ \dot{Y}_2 + Y_2 + 2e^t Y_0 Y_1 - 2Y_1 = 0\end{aligned} \tag{3.52}$$

Hosein considered $y_0 = 0$, so that $\dot{y}_0 = 0$, then:

$$\begin{aligned} &p^0: \ \dot{Y}_0 + Y_0 = 0, && Y_0(0) = c \\ &p^1: \ \dot{Y}_1 + Y_1 + e^t Y_0^{\,2} - 2Y_0 = 0, && Y_1(0) = 0 \\ &p^2: \ \dot{Y}_2 + Y_2 + 2e^t Y_0 Y_1 - 2Y_1 = 0, && Y_2(0) = 0 \end{aligned} \tag{3.53}$$

Previously Eq. (3.9) was solved using the Laplace transform, now Eq. (3.47) is solved using the integration method. Solving Eq. (3.53), the differential equation at p^0 can be expressed as $dY_0/dt = -Y_0$, so it can be presented as $dY_0/Y_0 = -dt$. By integrating the equation, we have

$$\begin{aligned} &\int \frac{dY_0}{Y_0} = -\int dt \\ &\ln(Y_0) = -t + const \end{aligned} \tag{3.54}$$

applying the properties of logarithmic functions and exponentials, equation (3.54) is presented as follows:

$$\begin{aligned} &e^{\ln(Y_0)} = e^{-t+const} \\ &Y_0 = e^{-t} e^{const} \end{aligned} \tag{3.55}$$

Due that e^{const} will be a constant, the solution of Y_0 is:

$$Y_0 = ce^{-t} \tag{3.56}$$

Using the solution of Y_0, it is solved for Y_1 at p^1, the equation is rewritten as:

$$\begin{aligned} &\frac{dY_1}{dt} + Y_1 = -e^t \left(ce^{-t}\right)^2 + 2\left(ce^{-t}\right) \\ &\frac{dY_1}{dt} + Y_1 = -c^2 e^{-t} + 2ce^{-t} \\ &\frac{dY_1}{dt} + Y_1 = \left(2c - c^2\right) e^{-t} \end{aligned} \tag{3.57}$$

Equation (3.57) has the form of first order linear ordinary differential equation:

$$y'(x) + p(x)y = q(x) \tag{3.58}$$

Notice that equation (3.57) can be expressed as

$$e^{t}\frac{dY_1}{dt}+e^{t}Y_1=\left(2c-c^2\right) \tag{3.59}$$

The reverse product rule for the differential equation states that

$$f\frac{dg}{dt}+g\frac{df}{dt}=\frac{d\left(f\ g\right)}{dt} \tag{3.60}$$

so, substituting $e^t=\frac{d}{dt}(e^t)$ in the second term of the (3.59), we have:

$$e^{t}\frac{dY_1}{dt}+\frac{d\left(e^{t}\right)}{dt}Y_1=\left(2c-c^2\right) \tag{3.61}$$

applying the reverse product rule to the left-hand side, we obtain:

$$\frac{d}{dt}\left(e^{t}Y_1\right)=\left(2c-c^2\right) \tag{3.62}$$

integrating both sides with respect to t:

$$\int\frac{d}{dt}\left(e^{t}Y_1\right)dt=\int\left(2c-c^2\right)dt \tag{3.63}$$

$$Y_1=e^{-t}\left(2c-c^2\right)t+c_1 \tag{3.64}$$

evaluating to find c_1 by substituting the initial condition $Y_1(0)=0$, at eq. (3.64)

$$0=e^{-0}\left(2c-c^2\right)0+c_1 \tag{3.65}$$

we find that $c_1=0$, so,

$$Y_1=\left(2c-c^2\right)te^{-t} \tag{3.66}$$

Using the solution of Y_0, and Y_1, now it is solved for Y_2 at p^2,

$$\dot{Y}_2+Y_2=-2e^{t}\left(ce^{-t}\right)\left(2c-c^2\right)te^{-t}+2\left(\left(2c-c^2\right)te^{-t}\right),\quad Y_2(0)=0 \tag{3.67}$$

Equation (3.67) can be rewritten as

$$\dot{Y}_2 + Y_2 = 2ce^{-t}t\left(c^2 - 3c + 2\right) \tag{3.68}$$

$$e^t\dot{Y}_2 + e^tY_2 = 2ct\left(c^2 - 3c + 2\right) \tag{3.69}$$

we substitute $e^t = \frac{d}{dt}(e^t)$ in the second term of (3.69), then, the equation becomes:

$$e^t\frac{dY_2}{dt} + \frac{d\left(e^t\right)}{dt}Y_2 = 2ct\left(c^2 - 3c + 2\right) \tag{3.70}$$

applying the reverse product rule to the left-hand side of (3.70), we obtain

$$\frac{d\left(e^tY_2\right)}{dt} = 2ct\left(c^2 - 3c + 2\right) \tag{3.71}$$

integrating both sides with respect to t, we have

$$\int\frac{d\left(e^tY_2\right)}{dt}dt = \int 2ct\left(c^2 - 3c + 2\right)dt \tag{3.72}$$

$$Y_2 = e^{-t}ct^2\left(c^2 - 3c + 2\right) + c_1 \tag{3.73}$$

evaluating to find c_1 by substituting the initial condition $Y_2(0) = 0$, at eq. (3.73)

$$0 = e^{-0}c(0)^2\left(c^2 - 3c + 2\right) + c_1 \tag{3.74}$$

we find that $c_1 = 0$, so, the solution of Y_2 is given by

$$Y_2 = e^{-t}ct^2\left(c^2 - 3c + 2\right) \tag{3.75}$$

Application of the HPM through the Taylor series

To improve the convergence of the HPM, Odibat in [51] proposed the expansion of the independent variable by using Taylor series, in such a way that it is possible to rewrite equation (3.9) as:

$$\dot{Y}\text{-}\,Y+\sum_{n=0}^{\infty}\frac{t^n}{n!}Y^2=0,\ Y(0)=c \tag{3.76}$$

For simplicity, the linear operator $L(y_0)=\frac{dy_0}{dt}$ is used, so that the homotopy of Eq. (3.76) can be represented as follows:

$$\mathcal{H}(Y,p)=\dot{Y}-\dot{y}_0+p\dot{y}_0-pY+\sum p^{n+1}\frac{t^n}{n!}Y^2 \tag{3.77}$$

To force the initial approximation $Y_0=c$, it was necessary to include the term p^{n+1}. Substituting the fourth order expansion $Y=Y_0+pY_1+p^2Y_2+p^3Y_3+p^4Y^4$ in equation (3.77), we have:

$$\begin{aligned}\mathcal{H}(Y,p)=&\left(\dot{Y}_0+p\dot{Y}_1+p^2\dot{Y}_2+p^3\dot{Y}_3+p^4\dot{Y}_4\right)-\dot{y}_0+p\dot{y}_0-p\left(Y_0+pY_1+p^2Y_2+p^3Y_3+p^4Y_4\right)+\\&p\left(Y_0+pY_1+p^2Y_2+p^3Y_3+p^4Y_4\right)^2+p^2t\left(Y_0+pY_1+p^2Y_2+p^3Y_3+p^4Y_4\right)^2+\\&p^3\frac{t^2}{2}\left(Y_0+pY_1+p^2Y_2+p^3Y_3+p^4Y_4\right)^2+p^4\frac{t^3}{6}\left(Y_0+pY_1+p^2Y_2+p^3Y_3+p^4Y_4\right)^2+\\&p^5\frac{t^4}{24}\left(Y_0+pY_1+p^2Y_2+p^3Y_3+p^4Y_4\right)^2\end{aligned} \tag{3.78}$$

By expanding and grouping the terms of equal order up to p^4, we have:

$$\begin{aligned}&p^0:\ \dot{Y}_0-\dot{y}_0=0\\&p^1:\ \dot{Y}_1+\dot{y}_0-Y_0+Y_0^2=0\\&p^2:\ \dot{Y}_2-Y_1+2Y_0Y_1+tY_0^2=0\\&p^3:\ \dot{Y}_3-Y_2+2Y_0Y_2+Y_1^2+2tY_0Y_1+\frac{t^2}{2}Y_0^2=0\\&p^4:\ \dot{Y}_4-Y_3+2Y_0Y_3+2Y_1Y_2+2tY_0Y_2+tY_1^2+t^2Y_0Y_1+\frac{t^3}{6}Y_0^2=0\end{aligned} \tag{3.79}$$

solving, and considering that $y_0=c$, we have, for p^0:

$$\int\frac{dY_0}{dt}=-\int\frac{dy_0}{dt},\ Y_0=y_0,\ Y_0=c \tag{3.80}$$

Substituting Y_0 in p^1, we have $\dot{Y}_1=Y_0-Y_0^2=c-c^2$, so that when applying the integral $\int\dot{Y}_1\,dt=\int(c-c^2)\,dt$, the solution of Y_1 is obtained.

$$Y_1=\left(c-c^2\right)t \tag{3.81}$$

Similarly, solving for p^2 we have $\dot{Y}_2 = (c - c^2)t - 2c\big((c - c^2)t\big) - tc^2 = ct - c^2t - 2c^2t + 2c^3t - tc^2$, so the integral $\int \dot{Y}_2\, dt = \int t(c - 4c^2 + 2c^3)\, dt$ is applied to obtain:

$$Y_2 = \frac{t^2}{2}\left(c - 4c^2 + 2c^3\right) \tag{3.82}$$

rearranging, the solution to Y_2 is:

$$Y_2 = \left(c^3 - 2c^2 + \frac{c}{2}\right)t^2 \tag{3.83}$$

At p^3, from Eq. (3.79) we have that $\dot{Y}_3 = Y_2 - 2Y_0Y_2 - Y_1^2 - 2tY_0Y_1 - \frac{t^2}{2}Y_0^2$ so, the same procedure is followed to apply the integral

$$\int \dot{Y}_3 dt = \int\left(\left(c^3 - 2c^2 + \frac{c}{2}\right)t^2 - 2c\left(\left(c^3 - 2c^2 + \frac{c}{2}\right)t^2\right) - \left(\left(c - c^2\right)t\right)^2 - 2tc\left(\left(c - c^2\right)t\right) - \frac{c^2t^2}{2}\right)dt \tag{3.84}$$

then, the solution of Y_3 is:

$$Y_3 = \left(-c^4 + 3c^3 - \frac{13}{6}c^2 + \frac{c}{6}\right)t^3 \tag{3.85}$$

Similarly, to p^4 we have

$$\begin{aligned}\int \dot{Y}_4 dt = &\int\left(\left(-c^4 + 3c^3 - \frac{13}{6}c^2 + \frac{c}{6}\right)t^3 - 2c\left(\left(-c^4 + 3c^3 - \frac{13}{6}c^2 + \frac{c}{6}\right)t^3\right) - 2\left(\left(c - c^2\right)t\right)\left(\left(c^3 - 2c^2 + \frac{c}{2}\right)t^2\right)\right)dt - \\ &\int\left(2tc\left(\left(c^3 - 2c^2 + \frac{c}{2}\right)t^2\right) - t\left(\left(c - c^2\right)t\right)^2 - t^2c\left(\left(c - c^2\right)t\right) - \frac{t^3}{6}c^2\right)dt\end{aligned} \tag{3.86}$$

by solving Eq. (3.86) we have:

$$\begin{aligned}Y_4 = &\left(-c^4 + 3c^3 - \frac{13}{6}c^2 + \frac{c}{6}\right)\frac{t^4}{4} + \left(2c^5 - 6c^4 + \frac{13}{3}c^3 - \frac{c^2}{3}\right)\frac{t^4}{4} + \left(-2c^4 + 4c^3 - c^2 + 2c^5 - 4c^4 + c^3\right)\frac{t^4}{4} + \\ &\left(-2c^4 + 4c^3 - c^2\right)\frac{t^4}{4} + \left(-c^2 + 2c^3 - c^4\right)\frac{t^4}{4} + \left(-c^2 + c^3\right)\frac{t^4}{4} - c^2\,\frac{t^4}{24}\end{aligned} \tag{3.87}$$

after solving we get:

$$Y_4 = \left(c^5 - 4c^4 + \frac{29}{6}c^3 - \frac{5}{3}c^2 + \frac{c}{24}\right)t^4 \tag{3.88}$$

The second-order solution obtained from Hosein is compared with the second-order solution, using the homotopy method from He, with Odibat's fourth-order equation and with the numerical solution calculated from the fourth-order Runge-Kutta method in Matlab (ode45). It is clearly observed in Figure 3.1 that the Hosein solution tends to coincide with the numerical solution while the other solutions diverge.

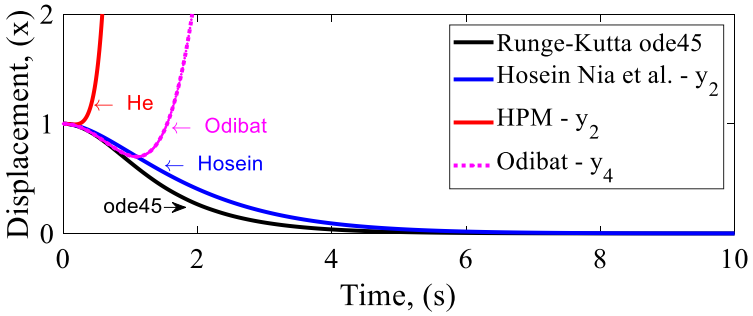

Figure 3.1 Solution comparison between Runge-Kutta and other authors of (3.9)

Application of the EMHPM

Since the solutions obtained by the MHPM diverge when the coefficients are dependent on time, to improve this drawback, Olvera in [57], proposed an extension of the MHPM to consider the general case in which the non-linear equation contains terms of the independently variable, he called this extension Enhanced Multistage Homotopy Perturbation Method (EMHPM).

In the algorithm proposed by Olvera in EMHPM, the HPM solution is sought by subintervals using the transformation $u(t) = U_i(T)$ where U_i represents a single approximate solution by subinterval and also satisfies the initial condition $U_i(0) = u_{i-1}(t_{i-1})$. The new time variable is subject to the condition: $0 \leq T \leq (t_i - t_{i-1})$; furthermore, $u_i(t)$ represents the approximate solution in the i-th subinterval. The initial proposed solution is given by: $U_{i0} = u_{i-1}(t_{i-1})$ where t_{i-1} represents the time at the end of the previous subinterval, that is, the final value of the approximate solution of a subinterval corresponds to the initial condition of the next subinterval.

To establish the homotopy that allows finding the solution of a differential equation, the following assumptions are made:

1. The linear operator $L(U_i)$ is chosen as $L(U_i) = \frac{d}{dT}U_i$ where the initial solution proposed is the initial condition $u_{i-1}(t_{i-1})$, that is, $U_{i0} = u_{i-1}(t_{i-1})$. To simplify the notation, it is used: $u_{i-1} \equiv u_{i-1}(t_{i-1})$.
2. Since the homotopy is defined in the i-th subinterval, the relation $T = t - t_{i-1}$ is introduced which must satisfy the condition: $0 \leq T \leq (t_i - t_{i-1})$; where t represents the current time. So, the solutions of k-th order are obtained by

integrating with respect to T while the terms related to the independent variable t are assumed to be constant in this i-th subinterval.

Therefore, the approximate solution of order m of the differential equation, according to the methodology proposed by the EMHPM, can be written as

$$u_i\left(T,t,u_{i-1}\right)=\sum_{k=0}^{m}U_{ik}\left(T,t,u_{i-1}\right) \tag{3.89}$$

The solution $u_{ik}(T,t,u_{i-1})$ is valid only in the i-th subinterval $(t_{i-1},t_i]$. To construct the solution $u(t)$ in this i-th subinterval, the next relation is used

$$u(t)\approx u_i\left(t-t_{i-1}\right) \tag{3.90}$$

So, the approximate solution of u at time t_i is given by:

$$u(t_i)\approx u_i\left(t_i-t_{i-1},t_i,u_{i-1}\right)=u_{i+1}\left(0,t_i,u_i\right)=u_i \tag{3.91}$$

Also, it is considered that the solution $u(t)$ for a subinterval (t_0,t_1) is divided into j subintervals which do not have to be equally spaced: $(t_0,t_1],(t_1,t_2],\ldots,\left(t_{j-1},t_j\right]$, but for simplicity it will be used in the work equidistant, unless otherwise specified. Finally, the approximate solution of $u(t)$ is obtained by coupling the solutions $u_i(t)$. To know the level of precision of the modifications proposed to the method, Olvera analyzed equation (3.9) in which the solutions developed by other authors do not converge. The homotopy of equation (3.9) is represented by eq. (3.11), the linear operator is $L(Y_i)=\dot{Y}_i$, while the non-linear one is given by $N(Y_i)=e^tY_i^2-Y_i$.

The third-order expansion $Y_i=Y_{i0}+pY_{i1}+p^2Y_{i2}+p^3Y_{i3}$, is used to rewrite the set of first-order linear equations that results from grouping the terms of equal power of p.

$$\begin{aligned}\mathcal{H}\left(Y_i,p\right)=&\left(\dot{Y}_{i0}+p\dot{Y}_{i1}+p^2\dot{Y}_{i2}+p^3\dot{Y}_{i3}\right)-\dot{y}_{i0}+p\dot{y}_{i0}+p\Big[e^t\left(Y_{i0}+pY_{i1}+p^2Y_{i2}+p^3Y_{i3}\right)^2-\\&\left(Y_{i0}+pY_{i1}+p^2Y_{i2}+p^3Y_{i3}\right)\Big]\end{aligned} \tag{3.92}$$

Also, knowing that

$$\begin{aligned}pe^t\left(Y_{i0}+pY_{i1}+p^2Y_{i2}+p^3Y_{i3}\right)^2=&\,pe^t\Big(Y_{i0}{}^2+2pY_{i0}Y_{i1}+2p^2Y_{i0}Y_{i2}+2p^3Y_{i0}Y_{i3}+p^2Y_{i1}{}^2+2p^3Y_{i1}Y_{i2}+\\&2p^4Y_{i1}Y_{i3}+p^4Y_{i2}{}^2+2p^5Y_{i2}Y_{i3}+p^6Y_{i3}{}^2\Big)\end{aligned} \tag{3.93}$$

by solving the equation (3.93), we have

$$\mathcal{H}(Y_i,p)=\left(\dot{Y}_{i0}+p\dot{Y}_{i1}+p^2\dot{Y}_{i2}+p^3\dot{Y}_{i3}\right)-\dot{y}_{i0}+p\dot{y}_{i0}+pe^t\left({Y_{i0}}^2+2pY_{i0}Y_{i1}+2p^2Y_{i0}Y_{i2}+2p^3Y_{i0}Y_{i3}+p^2{Y_{i1}}^2+2p^3Y_{i1}Y_{i2}+2p^4Y_{i1}Y_{i3}+p^4{Y_{i2}}^2+2p^5Y_{i2}Y_{i3}+p^6{Y_{i3}}^2\right)-\left(pY_{i0}+p^2Y_{i1}+p^3Y_{i2}+p^4Y_{i3}\right) \quad (3.94)$$

Grouping by powers of p, we have the general solution for equation (3.9):

$$\begin{aligned} p^0&:\ \dot{Y}_{i0}-\dot{y}_{i0}=0, && Y_{i0}(0)=c\\ p^1&:\ \dot{Y}_{i1}+\dot{y}_{i0}+e^t{Y_{i0}}^2-Y_{i0}=0, && Y_{i1}(0)=0\\ p^2&:\ \dot{Y}_{i2}+2e^tY_{i0}Y_{i1}-Y_{i1}=0, && Y_{i2}(0)=0\\ p^3&:\ \dot{Y}_{i3}+2e^tY_{i0}Y_{i2}+e^t{Y_{i1}}^2-Y_{i2}=0, && Y_{i3}(0)=0 \end{aligned} \quad (3.95)$$

Solving and considering that $y_{i0}=c$, and $\dot{y}_{i0}=0$ we have for p^0:

$$\int\dot{Y}_{i0}dT=\int\dot{y}_{i0}dT,\ \ Y_{i0}=y_{i0},\ Y_{i0}=c \quad (3.96)$$

Y_{i0} is replaced at p^1: $\dot{Y}_{i1}+e^tc^2-c=0$ and then it is integrated $\int\dot{Y}_{i1}\,dT=\int(c-e^tc^2)\,dT$ in order to have the value of Y_{i1}

$$Y_{i1}=cT-e^tc^2T \quad (3.97)$$

Similarly it is solved in p^2, so that $\dot{Y}_{i2}+2e^tc(cT-e^tc^2T)-(cT-e^tc^2T)=0$. The integral $\int\dot{Y}_{i2}\,dT=\int\left((cT-e^tc^2T)-2e^tc^2T+2e^{2t}c^3T\right)dT$, is applied, so that we have:

$$Y_{i2}=\frac{cT^2}{2}-\frac{e^tc^2T^2}{2}-e^tc^2T^2+e^{2t}c^3T^2 \quad (3.98)$$

rearranging, the solution to Y_{i2} is written as

$$Y_{i2}=\frac{1}{2}cT^2\left(2e^{2t}c^2-3e^tc+1\right) \quad (3.99)$$

Now, by substituting the found values of Y_{i0},Y_{i1},Y_{i2} in p^3,

$$\dot{Y}_{i3}+2e^tc\left(\frac{1}{2}cT^2\left(2e^{2t}c^2-3e^tc+1\right)\right)+e^t\left(cT-e^tc^2T\right)^2-\frac{1}{2}cT^2\left(2e^{2t}c^2-3e^tc+1\right)=0 \quad (3.100)$$

rearranging, we have

$$\dot{Y}_{i3}=\frac{1}{2}cT^2\left(2e^{2t}c^2-3e^tc+1\right)-c^2e^tT^2\left(2e^{2t}c^2-3e^tc+1\right)-e^tc^2T^2+2e^{2t}c^3T^2-e^{3t}c^4T^2 \quad (3.101)$$

applying the integral to (3.101),

$$\begin{aligned}\int \dot{Y}_{i3} dT &= \int \left(\frac{1}{2} cT^2 \left(2e^{2t}c^2 - 3e^t c + 1\right) - c^2 e^t T^2 \left(2e^{2t}c^2 - 3e^t c + 1\right) - e^t c^2 T^2 + 2e^{2t} c^3 T^2 - e^{3t} c^4 T^2 \right) dT \\ Y_{i3} &= \frac{1}{6} cT^3 \left(2e^{2t}c^2 - 3e^t c + 1\right) - \frac{1}{3} c^2 e^t T^3 \left(2e^{2t}c^2 - 3e^t c + 1\right) - \frac{1}{3} e^t c^2 T^3 + \frac{2}{3} e^{2t} c^3 T^3 - \frac{1}{3} e^{3t} c^4 T^3\end{aligned} \tag{3.102}$$

after simplifying,

$$Y_{i3} = -\frac{1}{6} cT^3 \left(4e^{3t}c^3 - 12e^{2t}c^2 + 7e^t c - 1\right) \tag{3.103}$$

so, the solution of equations (3.95) generates

$$\begin{aligned} Y_{i0} &= c \\ Y_{i1} &= cT - e^t c^2 T \\ Y_{i2} &= \frac{1}{2} cT^2 \left(2e^{2t}c^2 - 3e^t c + 1\right) \\ Y_{i3} &= -\frac{1}{6} cT^3 \left(4e^{3t}c^3 - 12e^{2t}c^2 + 7e^t c - 1\right) \end{aligned} \tag{3.104}$$

It is observed that the solutions can be generalized recursively:

$$Y_{ik} = \frac{T}{k} \left(Y_{i(k-1)} - e^t \sum_{n_1=0}^{k-1} Y_{in_1} Y_{i(k-1-n_1)} \right) \tag{3.105}$$

with the condition $k > 0$.

In Figure 3.2 the solution obtained by the EMHPM using the third approximation and subintervals of size $\Delta t = 0.01$ is compared with the solution obtained with ode45. It can be seen right there how a third order approximation is enough for the proposed solution of Eq. (3.9) to tend to converge towards the solution obtained by means of numerical integration with high precision, which none of the previously discussed solutions could achieve.

Also, to analyze the scope of the EMHPM method, this methodology will be applied to obtain approximate solutions of non-linear differential equations which are of great importance in engineering.

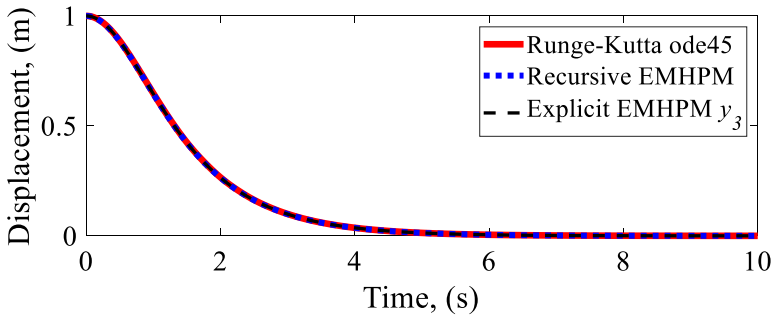

Figure 3.2 Solution of (3.9) with Runge Kutta ode45 vs. EMHPM

3.3 Delay Differential Equations

In the mathematical description of a physical process, it is generally assumed that the behavior of the process under consideration depends only on the current state; however, there are situations in which this assumption is not fulfilled and the use of a "classical" model in systems analysis and design can lead to poor performance. In such cases, the best is to consider that the behavior of the system also includes information about the previous state. These systems are called time delay systems. In fact, time delays occur so frequently, in almost all situations, that to ignore them is to ignore reality [61].

Delay Differential Equations (DDE) are widely used to describe physical phenomena of interest in mechanics, biology, medicine, chemistry, physics, engineering, economics, robotics, among others. Since the introduction of the first lag models, many publications have appeared with theorems and solution methods that also include stability issues [62–65].

In this work we develops the generalized EMHPM procedure proposed by Olvera in [57] to solve DDEs from the introduction of a “new time scale” in the MHPM derived by Hashim and Chowdhury, which was used to obtain solutions approximates of ordinary differential equations [52].

With the EMHPM, which is based on the solution by subintervals, precise solutions are achieved under a numerical-analytical procedure, the method is programmed as a routine in Matlab © and then compared with the numerical solutions of the routine dde23 in the same environment described by Shampine and Thompson in [66].

Let us consider the simplest delay differential equation of the form

$$\dot{x}(t)+x(t-\tau)=0 \tag{3.106}$$

with initial condition $x(0)=c$, the independent variable x is scalar $x(t)\in\Re$, the point on x means differentiation with respect to the time t, and τ is the value of the delay. To evaluate Eq. (3.106) at $a\le t\le b$, the term $x(t-\tau)$ must be represented by a known function $x(t)$ at $[a-\tau\le t\le a]$. That is, if at $a=0$, the solution of Eq. (3.106) can be

obtained on the interval $(0, \tau]$ assuming that the function in the initial period must satisfy the initial condition. Using this first solution, it is possible obtain the solution of Eq. (3.106) in the next i-th interval $[(i-1)\tau, i\tau], i = 2,3 \ldots, j$ where j is an integer $2 \leq j \leq \infty$ that determines up to what value of time the equation is solved with. With this approach, the HPM can be applied assuming that the function that describes the interval of size equal to the delay is $\boldsymbol{x}^{\tau_0}(T) = c$, hence the first interval of the solution is given by $\boldsymbol{x}^{\tau_1}(T)$, valid in $[0, \tau]$. Applying it, in terms of Eq. (3.5), the homotopy function for Eq. (3.106) is constructed.

$$\mathcal{H}\left(\mathbf{X}^{\tau_1}, p\right) = \dot{\mathbf{X}}^{\tau_1} + p\mathbf{x}^{\tau_0} = 0 \tag{3.107}$$

Substituting in equation (3.107) the first order expansion $\boldsymbol{X}^{\tau_1} = \boldsymbol{X}_0^{\tau_1} + p\boldsymbol{X}_1^{\tau_1}$, we have

$$\mathcal{H}\left(\mathbf{X}^{\tau_1}, p\right) = \left(\dot{\mathbf{X}}_0^{\tau_1} + p\dot{\mathbf{X}}_1^{\tau_1}\right) + p\mathbf{x}^{\tau_0} = 0 \tag{3.108}$$

expressing in terms of the identical powers of p:

$$\begin{aligned} p^0 &: \ \dot{\mathbf{X}}_0^{\tau_1} = 0, && \mathbf{X}_0^{\tau_1}(0) = c = \mathbf{X}^{\tau_0}(\tau) \\ p^1 &: \ \dot{\mathbf{X}}_1^{\tau_1} + \mathbf{x}^{\tau_0} = 0, && \mathbf{X}_1^{\tau_1} = -\mathbf{X}^{\tau_0}, \quad \mathbf{X}_1^{\tau_1}(0) = 0 \end{aligned} \tag{3.109}$$

solving, we have for p^0:

$$\int \dot{\mathbf{X}}_0^{\tau_1} dT = \int 0\, dT, \quad \mathbf{X}_0^{\tau_1} = c \tag{3.110}$$

at p^1:

$$\int \dot{\mathbf{X}}_1^{\tau_1} dT = -\int \mathbf{X}^{\tau_0} dT = -\int c\, dT \tag{3.111}$$

by solving we have

$$\mathbf{X}_1^{\tau_1} = -cT \tag{3.112}$$

Hence, the first order solution of (3.107) is given by:

$$\mathbf{x}^{\tau_1}(T) = c - cT \tag{3.113}$$

Eq. (3.113) represents the exact solution of Eq. (3.106) over the first interval. If the same procedure is continued, it can be shown that the exact solution of Eq. (3.107) for the second and third intervals, respectively, is given by

$$\begin{aligned}\mathbf{x}^{\tau_2}(T) &= c - c\tau - cT + \frac{1}{2}cT^2 \\ \mathbf{x}^{\tau_3}(T) &= c - 2c\tau + \frac{1}{2}c\tau^2 - (c - c\tau)T + \frac{1}{2}cT^2 - \frac{1}{6}cT^3\end{aligned} \tag{3.114}$$

The EMHPM can be applied for delayed nonlinear differential equations with variable coefficients, using the following equation

$$\dot{\mathbf{x}}(t) + \mathbf{x}(t-\tau) - \cos(\pi t)\mathbf{x}^2 = 0,\ \tau = 1 \ \text{ and } \ x(0) = c = \mathbf{x}^{\tau_0}(\tau) \tag{3.115}$$

where the solution $\boldsymbol{x}^{\tau_0}(T) = c_1$ is defined in the interval $(-\tau, 0]$. To find the solution $\boldsymbol{x}^{\tau_1}$ corresponding to the interval $[0, \tau]$ the representation of the equation (3.115) is proposed as

$$\mathcal{H}\left(\mathbf{X}^{\tau_1}, p\right) = \dot{\mathbf{X}}^{\tau_1} + p\left[\mathbf{x}^{\tau_0} - \cos(\pi t)\left(\mathbf{X}^{\tau_1}\right)^2\right] = 0 \tag{3.116}$$

The variable $\boldsymbol{X}$ depends on the time T for which $0 \le T \le \tau$. Substituting in equation (3.116) the second order expansion $\boldsymbol{X}^{\tau_1} = \boldsymbol{X}_0^{\tau_1} + p\boldsymbol{X}_1^{\tau_1} + p^2\boldsymbol{X}_2^{\tau_1}$, we have:

$$\mathcal{H}\left(\mathbf{X}^{\tau_1}, p\right) = \left(\dot{\mathbf{X}}_0^{\tau_1} + p\dot{\mathbf{X}}_1^{\tau_1} + p^2\dot{\mathbf{X}}_2^{\tau_1}\right) + p\left[\mathbf{x}^{\tau_0} - \cos(\pi t)\left(\mathbf{X}_0^{\tau_1} + p\mathbf{X}_1^{\tau_1} + p^2\mathbf{X}_2^{\tau_1}\right)^2\right] = 0 \tag{3.117}$$

which is expanded as

$$\begin{aligned}\mathcal{H}\left(\mathbf{X}^{\tau_1}, p\right) = \left(\dot{\mathbf{X}}_0^{\tau_1} + p\dot{\mathbf{X}}_1^{\tau_1} + p^2\dot{\mathbf{X}}_2^{\tau_1}\right) + p\Big[\mathbf{x}^{\tau_0} - \cos(\pi t)\Big(\left(\mathbf{X}_0^{\tau_1}\right)^2 + p\mathbf{X}_0^{\tau_1}\mathbf{X}_1^{\tau_1} + p^2\mathbf{X}_0^{\tau_1}\mathbf{X}_2^{\tau_1} + p\mathbf{X}_0^{\tau_1}\mathbf{X}_1^{\tau_1} + \\ p^2\left(\mathbf{X}_1^{\tau_1}\right)^2 + p^3\mathbf{X}_1^{\tau_1}\mathbf{X}_2^{\tau_1} + p^2\mathbf{X}_0^{\tau_1}\mathbf{X}_2^{\tau_1} + p^3\mathbf{X}_1^{\tau_1}\mathbf{X}_2^{\tau_1} + p^4\left(\mathbf{X}_2^{\tau_1}\right)^2\Big)\Big]\end{aligned} \tag{3.118}$$

expressing in terms of the identical powers of p:

$$\begin{aligned}&p^0:\ \dot{\mathbf{X}}_0^{\tau_1} = 0, && \mathbf{X}_0(T=0) = c_1 = \mathbf{X}^{\tau_0}(T=\tau) \\ &p^1:\ \dot{\mathbf{X}}_1^{\tau_1} = -\mathbf{x}^{\tau_0} + \cos(\pi t)\left(\mathbf{X}_0^{\tau_1}\right)^2 = 0, && \mathbf{X}_1^{\tau_1}(0) = 0 \\ &p^2:\ \dot{\mathbf{X}}_2^{\tau_1} = 2\cos(\pi t)\mathbf{X}_0^{\tau_1}\mathbf{X}_1^{\tau_1} = 0, && \mathbf{X}_2^{\tau_1}(0) = 0 \\ &p^3:\ \dot{\mathbf{X}}_3^{\tau_1} = \cos(\pi t)\left(2\mathbf{X}_0^{\tau_1}\mathbf{X}_2^{\tau_1} + \left(\mathbf{X}_1^{\tau_1}\right)^2\right) = 0, && \mathbf{X}_3^{\tau_1}(0) = 0\end{aligned} \tag{3.119}$$

Solving, we have for p^0:

$$\int \dot{\mathbf{X}}_0^{\tau_1} dT = \mathbf{X}_0^{\tau_1} = c_1 \tag{3.120}$$

at p^1:

$$\int \dot{\mathbf{X}}_1^{\tau_1} dT = \int -\mathbf{x}^{\tau_0} + \cos(\pi t)\left(\mathbf{X}_0^{\tau_1}\right)^2 dT \tag{3.121}$$

As it integrates with respect to T, and considering that $\boldsymbol{X}_0^{\boldsymbol{\tau_1}} = c_1$, the solution is expressed as follows:

$$\mathbf{X}_1^{\tau_1} = T\left(-\mathbf{x}^{\tau_0} + c_1^2 \cos(\pi t)\right) = -T\left(\mathbf{x}^{\tau_0} - c_1^2 \cos(\pi t)\right) \tag{3.122}$$

at p^2:

$$\int \dot{\mathbf{X}}_2^{\tau_1} dT = \int 2\cos(\pi t)\left(\mathbf{X}_0^{\tau_1}\mathbf{X}_1^{\tau_1}\right) dT \tag{3.123}$$

$$\mathbf{X}_2^{\tau_1} = \int 2\cos(\pi t)\left(c_1\left(-T\left(\mathbf{x}^{\tau_0} - c_1^2 \cos(\pi t)\right)\right)\right) dT \tag{3.124}$$

$$\mathbf{X}_2^{\tau_1} = -c_1 T^2\left(\cos(\pi t)\left(\mathbf{x}^{\tau_0} - c_1^2 \cos(\pi t)\right)\right) \tag{3.125}$$

at p^3:

$$\int \dot{\mathbf{X}}_3^{\tau_1} dT = \int \cos(\pi t)\left(2\mathbf{X}_0^{\tau_1}\mathbf{X}_2^{\tau_1} + \left(\mathbf{X}_1^{\tau_1}\right)^2\right) dT \tag{3.126}$$

by substituting $\boldsymbol{X}_0^{\boldsymbol{\tau_1}}, \boldsymbol{X}_1^{\boldsymbol{\tau_1}}$ and $\boldsymbol{X}_2^{\boldsymbol{\tau_1}}$ and solving we have:

$$\mathbf{X}_3^{\tau_1} = \frac{T^3}{3}\cos(\pi t)\left(3c_1^4 \cos^2(\pi t) - 4c_1^2 \mathbf{x}^{\tau_0} \cos(\pi t) + \left(\mathbf{x}^{\tau_0 2}\right)\right) \tag{3.127}$$

so, the solutions for the powers of p are:

$$\begin{aligned}
\mathbf{X}_0^{\tau_1} &= c_1 \\
\mathbf{X}_1^{\tau_1} &= T\left(-\mathbf{x}^{\tau_0} + c_1^2 \cos(\pi t)\right) = -T\left(\mathbf{x}^{\tau_0} - c_1^2 \cos(\pi t)\right) \\
\mathbf{X}_2^{\tau_1} &= -c_1 T^2\left(\cos(\pi t)\left(\mathbf{x}^{\tau_0} - c_1^2 \cos(\pi t)\right)\right) \\
\mathbf{X}_3^{\tau_1} &= \frac{T^3}{3}\cos(\pi t)\left(3c_1^4 \cos^2(\pi t) - 4c_1^2 \mathbf{x}^{\tau_0} \cos(\pi t) + \left(\mathbf{x}^{\tau_0}\right)^2\right)
\end{aligned} \tag{3.128}$$

Then, the approximate solution of Eq. (3.115), using the EMHPM, is given by

$$\mathbf{x}^{\tau_1}(T) \approx \mathbf{X}_0^{\tau_1} + \mathbf{X}_1^{\tau_1} + \mathbf{X}_2^{\tau_1} + \mathbf{X}_3^{\tau_1} \tag{3.129}$$

In this case, the solution of $\boldsymbol{x}^{\tau_1}(T)$ is approximate because its exact solution is not known. To obtain $\boldsymbol{x}^{\tau_2}$, we calculate again the approximation of by means of the EMHPM with the assumption that the function that describes the delay remains constant. Therefore, to determine $\boldsymbol{x}^{\tau_2}$, the homotopy of Eq. (3.115) is used for the interval $(\tau, 2\tau]$

$$\mathcal{H}\left(\mathbf{X}^{\tau_2}, p\right) = \dot{\mathbf{X}}^{\tau_2} + p\left[\mathbf{x}^{\tau_1} - \cos(\pi t)\left(\mathbf{X}^{\tau_2}\right)^2\right] = 0 \tag{3.130}$$

substituting in equation (3.130) the second order expansion $\boldsymbol{X}^{\tau_2} = \boldsymbol{X}_0^{\tau_2} + p\boldsymbol{X}_1^{\tau_2} + p^2\boldsymbol{X}_2^{\tau_2}$, we have:

$$\mathcal{H}\left(\mathbf{X}^{\tau_2}, p\right) = \left(\dot{\mathbf{X}}_0^{\tau_2} + p\dot{\mathbf{X}}_1^{\tau_2} + p^2\dot{\mathbf{X}}_2^{\tau_2}\right) + p\left[\mathbf{x}^{\tau_1} - \cos(\pi t)\left(\mathbf{X}_0^{\tau_2} + p\mathbf{X}_1^{\tau_2} + p^2\mathbf{X}_2^{\tau_2}\right)^2\right] = 0 \tag{3.131}$$

After solving the previous equation, we obtain:

$$\begin{aligned}
\mathbf{X}_0^{\tau_2} &= c_2 \\
\mathbf{X}_1^{\tau_2} &= T\left(-\mathbf{x}^{\tau_1} + c_2{}^2\cos(\pi t)\right) \\
\mathbf{X}_2^{\tau_2} &= -c_2 T^2\left(\cos(\pi t)\left(\mathbf{x}^{\tau_1} - c_2{}^2\cos(\pi t)\right)\right) \\
\mathbf{X}_3^{\tau_2} &= \frac{T^3}{3}\cos(\pi t)\left(3c_2{}^4\cos^2(\pi t) - 4c_2{}^2\mathbf{x}^{\tau_1}\cos(\pi t) + \left(\mathbf{x}^{\tau_1}\right)^2\right)
\end{aligned} \tag{3.132}$$

It is observed that Eq. (3.128) and (3.132) represent approximate solutions to Eq. (3.115) but evaluated at different intervals of size equal to the delay. Therefore, the approximate third-order solution of Eq. (3.115) can be generalized if it is solved by intervals using the homotopy of the form

$$\mathcal{H}\left(\mathbf{X}^{\tau_i}, p\right) = \dot{\mathbf{X}}^{\tau_i} + p\left[\mathbf{x}^{\tau_{i-1}} - \cos(\pi t)\left(\mathbf{X}^{\tau_i}\right)^2\right] = 0 \tag{3.133}$$

Following the previous methodology,

$$\begin{aligned}
\mathbf{X}_0^{\tau_i} &= c \\
\mathbf{X}_1^{\tau_i} &= T\left(-\mathbf{x}^{\tau_{i-1}} + c^2\cos(\pi t)\right) \\
\mathbf{X}_2^{\tau_i} &= -cT^2\left(\cos(\pi t)\left(\mathbf{x}^{\tau_{i-1}} - c^2\cos(\pi t)\right)\right) \\
\mathbf{X}_3^{\tau_i} &= \frac{T^3}{3}\cos(\pi t)\left(3c^4\cos^2(\pi t) - 4c^2\mathbf{x}^{\tau_{i-1}}\cos(\pi t) + \left(\mathbf{x}^{\tau_{i-1}}\right)^2\right)
\end{aligned} \tag{3.134}$$

from Eq. (3.134), the k-th order approximation of Eq. (3.115) can be written as

$$\begin{aligned}\mathbf{X}_0^{\tau_i} &= c \\ \mathbf{X}_k^{\tau_i} &= \frac{T}{k}\left(-\left(\mathbf{x}^{\tau_{i-1}}\right)g(k)+\cos(\pi t)\sum_{n_1=0}^{k-1}\mathbf{X}_{n_1}^{\tau_i}\mathbf{X}_{k-1-n_1}^{\tau_i}\right)\end{aligned} \tag{3.135}$$

where $k > 0, g(k) = 1$ when $k = 1$ and $g(k) = 0$ otherwise.

Figure 3.3 shows the approximate solution of Eq. (3.115) obtained by the EMHPM compared with the numerical solution provided by the dde23 routine in Matlab, assuming the initial solution scenarios $x^{\tau_0}(T) = \cos(\pi(T+1))$, $x^{\tau_0}(T) = e^{T+1}$, $x^{\tau_0}(T) = 1$ and subintervals of size $\Delta t = 0.01$. The dde23 routine is an algorithm based on the Runge-Kutta formula for the solution of delayed differential equations with constant delays. It is observed that both solutions coincide for the time interval shown.

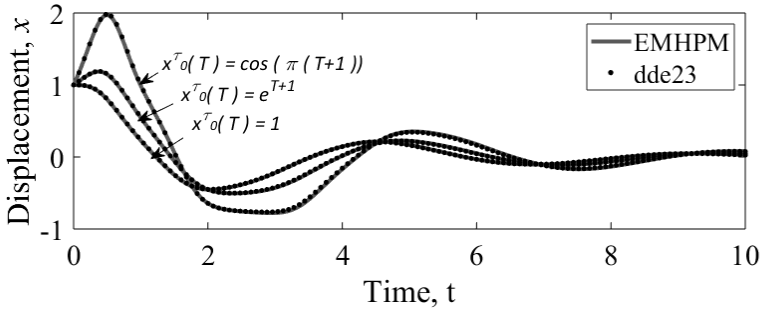

Figure 3.3 Solutions of Eq. (3.115) by the EMHPM and the dde23 routine.

Generalized EMHPM for DDE solutions

Consider the periodic differential equation with -dimensional delay of the form

$$\dot{\mathbf{x}}(t) = \mathbf{A}(t)x + \mathbf{B}(t)\mathbf{x}(t-\tau) \tag{3.136}$$

where $\boldsymbol{A}(t-\tau) = \boldsymbol{A}(t)$, $\boldsymbol{B}(t-\tau) = \boldsymbol{B}(t)$, $\boldsymbol{x} = [\boldsymbol{x}, \dot{\boldsymbol{x}}]^T$ is the vector of states and τ is the delay time, following the procedure proposed by the EMHPM, the above equation can be written equivalently as

$$\dot{\mathbf{x}}_i(T) - \mathbf{A}_t\mathbf{x}_i(t) \approx \mathbf{B}_t\mathbf{x}_i^{\tau}(T) \tag{3.137}$$

where $\boldsymbol{x}_i(T)$ expresses the solution of order m for Eq. (3.137) in the $i-$th subinterval that must also satisfy the vector of initial conditions $\boldsymbol{x}_i(0) = \boldsymbol{x}_{i-1}$. $\boldsymbol{A}_t$ and $\boldsymbol{B}_t$ represent the matrices in which each of its elements are evaluated at time t. In order to approximate the delay term in Eq. (3.137), the period $[t_0 - \tau, t_0]$ is discretized by N equally spaced

points as shown in Figure 3.4. As part of the proposed methodology, it is assumed that the function that describes the term of the delay $\boldsymbol{x}_i^{\tau}(T)$ that corresponds to the subinterval $[t_{i-N}, t_{i-N+1}]$ is approximated by a constant value, that is:

$$\mathbf{x}_i^{\tau}(T) = \mathbf{x}_{i-N+1}(T) \approx \mathbf{x}_{i-N} \tag{3.138}$$

Olvera in [67], proposed to call it zero-order EMHPM when the delay term is approached by a constant, and it should not be confused with the approximation order m of the solution. Figure 3.4 shows graphically this procedure.

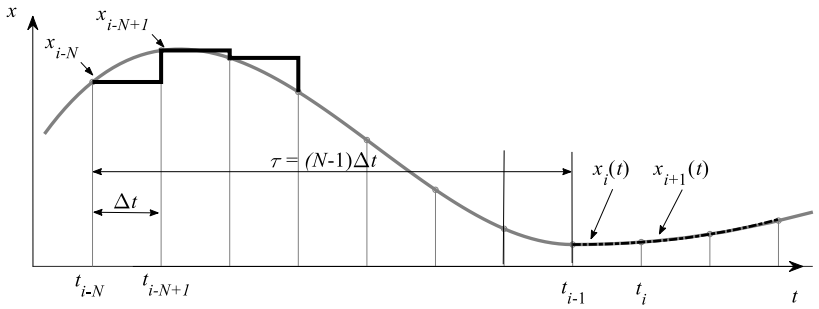

Figure 3.4 Scheme for the approximation of the delayed term by a zeroth-order (solid black line)

Continuing with the HPM technique, the homotopy of Eq. (3.137) can be written as:

$$\mathcal{H}(\mathbf{X}_i, p) = L(\dot{\mathbf{X}}_i) - L(\dot{\mathbf{x}}_{i0}) + pL(\dot{\mathbf{x}}_{i0}) - p(\mathbf{A}_t\mathbf{X}_i + \mathbf{B}_t x_{i-N}) = 0 \tag{3.139}$$

Substituting the expansion of order m, $\boldsymbol{X}_i = \boldsymbol{X}_{i0} + p\boldsymbol{X}_{i1} + p^2\boldsymbol{X}_{i2} + \cdots + p^m$ and considering that the initial condition is equal to the final value of the previous subinterval, that is, $\boldsymbol{x}_{i0} = \boldsymbol{x}_{i-1}$, we obtain:

$$\begin{aligned}\mathcal{H}(\mathbf{X}_i, p) = {} & \left(\dot{\mathbf{X}}_{i0} + p\dot{\mathbf{X}}_{i1} + p^2\dot{\mathbf{X}}_{i2} + \ldots + p^m\dot{\mathbf{X}}_{im}\right) - \left(\dot{\mathbf{x}}_{i0}\right) + p\left(\dot{\mathbf{x}}_{i0}\right) - p\left[A_t\left(\dot{\mathbf{X}}_{i0} + p\dot{\mathbf{X}}_{i1} + p^2\dot{\mathbf{X}}_{i2} + \right.\right. \\ & \left.\left. \ldots + p^m\dot{\mathbf{X}}_{im}\right) + B_t\mathbf{x}_{i-N}\right]\end{aligned} \tag{3.140}$$

grouping by powers of p:

$$\begin{aligned}
p^0 &: \ \dot{\mathbf{X}}_{i0} - \dot{\mathbf{x}}_{i0} = 0,\ \dot{\mathbf{X}}_{i0} - \dot{\mathbf{x}}_{i-1} = 0, && \mathbf{X}_{i0} = \mathbf{x}_{i-1} \\
p^1 &: \ \dot{\mathbf{X}}_{i1} + \dot{\mathbf{x}}_{i0} = \mathbf{A}_t\mathbf{X}_{i0} + \mathbf{B}_t\left(\mathbf{x}_{i-N}\right), && \mathbf{X}_{i1}(0) = 0 \\
p^2 &: \ \dot{\mathbf{X}}_{i2} = \mathbf{A}_t\mathbf{X}_{i1}, && \mathbf{X}_{i2}(0) = 0 \\
&\ \ \vdots \\
p^m &: \ \dot{\mathbf{X}}_{im} = \mathbf{A}_t\mathbf{X}_{i(m-1)}, && \mathbf{X}_{im}(0) = 0
\end{aligned} \tag{3.141}$$

Knowing that $\dot{\boldsymbol{x}}_{i0} = \dot{\boldsymbol{x}}_{i-1} = 0$, when integrating the previous equations, we have, at p^0:

$$\int \dot{\mathbf{X}}_{i0} dT = \int \dot{\mathbf{x}}_{i-1} dT = const \tag{3.142}$$

The initial constant is $\boldsymbol{x}_{i-1}$, so:

$$\mathbf{X}_{i0} = const = \mathbf{x}_{i-1} \tag{3.143}$$

at p^1:

$$\int \dot{\mathbf{X}}_{i1} dT = \int \left(\mathbf{A}_t \mathbf{X}_{i0} + \mathbf{B}_t x_{i-N} \right) dT \tag{3.144}$$

solving and knowing that $\boldsymbol{X}_{i0} = \boldsymbol{x}_{i-1}$

$$\mathbf{X}_{i1} = T\mathbf{A}_t \mathbf{x}_{i-1} + T\,\mathbf{B}_t \mathbf{x}_{i-N} \tag{3.145}$$

at p^2:

$$\int \dot{\mathbf{X}}_{i2} dT = \int \left(\mathbf{A}_t \mathbf{X}_{i1} \right) dT = \int \mathbf{A}_t \left(T\mathbf{A}_t \mathbf{x}_{i-1} + T\,\mathbf{B}_t x_{i-N} \right) dT \tag{3.146}$$

$$\mathbf{X}_{i2} = \frac{T^2}{2} \mathbf{A}_t^{\,2} \mathbf{x}_{i-1} + \frac{T^2}{2} \mathbf{A}_t \mathbf{B}_t \mathbf{x}_{i-N} \tag{3.147}$$

for p^m:

$$\mathbf{X}_{im} = \frac{T^m}{m!} \left(\mathbf{A}_t^{\,m} \mathbf{x}_{i-1} + \mathbf{A}_t^{\,m-1} \mathbf{B}_t \mathbf{x}_{i-N} \right) \tag{3.148}$$

So, the solution of equations (3.141) can be expressed recursively:

$$\mathbf{X}_{ik} = \frac{T}{k} \left(\mathbf{A}_t \mathbf{X}_{i(k-1)} + g(k) \mathbf{B}_t \left(\mathbf{x}_{i-N} \right) \right), k = 1, 2, 3... \tag{3.149}$$

Finally, the solution of Equation (3.136) is obtained by adding each approximation $\boldsymbol{X}_{ik}$:

$$\mathbf{X}_i (T) \approx \sum_{k=0}^{m} \mathbf{X}_{ik} (T) \tag{3.150}$$

First-order EMHPM

The solution of equation (3.136) given by equation (3.150) can be improved if a higher-order polynomial representation is used for $\boldsymbol{x}_i^{\tau}(T)$. If a first-order polynomial representation is used for $\boldsymbol{x}_i^{\tau}(T)$, it is called first-order EMHPM, and the function that describes the subinterval of the delay $[t_{i-N}, t_{i-N+1}]$ will have the form:

$$\mathbf{x}_i^{\tau}(T) \approx \mathbf{x}_{i-N} + \frac{N-1}{\tau}\left(\mathbf{x}_{i-N+1} - \mathbf{x}_{i-N}\right)T \tag{3.151}$$

Figure 3.5 shows the representation of the solution if a first-order approximation is used.

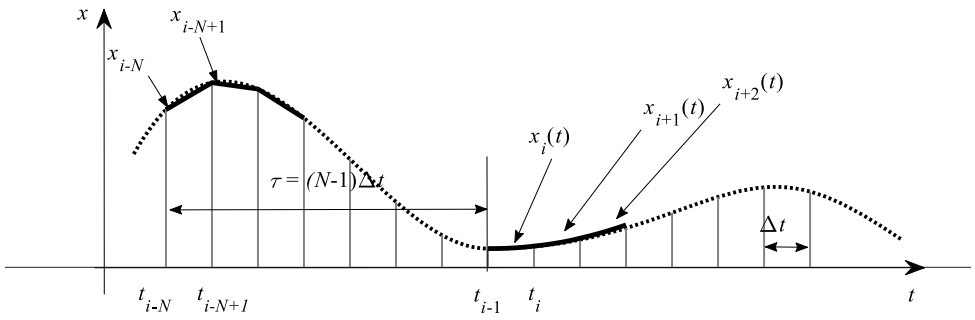

Figure 3.5 a) Scheme for the approximation of the delayed term by a first-order.

by substituting equation (3.151) in Eq. (3.137) we obtain:

$$\dot{\mathbf{x}}_i(T) - \mathbf{A}_t\mathbf{x}_i(T) \approx \mathbf{B}_t\mathbf{x}_{i-N} - \left(\frac{N-1}{\tau}\right)\mathbf{B}_t\left(\mathbf{x}_{i-N}\right)T + \left(\frac{N-1}{\tau}\right)\mathbf{B}_t\left(\mathbf{x}_{i-N+1}\right)T \tag{3.152}$$

Constructing the homotopy for the previous equation:

$$\mathcal{H}\left(\mathbf{X}_i, p\right) = L\left(\dot{\mathbf{X}}_i\right) - L\left(\dot{\mathbf{x}}_{i0}\right) + pL\left(\dot{\mathbf{x}}_{i0}\right) - p\left(\mathbf{A}_t\mathbf{X}_i + \mathbf{B}_t\mathbf{x}_{i-N} - \left(\frac{N-1}{\tau}\right)\mathbf{B}_t\left(\mathbf{x}_{i-N}\right)T + \left(\frac{N-1}{\tau}\right)\mathbf{B}_t\left(\mathbf{x}_{i-N+1}\right)T\right) \tag{3.153}$$

Substituting the expansion of order m, $\boldsymbol{X}_i = \boldsymbol{X}_{i0} + p\boldsymbol{X}_{i1} + p^2\boldsymbol{X}_{i2} + \cdots + p^m$ and considering that the initial condition is equal to the final value of the previous subinterval, that is, $\boldsymbol{x}_{i0} = \boldsymbol{x}_{i-1}$, and $\boldsymbol{x}_{i1}(0) = \boldsymbol{x}_{i2}(0) = \cdots = \boldsymbol{x}_{im}(0) = 0$ it is obtained:

$$\begin{aligned}\mathcal{H}\left(\mathbf{X}_i, p\right) = {} & \left(\dot{\mathbf{X}}_{i0} + p\dot{\mathbf{X}}_{i1} + p^2\dot{\mathbf{X}}_{i2} + \ldots + p^m\dot{\mathbf{X}}_{im}\right) - \left(\dot{\mathbf{x}}_{i0}\right) + p\left(\dot{\mathbf{x}}_{i0}\right) - p\Big[\mathbf{A}_t\left(\mathbf{X}_{i0} + p\mathbf{X}_{i1} + p^2\mathbf{X}_{i2} + \right. \\ & \left. \ldots + p^m\mathbf{X}_{im}\right) + \mathbf{B}_t\mathbf{x}_{i-N} - \left(\frac{N-1}{\tau}\right)\mathbf{B}_t\left(\mathbf{x}_{i-N}\right)T + \left(\frac{N-1}{\tau}\right)\mathbf{B}_t\left(\mathbf{x}_{i-N+1}\right)T\Big]\end{aligned} \tag{3.154}$$

grouping by powers of p:

$$\begin{aligned}
&p^0: \ \dot{\mathbf{X}}_{i0} - \dot{\mathbf{x}}_{i0} = 0,\ \dot{\mathbf{X}}_{i0} - \dot{\mathbf{x}}_{i-1} = 0, && \mathbf{X}_{i0} = \mathbf{x}_{i-1} \\
&p^1: \ \dot{\mathbf{X}}_{i1} + \dot{\mathbf{x}}_{i0} = \mathbf{A}_t \mathbf{X}_{i0} + \mathbf{B}_t \left(\mathbf{x}_{i-N}\right) - \mathbf{B}_t T\left(\frac{N-1}{\tau}\right)\left(\mathbf{x}_{i-N}\right) + \mathbf{B}_t T\left(\frac{N-1}{\tau}\right)\left(\mathbf{x}_{i-N+1}\right), && \mathbf{X}_{i1}(0) = 0 \\
&p^2: \ \dot{\mathbf{X}}_{i2} = \mathbf{A}_t \mathbf{X}_{i1}, && \mathbf{X}_{i2}(0) = 0 \\
&\ \ \vdots \\
&p^m: \ \dot{\mathbf{X}}_{im} = \mathbf{A}_t \mathbf{X}_{i(m-1)}, && \mathbf{X}_{im}(0) = 0
\end{aligned} \tag{3.155}$$

knowing that $\dot{\boldsymbol{x}}_{i0} = \dot{\boldsymbol{x}}_{i-1} = 0$, when integrating the previous equations, we have, at p^0:

$$\int \dot{\mathbf{X}}_{i0} dT = \int \dot{\mathbf{x}}_{i-1} dT = const \tag{3.156}$$

the initial constant is $\boldsymbol{x}_{i-1}$, so:

$$\mathbf{X}_{i0} = const = \mathbf{x}_{i-1} \tag{3.157}$$

at p^1:

$$\int \dot{\mathbf{X}}_{i1} dT = \int \left(\mathbf{A}_t \mathbf{X}_{i0} + \mathbf{B}_t x_{i-N} - \mathbf{B}_t T\left(\frac{N-1}{\tau}\right)\left(\mathbf{x}_{i-N}\right) + \mathbf{B}_t T\left(\frac{N-1}{\tau}\right)\left(\mathbf{x}_{i-N+1}\right) \right) dT \tag{3.158}$$

solving and knowing that $\boldsymbol{X}_{i0} = \boldsymbol{x}_{i-1}$

$$\mathbf{X}_{i1} = T\mathbf{A}_t \mathbf{x}_{i-1} + T\,\mathbf{B}_t \mathbf{x}_{i-N} - \mathbf{B}_t \frac{T^2}{2}\left(\frac{N-1}{\tau}\right)\left(\mathbf{x}_{i-N}\right) + \mathbf{B}_t \frac{T^2}{2}\left(\frac{N-1}{\tau}\right)\left(\mathbf{x}_{i-N+1}\right) \tag{3.159}$$

at p^2:

$$\begin{aligned}
&\int \dot{\mathbf{X}}_{i2} dT = \int \left(\mathbf{A}_t \mathbf{X}_{i1}\right) dT \\
&\int \dot{\mathbf{X}}_{i2} dT = \int \mathbf{A}_t \left(T\mathbf{A}_t \mathbf{x}_{i-1} + T\,\mathbf{B}_t x_{i-N} - \mathbf{B}_t \frac{T^2}{2}\left(\frac{N-1}{\tau}\right)\left(\mathbf{x}_{i-N}\right) + \mathbf{B}_t \frac{T^2}{2}\left(\frac{N-1}{\tau}\right)\left(\mathbf{x}_{i-N+1}\right) \right) dT
\end{aligned} \tag{3.160}$$

$$\mathbf{X}_{i2} = \frac{T^2}{2}\mathbf{A}_t{}^2 \mathbf{x}_{i-1} + \frac{T^2}{2}\mathbf{A}_t \mathbf{B}_t \mathbf{x}_{i-N} - \mathbf{A}_t \mathbf{B}_t \frac{T^3}{6}\left(\frac{N-1}{\tau}\right)\left(\mathbf{x}_{i-N}\right) + \mathbf{A}_t \mathbf{B}_t \frac{T^3}{6}\left(\frac{N-1}{\tau}\right)\left(\mathbf{x}_{i-N+1}\right) \tag{3.161}$$

for p^m:

$$\mathbf{X}_{im} = \frac{T^m}{m!}\left(\mathbf{A}_t{}^m \mathbf{x}_{i-1} + \mathbf{A}_t^{m-1}\mathbf{B}_t \mathbf{x}_{i-N}\right) + \frac{T^{m+1}}{(m+1)!}\mathbf{A}_t^{m-1}\mathbf{B}_t\left(\frac{N-1}{\tau}\right)\left(-\mathbf{x}_{i-N} + \mathbf{x}_{i-N+1}\right) \tag{3.162}$$

considering that $\boldsymbol{X}_{i0}^{a} = \boldsymbol{x}_{i-1}$ and $\boldsymbol{X}_{i0}^{b} = 0$, the equation $\boldsymbol{X}_{ik}$ is expressed recursively:

$$\mathbf{X}_{ik} = \mathbf{X}_{ik}^{a} + \mathbf{X}_{ik}^{b}, k = 1,2,3\ldots \tag{3.163}$$

$$\begin{aligned}
\mathbf{X}_{ik}^{a} &= \frac{T}{k}\left(\mathbf{A}_t \mathbf{X}_{i(k-1)}^{a} + g(k)\mathbf{B}_t\left(\mathbf{x}_{i-N}\right)\right) \\
\mathbf{X}_{ik}^{b} &= \frac{T}{k+1}\left(\mathbf{A}_t \mathbf{X}_{i(k-1)}^{b} + g(k)\mathbf{B}_t T\left(\frac{N-1}{\tau}\right)\left(-\mathbf{x}_{i-N} + \mathbf{x}_{i-N+1}\right)\right)
\end{aligned} \tag{3.164}$$

Finally, the approximate solution of Eq. (3.136), using the EMHPM, can be obtained by substituting Eq. (3.163) in Eq. (3.150).

Second-order EMHPM

If a second-order polynomial representation is used for $\boldsymbol{x}_i^{\tau}(T)$ in the equation (3.136) the solution obtained is called second-order EMHPM. Here it is performed using the Lagrange polynomial interpolating equation, the period $[t_0 - \tau, t_0]$ is discretized by N equally spaced points as shown in Figure 3.6.

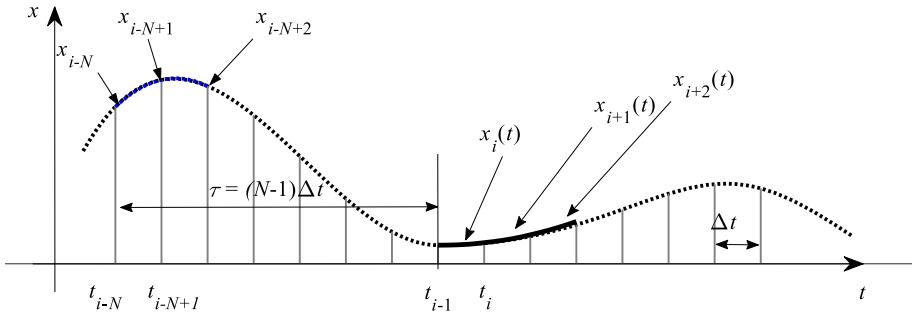

Figure 3.6 a) Scheme for the approximation of the delayed term by a second-order.

To obtain the function that describes the subinterval of the delay $[t_{i-N}, t_{i-N+2}]$ for $\boldsymbol{x}_i^{\tau}(T)$ we proceed to solve the Lagrange equation, which is presented below

$$\begin{aligned}
f_n(x) &= \sum_{i=0}^{n} L_i(x) f(x_i) \\
L_i(x) &= \prod_{i=0, i\neq k}^{n} \frac{x - x_i}{x_k - x_i}
\end{aligned} \tag{3.165}$$

In this case, it is necessary to make use of the discretization $\boldsymbol{x}_{i-N}, \boldsymbol{x}_{i-N+1}, \boldsymbol{x}_{i-N+2}$. Using the Lagrange Equation, we have:

$$P_2(x) = \frac{(x-x_1)(x-x_2)}{(x_0-x_1)(x_0-x_2)} f(x_0) + \frac{(x-x_0)(x-x_2)}{(x_1-x_0)(x_1-x_2)} f(x_1) + \frac{(x-x_0)(x-x_1)}{(x_2-x_0)(x_2-x_1)} f(x_2) \tag{3.166}$$

where $f(x_0) = \boldsymbol{x}_{i-N}, f(x_1) = \boldsymbol{x}_{i-N+1}, f(x_2) = \boldsymbol{x}_{i-N+2}$, and $x_0 = 0, x_1 = \Delta t, x_2 = 2\Delta t$. Here, the 2 from $P_2(x)$ is to represent that it applies in the second-order. The equation can be rewritten as follows:

$$P_2(x) = \frac{(x-\Delta t)(x-2\Delta t)}{(0-\Delta t)(0-2\Delta t)} (\mathbf{x}_{i-N}) + \frac{(x-0)(x-2\Delta t)}{(\Delta t-0)(\Delta t-2\Delta t)} (\mathbf{x}_{i-N+1}) + \frac{(x-0)(x-\Delta t)}{(2\Delta t-0)(2\Delta t-\Delta t)} (\mathbf{x}_{i-N+2}) \tag{3.167}$$

Considering $x = T$, and solving, the equation becomes:

$$P_2(x) = \frac{T^2 - T(2\Delta t) - T(\Delta t) + 2(\Delta t)^2}{2(\Delta t)^2} (\mathbf{x}_{i-N}) + \frac{T^2 - T(2\Delta t)}{-(\Delta t)^2} (\mathbf{x}_{i-N+1}) + \frac{T^2 - T(\Delta t)}{2(\Delta t)^2} (\mathbf{x}_{i-N+2}) \tag{3.168}$$

putting together the terms with common denominator:

$$P_2(x) = \frac{\left(T^2 - T(2\Delta t) - T(\Delta t) + 2(\Delta t)^2\right)(\mathbf{x}_{i-N}) + \left(T^2 - T(\Delta t)\right)(\mathbf{x}_{i-N+2})}{2(\Delta t)^2} - \frac{T^2 - T(2\Delta t)}{(\Delta t)^2} (\mathbf{x}_{i-N+1}) \tag{3.169}$$

then, the equation is:

$$P_2(x) = \left(\frac{T^2}{2(\Delta t)^2} - \frac{T}{\Delta t} - \frac{T}{2\Delta t} + 1 \right) (\mathbf{x}_{i-N}) + \left(\frac{T^2}{2(\Delta t)^2} - \frac{T}{2\Delta t} \right) (\mathbf{x}_{i-N+2}) - \left(\frac{T^2}{(\Delta t)^2} - \frac{2T}{\Delta t} \right) (\mathbf{x}_{i-N+1}) \tag{3.170}$$

From Figure 3.6, it is observed that $\Delta t = \frac{\tau}{N-1}$, then solving and grouping, the equation is rewritten:

$$P_2(x) = \mathbf{x}_{i-N} + \left(\frac{N-1}{\tau} \right) T \left(-\frac{3}{2} \mathbf{x}_{i-N} + 2\mathbf{x}_{i-N+1} - \frac{1}{2} \mathbf{x}_{i-N+2} \right) + \left(\frac{N-1}{\tau} \right)^2 \frac{T^2}{2} (\mathbf{x}_{i-N} - 2\mathbf{x}_{i-N+1} + \mathbf{x}_{i-N+2}) \tag{3.171}$$

so, the function that describes the delay subinterval is expressed as:

$$\mathbf{x}_i^{\tau}(T) \approx \mathbf{x}_{i-N} + \left(\frac{N-1}{\tau} \right) T \left(-\frac{3}{2} \mathbf{x}_{i-N} + 2\mathbf{x}_{i-N+1} - \frac{1}{2} \mathbf{x}_{i-N+2} \right) + \left(\frac{N-1}{\tau} \right)^2 \frac{T^2}{2} (\mathbf{x}_{i-N} - 2\mathbf{x}_{i-N+1} + \mathbf{x}_{i-N+2}) \tag{3.172}$$

Using the HPM technique, and considering (3.172), we proceed to construct the homotopy as follows,

$$H(\mathbf{X}_i,p)=L(\dot{\mathbf{X}}_i)-L(\dot{\mathbf{x}}_{i0})+pL(\dot{\mathbf{x}}_{i0})-p(\mathbf{A}_t\mathbf{X}_i+\mathbf{B}_t\mathbf{x}_{i-N}+\left(\frac{N-1}{\tau}\right)\mathbf{B}_tT\left(-\frac{3}{2}\mathbf{x}_{i-N}+2\mathbf{x}_{i-N+1}-\frac{1}{2}\mathbf{x}_{i-N+2}\right)+ \left(\frac{N-1}{\tau}\right)^2\mathbf{B}_t\frac{T^2}{2}\left(\mathbf{x}_{i-N}-2\mathbf{x}_{i-N+1}+\mathbf{x}_{i-N+2}\right) \tag{3.173}$$

Substituting in the previous equation the expansion of order m, $\boldsymbol{X}_i=\boldsymbol{X}_{i0}+p\boldsymbol{X}_{i1}+p^2\boldsymbol{X}_{i2}+\cdots+p^m\boldsymbol{X}_{im}$, grouping in powers of p and considering the initial condition $\boldsymbol{x}_{i0}=\boldsymbol{x}_{i-1}$, and $\boldsymbol{x}_{i1}(0)=\boldsymbol{x}_{i2}(0)=\cdots=\boldsymbol{x}_{im}(0)=0$, the following first order linear differential equations are obtained

$$\begin{aligned}
&p^0:\ \dot{\mathbf{X}}_{i0}-\dot{\mathbf{x}}_{i-1}=0,\\
&p^1:\ \dot{\mathbf{X}}_{i1}=\mathbf{A}_t\mathbf{x}_{i-1}+\mathbf{B}_t\mathbf{x}_{i-N}+\left(\frac{N-1}{\tau}\right)\mathbf{B}_tT\left(-\frac{3}{2}\mathbf{x}_{i-N}+2\mathbf{x}_{i-N+1}-\frac{1}{2}\mathbf{x}_{i-N+2}\right)+\left(\frac{N-1}{\tau}\right)^2\mathbf{B}_t\frac{T^2}{2}\left(\mathbf{x}_{i-N}-2\mathbf{x}_{i-N+1}+\mathbf{x}_{i-N+2}\right)\\
&p^2:\ \dot{\mathbf{X}}_{i2}=\mathbf{A}\mathbf{X}_{i1}\\
&\vdots\\
&p^m:\ \dot{\mathbf{X}}_{im}=\mathbf{A}\mathbf{X}_{i(m-1)}
\end{aligned} \tag{3.174}$$

integrating the set of Eq. (3.174), it is obtained that,

$$\begin{aligned}
&\mathbf{X}_{i0}=\mathbf{x}_{i-1}\\
&\mathbf{X}_{i1}=\mathbf{A}_t\mathbf{x}_{i-1}T+\mathbf{B}_t\mathbf{x}_{i-N}T+\left(\frac{N-1}{\tau}\right)\mathbf{B}_t\frac{T^2}{2}\left(-\frac{3}{2}\mathbf{x}_{i-N}+2\mathbf{x}_{i-N+1}-\frac{1}{2}\mathbf{x}_{i-N+2}\right)+\left(\frac{N-1}{\tau}\right)^2\mathbf{B}_t\frac{T^3}{6}\left(\mathbf{x}_{i-N}-2\mathbf{x}_{i-N+1}+\mathbf{x}_{i-N+2}\right)\\
&\mathbf{X}_{i2}=\frac{1}{2}\mathbf{A}_t^2\mathbf{x}_{i-1}T^2+\frac{1}{2}\mathbf{B}_t\mathbf{x}_{i-N}T^2+\frac{1}{6}\left(\frac{N-1}{\tau}\right)\mathbf{A}_t\mathbf{B}_tT^3\left(-\frac{3}{2}\mathbf{x}_{i-N}+2\mathbf{x}_{i-N+1}-\frac{1}{2}\mathbf{x}_{i-N+2}\right)+\\
&\quad\frac{1}{24}\left(\frac{N-1}{\tau}\right)^2\mathbf{A}_t\mathbf{B}_tT^4\left(\mathbf{x}_{i-N}-2\mathbf{x}_{i-N+1}+\mathbf{x}_{i-N+2}\right)\\
&\mathbf{X}_{im}=\frac{1}{m!}\mathbf{A}_t\mathbf{x}_{i-1}T^m+\frac{1}{m!}\mathbf{A}_t^{m-1}\mathbf{B}_t\mathbf{x}_{i-N}T^m+\frac{1}{(m+1)!}\frac{N-1}{\tau}\mathbf{A}_t^{m-1}\mathbf{B}_tT^{m+1}\left(-\frac{3}{2}\mathbf{x}_{i-N}+2\mathbf{x}_{i-N+1}-\frac{1}{2}\mathbf{x}_{i-N+2}\right)+\\
&\quad\frac{1}{(m+2)!}\frac{(N-1)^2}{\tau^2}\mathbf{A}_t^{m-1}\mathbf{B}_tT^{m+2}\left(\mathbf{x}_{i-N}-2\mathbf{x}_{i-N+1}+\mathbf{x}_{i-N+2}\right)
\end{aligned} \tag{3.175}$$

The solution for second order EMHPM is expressed in recursively form of $\boldsymbol{X}_{ik}(T)$ as

$$\mathbf{X}_{ik}=\mathbf{X}_{ik}^a+\mathbf{X}_{ik}^b+\mathbf{X}_{ik}^c,k=1,2,3.... \tag{3.176}$$

where

$$\mathbf{X}_{i0}^{a} = \mathbf{x}_{i-1,}\ \mathbf{X}_{i0}^{b} = \mathbf{X}_{i0}^{c} = 0 \tag{3.177}$$

and

$$\begin{aligned}
\mathbf{X}_{ik}^{a} &= \frac{T}{k}\left(\mathbf{A}_t \mathbf{X}_{i(k-1)}^{a} + g(k)\mathbf{B}_t \mathbf{x}_{i-N}\right) \\
\mathbf{X}_{ik}^{b} &= \frac{T}{k+1}\left(\mathbf{A}_t \mathbf{X}_{i(k-1)}^{b} + g(k)\left(\frac{N-1}{\tau}\right)\mathbf{B}_t T\left(-\frac{3}{2}\mathbf{x}_{i-N} + 2\mathbf{x}_{i-N+1} - \frac{1}{2}\mathbf{x}_{i-N+2}\right)\right) \\
\mathbf{X}_{ik}^{c} &= \frac{T}{k+2}\left(\mathbf{A}_t \mathbf{X}_{i(k-1)}^{c} + g(k)\left(\frac{N-1}{\tau}\right)^{2}\mathbf{B}_t \frac{T^2}{2}\left(\mathbf{x}_{i-N} - 2\mathbf{x}_{i-N+1} + \mathbf{x}_{i-N+2}\right)\right)
\end{aligned} \tag{3.178}$$

The solution of (3.136) is obtained by adding each of the approximations X_{ik} from (3.176) using (3.150).

Third-order EMHPM

For the polynomial representation of the third-degree, the function that describes the delayed term $\mathbf{x}_i^{\tau}(T)$ is approximated by a polynomial of order three. The Lagrange interpolator is used accordingly. In this case, it is necessary to employ the $\mathbf{x}_{i-N}$, $\mathbf{x}_{i-N+1}$, $\mathbf{x}_{i-N+2}$, $\mathbf{x}_{i-N+3}$ discrete values. Figure 3.7 presents the scheme used for the solution of a polynomial of order three.

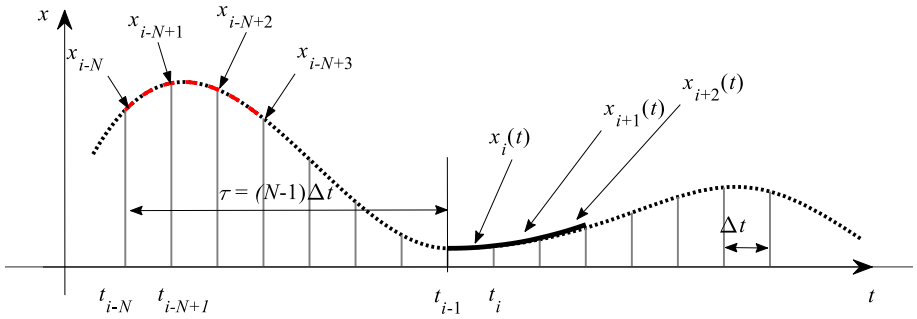

Figure 3.7 a) Scheme for the approximation of the delayed term by a third-order.

Following the same procedure described above for the second-order EMHPM, the function that describes the delayed interval is:

$$\begin{aligned}
P_3(x) = &\frac{(x-x_1)(x-x_2)(x-x_3)}{(x_0-x_1)(x_0-x_2)(x_0-x_3)} f(x_0) + \frac{(x-x_0)(x-x_2)(x-x_3)}{(x_1-x_0)(x_1-x_2)(x_1-x_3)} f(x_1) + \\
&\frac{(x-x_0)(x-x_1)(x-x_3)}{(x_2-x_0)(x_2-x_1)(x_2-x_3)} f(x_2) + \frac{(x-x_0)(x-x_1)(x-x_2)}{(x_3-x_0)(x_3-x_1)(x_3-x_2)} f(x_3)
\end{aligned} \tag{3.179}$$

where $f(x_0) = \boldsymbol{x}_{i-N}, f(x_1) = \boldsymbol{x}_{i-N+1}, f(x_2) = \boldsymbol{x}_{i-N+2}, f(x_3) = \boldsymbol{x}_{i-N+3}$, and $x_0 = 0$, $x_1 = \Delta t$, $x_2 = 2\Delta t$, and $x_3 = 3\Delta t$. Considering $x = T$, $\Delta t = \frac{\tau}{N-1}$ and solving, the equation becomes:

$$\begin{aligned} P_3(x) = &\left(-\frac{T^3}{6}\left(\frac{N-1}{\tau}\right)^3 + T^2\left(\frac{N-1}{\tau}\right)^2 - \frac{11}{6}T\left(\frac{N-1}{\tau}\right) + 1\right)\mathbf{x}_{i-N} + \left(\frac{T^3}{2}\left(\frac{N-1}{\tau}\right)^3 - \frac{5}{2}T^2\left(\frac{N-1}{\tau}\right)^2 + \right. \\ &\left. 3T\left(\frac{N-1}{\tau}\right)\right)\mathbf{x}_{i-N+1} - \left(\frac{T^3}{2}\left(\frac{N-1}{\tau}\right)^3 - 2T^2\left(\frac{N-1}{\tau}\right)^2 + \frac{3}{2}T\left(\frac{N-1}{\tau}\right)\right)\mathbf{x}_{i-N+2} + \\ &\left(\frac{T^3}{6}\left(\frac{N-1}{\tau}\right)^3 - \frac{T^2}{2}\left(\frac{N-1}{\tau}\right)^2 + \frac{T}{3}\left(\frac{N-1}{\tau}\right)\right)\mathbf{x}_{i-N+3} \end{aligned} \tag{3.180}$$

after rearranging, the function that describes the delayed interval is:

$$\begin{aligned} \mathbf{x}_i^{\tau}(T) \approx &\mathbf{x}_{i-N} + \left(\frac{N-1}{\tau}\right)T\left(-\frac{11}{6}\mathbf{x}_{i-N} + 3\mathbf{x}_{i-N+1} - \frac{3}{2}\mathbf{x}_{i-N+2} + \frac{1}{3}\mathbf{x}_{i-N+3}\right) + \\ &\left(\frac{N-1}{\tau}\right)^2\frac{T^2}{2}\left(2\mathbf{x}_{i-N} - 5\mathbf{x}_{i-N+1} + 4\mathbf{x}_{i-N+2} - \mathbf{x}_{i-N+3}\right) + \left(\frac{N-1}{\tau}\right)^3\frac{T^3}{6}\left(-\mathbf{x}_{i-N} + 3\mathbf{x}_{i-N+1} - 3\mathbf{x}_{i-N+2} + \mathbf{x}_{i-N+3}\right) \end{aligned} \tag{3.181}$$

Following the EMHPM procedure, the solution of (3.136) recursively $\mathbf{X}_{ik}(T)$ is expressed as

$$\mathbf{X}_{ik} = \mathbf{X}_{ik}^a + \mathbf{X}_{ik}^b + \mathbf{X}_{ik}^c + \mathbf{X}_{ik}^d, k = 1, 2, 3.... \tag{3.182}$$

where

$$\mathbf{X}_{i0}^a = \mathbf{x}_{i-1,}\mathbf{X}_{i0}^b = \mathbf{X}_{i0}^c = \mathbf{X}_{i0}^d = 0 \tag{3.183}$$

and

$$\begin{aligned} \mathbf{X}_{ik}^a &= \frac{T}{k}\left(\mathbf{A}_t\mathbf{X}_{i(k-1)}^a + g(k)\mathbf{B}_t\mathbf{x}_{i-N}\right) \\ \mathbf{X}_{ik}^b &= \frac{T}{k+1}\left(\mathbf{A}_t\mathbf{X}_{i(k-1)}^b + g(k)\left(\frac{N-1}{\tau}\right)\mathbf{B}_t T\left(-\frac{11}{6}\mathbf{x}_{i-N} + 3\mathbf{x}_{i-N+1} - \frac{3}{2}\mathbf{x}_{i-N+2} + \frac{1}{3}\mathbf{x}_{i-N+3}\right)\right) \\ \mathbf{X}_{ik}^c &= \frac{T}{k+2}\left(\mathbf{A}_t\mathbf{X}_{i(k-1)}^c + g(k)\left(\frac{N-1}{\tau}\right)^2\mathbf{B}_t\frac{T^2}{2}\left(2\mathbf{x}_{i-N} - 5\mathbf{x}_{i-N+1} + 4\mathbf{x}_{i-N+2} - \mathbf{x}_{i-N+3}\right)\right) \\ \mathbf{X}_{ik}^d &= \frac{T}{k+3}\left(\mathbf{A}_t\mathbf{X}_{i(k-1)}^d + g(k)\left(\frac{N-1}{\tau}\right)^3\mathbf{B}_t\frac{T^3}{6}\left(-\mathbf{x}_{i-N} + 3\mathbf{x}_{i-N+1} - 3\mathbf{x}_{i-N+2} + \mathbf{x}_{i-N+3}\right)\right) \end{aligned} \tag{3.184}$$

So, the solution of (3.136) is obtained by adding each of the approximations $\mathbf{X}_{ik}$.

3.4 Analysis of the EMHPM

Mathieu equation

Having clear the EMHPM procedure, its accuracy is evaluated through the differential Mathieu equation with delay, whose form is expressed as:

$$\ddot{\mathbf{x}} + k\dot{\mathbf{x}} + \left(\delta + \varepsilon\cos\left(\frac{2\pi t}{T}\right)\right)\mathbf{x} = b\mathbf{x}(t-\tau) \tag{3.185}$$

where $k, \delta, \varepsilon, \tau$ y T are system parameters. Therefore, following the EMHPM procedure, Eq. (3.185) is first written in its equivalent form by subintervals

$$\ddot{\mathbf{x}}_i(T) + k\dot{\mathbf{x}}_i(T) + \alpha_t\mathbf{x}_i \approx b\mathbf{x}_{i-N+1}(T) \tag{3.186}$$

where $\boldsymbol{x}_i(T)$ expresses the solution of order m for Eq. (3.186) in the $i-$th subinterval that must also satisfy the initial conditions $\boldsymbol{x}_i(0) = \boldsymbol{x}_{i-1}$, and $\dot{\boldsymbol{x}}_i(0) = \dot{\boldsymbol{x}}_{i-1}$. Through the representation in state space of (3.186), results the more general matrix equation given by

$$\dot{\mathbf{x}}_i(T) = \mathbf{A}_t\mathbf{x}_i(T) + \mathbf{B}_t\mathbf{x}_{i-N+1}(T) \tag{3.187}$$

where

$$\mathbf{A}_t = \begin{bmatrix} 1 & 0 \\ -\alpha_t & -k \end{bmatrix},\ \mathbf{B}_t = \begin{bmatrix} 0 & 0 \\ b_t & 0 \end{bmatrix} \tag{3.188}$$

and $\alpha_t = (\delta + \varepsilon\cos(t))$ is a periodic term.

Combinations of specific values have been chosen to show the capacity of the method in a case where the system is stable and unstable according to [68]. For an unstable case, the values for $k = 0.2, \delta = 3, \varepsilon = 1, T = \tau = 2\pi$ and $b = -1$.

Solution of Eq. (3.185) through the EMHPM is shown in Figure 3.8, compared with the numerical integration obtained using the Matlab routine dde23 in a time interval twice the period $2T$, considering $N = 50$ discretization and the following values that describe the solution: a period T before zero $x_{-50}(T) = x_{-49}(T) = \cdots x_0(T) = 0.001$ and $\dot{x}_{-50}(T) = \dot{x}_{-49}(T) = \cdots \dot{x}_0(T) = 0$.

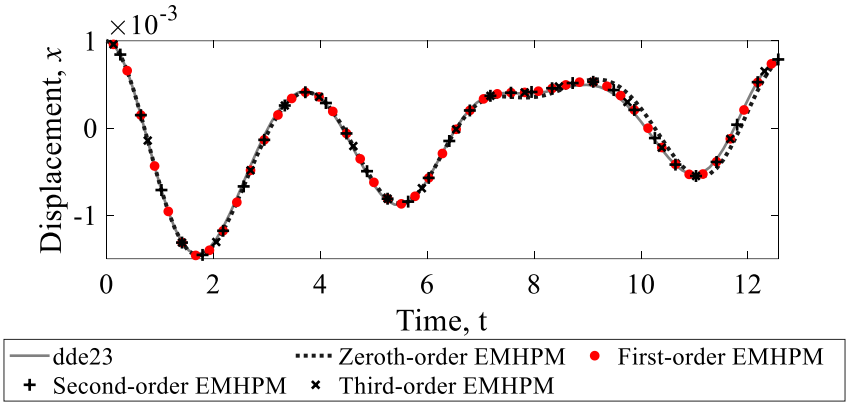

Figure 3.8 Solution of Mathieu's equation with delay, $N = 50$ and $m = 4$.

In Figure 3.8, it is observed that in the first interval of solution of size $T[0, T]$, the solutions with approximations to the delay of zero, first, second and third order are exactly the same since the displacement and velocity before $t = 0$ were assumed constants, that is, the delay approximation is reduced to a zeroth-order approximation. This is contrasted by the following interval of size equal to the period $T[T, 2T]$ where it is evident that with the first, second and third order approximations to the delay a better approximation to the delay subinterval is achieved. On the other hand, the computational time of the EMHPM implementation in Matlab is listed in Table 3.1.

Table 3.1 Computational time required for the solution of Mathieu's equation.

			EMHPM		
N	*m*	dde23 [ms]	First-order [ms]	Second-order [ms]	Third-order [ms]
15	5	5.2	0.09	1.5	2.5
20	4	6.0	1.0	1.8	2.8
40	3	7.5	1.6	2.8	4.4
50	2	7.8	1.7	3.3	4.0
60	2	8.4	2.2	3.2	4.9
80	5	8.5	4.9	8.9	15.9

The order of solution and number of discretization intervals in the EMHPM routine were chosen as the minimum sufficient to guarantee convergence.

Dynamic milling solution

To exemplify the use of the EMHPM to obtain the solution of the differential equation with delay, the mathematical model of milling in a degree of freedom commonly used in the literature is applied [23,67–69], which is given as

$$\ddot{x}(t)+2\zeta\omega_n\dot{x}(t)+\omega_n^2x(t)=-\frac{a_p h_{xx}(t)}{m_m}\left(x(t)-x(t-\tau)\right) \tag{3.189}$$

where ζ is the modal damping ratio, ω_n is the natural frequency of the workpiece, a_p is the axial depth of cut, m_m is the modal mass, τ represents the time delay corresponding to the hitting period between each tooth of the tool and $h_{xx}(t)$ is the specific cutting force in the x-direction due to flexibility in x-direction, which was calculated depending on the position of the tool

$$h_{xx}(t)=\sum_{iz=1}^{z_n} g\left(\phi_{iz}(t)\right)\sin\phi_{iz}(t)\left(K_{tc}\cos\phi_{iz}(t)+K_{nc}\sin\phi_{iz}(t)\right) \tag{3.190}$$

z_n is the number of edges of the tool, K_{tc} and K_{nc} are the average specific cut coefficients in the tangential and normal direction, respectively, and $\phi_{iz}(t)$ is the angular position of each left edge described by

$$\phi_{iz}=(2\pi n/60)t+2\pi iz/z_n \tag{3.191}$$

where n is the spindle speed in rpm and the function $g\left((\phi_{iz})(t)\right)$ is a window function, which is one while the current edge iz is cutting material, otherwise it takes the value zero.

$$g(\phi_{iz}(t))=\begin{cases}1\rightarrow \phi_{st}<\phi_j(t)<\phi_{ex}\\ 0\rightarrow otherwise\end{cases} \tag{3.192}$$

angles ϕ_{st} and ϕ_{ex} are the angular positions where each cutting edge enters and leaves the workpiece. In up-milling $\phi_{st}=0$ and $\phi_{ex}=\cos^{-1}(1-2a_d)$, conversely, in down-milling, $\phi_{st}=\cos^{-1}(2a_d-1)$ and $\phi_{ex}=\pi$, where a_d is the radial immersion ratio of the cut.

Radial immersion is the width of the cut in relation to the diameter of the cutter, it is expressed as $a_d=a_e/D$, a_e is the radial width of the cutter in engagement in the cut, and D is the diameter of the tool.

Using the EMHPM procedure, Eq. (3.189) is rewritten by subintervals

$$\ddot{\mathbf{x}}_i(T)+2\zeta\omega_n\dot{\mathbf{x}}_i(T)+\omega_n^2\mathbf{x}_i(T)\approx-\frac{a_p h_{xx,t}}{m_m}\left(\mathbf{x}_i(T)-\mathbf{x}_{i-N+1}(T)\right) \tag{3.193}$$

where $\boldsymbol{x}_i(T)$ represents the solution of order m for Eq. (3.189) in the i −th subinterval that satisfies the initial conditions $\boldsymbol{x}_i(0)=\boldsymbol{x}_{i-1}$, $\dot{\boldsymbol{x}}_i(0)=\dot{\boldsymbol{x}}_{i-1}, h_{xx,t}=h(t)$ and x_i^{τ} is

represented by Eq. (3.151). Making the transformation $\boldsymbol{x}_i = [\boldsymbol{x}_i, \dot{\boldsymbol{x}}_i]^T$, Eq. (3.193) can be rewritten as a system of first-order linear differential equations represented in matrix form as:

$$\dot{\mathbf{x}}_i(T) = \mathbf{A}_t \mathbf{x}_i(T) + \mathbf{B}_t \mathbf{x}_{i-N+1}(T) \tag{3.194}$$

where for a regular tool the matrix **A** and **B** are represented as:

$$\mathbf{A}_t = \begin{bmatrix} 0 & 1 \\ -\omega_n^2 - \dfrac{a_p h_{xx}(t)}{m_m} & -2\zeta\omega_n \end{bmatrix}, \mathbf{B}_t = \begin{bmatrix} 0 & 0 \\ \dfrac{a_p h_{xx}(t)}{m_m} & 0 \end{bmatrix} \tag{3.195}$$

$\mathbf{A}_t$ and $\mathbf{B}_t$ correspond to the periodic matrix evaluated at time t. For demonstration purposes, time-domain simulations were computed for a full-immersion down-milling operation to obtain the solution of Eq. (3.189). We used the parameters employed by Insperger et al., in [68] where the stability lobes were also calculated.

The modal parameters f_n = 922 Hz, $\omega_n = 5793$ rad/s, $\zeta = 0.011$ and $m_m = 0.03993$ kg corresponds to a single degree of freedom. The tangential and normal cutting coefficients are $K_{tc} = 6 \times 10^8$ N/m^2 and $K_{nc} = 2 \times 10^8$ N/m^2 respectively for an end-mill with $z_n = 2$. The time-domain solution was computed using the EMHPM considering $N = 76$ discrete intervals and $m = 7$.

Two sets of cutting conditions were chosen for a fixed spindle speed with value of $n = 12000$ rpm where the axial depth of cut of $a_p = 1.5$ mm corresponds to a stable cutting operation while that for an unstable operation $a_p = 3$ mm was chosen.

In Figure 3.9 we plot the second- and third-order EMHPM solutions and compare it with the zeroth- and first-order EMHPM and with the dde23 routine in Matlab, which is used to integrate DDE.

a)

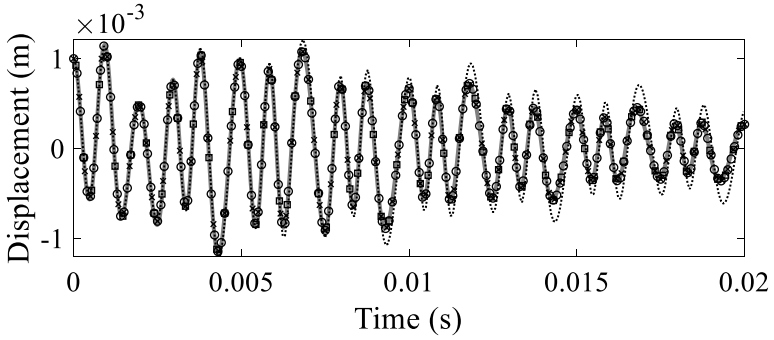

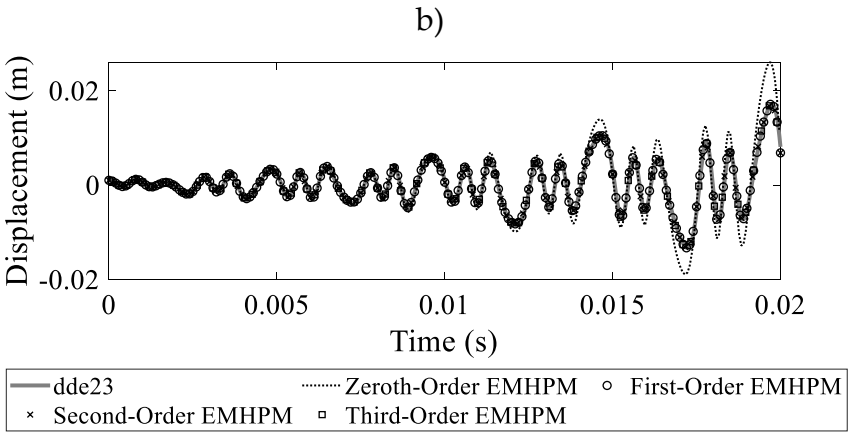

Figure 3.9 Approximate solution of Eq. (3.189) using the EMHPM, $n = 12000\ rpm$, $a_d = 1$, a) stable operation $a_p = 1.5\ mm$, b) unstable operation $a_p = 3$ mm

Numerical comparison between methods

In order to observe the rate of convergence of the zeroth-, first-, second- and third-order EMHPM, we chose the stable case with cutting conditions $a_p = 1.5$ mm, $a_d = 1$ and $n = 12000$ rpm presented in Figure 3.10a, and the unstable case with cutting conditions $a_p = 3$ mm, $a_d = 1$ and $n = 12000$ rpm showed in Figure 3.10b. The rate of convergence was analyzed by computing the absolute error between the solution with N discrete intervals and a converged solution. All methods were compared against itself using the solution provided with N = 200 discrete intervals, which are considered the converged solution.

In Figure 3.10a it is observed that the convergence is better for the second- and third-order than the zeroth and first-order, however, the difference of convergence between second- and third-order with the parameters used was negligible. On the other hand, Figure 3.10b shows that for few discrete intervals the third-order EMHPM had the fastest convergence in comparison with the second-, the first and the zeroth-order EMHPM. However, the second- and third-order curves behaved very similarly after N = 50 discrete intervals.

It is important to mention that for a typical stability solution in the ranges of spindle speed 5000–10000 rpm, N = 40 discrete intervals will be enough to have accurate predictions.

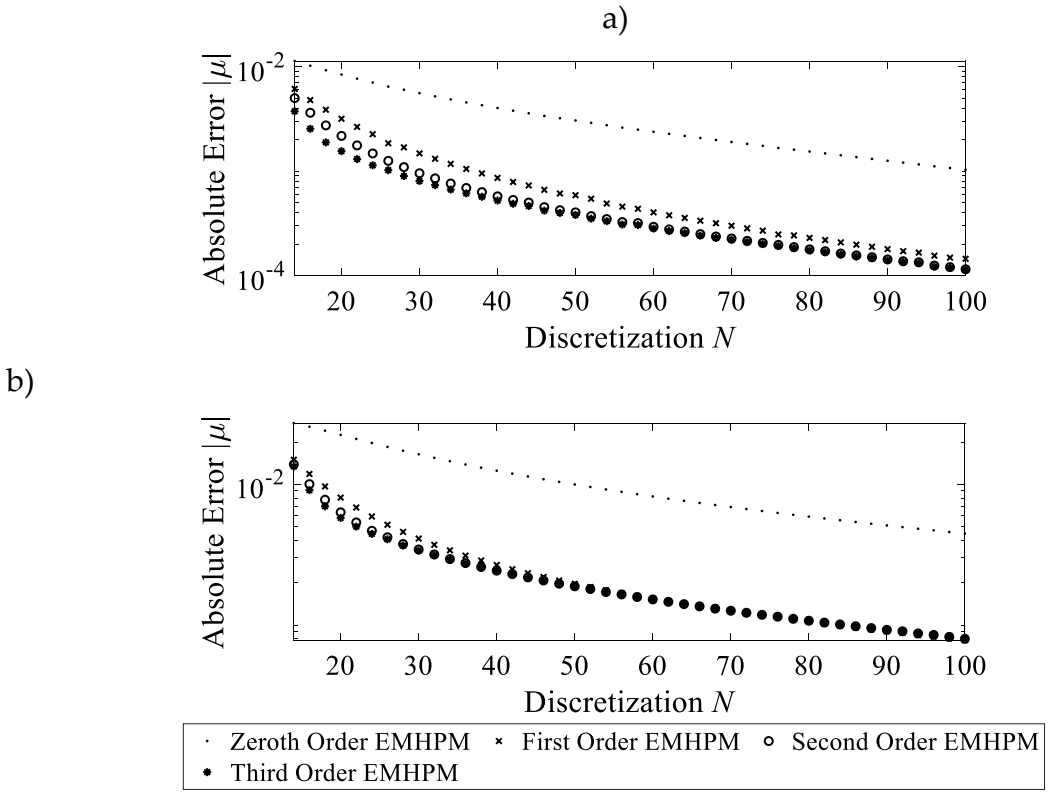

Figure 3.10 Convergence rate of absolute error between zeroth-, first-, second- and third-order EMHPM for down-milling operation. Cutting parameters for a) $a_p = 1.5$ mm, $a_d = 1$ and n=12000 rpm, b) $a_p = 3$ mm, $a_d = 1$ and n=12000 rpm.

At Figure 3.11 the comparison of the absolute error between zeroth-, first-, second- and third-order is plotted, using as reference the Matlab solution dde23 with $N = 1000$. Here, the parameters employed are $a_p = 1.5$ mm, and $n = 12000$ rpm and the radial immersion is varied as shown in Figure 3.11. A step of 10 is used from 10 to 200 discretization, while from 200 to 1000 a step of 100 is used. An initial condition of a constant $c = 0.001$ for the position is used and 0 for the velocity. It is evident that the convergence of the first, second and third order solutions occurs with fewer discretization than with the zero-order one.

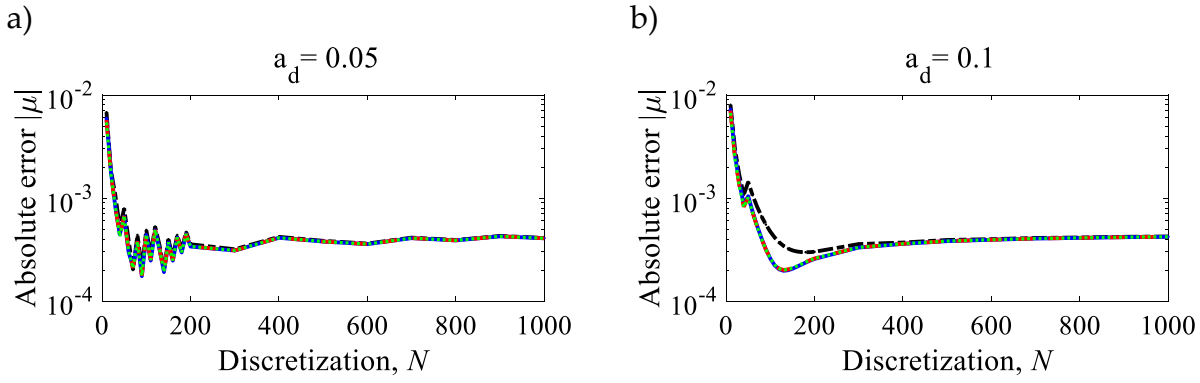

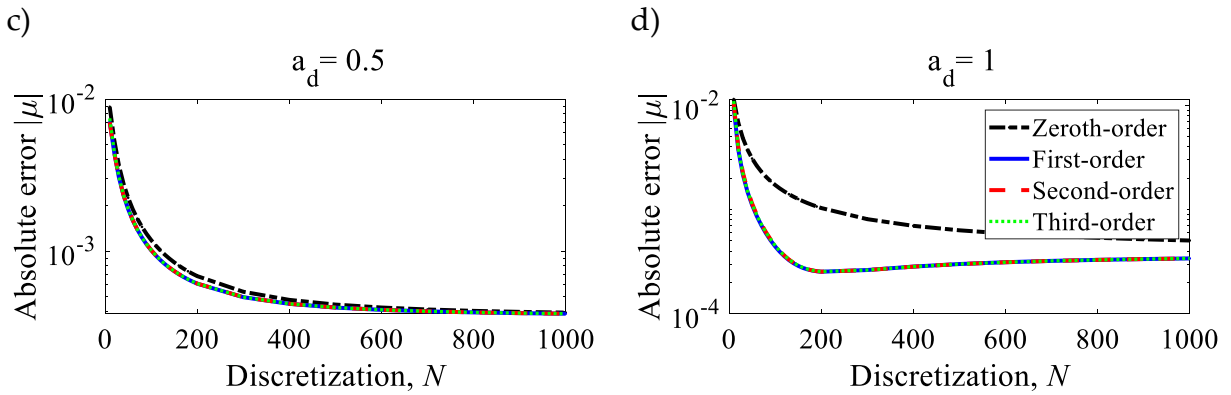

Figure 3.11 Absolute error with different discretization for zeroth-, first-, second- and third-order vs solution dde23

The computation time for different discretization in the time-domain simulations with different order of solution is presented in Figure 3.12 for values of a_d=0.05, 0.1, 0.5 and 1. The computational time presented in the figure is the minimum obtained of 10 samples. It is observed that as the order of solution increases, the time also increases slightly. However, since it is not significant, the feasibility of being able to use the second- and the third-order solution is considered, in addition to the fact that a faster convergence has been observed in those solutions as showed in Figure 3.10.

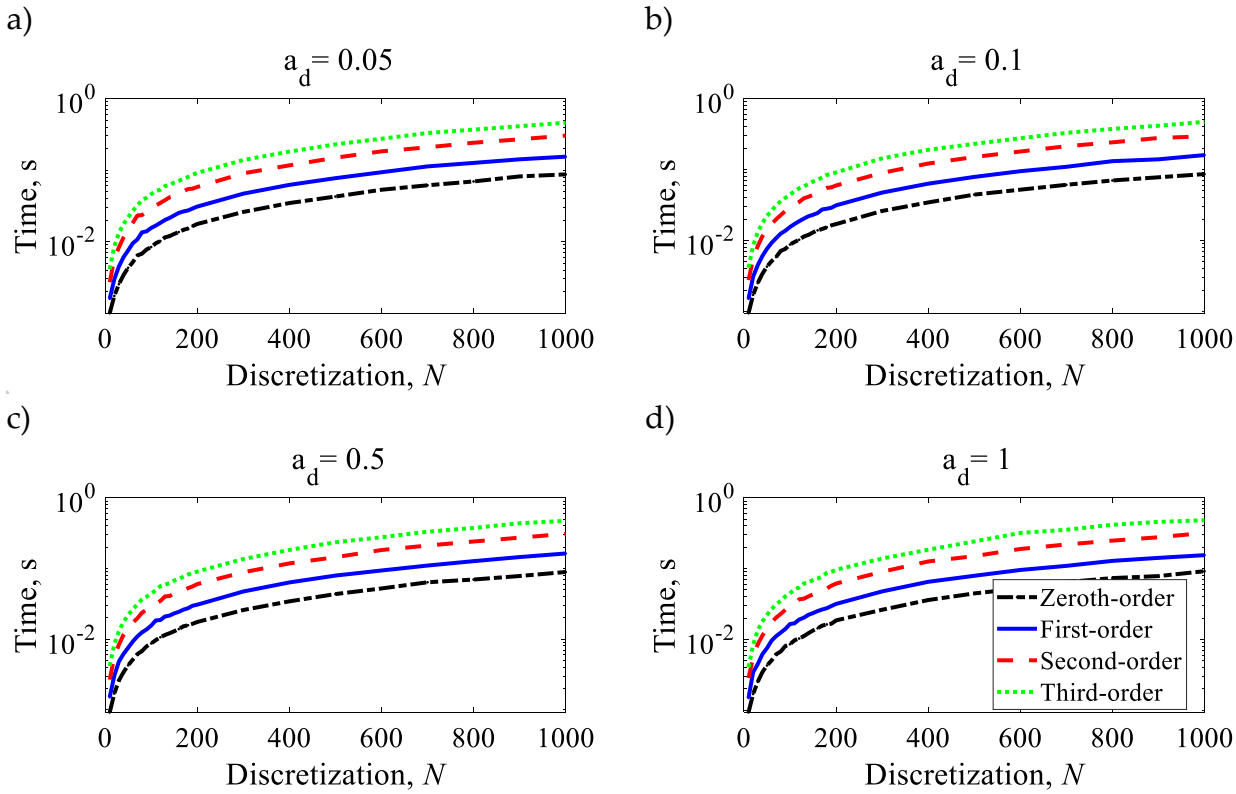

Figure 3.12 Computation time for different discretization in zeroth-, first-, second- and third-order EMHPM vs solution dde23 of Matlab with a) a_d=0.05, b) a_d=0.1, c) a_d=0.5, d) a_d=1.

Knowing that the second- and the third-order EMHPM are better than the zeroth- and the first-order EMHPM, in Figure 3.13 the second- and the third-order solutions are analyzed varying the number of discretization N, and the order m of the solution.

Figure 3.13a shows the influence on the second-order solution of the EMHPM when compared against the evaluation of itself for $N = 1001$, while that Figure 3.13b corresponds to the solution of the third-order EMHPM. The initial constant $c = 0.001$ is used for the position and 0 for the velocity, with parameters $zn = 2$, $a_d = 1$, $a_p = 1.5\ mm$ and $n = 12000\ rpm$.

To be able to compare with the different discretization, interpolations are carried out in such a way that it is guaranteed to have the values in the same time that is evaluated for the different discretization.

To select the solution with the smallest absolute error and with the smallest approximation order $m = 4$, it is observed in the Figure 3.13 that discretization with $N \geq 40$ must be chosen, also, it is observed a very similar result when comparing the two methods.

a)

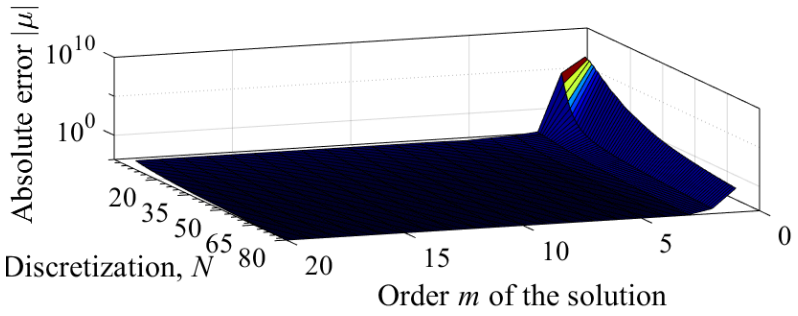

b)

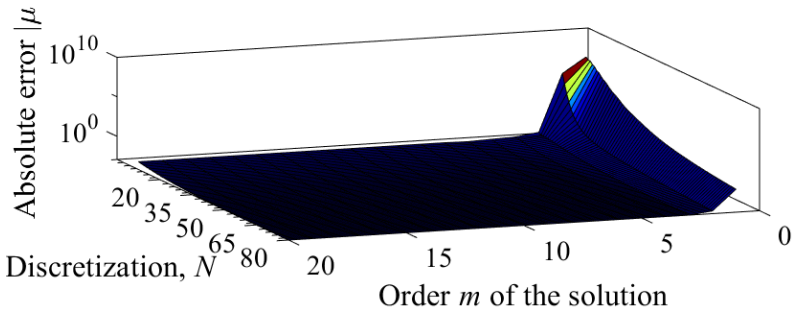

Figure 3.13 Influence of the number of discretization N and the order m of solution for the EHPM of a) second and b) third order with constant initial condition

Similarly, the influence of the discretization N and of the order m for the third-order EMHPM is analyzed if a quadratic curve is taken as an initial condition instead of a constant value, Figure 3.14a, and if a straight line is taken as the initial condition.

For the quadratic curve the function for the position is $d = x^2$, evaluated from $\sqrt{0.002}$ to $\sqrt{0.001}$ and for the velocity is $v = x^2$, evaluated from -3 to $\sqrt{0.001}$ both with N points.

a)

b)

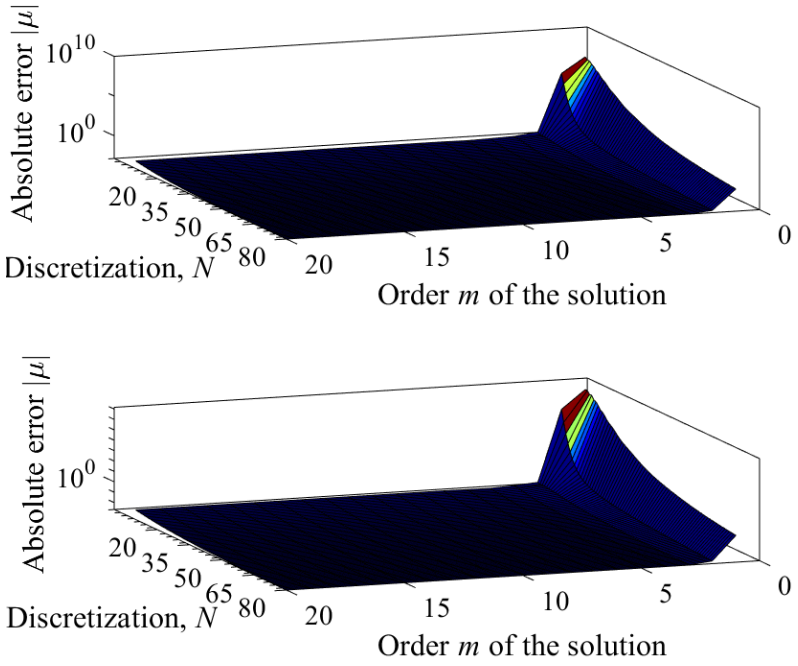

Figure 3.14 Influence of the number of discretization N and the order m of solution for the third-order EHPM with a) cuadratic initial condition, b) straigth line initial condition.

For the initial condition with a straight line, the position and the velocity used a line evaluated from 0.005 to 0.001 with N points. By observing Figure 3.14, and Figure 3.13 the results are similar, so it is not observed an improvement from a constant initial condition.

Chapter 4. Stability in Delay Differential Equations

4.1 Introduction to the stability of systems with time delay

In the field of engineering and research, Delay Differential Equations (DDE) play a very important role. Many phenomena that occur are modeled with this type of equations, and to understand their behavior it is necessary to know the influence of each of the parameters influencing the system. The stability graphs are diagrams in the plane of two or more parameters of the system that allow to observe graphically under which combination of these parameters the system becomes stable or unstable. In some cases, it is possible to construct the stability graphs in a closed form by analyzing the characteristic equation, but in many other cases it is only possible by approximating the monodromic operator. Another way is to perform numerical simulations in the time domain to capture the interrupted nature of the process, then the evolution over time of the phenomenon is visualized and analyzed to determine whether it was stable. However, this technique as a tool for determining stability graphs is computationally inefficient compared to those based on the monodromic operator approximation.

Because the reliability of the chatter prediction is limited by the inaccuracy of the dynamic model of the system, some researchers have proposed using the parameters as random variables and basing the stability calculation on estimating the probability for each combination of cutoff parameters among them is the work of Totis [70] where the calculation can be very computationally demanding. Pérez-Canales [71] proposed the entropy approximation method which is an approach with high robustness, high computational efficiency and with a sense of online monitoring; relates the randomness of the content of the acceleration signal in unstable cases, in contrast to stable cases, in order to characterize the milling process with a reduced number of samples.

There are several models based on the time domain using the Floquet monodromic operator approach that seek the optimization of the process to increase vibration-free productivity. According to the theory developed by Floquet, the stability properties are determined by the monodromic operator of the finite system that approximates the DDE. Various approaches to prediction of stability lobes are found in the literature. Stability lobes are design maps that allow you to visually identify areas that suggest higher productivity without unstable vibrations. These are calculated based on the process variables, which directly or indirectly affect the equation of motion. Commonly, the parameters are the spindle speed as it defines the delay or delays, and the cutting area that is a function of the axial depth of cut a_p and the immersion in the radial direction a_e.

Altintas and Budak [72] developed the first analytical solution in the frequency domain that allows the prediction of the lobes through the average of the directional

coefficients that define the force during the process. This method allows accurate analytical predictions except for cuts with very low radial immersion which causes a highly uninterrupted cut. Davies [73] showed that at low radial immersions, traditional vibration regeneration theory is not able to predict accurately; however, shortly afterwards, Merdol and Altintas in demonstrated that stability frontiers at low radial immersions can be predicted through the so-called multifrequency method if a higher number of harmonics of the shear force is considered on the eigenvalue solution. Bayly [69] analyzed the double-period bifurcation phenomenon that appears in low radial inmersions using the Time Finite Element Analysis (TFEA) approach. The approximate solution is obtained by means of a discrete map that relates the position and velocity at the beginning of each element with the end, so that the eigenvalues of the discrete map are used to determine the stability boundaries.

Another method that forms a finite transition matrix, as an approximation of the monodromic operator of infinite dimension, is the Semi-Discretization method proposed by Insperger and Stépán in [74], in this, the delay terms are discretized while those that are not dependent on the delay remain unchanged, and the periodic coefficients in time are approximated by piecewise constant functions, later they made an update of the method for periodic systems for a single delay [68]. In addition, they demonstrated that second or higher order approximations of the delay term do not produce a solution with better convergence compared to the first order one, but rather generate an increase in computational time [75,76]. On the other hand, Butcher et al. [77] developed a technique based on Chebyshev polynomials and the use of placement points to obtain the solution of the delay equation by using a differentiation matrix, the stability boundaries are determined from the eigenvalues of the transition matrix that maps the solution over the placement points from one period to another.

Ding et al. [78] presented a method that they named Full-Discretization Method (FD) based on a direct integration scheme for the prediction of milling stability, which indicated that it provided greater computational efficiency than the Semi-Discretization method developed by Insperger in [68]. However, Insperger in [79] describes that the methods are similar since they both approximate the differential equation with delay by means of a series of ordinary differential equations, in addition he indicates that the FD is an alternative method of the SD but with a slightly different conception that produces a slow convergence. Soon after, Ding et al. [80] proposed an improvement called Second-order Full-Discretization Method that indicates improved convergence, so they indicate that they developed a method with computational accuracy and efficiency, then, in [81] they released another numerical scheme based on the equation integral and numerical integration formulas. They divide the shear period into free vibration (when the analytical solution is known) and forced vibration, whose approximate solution is required to solve the resulting integral equation.

To obtain the numerical solution of the integral equation during the forced vibration phase, the time interval of interest is equally discretized. By applying milling to a degree of freedom with respect to the FD method, there is an improvement in the computation time of 63% up to 95% for full immersion and 0.05% immersion operations. All the exposed methods offer the same solutions.

4.2 Stability for regular tools with EMHPM

Stability by first-order EMHPM

The matrix representation for the calculation of the dynamic stability of differential equations with delay with the EMHPM is given by

$$\dot{\mathbf{x}}(t) = \mathbf{A}(t)x + \mathbf{B}(t)\mathbf{x}(t-\tau) \tag{4.1}$$

where $\mathbf{A}(\mathrm{t}+\tau) = \mathbf{A}(\mathrm{t})$, $\mathbf{B}(\mathrm{t}+\tau) = \mathbf{B}(\mathrm{t})$, $\boldsymbol{x} = [\boldsymbol{x}, \dot{\boldsymbol{x}}]^{\boldsymbol{T}}$ is the vector of states and τ is the value of the delay in time; which was described in section 3.3 by the EMHPM and written equivalently as

$$\dot{\mathbf{x}}_i(T) - \mathbf{A}_t\mathbf{x}_i(t) \approx \mathbf{B}_t\mathbf{x}_i^{\tau}(T) \tag{4.2}$$

where $\boldsymbol{x}_i(T)$ expresses the solution of order m for Eq. (4.1) in the i −th subinterval that must also satisfy the vector of initial conditions $\boldsymbol{x}_i(0) = \boldsymbol{x}_{i-1}$, $\boldsymbol{A}_t$ and $\boldsymbol{B}_t$ represent the matrices in which each of its elements are evaluated at time t.

To approximate the delay term $\boldsymbol{x}_i^{\tau}(T)$ in Eq. (4.2), the time interval of size equal to the delay value $[t_0 - \tau, t_0]$ is discretized by N points not strictly equal spaced, however, for simplicity and without losing generality, the subintervals are considered to be of equal size.

To calculate the stability of the differential equation (4.1) using the first-order EMHPM, the solution (3.150) for first-order EMHPM reviewed in Chapter 3 must be rewritten by grouping each of the discrete values $\mathbf{x}_\mathbf{i}, \mathbf{x}_{i-N+1}, \mathbf{x}_{i-N}$, resulting

$$\mathbf{x}_i(T) \approx \mathbf{P}_i(T)\mathbf{x}_{i-1} + \mathbf{Q}_i(T)\mathbf{x}_{i-N+1} + \mathbf{R}_i(T)\mathbf{x}_{i-N} \tag{4.3}$$

where

$$\begin{aligned}
&\mathbf{P}_i(T) = \sum_{k=0}^{m} \frac{1}{k!} \mathbf{A}_t^k T^k, \\
&\mathbf{Q}_i(T) = \sum_{k=1}^{m} \frac{1}{(k+1)!} \left(\frac{N-1}{\tau} \right) \mathbf{A}_t^{k-1} \mathbf{B}_t T^{k+1}, \quad m \geq 1 \\
&\mathbf{R}_i(T) = \sum_{k=1}^{m} \frac{1}{k!} \mathbf{A}_t^{k-1} \mathbf{B}_t T^k - \mathbf{Q}_i, \qquad m \geq 1
\end{aligned} \tag{4.4}$$

Stability by second-order EMHPM

To calculate the stability of the differential equation (4.1) using the second-order EMHPM, the solution (3.150) for second-order EMHPM must be rewritten by grouping each of the discrete values $\mathbf{x_i}, \mathbf{x}_{i-N+2}, \mathbf{x}_{i-N+1}, \mathbf{x}_{i-N}$, resulting

$$\mathbf{x}_i(T) \approx \mathbf{P}_i(T)\mathbf{x}_{i-1} + \mathbf{Q}_i^{'}(T)\mathbf{x}_{i-N+2} + \mathbf{Q}_i(T)\mathbf{x}_{i-N+1} + \mathbf{R}_i(T)\mathbf{x}_{i-N} \tag{4.5}$$

where

$$\begin{aligned}
&\mathbf{P}_i(T) = \sum_{k=0}^{m} \frac{1}{k!} \mathbf{A}_t^k T^k, \\
&\mathbf{Q}_i^{'}(T) = \sum_{k=1}^{m} \left(\frac{1}{(k+2)!} \left(\frac{N-1}{\tau} \right)^2 \mathbf{A}_t^{k-1} \mathbf{B}_t T^{k+2} - \frac{1}{2(k+1)!} \left(\frac{N-1}{\tau} \right) \mathbf{A}_t^{k-1} \mathbf{B}_t T^{k+1} \right) \\
&\mathbf{Q}_i(T) = \sum_{k=1}^{m} \frac{1}{(k+1)!} \left(\frac{N-1}{\tau} \right) \mathbf{A}_t^{k-1} \mathbf{B}_t T^{k+1} - 2\mathbf{Q}_i^{'} \\
&\mathbf{R}_i(T) = \sum_{k=1}^{m} \frac{1}{k!} \mathbf{A}_t^{k-1} \mathbf{B}_t T^k - \mathbf{Q}_i^{'} - \mathbf{Q}_i
\end{aligned} \tag{4.6}$$

Stability by third-order EMHPM

Similarly, to compute the stability lobes for the third-order EMHPM, the solution of the differential equation (4.1) for third-order EMHPM is rewritten, which results

$$\mathbf{x}_i(T) \approx \mathbf{P}_i(T)\mathbf{x}_{i-1} + \mathbf{Q}_i^{''}(T)\mathbf{x}_{i-N+3} + \mathbf{Q}_i^{'}(T)\mathbf{x}_{i-N+2} + \mathbf{Q}_i(T)\mathbf{x}_{i-N+1} + \mathbf{R}_i(T)\mathbf{x}_{i-N} \tag{4.7}$$

where

$$\mathbf{P}_i(T)=\sum_{k=0}^{m}\frac{1}{k!}\mathbf{A}_t^k T^k,$$

$$\mathbf{Q}_i^{''}(T)=\sum_{k=1}^{m}\left(\frac{1}{(k+1)!}\left(\frac{N-1}{\tau}\right)\mathbf{A}_t^{k-1}\mathbf{B}_t T^{k+1}\left(\frac{1}{3}\right)-\frac{1}{(k+2)!}\left(\frac{N-1}{\tau}\right)^2\mathbf{A}_t^{k-1}\mathbf{B}_t T^{k+2}+\frac{1}{(k+3)!}\left(\frac{N-1}{\tau}\right)^3\mathbf{A}_t^{k-1}\mathbf{B}_t T^{k+3}\right)$$

$$\mathbf{Q}_i^{'}(T)=\sum_{k=1}^{m}\left(\begin{array}{l}\frac{1}{(k+1)!}\left(\frac{N-1}{\tau}\right)\mathbf{A}_t^{k-1}\mathbf{B}_t T^{k+1}+\frac{1}{(k+2)!}\left(\frac{N-1}{\tau}\right)^2\mathbf{A}_t^{k-1}\mathbf{B}_t T^{k+2}\left(-\frac{7}{2}\right)\\ +\frac{1}{(k+3)!}\left(\frac{N-1}{\tau}\right)^3\mathbf{A}_t^{k-1}\mathbf{B}_t T^{k+3}\left(\frac{9}{2}\right)\end{array}\right)-\frac{15}{2}\mathbf{Q}_i^{''} \tag{4.8}$$

$$\mathbf{Q}_i(T)=\sum_{k=1}^{m}\left(\frac{1}{(k+1)!}\left(\frac{N-1}{\tau}\right)\mathbf{A}_t^{k-1}\mathbf{B}_t T^{k+1}\right)-3\mathbf{Q}_i^{''}-2\mathbf{Q}_i^{'}$$

$$\mathbf{R}_i(T)=\sum_{k=1}^{m}\frac{1}{k!}\mathbf{A}_t^{k-1}\mathbf{B}_t T^k-\mathbf{Q}_i^{''}-\mathbf{Q}_i^{'}-\mathbf{Q}_i$$

For this case, only the solution of Eq. (4.3) is a function of the vectors $\boldsymbol{x}_i, \boldsymbol{x}_{i-N+3}$, $\boldsymbol{x}_{i-N+2}$, $\boldsymbol{x}_{i-N+1}$ and $\boldsymbol{x}_{i-N}$, since the subinterval is defined by the vectors $\boldsymbol{x}_{i-N+3}$, $\boldsymbol{x}_{i-N+2}$, $\boldsymbol{x}_{i-N+1}, \boldsymbol{x}_{i-N}$, and the initial condition is always $\boldsymbol{x}_i$.

From Eq. (4.3) a discrete mapping can be defined through a matrix that allows calculating the behavior of the next discretization based on the previous ones. The equality that defines this relationship is given by:

$$\mathbf{w}_i=\mathbf{D}_i\mathbf{w}_{i-1} \tag{4.9}$$

where $\boldsymbol{w}_i$ is a vector of coefficients of dimension equal to the number of states by the number of discretization N, which contains all vectors from $\boldsymbol{x}_{i-1}$ to $\boldsymbol{x}_{i-N}$

$$\mathbf{w}_{i-1}=\left[\mathbf{x}_{i-1},\dot{\mathbf{x}}_{i-1},\mathbf{x}_{i-2},\ldots,\mathbf{x}_{i-N}\right]^T \tag{4.10}$$

The matrix $\mathbf{D}_i$ for the third-order EMHPM has the form:

$$\mathbf{D}_i=\begin{bmatrix}\mathbf{P} & 0 & 0 & 0 & \cdots & 0 & \mathbf{Q}''_i & \mathbf{Q}'_i & \mathbf{Q}_i & \mathbf{R}_i\\ \mathbf{I} & 0 & 0 & 0 & \cdots & 0 & 0 & 0 & 0 & 0\\ 0 & \mathbf{I} & 0 & 0 & \cdots & 0 & 0 & 0 & 0 & 0\\ 0 & 0 & \mathbf{I} & 0 & \cdots & 0 & 0 & 0 & 0 & 0\\ \vdots & \vdots & \vdots & \ddots & \vdots & \vdots & \vdots & \vdots & \vdots & \vdots\\ 0 & 0 & 0 & 0 & \ddots & 0 & 0 & 0 & 0 & 0\\ 0 & 0 & 0 & 0 & \cdots & \mathbf{I} & 0 & 0 & 0 & 0\\ 0 & 0 & 0 & 0 & \cdots & 0 & \mathbf{I} & 0 & 0 & 0\\ 0 & 0 & 0 & 0 & \cdots & 0 & 0 & \mathbf{I} & 0 & 0\\ 0 & 0 & 0 & 0 & \cdots & 0 & 0 & 0 & \mathbf{I} & 0\end{bmatrix} \tag{4.11}$$

The Floquet transition matrix $\mathbf{\Phi}$ is calculated over the main period $\tau = (N-1)/\Delta t$, coupling each of the discrete maps D_i, $i = 1, 2, \ldots, (N-1)$, to obtain:

$$\mathbf{\Phi} = \mathbf{D}_{N-1}\mathbf{D}_{N-2}\ldots\mathbf{D}_2\mathbf{D}_1 \tag{4.12}$$

Thus, the stability of Eq. (4.1) is determined by calculating the eigenvalues of the transition matrix given by Eq. (4.12). The eigenvalues of the transition matrix (4.12) are actually the Floquet multipliers. If the modulus of greatest magnitude is greater than or equal to one, it implies that the system will behave in an unstable way, otherwise it will have a stable behavior.

It is important to point out that in the case of the second-order EMHPM, the matrix $\mathbf{D}_\mathrm{i}$ is like the matrix of the third-order EMHPM but without the matrix $\mathbf{Q}_i''$, while that in the case of the first-order EMHPM the matrix $\mathbf{D}_\mathrm{i}$ is like the matrix of the third-order EMHPM but without the matrix $\mathbf{Q}_i''$ and without the matrix $\mathbf{Q}_i'$.

4.3 Analysis of stability in milling for a regular tool in one degree of freedom

Sometimes, when vibration is present, a single, well-defined dominant mode may occur, as in thin-wall milling. In this case the stability graphs consist of an infinite series of stability lobes that are associated to the Hopf bifurcation or to the bifurcation of a period. The equation that describes the movement of the milling model in a degree of freedom analyzed by Bayly in [82] is written as

$$\ddot{x}(t) + 2\zeta\omega_n\dot{x}(t) + \omega_n^2 x(t) = -\frac{a_p h_{xx}(t)}{m_m}\left(x(t) - x(t-\tau)\right) \tag{4.13}$$

where ω_n is the natural frequency of the workpiece, ζ is the modal damping ratio, a_p is the axial depth of cut, m_m is the modal mass of the tool, the chip thickness is described from the difference of the current position and the delay period τ (which corresponds to the striking period between each tooth of the tool), $h(t)$ represents the specific cutting coefficient, which is calculated depending on the angular position in time of each of the teeth on the tool neglecting the helix angle,

$$h_{xx}(t) = \sum_{iz=1}^{z_n} g\left(\phi_{iz}(t)\right)\sin\phi_{iz}(t)\left(K_{tc}\cos\phi_{iz}(t) + K_{nc}\sin\phi_{iz}(t)\right) \tag{4.14}$$

z_n is the number of edges of the tool, K_{tc} and K_{nc} are the average specific cut coefficients in the tangential and normal direction, respectively, and $\phi_{iz}(t)$ is the angular position of each left edge described by

$$\phi_{iz}(t) = (2\pi n/60)t + 2\pi iz/z_n \tag{4.15}$$

where n is the spindle speed in rpm and the function $g\big((\phi_{iz})(t)\big)$ is a window function, which is one while the current edge iz is cutting material, otherwise it takes the value zero.

$$g(\phi_{iz}(t)) = \begin{cases} 1 \to \phi_{st} < \phi_j(t) < \phi_{ex} \\ 0 \to otherwise \end{cases} \tag{4.16}$$

angles ϕ_{st} and ϕ_{ex} are the angular positions where each cutting edge enters and leaves the workpiece. For up-milling $\phi_{st} = 0$ and $\phi_{ex} = \cos^{-1}(1 - 2a_d)$, while that for down-milling, $\phi_{st} = \cos^{-1}(2a_d - 1)$ and $\phi_{ex} = \pi$, a_d is the radial immersion ratio of the cut.

Using the EMHPM procedure, Eq. (4.13) is rewritten by subintervals

$$\dot{\mathbf{x}}_i(T) - \mathbf{A}_t\mathbf{x}_i(T) \approx \mathbf{B}_t\mathbf{x}_{i-N} - \left(\frac{N-1}{\tau}\right)\mathbf{B}_t(\mathbf{x}_{i-N})T + \left(\frac{N-1}{\tau}\right)\mathbf{B}_t(\mathbf{x}_{i-N+1})T \tag{4.17}$$

where

$$\mathbf{A}_t = \begin{pmatrix} 0 & 1 \\ -\omega_n^2 - \dfrac{a_p}{m_m}h_{xx,t} & -2\zeta\omega_n \end{pmatrix}, \mathbf{B}_t = \begin{pmatrix} 0 & 0 \\ \dfrac{a_p}{m_m}h_{xx,t} & 0 \end{pmatrix} \tag{4.18}$$

In order to validate its effectiveness, and determine the minimum order of solution that allows obtaining a reliable answer, Eq. (4.18) is solved using the third-order EMHPM, with parameters . $\omega_n = 5793\ rad/s$, $\zeta = 0.011$, $K_{tc} = 6 \times 10^8\ N/m^2$, $K_{nc} = 2 \times 10^8\ N/m^2$, and $m_m = 0.03993\ kg$ as used in [68] for approximations of $m = 3, 4, 5$ and 7 using two different numbers of discretization $N = 21$, and $N = 41$. $N = 41$ is used to compare with Insperger's work [68] while that $N = 21$ demonstrates convergence limitations.

The results are shown in Figure 4.1 with grid resolution of 401×201 for spindle speed and axial depth respectively. It is observed that the fifth order solution $m = 5$ (in red color) matches well with the higher order solution $m = 7$ when using $N = 41$; however, it is perceived that this does not imply that the convergent solution for $N = 21$ is the same for a greater number of discretization.

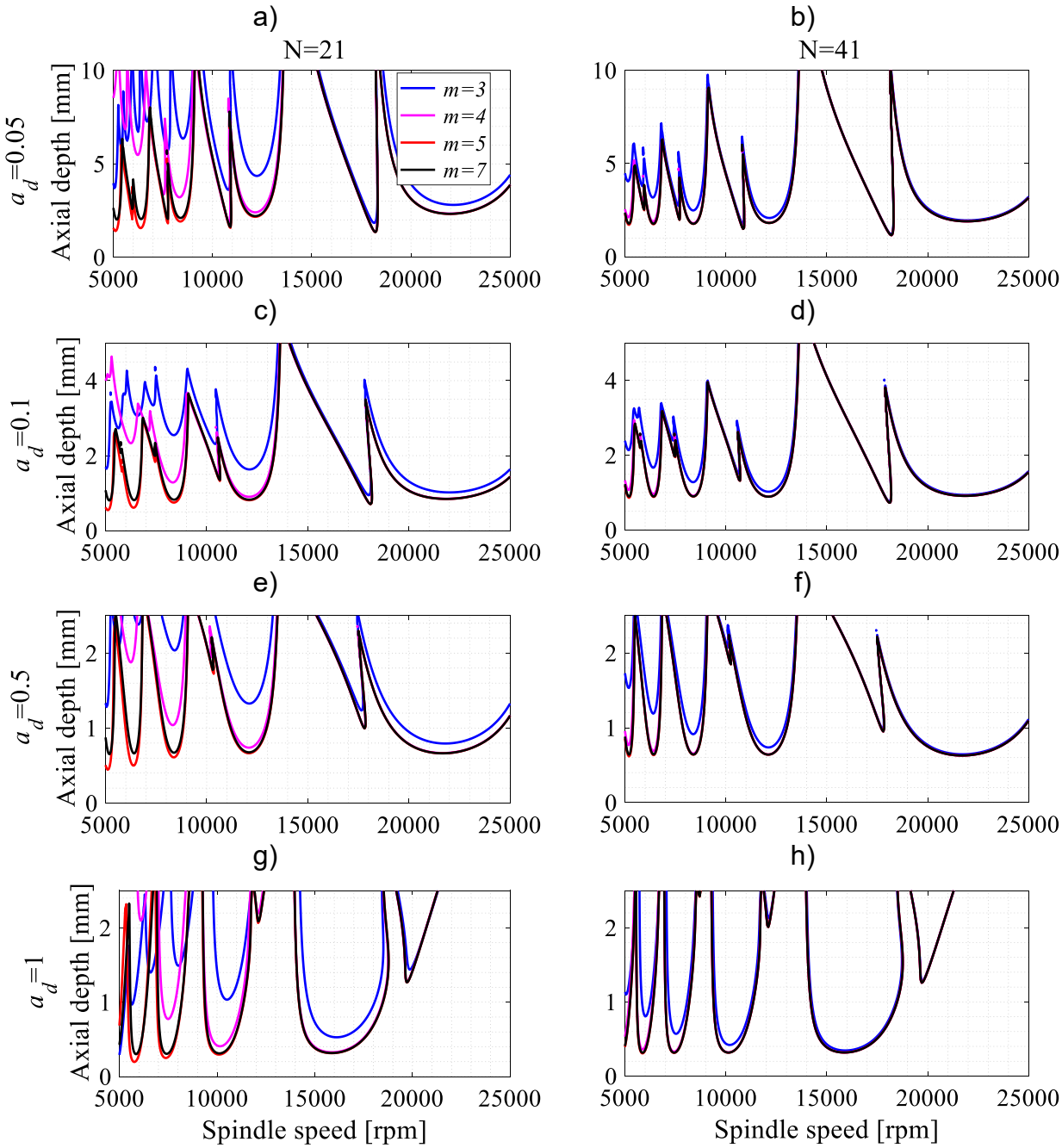

Figure 4.1 Comparison of the order of the solution using the EMHPM with first- order approximation for stability analysis in one degree of freedom

When both columns of Figure 4.1 are compared, it is also observed that, for lower revolutions, the dynamics demands a greater number of discretization to capture the phenomenon in greater detail. However, when increasing the number of discretization, the subintervals become smaller, which, without losing precision, tolerates a lower order of solution and consequently a decrease in the computation time.

In short, when $N = 21$ discretization, the EMHPM converges to a solution when the order of the approximation $m = 5$ but by increasing the number of discretized intervals to $N = 41$, the solution can be converged from $m = 4$ (in magenta color). This is valid regardless of the cut immersion.

EMHPM convergence for milling in ODF

A common practice is to analyze the convergence of the modulus of a certain multiplier of the transition matrix for a specific combination of system parameters [68]. However, here the convergence is analyzed according to the order of the solution as a function of the number of discretization $N = 20, 40, 60, 80, 100$ (see Figure 4.2) by calculating the norm of the matrices of size 11×11 that collect equally spaced combinations of chosen parameters from the mesh of Figure 4.2.

The first, second and third column represents the solution for the first-, second- and third-order EMHPM, and the first, second, third and fourth row represents values of ad 0.05, 0.1, 0.5 and 1 respectively. The purpose is to analyze how the solution order m affects, since as seen in Figure 4.2, when there are lower spindle speeds, a higher order solution is required.

From the analysis of Figure 4.1 it can be deduced that for N=41 discretization and any radial immersion value, it is sufficient to use a fourth order solution m=4 to calculate reliable stability boundaries, since it is observed that higher-order solutions do not provide an improvement over the stability frontiers.

Figure 4.2 was graphed varying the discretization, as well as the order of solution and it was compared against $N = 100$ and $m = 10$ using the square norm.

It is observed that for immersion of 0.05 for first, second and third order, the stability of all the N occurs approximately with $m = 5$, for $a_d = 0.1$ approximately it occurs with $m = 6$, with $a_d = 0.5$ for N>40 the stability also occurs with m=6, while with full immersion for $N > 40$ stability occurs with $m = 8$.

In addition, it is observed that there is no significant difference in the comparison for immersion of $0.05, 0.1$ and 0.5 but for full immersion it is observed that, by increasing the discretization, there is an improvement when going from first order to second and third order.

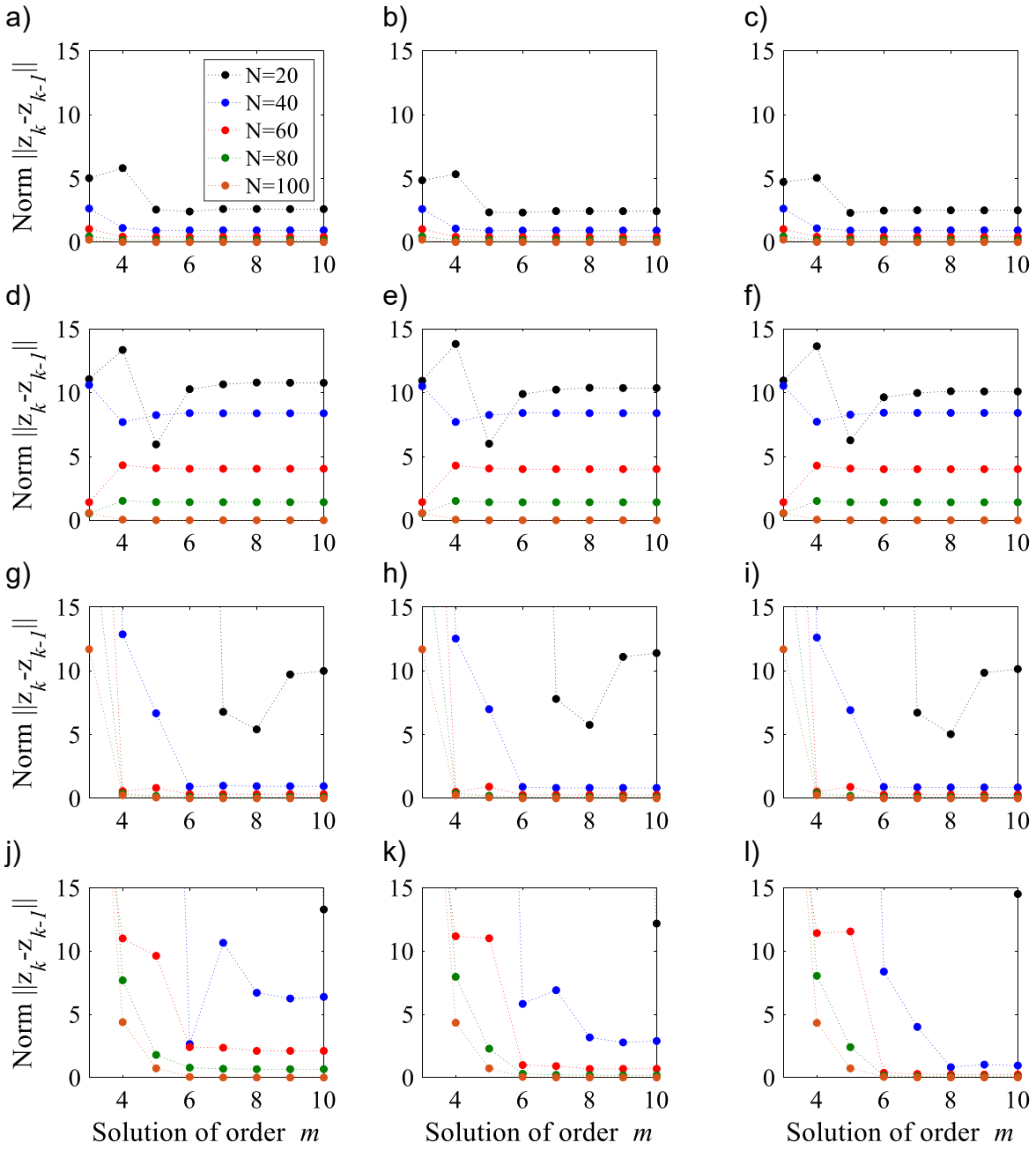

Figure 4.2 Convergence of the EMHPM, first, second and third column represents the solution for the first-, second- and third-order EMHPM, and the first, second, third and fourth row represents values of ad 0.05, 0.1, 0.5 and 1 respectively.

It was decided to analyze how the stability for full immersion behaves when increasing the mesh from 11x11 to 100x100 (Figure 4.3). The results show that when increasing the mesh, the stability for the first order with N=40 looks smoother than with the 11x11, but in the others there is no significant improvement, and considering that the computation time becomes much larger, it is concluded that it is not feasible to increase

the mesh to that degree. The line for $N = 20$ is not observed since it is outside the range shown, and neither does it present an improvement.

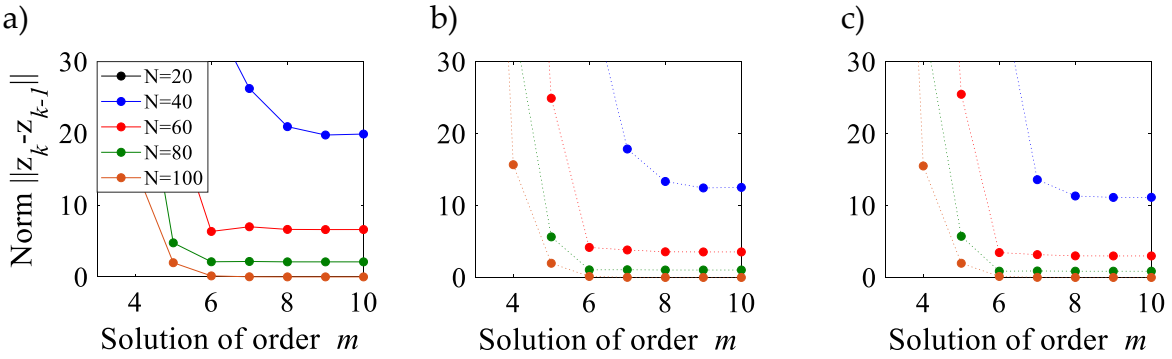

Figure 4.3 Convergence of the EMHPM of a) first-, b) second- and c) third-order for a degree of freedom as the order of the solution varies for different values of discretization for full immersion.

In Figure 4.4 the comparison between the computation times for first, second and third order is shown using $a_d = 0.05$. To obtain the computation time for each order, it was decided to keep $m = 6$, it was analyzed for different discretization and the time obtained was divided between the $11x11$ mesh. It is observed that for small discretization the computation time is slightly longer for third-order, this is because the number of operations carried out with third-order is more; however, by increasing the discretization the difference is smaller, since the operations become recursive and tend to be similar to those of the first and second order.

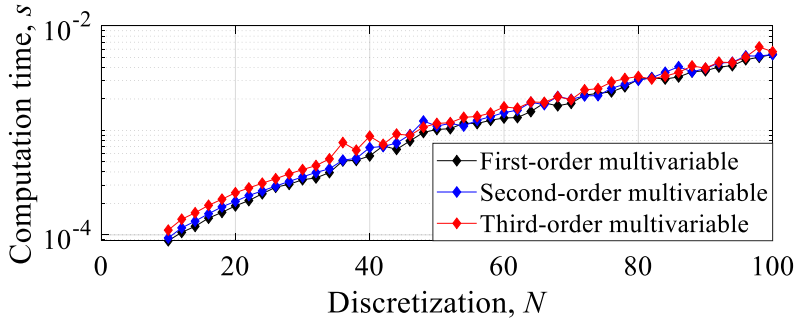

Figure 4.4 Computation time with different discretization for the first-, second-, and third-order solution of the EMHPM with a_d=0.05, m=6 vs the reference with $N = 100$ and $m = 10$.

Since the rate of convergence was proved in Chapter 3 for time-domain simulations, we explored the convergence of the methods applied to the stability analysis. The stability lobes computed with the second- and third-order EMHPM for regular milling tools were compared with its predecessor for radial immersion value of a_d =1 and the other parameters indicated above as it was used in [79].

Figure 4.5 shows the stability diagrams for spindle speed in the range 2000–3000 rev/min where the precision of the method was compromised due to the higher value of the time delay. While the shaded gray area represents the stability lobes computed with N = 200 discrete intervals in all subfigures, in each subfigure solid black lines draw the stability frontier for a specific discrete interval and using the first-, second- or third-order EMHPM. In Figure 4.5 the first, second and third column represents the solution for the first-, the second- and the third-order EMHPM respectively, while the first and the second row was for N = 60 and N = 100 discrete intervals, respectively.

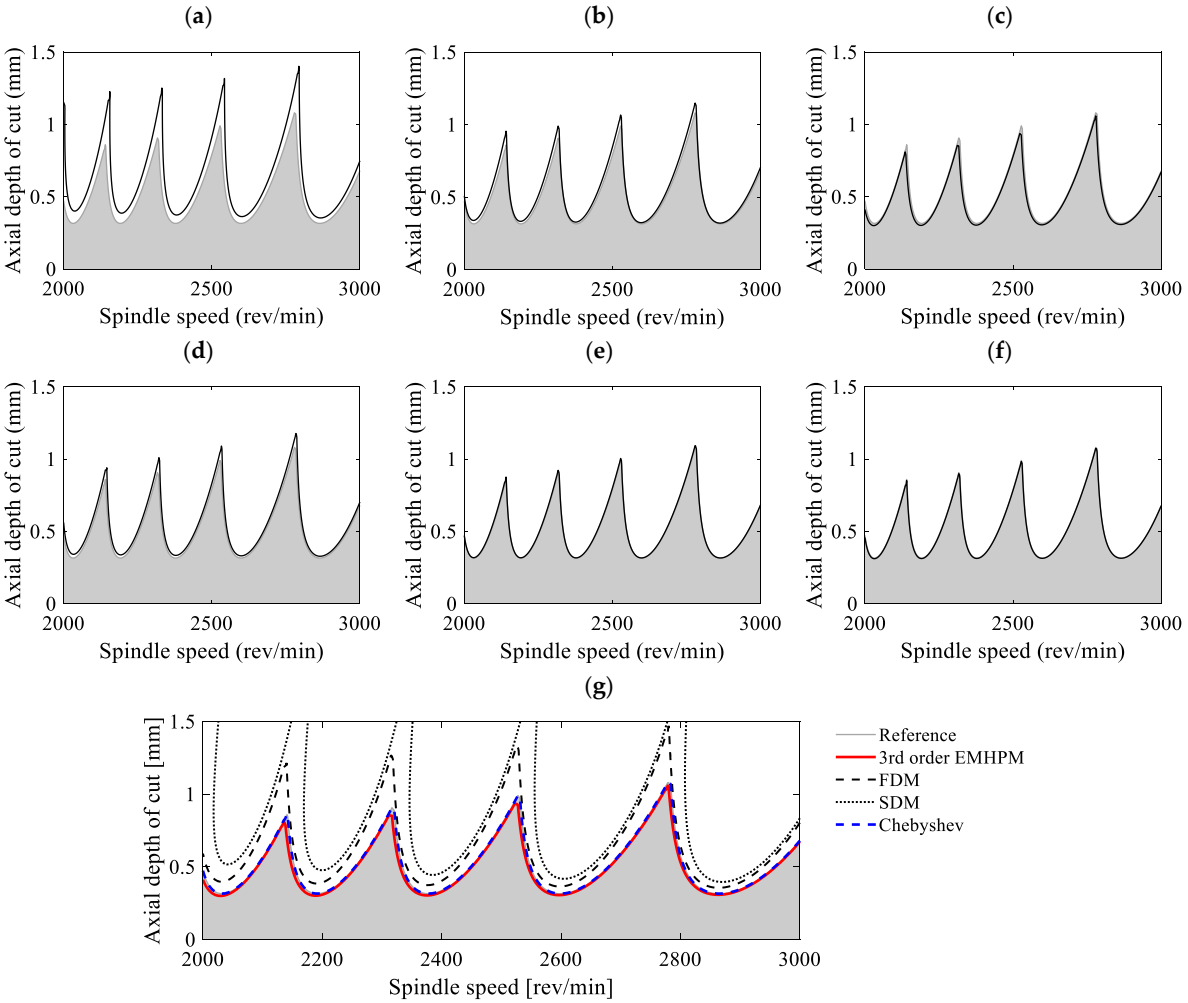

Figure 4.5 Stability diagrams for down-milling operation. The first (a,b,c) and second (d,e,f) rows of subfigures correspond to N = 60 and N = 100 discrete intervals, respectively. First (a,d), second (b,e) and third (c,f) columns correspond to the first-, second- and third-order EMHPM, respectively. Subfigure (g) shows a comparison between the third-order EMHPM (red line), SDM (dot black line), FDM (dash black line), and Chebyshev (dot blue line) methods with N = 60 discrete intervals.

It is observed that the error achieved in the third-order EMHPM was less than those attained for the first-order and second-order EMHPM solutions. This confirms that the third-order EMHPM had the highest rate of convergence.

The results were also compared, in Figure 4.5g, with the semi-discretization method (SDM) presented by Insperger and Stépán in [68] (dot black line) and with the full-discretization method (FDM) presented by Ding et al. in [78] (dash black line), and the Chebyshev collocation method (dot blue line) discussed in [83,84]. It is observed that the EMHPM converged faster than the SDM and FDM, although the solution with the Chebyshev method converges faster.

Table 4.1 list the results for computation times for a different number of discretized intervals together with the absolute error between stability frontiers. Notice that the solution obtained with the EMHPM with N = 60 discrete intervals was faster than the SDM and the FDM and even the error was less in the solution by the EMHPM. For N = 100 discrete intervals the computation time for the FDM was similar to the solution obtained with the EMHPM but it was demonstrated that the solution by second- and third-order EMHPM requires a smaller number of discretized intervals to converge to the solution and using a smaller amount of computation time. Notice the error for the SDM was not calculated since there was no stability frontier in some values of spindle speed.

It is noticeable that exists a significant improvement in the rate of convergence from first-order to second-order and third-order EMHPM, however, the difference between the second- and the third-order EMHPM is negligible if the number of discretized intervals increase. There is no best method between second- and third-order EMHPM in terms of rate of convergence and computation time since the precision depends on the nature of the studied problem. However, it is easy to prove that a higher-order approximation (fourth- and fifth-order EMHPM) could drastically increase the computational time without a significant improvement in the solution. The solution also was compared with the Chebyshev method, which, as far as we know is the method that converges faster.

Table 4.1 Comparison of convergence for different methods for down-milling operation with $\boldsymbol{a_d = 1}$.

Method	$\boldsymbol{N}$ **= 60**		$\boldsymbol{N}$ **= 100**	
	Time (s)	**Error**	**Time (s)**	**Error**
First-order EMHPM	46.98	1.6276	171.03	0.3203
Second-order EMHPM	54.85	0.3507	194.53	0.0568
Third-order EMHPM	60.58	0.3458	208.69	0.0563
FDM	61.26	1.4097	200.49	0.3998
SDM	278.03	-	570.04	-
Chebyshev	36.02	0.0024	90.11	4.385E-13

Chebyshev is a spectral convergence method, but it does not necessarily mean that there is convergence to the solution we are looking for (although for this solution Chebyshev had a faster convergence and precision), Chebyshev is based on a linear theory while the EMHPM allows to solve non-linear problems, in addition the EMHPM has the flexibility to improve the time of computation by decreasing the number of discretization and increasing the order of solution.

It is important to point out that the level of convergence does not depend only on the number of discretization but is a ratio of the natural frequency with respect to the discretization value of the delay. The influence of the size of the subinterval as well as the ratio of the natural frequency with respect to the size of the subinterval are key points.

4.4 Stability of DDE with multiple delays through the EMHPM

The EMHPM can be generalized for stability analysis of DDEs having multiple delays. A multivariable tool contains some of the following characteristics: uneven pitch between teeth, and/or at least one helix angle with a different value from the others. This analysis was developed by Compeán et al., in [85] by using the first-order EMHPM, where the methodology for the characterization of the cutting coefficients for a multivariable tool was discussed, and the dynamic behavior was studied from the productivity point of view. Since the angular spacing at the beginning of the edge is different between teeth (pitch) and the different values of helix angles of the edges between adjacent teeth, the angular spacing between teeth at a specific height changes continuously, which produces an infinite number of delays. A common approach to deal with the DDE with an infinite number of delay is to discretize the tool by cutting disks in the axial direction with a thickness Δa_{dsk} to induce a DDE with a finite number of delays. A single disk still has the same number of flutes (discrete flutes) and considering that the maximum delay in the process is the period of rotation of the tool or the spindle rotation period τ_T, then, it can be discretized in $N-1$ intervals.

The angular position between two adjacent teeth in each cutting disk changes according to the axial position of the referred disk and is related to the expression $\psi = k_\beta a_p$, where $k_\beta = 2\tan\beta/2D$. Here D is the diameter of the tool and ψ represents the cutting-edge offset angle due to the helix angle. A certain interval can be associated with a discrete time delay of each tooth iz and disk l using the following formulation.

$$N_{iz,l} = round\left((N-1)\frac{\delta\phi_{iz,l}}{2\pi}\right) \tag{4.19}$$

where $\delta\phi_{iz,l}$ is the angular pitch between consecutive teeth for each disk, the round function converts the argument to the nearest integer. In (4.19) $N_{iz,}$ is a table (matrix) of dimension $iz \times l$. Since this procedure could generate several delayed terms and some

of them with the same value of discrete time delay due to the discretization scheme, it is required to collect all the different (non-repeated) discrete time delays d_n from $N_{iz,l}$.

So, without losing generality, the DDE with multiple delays is read as

$$\dot{\mathbf{x}}(t) = \mathbf{A}(t)\mathbf{x}(t) + \sum_{d=\min(d_n)}^{\max(d_n)} \mathbf{B}^d \mathbf{x}(t-\tau) \tag{4.20}$$

where $\mathbf{x}$ is the vector of states, $\mathbf{A}(t+\tau_T) = \mathbf{A}(\tau_T)$, $\mathbf{B}^d(t+\tau_T) = \mathbf{B}^d(\tau_T)$ and τ_T is the period of rotation of the spindle. Following the EMHPM procedure, Eq. (4.20) can be written equivalently by intervals as:

$$\dot{\mathbf{x}}_i(T) - \mathbf{A}_t \mathbf{x}_i(T) \approx \sum_{d=\min(d_n)}^{\max(d_n)} \mathbf{B}_t{}^d \mathbf{x}_i^{\tau_d}(T) \tag{4.21}$$

being $\mathbf{x}_i(T)$ the solution by intervals of order m for Eq. (4.20) in the $i-th$ interval that satisfies the initial condition $\mathbf{x}_i(0) = \mathrm{x}_{i-1}$, the matrices $\mathbf{A_t}$ and $\mathbf{B}_t^d$ represent the values of the matrices $\mathbf{A}(t)$ and $\mathbf{B}^d(t)$ evaluated at time t respectively.

Multivariable tool milling stability using First-order EMHPM.

To approximate the term associated with the discrete delays $\boldsymbol{x}_i^{\tau_d}(T)$ of Eq. (4.21), similar to the methodology used for regular tools, the interval of the period τ_T, $[t_0 - \tau_T, t_0]$ is discretized in $N-1$ intervals that can be equal size as seen in Figure 4.6. For simplicity, intervals of equal size $\Delta t = \tau_T/(N-1)$ are chosen. Then it is assumed that the function $\mathbf{x}_i^{\tau_d}$ (T), which is defined in the interval $[t_{i-d-1}, t_{i-d}]$, for the first-order EMHPM has the representation of the form:

$$\mathbf{x}_i^{\tau_d}(T) = \mathbf{x}_{i-d}(T) \approx \mathbf{x}_{i-d-1} + \left(\frac{N-1}{\tau_T}\right) T\left(\mathbf{x}_{i-d} - \mathbf{x}_{i-d-1}\right) \tag{4.22}$$

Defining $\boldsymbol{x_i} \equiv \boldsymbol{x_i}(\boldsymbol{T_i})$ o simplify the notation, and substituting Eq. (4.22) in Eq. (4.21), the following equation is obtained:

$$\dot{\mathbf{x}}_i(T) = \mathbf{A}_t \mathbf{x}_i(T) + \sum_{d=\min(d_n)}^{max(d_n)} \left(\mathbf{B}_t^d \mathbf{x}_{i-d-1} + \mathbf{B}_t^d T \left(\frac{N-1}{\tau}\right)\left(\mathbf{x}_{i-d} - \mathbf{x}_{i-d-1}\right)\right) \tag{4.23}$$

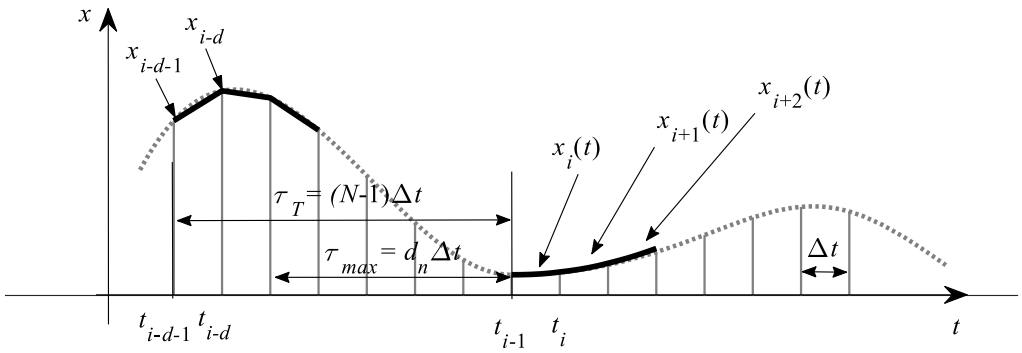

Figure 4.6 Representation of the first-order polynomial approximation for the delay subinterval

where

$$\mathbf{A}_t = \begin{pmatrix} 0 & 1 \\ -\omega_n^2 - \dfrac{\Delta a_{disk}}{m_m} \displaystyle\sum_{d=\min(d_n)}^{\max(d_n)} h_{yy}^d & -2\zeta\omega_n \end{pmatrix}, \ \mathbf{B}_t^{\ d} = \begin{pmatrix} 0 & 0 \\ \dfrac{\Delta a_{disk}}{m_m} \displaystyle\sum_{d=\min(d_n)}^{\max(d_n)} h_{yy}^d & 0 \end{pmatrix} \tag{4.24}$$

here h_{yy} is the specific cutting coefficient, which is calculated depending on the position in time of the tool:

$$h_{yy}(t) = \sum_{iz=1}^{z_n} g\left(\phi_{iz}(t)\right)\cos\phi_{iz}(t)\left(-K_{tc}\sin\phi_{iz}(t) + K_{nc}\cos\phi_{iz}(t)\right) \tag{4.25}$$

Continuing with the EMHPM procedure, it is assumed that the homotopy for the solution of Eq. (4.23) has the form

$$\mathcal{H}\left(\mathbf{X}_i, p\right) = L\left(\ddot{\mathbf{X}}_i\right) - L\left(\ddot{\mathbf{x}}_{i0}\right) + pL\left(\ddot{\mathbf{x}}_{i0}\right) - p\left(\mathbf{A}_t\mathbf{X}_i + \sum_{d=\min(d_n)}^{\max(d_n)}\left(\mathbf{B}_t^d\mathbf{x}_{i-d-1} + \mathbf{B}_t^d T\left(\frac{N-1}{\tau_T}\right)\left(\mathbf{x}_{i-d} - \mathbf{x}_{i-d-1}\right)\right)\right) \tag{4.26}$$

Substituting the expansion of order m, $\boldsymbol{X_i} = \boldsymbol{X_{i0}} + p\boldsymbol{X_{i1}} + p^2\boldsymbol{X_{i2}} + \cdots + p^m$ and considering that the initial condition is equal to the final value of the previous subinterval, that is, $\boldsymbol{x_{i0}} = \boldsymbol{x_{i-1}}$, and $\boldsymbol{x_{i1}}(0) = \boldsymbol{x_{i2}}(0) = \cdots = \boldsymbol{x_{im}}(0) = 0$, it is obtained:

$$\begin{aligned}\mathcal{H}\left(\mathbf{X}_i, p\right) = &\left(\ddot{\mathbf{X}}_{i0} + p\ddot{\mathbf{X}}_{i1} + p^2\ddot{\mathbf{X}}_{i2} + \ldots + p^m\ddot{\mathbf{X}}_{im}\right) - \left(\ddot{\mathbf{x}}_{i0}\right) + p\left(\ddot{\mathbf{x}}_{i0}\right) - p\Big[\mathbf{A}_t\left(\mathbf{X}_{i0} + p\mathbf{X}_{i1} + p^2\mathbf{X}_{i2} + \right. \\ &\left. \ldots + p^m\mathbf{X}_{im}\right) + \sum_{d=\min(d_n)}^{\max(d_n)}\left(\mathbf{B}_t^d\mathbf{x}_{i-d-1} + \mathbf{B}_t^d T\left(\frac{N-1}{\tau_T}\right)\left(\mathbf{x}_{i-d} - \mathbf{x}_{i-d-1}\right)\right)\Big]\end{aligned} \tag{4.27}$$

grouping by powers of p:

$$
\begin{aligned}
&p^0:\ \dot{\mathbf{X}}_{i0}-\dot{\mathbf{x}}_{i0}=0,\ \dot{\mathbf{X}}_{i0}-\dot{\mathbf{x}}_{i-1}=0, && \mathbf{X}_{i0}(0)=\mathbf{x}_{i-1}\\
&p^1:\ \dot{\mathbf{X}}_{i1}+\dot{\mathbf{x}}_{i0}=\mathbf{A}_t\mathbf{X}_{i0}+\sum_{d=\min(d_n)}^{\max(d_n)}\left(\mathbf{B}_t^d\mathbf{x}_{i-d-1}+\mathbf{B}_t^d T\left(\frac{N-1}{\tau_T}\right)\left(\mathbf{x}_{i-d}-\mathbf{x}_{i-d+1}\right)\right), && \mathbf{X}_{i1}(0)=0\\
&p^2:\ \dot{\mathbf{X}}_{i2}=\mathbf{A}\mathbf{X}_{i1}, && \mathbf{X}_{i2}(0)=0\\
&\vdots\\
&p^m:\ \dot{\mathbf{X}}_{im}=\mathbf{A}\mathbf{X}_{i(m-1)}, && \mathbf{X}_{im}(0)=0
\end{aligned}
\tag{4.28}
$$

by solving (4.28), we get

$$
\begin{aligned}
&\mathbf{X}_{i0}=\mathbf{x}_{i-1}\\
&\mathbf{X}_{i1}=T\mathbf{A}_t\left(\mathbf{x}_{i-1}\right)+\sum_{d=\min(d_n)}^{\max(d_n)}\left(TB_t^{\,d}\left(\mathbf{x}_{i-d-1}\right)+B_t^{\,d}\frac{T^2}{2}\left(\frac{N-1}{\tau_T}\right)\left(\mathbf{x}_{i-d}-\mathbf{x}_{i-d-1}\right)\right)\\
&\mathbf{X}_{i2}=\frac{T^2}{2}\mathbf{A}_t^{\,2}\left(\mathbf{x}_{i-1}\right)+\mathbf{A}_t\sum_{d=\min(d_n)}^{\max(d_n)}\left(\frac{T^2}{2}B_t^{\,d}\left(\mathbf{x}_{i-d-1}\right)+B_t^{\,d}\frac{T^3}{6}\left(\frac{N-1}{\tau_T}\right)\left(\mathbf{x}_{i-d}-\mathbf{x}_{i-d-1}\right)\right)\\
&\vdots\\
&\mathbf{X}_{ik}=\frac{1}{k!}T^k\mathbf{A}_t^{\,k}\left(\mathbf{x}_{i-1}\right)+\mathbf{A}_t^{\,k-1}\sum_{d=\min(d_n)}^{\max(d_n)}\left(\frac{1}{k!}T^k\mathbf{B}_t^{\,d}\left(\mathbf{x}_{i-d-1}\right)+\frac{1}{(k+1)!}T^{k+1}\mathbf{B}_t^{\,d}\left(\frac{N-1}{\tau_T}\right)\left(\mathbf{x}_{i-d}-\mathbf{x}_{i-d-1}\right)\right)
\end{aligned}
\tag{4.29}
$$

Eq. (4.29) can be written recursively as

$$
\mathbf{X}_{ik}=\mathbf{X}_{ik}^a+\mathbf{X}_{ik}^b, k=1,2,3....
\tag{4.30}
$$

where $\mathbf{X}_{i0}^a=\mathbf{x}_{i-1},\mathbf{X}_{i0}^b,=0$ and

$$
\begin{aligned}
\mathbf{X}_{ik}^a&=\frac{T}{k}\left(\mathbf{A}_t\mathbf{X}_{i(k-1)}^a+g(k)\sum_{d=\min(d_n)}^{\max(d_n)}\mathbf{B}_t^d\mathbf{x}_{i-d-1}\right)\\
\mathbf{X}_{ik}^b&=\frac{T}{k+1}\left(\mathbf{A}_t\mathbf{X}_{i(k-1)}^b+g(k)\sum_{d=\min(d_n)}^{\max(d_n)}\left(\frac{N-1}{\tau}\right)\mathbf{B}_t^d T\left(\mathbf{x}_{i-d}-\mathbf{x}_{i-d-1}\right)\right)
\end{aligned}
\tag{4.31}
$$

the solution of order m for Eq. (4.23) is obtained by adding each of the approximations k of Eq. (4.30).

Similar to Eq. (4.3), to obtain the stability graphs of Eq. (4.20) the solution of Eq. (4.30) is rewritten by grouping the discrete states, which results:

$$
\mathbf{x}_i(T)\approx\mathbf{P}_i(T)\mathbf{x}_{(i-1)}+\sum_{d=\min(d_n)}^{\max(d_n)}\left(\mathbf{Q}_i^d(T)\mathbf{x}_{i-d}+\mathbf{R}_i^d(T)\mathbf{x}_{i-d-1}\right)
\tag{4.32}
$$

where

$$\begin{aligned}
\mathbf{P}_i(T) &= \sum_{k=0}^{m} \frac{1}{k!}\mathbf{A}_t^k T^k, \\
\mathbf{Q}_i^d(T) &= \sum_{k=1}^{m}\left(\frac{1}{(k+1)!}\left(\frac{N-1}{\tau_T}\right)\mathbf{A}_t^{k-1}\mathbf{B}_t^d T^{k+1}\right), \quad m \geq 1 \\
\mathbf{R}_i^d(T) &= \sum_{k=1}^{m} \frac{1}{k!}\mathbf{A}_t^{k-1}\mathbf{B}_t^d T^k - \mathbf{Q}_i^d, \qquad m \geq 1
\end{aligned} \tag{4.33}$$

the approximate solution using the EMHPM given by Eq. (4.32) is used to define a discrete map such as shown in (4.9), with a matrix of coefficients $\boldsymbol{D}_i$ with dimension $(N-1)(z_n) \times (N-1)(z_n)$. The coefficients of the matrix $\boldsymbol{D}_i$ are given by:

$$D_i = \begin{bmatrix}
P_i & 0 & 0 & \cdots & Q_i^1 & R_i^1 & \cdots & Q_i^2 & R_i^2 & \cdots & Q_i^{d_n} & R_i^{d_n} & \cdots & 0 \\
I & 0 & 0 & \cdots & 0 & 0 & \cdots & 0 & 0 & \cdots & 0 & 0 & \cdots & 0 \\
0 & I & 0 & \cdots & 0 & 0 & \cdots & 0 & 0 & \cdots & 0 & 0 & \cdots & 0 \\
0 & 0 & I & \cdots & 0 & 0 & \cdots & 0 & 0 & \cdots & 0 & 0 & \cdots & 0 \\
0 & 0 & 0 & \ddots & 0 & 0 & \cdots & 0 & 0 & \cdots & 0 & 0 & \cdots & 0 \\
\vdots & \vdots & \vdots & \vdots & I & 0 & \cdots & 0 & 0 & \cdots & 0 & 0 & \cdots & 0 \\
0 & 0 & 0 & \cdots & 0 & I & \cdots & 0 & 0 & \cdots & 0 & 0 & \cdots & 0 \\
0 & 0 & 0 & \cdots & 0 & 0 & \ddots & 0 & 0 & \cdots & 0 & 0 & \cdots & 0 \\
0 & 0 & 0 & \cdots & 0 & 0 & \cdots & I & 0 & \cdots & 0 & 0 & \cdots & 0 \\
0 & 0 & 0 & \cdots & 0 & 0 & \cdots & 0 & I & \cdots & 0 & 0 & \cdots & 0 \\
0 & 0 & 0 & \cdots & 0 & 0 & \cdots & 0 & 0 & \ddots & 0 & 0 & \cdots & 0 \\
0 & 0 & 0 & \cdots & 0 & 0 & \cdots & 0 & 0 & \cdots & I & 0 & \cdots & 0 \\
\vdots & \vdots & \vdots & \cdots & \vdots & \vdots & \cdots & \vdots & \vdots & \cdots & \vdots & I & \cdots & \vdots \\
0 & 0 & 0 & \cdots & 0 & 0 & \cdots & 0 & 0 & 0 & 0 & 0 & \cdots & 0
\end{bmatrix} \tag{4.34}$$

The transition matrix $\boldsymbol{\Phi}$ over the period $\tau_T = (N-1)/\Delta t$ is determined by coupling each solution x_i through the discrete map $\boldsymbol{D}_i$, $i = 1, 2, \ldots, (N-1)$. However, it is important to note that the computational cost can be significantly reduced by computing only the transition matrix up to the maximum delay without losing precision in the calculation of the eigenvalues:

$$\boldsymbol{\Phi} = \mathbf{D}_{N\max}\mathbf{D}_{N\max-1}\ldots\mathbf{D}_2\mathbf{D}_1 \tag{4.35}$$

The stability graphs of Eq. (4.20) are determined by computing the eigenvalues of the transition matrix calculated by Eq. (4.35).

Multivariable tool milling stability using Second Order EMHPM.

Following a similar procedure to that used for the multivariate tool with first-order EMHPM, the stability prediction for the multivariate tool with second-order EMHPM can be performed.

To approximate the term associated with the discrete delays $\boldsymbol{x}_i^{\tau_d}(T)$ of Eq. (4.21), the interval of the period $\tau_T, [t_0 - \tau_T, t_0]$ is discretized in $N-1$ subintervals. Figure 4.7 schematize the second-order polynomial approximation.

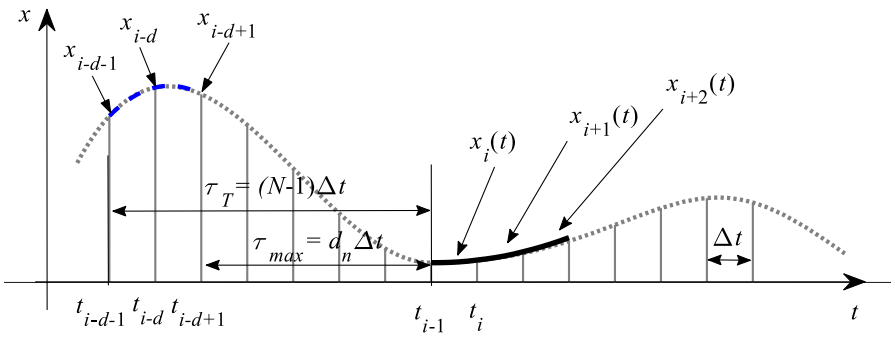

Figure 4.7 Representation of the second-order polynomial approximation for the delay subinterval.

Then it is assumed that the function $\boldsymbol{x}_i^{\tau_d}(T)$, which is defined in the subinterval $[t_{i-d-1}, t_{i-d+1}]$, for the second order EMHPM has the representation of the form:

$$\mathbf{x}_i^{\tau_d}(T) \approx \mathbf{x}_{i-d-1} + \left(\frac{N-1}{\tau_T}\right) T\left(-\frac{3}{2}\left(\mathbf{x}_{i-d-1}\right) + 2\left(\mathbf{x}_{i-d}\right) - \frac{1}{2}\left(\mathbf{x}_{i-d+1}\right)\right) + \left(\frac{N-1}{\tau_T}\right)^2 \frac{T^2}{2}\left(\mathbf{x}_{i-d-1} - 2\mathbf{x}_{i-d} + \mathbf{x}_{i-d+1}\right) \tag{4.36}$$

Defining $\boldsymbol{x}_i \equiv \boldsymbol{x}_i(T_i)$ to simplify the notation, and substituting Eq. (4.36) in Eq. (4.21), the following equation is obtained:

$$\dot{\mathbf{x}}_i(T) = \mathbf{A}_i \mathbf{x}_i(T) + \sum_{d=\min(d_n)}^{\max(d_n)} \left(\begin{array}{l} \mathbf{B}_t^d \mathbf{x}_{i-d-1} + \mathbf{B}_t^d T\left(\frac{N-1}{\tau_T}\right)\left(-\frac{3}{2}\left(\mathbf{x}_{i-d-1}\right) + 2\left(\mathbf{x}_{i-d}\right) - \frac{1}{2}\left(\mathbf{x}_{i-d+1}\right)\right) + \\ \mathbf{B}_t^d \frac{T^2}{2}\left(\frac{N-1}{\tau_T}\right)^2 \left(\mathbf{x}_{i-d-1} - 2\mathbf{x}_{i-d} + \mathbf{x}_{i-d+1}\right) \end{array} \right) \tag{4.37}$$

Continuing with the HPM, and substituting the expansion of order m, $\boldsymbol{X}_i = \boldsymbol{X}_{i0} + p\boldsymbol{X}_{i1} + p^2\boldsymbol{X}_{i2} + \cdots + p^m$, considering that the initial condition is equal to the final value of the previous subinterval, that is, $\boldsymbol{x}_{i0} = \boldsymbol{x}_{i-1}$, and $\boldsymbol{x}_{i1}(0) = \boldsymbol{x}_{i2}(0) = \cdots = \boldsymbol{x}_{im}(0) = 0$, (4.37) has the form:

$$\begin{aligned}\mathcal{H}\left(\mathbf{X}_i, p\right) = &\left(\dot{\mathbf{X}}_{i0} + p\dot{\mathbf{X}}_{i1} + p^2\dot{\mathbf{X}}_{i2} + \ldots + p^m\dot{\mathbf{X}}_{im}\right) - \left(\dot{\mathbf{x}}_{i0}\right) + p\left(\dot{\mathbf{x}}_{i0}\right) - p\Big[\mathbf{A}_t\left(\mathbf{X}_{i0} + p\mathbf{X}_{i1} + p^2\mathbf{X}_{i2} + \ldots + p^m\mathbf{X}_{im}\right) \\ &+ \sum_{d=\min(d_n)}^{\max(d_n)} \begin{pmatrix} \mathbf{B}_t^d\mathbf{x}_{i-d-1} + \mathbf{B}_t^d T\left(\dfrac{N-1}{\tau_T}\right)\left(-\dfrac{3}{2}\left(\mathbf{x}_{i-d-1}\right) + 2\left(\mathbf{x}_{i-d}\right) - \dfrac{1}{2}\left(\mathbf{x}_{i-d+1}\right)\right) + \\ \mathbf{B}_t^d\dfrac{T^2}{2}\left(\dfrac{N-1}{\tau_T}\right)^2\left(\mathbf{x}_{i-d-1} - 2\mathbf{x}_{i-d} + \mathbf{x}_{i-d+1}\right) \end{pmatrix}\Big]\end{aligned} \tag{4.38}$$

after applying the EMHPM to solve the set of second-order differential delay equations, we get:

$$\begin{aligned}&\mathbf{X}_{i0} = \mathbf{x}_{i-1} \\ &\mathbf{X}_{i1} = T\mathbf{A}_t\left(\mathbf{x}_{i-1}\right) + \sum_{d=\min(d_n)}^{\max(d_n)} \begin{pmatrix} T\mathbf{B}_t^d\left(\mathbf{x}_{i-d-1}\right) + \mathbf{B}_t^d\dfrac{T^2}{2}\left(\dfrac{N-1}{\tau_T}\right)\left(-\dfrac{3}{2}\left(\mathbf{x}_{i-d-1}\right) + 2\left(\mathbf{x}_{i-d}\right) - \dfrac{1}{2}\left(\mathbf{x}_{i-d+1}\right)\right) + \\ \mathbf{B}_t^d\dfrac{T^3}{6}\left(\dfrac{N-1}{\tau_T}\right)^2\left(\mathbf{x}_{i-d-1} - 2\mathbf{x}_{i-d} + \mathbf{x}_{i-d+1}\right) \end{pmatrix} \\ &\mathbf{X}_{i2} = \frac{T^2}{2}\mathbf{A}_t{}^2\left(\mathbf{x}_{i-1}\right) + \mathbf{A}_t\sum_{d=\min(d_n)}^{\max(d_n)} \begin{pmatrix} \dfrac{T^2}{2}\mathbf{B}_t^d\left(z_{i-d-1}\right) + \mathbf{B}_t^d\dfrac{T^3}{6}\left(\dfrac{N-1}{\tau_T}\right)\left(-\dfrac{3}{2}\left(\mathbf{x}_{i-d-1}\right) + 2\left(\mathbf{x}_{i-d}\right) - \dfrac{1}{2}\left(\mathbf{x}_{i-d+1}\right)\right) + \\ \mathbf{B}_t^d\dfrac{T^4}{24}\left(\dfrac{N-1}{\tau_T}\right)^2\left(\mathbf{x}_{i-d-1} - 2\mathbf{x}_{i-d} + \mathbf{x}_{i-d+1}\right) \end{pmatrix} \\ &\vdots \\ &\mathbf{X}_{ik} = \frac{1}{k!}T^k\mathbf{A}_t^k\left(\mathbf{x}_{i-1}\right) + \mathbf{A}_t{}^{k-1}\sum_{d=\min(d_n)}^{\max(d_n)} \begin{pmatrix} \dfrac{1}{k!}T^k\mathbf{B}_t^d\left(z_{i-d-1}\right) + \dfrac{1}{(k+1)!}T^{k+1}\mathbf{B}_t^d\left(\dfrac{N-1}{\tau_T}\right)\left(-\dfrac{3}{2}\left(\mathbf{x}_{i-d-1}\right) + 2\left(\mathbf{x}_{i-d}\right) - \right. \\ \left.\dfrac{1}{2}\left(\mathbf{x}_{i-d+1}\right)\right) + \dfrac{1}{(k+2)!}T^{k+2}\mathbf{B}_t^d\left(\dfrac{N-1}{\tau_T}\right)^2\left(\mathbf{x}_{i-d-1} - 2\mathbf{x}_{i-d} + \mathbf{x}_{i-d+1}\right) \end{pmatrix}\end{aligned} \tag{4.39}$$

Eq. (4.39) can be written recursively as

$$\mathbf{X}_{ik} = \mathbf{X}_{ik}^a + \mathbf{X}_{ik}^b + \mathbf{X}_{ik}^c, k = 1, 2, 3.... \tag{4.40}$$

where $\boldsymbol{X}_{i0}^a = \boldsymbol{x}_{i-1}, \boldsymbol{X}_{i0}^b, = \boldsymbol{X}_{i0}^c = 0$ and

$$\begin{aligned}
\mathbf{X}_{ik}^{a} &= \frac{T}{k}\left(\mathbf{A}_t\mathbf{X}_{i(k-1)}^{a} + g(k)\sum_{d=\min(d_n)}^{\max(d_n)}\mathbf{B}_t^{d}\mathbf{x}_{i-d-1}\right)\\
\mathbf{X}_{ik}^{b} &= \frac{T}{k+1}\left(\mathbf{A}_t\mathbf{X}_{i(k-1)}^{b} + g(k)\sum_{d=\min(d_n)}^{\max(d_n)}\left(\frac{N-1}{\tau}\right)\mathbf{B}_t^{d}T\left(-\frac{3}{2}\left(\mathbf{x}_{i-d-1}\right)+2\left(\mathbf{x}_{i-d}\right)-\frac{1}{2}\left(\mathbf{x}_{i-d+1}\right)\right)\right)\\
\mathbf{X}_{ik}^{c} &= \frac{T}{k+2}\left(\mathbf{A}_t\mathbf{X}_{i(k-1)}^{c} + g(k)\sum_{d=\min(d_n)}^{\max(d_n)}\left(\frac{N-1}{\tau}\right)^{2}\mathbf{B}_t^{d}\frac{T^2}{2}\left(\mathbf{x}_{i-d-1}-2\mathbf{x}_{i-d}+\mathbf{x}_{i-d+1}\right)\right)
\end{aligned} \tag{4.41}$$

the solution of order m for Eq. (4.37) is obtained by adding each of the approximations k of Eq. (4.40).

Similar to Eq. (4.5), to obtain the stability graphs, the solution of Eq. (4.40). is rewritten by grouping the discrete states, which results in:

$$\mathbf{x}_i(T) \approx \mathbf{P}_i(T)\mathbf{x}_{(i-1)} + \sum_{d=\min(d_n)}^{\max(d_n)}\left(\mathbf{Q}_i^{'d}(T)\mathbf{x}_{i-d+1} + \mathbf{Q}_i^{d}(T)\mathbf{x}_{i-d} + \mathbf{R}_i^{d}(T)\mathbf{x}_{i-d-1}\right) \tag{4.42}$$

where

$$\begin{aligned}
\mathbf{P}_i(T) &= \sum_{k=0}^{m}\frac{1}{k!}\mathbf{A}_t^{k}T^{k},\\
\mathbf{Q}_i^{'d}(T) &= \sum_{k=1}^{m}\left(-\frac{1}{2(k+1)!}\left(\frac{N-1}{\tau_T}\right)\mathbf{A}_t^{k-1}\mathbf{B}_t^{d}T^{k+1} + \frac{1}{(k+2)!}\left(\frac{N-1}{\tau_T}\right)^{2}\mathbf{A}_t^{k-1}\mathbf{B}_t^{d}T^{k+2}\right)\\
\mathbf{Q}_i^{d}(T) &= \sum_{k=1}^{m}\left(\frac{1}{(k+1)!}\left(\frac{N-1}{\tau_T}\right)\mathbf{A}_t^{k-1}\mathbf{B}_t^{d}T^{k+1}\right) - 2\mathbf{Q}_i^{'d}\\
\mathbf{R}_i^{d}(T) &= \sum_{k=1}^{m}\frac{1}{k!}\mathbf{A}_t^{k-1}\mathbf{B}_t^{d}T^{k} - \mathbf{Q}_i^{'d} - \mathbf{Q}_i^{d}
\end{aligned} \tag{4.43}$$

The approximate solution given by Eq. (4.42) is used to define a discrete map following the same procedure as semi-discretization method in [68], as showed in the solution of the first-order EMHPM presented above.

Multivariable tool milling stability using Third-order EMHPM.

In a similar way to the solution described for the second order EMHPM, it is performed for the third order approximation as observed in Figure 4.8.

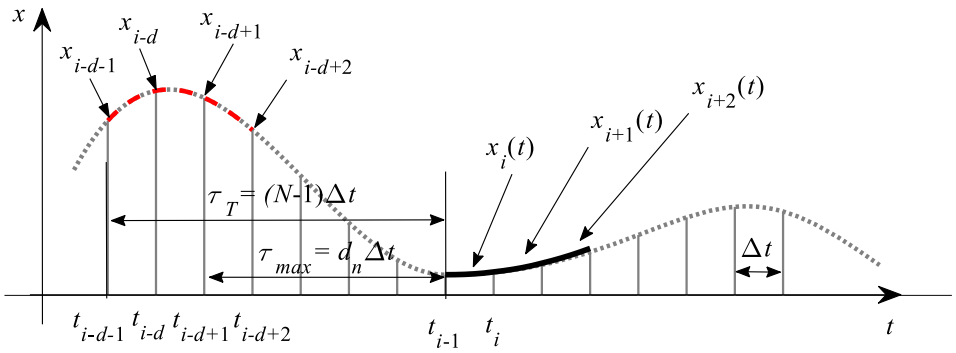

Figure 4.8 Representation of the third-order polynomial approximation for the delay subinterval.

It is assumed that the function $\mathbf{x}_i^{\tau_d}(T)$, which is defined in the interval $[t_{i-d-1}, t_{i-d+2}]$, for the third-order EMHPM has the representation of the form:

$$\begin{aligned}\mathbf{x}_i^{\tau_d}(T) \approx \mathbf{x}_{i-d-1} &+ \left(\frac{N-1}{\tau_T}\right) T\left(-\frac{11}{6}(\mathbf{x}_{i-d-1}) + 3(\mathbf{x}_{i-d}) - \frac{3}{2}(\mathbf{x}_{i-d+1}) + \frac{1}{3}(\mathbf{x}_{i-d+2})\right) + \\ &\left(\frac{N-1}{\tau_T}\right)^2 \frac{T^2}{2}\left(2(\mathbf{x}_{i-d-1}) - 5(\mathbf{x}_{i-d}) + 4(\mathbf{x}_{i-d+1}) - (\mathbf{x}_{i-d+2})\right) + \\ &\left(\frac{N-1}{\tau_T}\right)^3 \frac{T^3}{6}\left(-\mathbf{x}_{i-d-1} + 3(\mathbf{x}_{i-d}) - 3(\mathbf{x}_{i-d+1}) + \mathbf{x}_{i-d+2}\right)\end{aligned} \tag{4.44}$$

Defining $\mathbf{x}_i \equiv \mathbf{x}_i(T_i)$ to simplify the notation, and substituting (4.44) in Eq. (4.21), the following equation is obtained:

$$\dot{\mathbf{x}}_i(T) = \mathbf{A}_t \mathbf{x}_i(T) + \sum_{d=\min(d_n)}^{max(d_n)} \begin{pmatrix} \mathbf{B}_t^{\,d}\mathbf{x}_{i-d-1} + \mathbf{B}_t^{\,d} T\left(\frac{N-1}{\tau_T}\right)\left(-\frac{11}{6}(\mathbf{x}_{i-d-1}) + 3(\mathbf{x}_{i-d}) - \frac{3}{2}(\mathbf{x}_{i-d+1}) + \frac{1}{3}(\mathbf{x}_{i-d+2})\right) + \\ \mathbf{B}_t^{\,d}\frac{T^2}{2}\left(\frac{N-1}{\tau_T}\right)^2\left(2(\mathbf{x}_{i-d-1}) - 5(\mathbf{x}_{i-d}) + 4(\mathbf{x}_{i-d+1}) - \mathbf{x}_{i-d+2}\right) + \\ \mathbf{B}_t^{\,d}\frac{T^3}{6}\left(\frac{N-1}{\tau_T}\right)^3\left(-\mathbf{x}_{i-d-1} + 3(\mathbf{x}_{i-d}) - 3(\mathbf{x}_{i-d+1}) + \mathbf{x}_{i-d+2}\right) \end{pmatrix} \tag{4.45}$$

by solving Eq. (4.45), we get

$$\mathbf{X}_{i0} = \mathbf{x}_{i-1}$$

$$\mathbf{X}_{i1} = T\mathbf{A}_t\left(\mathbf{x}_{i-1}\right) + \sum_{d=\min(d_n)}^{\max(d_n)} \begin{pmatrix} TB_t^{\,d}\left(\mathbf{x}_{i-d-1}\right) + B_t^{\,d}\dfrac{T^2}{2}\left(\dfrac{N-1}{\tau_T}\right)\left(-\dfrac{11}{6}\left(\mathbf{x}_{i-d-1}\right)+3\left(\mathbf{x}_{i-d}\right)-\dfrac{3}{2}\left(\mathbf{x}_{i-d+1}\right)+\dfrac{1}{3}\left(\mathbf{x}_{i-d+2}\right)\right) \\ +B_t^{\,d}\dfrac{T^3}{6}\left(\dfrac{N-1}{\tau_T}\right)^2\left(2\left(\mathbf{x}_{i-d-1}\right)-5\left(\mathbf{x}_{i-d}\right)+4\left(\mathbf{x}_{i-d+1}\right)-\mathbf{x}_{i-d+2}\right) \\ +B_t^{\,d}\dfrac{T^4}{24}\left(\dfrac{N-1}{\tau_T}\right)^3\left(-\mathbf{x}_{i-d-1}+3\left(\mathbf{x}_{i-d}\right)-3\left(\mathbf{x}_{i-d+1}\right)+\mathbf{x}_{i-d+2}\right) \end{pmatrix}$$

$$\mathbf{X}_{i2} = \frac{T^2}{2}\mathbf{A}_t^{\,2}\left(\mathbf{x}_{i-1}\right) + \mathbf{A}_t \sum_{d=\min(d_n)}^{\max(d_n)} \begin{pmatrix} \dfrac{T^2}{2}B_t^{\,d}\left(\mathbf{x}_{i-d-1}\right) + B_t^{\,d}\dfrac{T^3}{6}\left(\dfrac{N-1}{\tau_T}\right)\left(-\dfrac{11}{6}\left(\mathbf{x}_{i-d-1}\right)+3\left(\mathbf{x}_{i-d}\right)-\dfrac{3}{2}\left(\mathbf{x}_{i-d+1}\right)+\dfrac{1}{3}\left(\mathbf{x}_{i-d+2}\right)\right)+ \\ B_t^{\,d}\dfrac{T^4}{24}\left(\dfrac{N-1}{\tau_T}\right)^2\left(2\left(\mathbf{x}_{i-d-1}\right)-5\left(\mathbf{x}_{i-d}\right)+4\left(\mathbf{x}_{i-d+1}\right)-\mathbf{x}_{i-d+2}\right)+ \\ B_t^{\,d}\dfrac{T^5}{120}\left(\dfrac{N-1}{\tau_T}\right)^3\left(-\mathbf{x}_{i-d-1}+3\left(\mathbf{x}_{i-d}\right)-3\left(\mathbf{x}_{i-d+1}\right)+\mathbf{x}_{i-d+2}\right) \end{pmatrix}$$

$$\vdots$$

$$\mathbf{X}_{ik} = \frac{1}{k!}T^k\mathbf{A}_t^{\,k}\left(\mathbf{x}_{i-1}\right) + \mathbf{A}_t^{\,k-1}\sum_{d=\min(d_n)}^{\max(d_n)} \begin{pmatrix} \dfrac{1}{k!}T^k\mathbf{B}_t^{\,d}\left(\mathbf{x}_{i-d-1}\right) + \dfrac{1}{(k+1)!}T^{k+1}\mathbf{B}_t^{\,d}\left(\dfrac{N-1}{\tau_T}\right)\left(-\dfrac{11}{6}\left(\mathbf{x}_{i-d-1}\right)+3\left(\mathbf{x}_{i-d}\right)-\dfrac{3}{2}\left(\mathbf{x}_{i-d+1}\right)+\right. \\ \left.\dfrac{1}{3}\left(\mathbf{x}_{i-d+2}\right)\right)+\dfrac{1}{(k+2)!}T^{k+2}B_t^{\,d}\left(\dfrac{N-1}{\tau_T}\right)^2\left(2\left(\mathbf{x}_{i-d-1}\right)-5\left(\mathbf{x}_{i-d}\right)+4\left(\mathbf{x}_{i-d+1}\right)-\mathbf{x}_{i-d+2}\right)+ \\ \dfrac{1}{(k+3)!}T^{k+3}\mathbf{B}_t^{\,d}\left(\dfrac{N-1}{\tau_T}\right)^3\left(-\mathbf{x}_{i-d-1}+3\left(\mathbf{x}_{i-d}\right)-3\left(\mathbf{x}_{i-d+1}\right)+\mathbf{x}_{i-d+2}\right) \end{pmatrix} \tag{4.46}$$

Eq. (4.46) can be written recursively as

$$\mathbf{X}_{ik} = \mathbf{X}_{ik}^a + \mathbf{X}_{ik}^b + \mathbf{X}_{ik}^c + \mathbf{X}_{ik}^d, k = 1,2,3.... \tag{4.47}$$

where $\mathbf{X}_{i0}^a = \mathbf{x}_{i-1}, \mathbf{X}_{i0}^b, = \mathbf{X}_{i0}^c = \mathbf{X}_{i0}^d = 0$ and

$$\begin{aligned}
\mathbf{X}_{ik}^a &= \frac{T}{k}\left(\mathbf{A}_t\mathbf{X}_{i(k-1)}^a + g\left(k\right)\sum_{d=\min(d_n)}^{\max(d_n)}\mathbf{B}_t^d\mathbf{x}_{i-d-1}\right) \\
\mathbf{X}_{ik}^b &= \frac{T}{k+1}\left(\mathbf{A}_t\mathbf{X}_{i(k-1)}^b + g(k)\sum_{d=\min(d_n)}^{\max(d_n)}\left(\frac{N-1}{\tau}\right)\mathbf{B}_t^d T\left(-\frac{11}{6}\left(\mathbf{x}_{i-d-1}\right)+3\left(\mathbf{x}_{i-d}\right)-\frac{3}{2}\left(\mathbf{x}_{i-d+1}\right)+\frac{1}{3}\left(\mathbf{x}_{i-d+2}\right)\right)\right) \\
\mathbf{X}_{ik}^c &= \frac{T}{k+2}\left(\mathbf{A}_t\mathbf{X}_{i(k-1)}^c + g(k)\sum_{d=\min(d_n)}^{\max(d_n)}\left(\frac{N-1}{\tau}\right)^2\mathbf{B}_t^d\frac{T^2}{2}\left(2\left(\mathbf{x}_{i-d-1}\right)-5\left(\mathbf{x}_{i-d}\right)+4\left(\mathbf{x}_{i-d+1}\right)-\mathbf{x}_{i-d+2}\right)\right) \\
\mathbf{X}_{ik}^d &= \frac{T}{k+3}\left(\mathbf{A}_t\mathbf{X}_{i(k-1)}^d + g(k)\sum_{d=\min(d_n)}^{\max(d_n)}\left(\frac{N-1}{\tau}\right)^3\mathbf{B}_t^d\frac{T^3}{6}\left(-\mathbf{x}_{i-d-1}+3\left(\mathbf{x}_{i-d}\right)-3\left(\mathbf{x}_{i-d+1}\right)+\mathbf{x}_{i-d+2}\right)\right)
\end{aligned} \tag{4.48}$$

the solution of order m for Eq. (4.45) is obtained by adding each of the approximations k of Eq. (4.47). To obtain the stability graphs the solution of Eq. (4.47) is rewritten by grouping the discrete states, which results in:

$$\mathbf{x}_i(T) \approx \mathbf{P}_i(T)\mathbf{x}_{(i-1)} + \sum_{d=\min(d_n)}^{\max(d_n)} \left(\mathbf{Q}_i^{''d}(T)\mathbf{x}_{i-d+2} + \mathbf{Q}_i^{'d}(T)\mathbf{x}_{i-d+1} + \mathbf{Q}_i^{d}(T)\mathbf{x}_{i-d} + \mathbf{R}_i^{d}(T)\mathbf{x}_{i-d-1} \right) \tag{4.49}$$

where

$$\begin{aligned}
\mathbf{P}_i(T) &= \sum_{k=0}^{m} \frac{1}{k!}\mathbf{A}_t^k T^k, \\
\mathbf{Q}_i^{''d}(T) &= \sum_{k=1}^{m} \left(\begin{array}{l} \frac{1}{(k+1)!}\left(\frac{N-1}{\tau_T}\right)\mathbf{A}_t^{k-1}\mathbf{B}_t^d T^{k+1}\left(\frac{1}{3}\right) - \frac{1}{(k+2)!}\left(\frac{N-1}{\tau_T}\right)^2 \mathbf{A}_t^{k-1}\mathbf{B}_t^d T^{k+2} + \\ \frac{1}{(k+3)!}\left(\frac{N-1}{\tau_T}\right)^3 \mathbf{A}_t^{k-1}\mathbf{B}_t^d T^{k+3} \end{array} \right) \\
\mathbf{Q}_i^{'d}(T) &= \sum_{k=1}^{m} \left(\begin{array}{l} \frac{1}{(k+1)!}\left(\frac{N-1}{\tau_T}\right)\mathbf{A}_t^{k-1}\mathbf{B}_t^d T^{k+1} + \frac{1}{(k+2)!}\left(\frac{N-1}{\tau_T}\right)^2 \mathbf{A}_t^{k-1}\mathbf{B}_t^d T^{k+2}\left(-\frac{7}{2}\right) + \\ \frac{1}{(k+3)!}\left(\frac{N-1}{\tau_T}\right)^3 \mathbf{A}_t^{k-1}\mathbf{B}_t^d T^{k+3}\left(\frac{9}{2}\right) \end{array} \right) - \frac{15}{2}\mathbf{Q}_i^{''d} \\
\mathbf{Q}_i^{d}(T) &= \sum_{k=1}^{m} \left(\frac{1}{(k+1)!}\left(\frac{N-1}{\tau_T}\right)\mathbf{A}_t^{k-1}\mathbf{B}_t^d T^{k+1} \right) - 3\mathbf{Q}_i^{''d} - 2\mathbf{Q}_i^{'d} \\
\mathbf{R}_i^{d}(T) &= \sum_{k=1}^{m} \frac{1}{k!}\mathbf{A}_t^{k-1}\mathbf{B}_t^d T^k - \mathbf{Q}_i^{''d} - \mathbf{Q}_i^{'d} - \mathbf{Q}_i^{d}
\end{aligned} \tag{4.50}$$

The approximate solution given by Eq. (4.49) is used to define a discrete map such as (4.9), where the coefficients of the matrix $\boldsymbol{D_i}$ are given by

$$
D_i = \begin{bmatrix}
P_{i(1,1)} & P_{i(1,2)} & 0 & \cdots & Q''^{1}_{i(1,1)} & Q'^{1}_{i(1,1)} & Q^{1}_{i(1,1)} & R^{1}_{i(1,1)} & \cdots & Q''^{2}_{i(1,1)} & Q'^{2}_{i(1,1)} & Q^{2}_{i(1,1)} & R^{2}_{i(1,1)} & \cdots & Q''^{d_n}_{i(1,1)} & Q'^{d_n}_{i(1,1)} & Q^{d_n}_{i(1,1)} & R^{d_n}_{i(1,1)} & \cdots & 0 \\
P_{i(2,1)} & P_{i(2,2)} & 0 & \cdots & Q''^{1}_{i(2,1)} & Q'^{1}_{i(2,1)} & Q^{1}_{i(2,1)} & R^{1}_{i(2,1)} & \cdots & Q''^{2}_{i(2,1)} & Q'^{2}_{i(2,1)} & Q^{2}_{i(2,1)} & R^{2}_{i(2,1)} & \cdots & Q''^{d_n}_{i(2,1)} & Q'^{d_n}_{i(2,1)} & Q^{d_n}_{i(2,1)} & R^{d_n}_{i(2,1)} & \cdots & 0 \\
1 & 0 & 0 & \cdots & 0 & 0 & 0 & 0 & \cdots & 0 & 0 & 0 & 0 & \cdots & 0 & 0 & 0 & 0 & \cdots & 0 \\
0 & 0 & 1 & \cdots & 0 & 0 & 0 & 0 & \cdots & 0 & 0 & 0 & 0 & \cdots & 0 & 0 & 0 & 0 & \cdots & 0 \\
0 & 0 & 0 & \ddots & 0 & 0 & 0 & 0 & \cdots & 0 & 0 & 0 & 0 & \cdots & 0 & 0 & 0 & 0 & \cdots & 0 \\
\vdots & \vdots & \vdots & \vdots & 1 & 0 & 0 & 0 & \cdots & 0 & 0 & 0 & 0 & \cdots & 0 & 0 & 0 & 0 & \cdots & 0 \\
0 & 0 & 0 & \cdots & 0 & 1 & 0 & 0 & \cdots & 0 & 0 & 0 & 0 & \cdots & 0 & 0 & 0 & 0 & \cdots & 0 \\
0 & 0 & 0 & \cdots & 0 & 0 & 1 & 0 & \cdots & 0 & 0 & 0 & 0 & \cdots & 0 & 0 & 0 & 0 & \cdots & 0 \\
0 & 0 & 0 & \cdots & 0 & 0 & 0 & 1 & \cdots & 0 & 0 & 0 & 0 & \cdots & 0 & 0 & 0 & 0 & \cdots & 0 \\
0 & 0 & 0 & \cdots & 0 & 0 & 0 & 0 & \ddots & 0 & 0 & 0 & 0 & \cdots & 0 & 0 & 0 & 0 & \cdots & 0 \\
0 & 0 & 0 & \cdots & 0 & 0 & 0 & 0 & \cdots & 1 & 0 & 0 & 0 & \cdots & 0 & 0 & 0 & 0 & \cdots & 0 \\
0 & 0 & 0 & \cdots & 0 & 0 & 0 & 0 & \cdots & 0 & 1 & 0 & 0 & \cdots & 0 & 0 & 0 & 0 & \cdots & 0 \\
0 & 0 & 0 & \cdots & 0 & 0 & 0 & 0 & \cdots & 0 & 0 & 1 & 0 & \cdots & 0 & 0 & 0 & 0 & \cdots & 0 \\
0 & 0 & 0 & \cdots & 0 & 0 & 0 & 0 & \cdots & 0 & 0 & 0 & 1 & \cdots & 0 & 0 & 0 & 0 & \cdots & 0 \\
0 & 0 & 0 & \cdots & 0 & 0 & 0 & 0 & \cdots & 0 & 0 & 0 & 0 & \ddots & 0 & 0 & 0 & 0 & \cdots & 0 \\
0 & 0 & 0 & \cdots & 0 & 0 & 0 & 0 & \cdots & 0 & 0 & 0 & 0 & \cdots & 1 & 0 & 0 & 0 & \cdots & 0 \\
0 & 0 & 0 & \cdots & 0 & 0 & 0 & 0 & \cdots & 0 & 0 & 0 & 0 & \cdots & 0 & 1 & 0 & 0 & \cdots & 0 \\
0 & 0 & 0 & \cdots & 0 & 0 & 0 & 0 & \cdots & 0 & 0 & 0 & 0 & \cdots & 0 & 0 & 1 & 0 & \cdots & 0 \\
\vdots & \vdots & \vdots & \cdots & \vdots & \vdots & \vdots & \vdots & \cdots & \vdots & \vdots & \vdots & \vdots & \cdots & 0 & 0 & 0 & 1 & \cdots & \vdots \\
0 & 0 & 0 & \cdots & 0 & 0 & 0 & 0 & \cdots & 0 & 0 & 0 & 0 & \cdots & 0 & 0 & 0 & 0 & \cdots & 0
\end{bmatrix} \tag{4.51}
$$

For the second order approximation, the matrix $\mathbf{D_i}$ is like the matrix of the third order but without the terms having $\boldsymbol{Q_i''}$, instead it will be a zero.

The transition matrix $\boldsymbol{\Phi}$ over the period $\tau_T = (N-1)/\Delta t$ is determined by coupling each solution $\boldsymbol{z}_i$ through the discrete map $\boldsymbol{D_i}$, $i = 1, 2, \ldots, (N-1)$. However, the computational cost can be reduced by computing only the transition matrix up to the maximum delayed term without losing precision in the calculation of the eigenvalues:

$$\boldsymbol{\Phi} = \mathbf{D}_{N\max}\mathbf{D}_{N\max-1}\ldots\mathbf{D}_2\mathbf{D}_1 \tag{4.52}$$

The stability graphs of (4.20) are determined by computing the eigenvalues of the transition matrix calculated by Eq. (4.52). The results of the EMHPM have been corroborated with the stability lobes in the study of multivariate tools [86–93].

4.5 Numerical Analysis of the algorithm for multivariable tool

The solution of tools with variable pitch and helix angles for milling operation with one degree of freedom is plotted over time and compared with the solution of the algorithm for regular tools, this is done for the solution of third order EMHPM (Figure 4.9) the parameters used for the multivariate tool algorithm are tool diameter $D = 10\ mm$, number of disks=10, $z_n = 2$, the pitch angle between the cutting edges is 180°, the helix angle is maintained 1°, $\omega_n = 5793\ rad/s$, $\zeta = 0.011$, $m_m = 0.03993\ kg$, $K_{tc} = 6 \times 10^8\ N/m^2$, $K_{nc} = 2 \times 10^8\ N/m^2$, $a_d = 1$, $n = 12000\ rpm$, $\Delta a_p = 0.15$, $m = 7$, $N = (75 \times z_n) + 1$. For the regular tool algorithm, we use $\omega_n = 5793\ rad/s$, $\zeta = 0.011$, $m_m = 0.03993\ kg$, $K_{tc} = 6 \times 10^8\ N/m^2$, $K_{nc} = 2 \times 10^8\ N/m^2$, $a_d = 1$, $n = 12000\ rpm$, $a_p = 1.5\ mm$, $m = 7$, $N = 76$. In both, we start from a constant initial condition for the period prior to time zero of $c = 0.001\ m$ for position and zero for velocity. It is clearly observed in Figure 4.9 that the solution of the algorithm proposed by Compeán in [85] of a multivariate tool converges with the algorithm used in Chapter 3 for a regular tool.

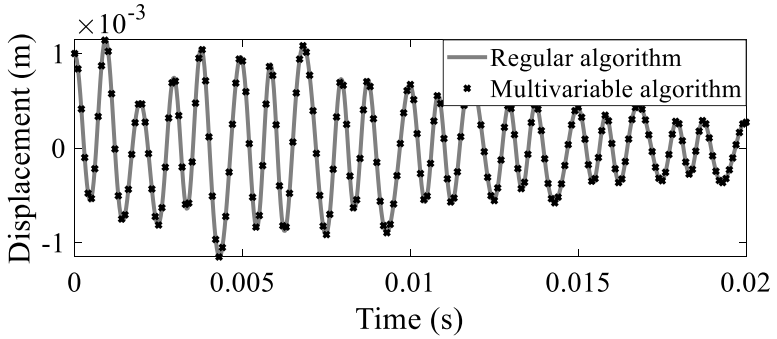

Figure 4.9 Comparison of solution with regular tool algorithm vs multivariate tool algorithm for third-order EMHPM, with values of $n = 12000\ rpm$, $z_n = 4$, $a_d = 1$, $a_p = 1.5\ mm$.

The solutions of the first-, second-, and third-order approximations of the EMHPM are solved using the multivariable tool algorithm and they are compared with the solution of dde23 from Matlab (Figure 4.10). Although the three solutions are very similar, the second and third order are better aligned, which is due to a better approximation by increasing the order from solution.

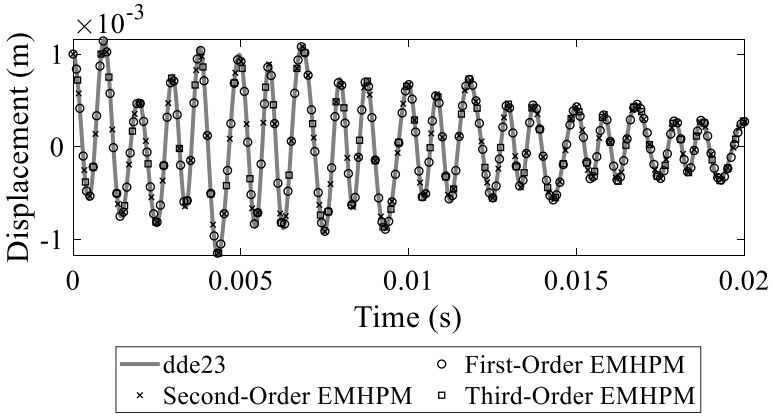

Figure 4.10 Numerical comparison of the EMHPM solutions of milling equation Eq. (4.13) with the dde23 MATLAB routine. For a stable milling operation $a_p = 1.5$ mm, $a_d = 1$ and $n = 12000$ rpm with 10 disks.

The solutions of the multivariable tool algorithm showed in Figure 4.11 are obtained for a tool of diameter of 10 mm with 4 flutes, a 400 x 200 mesh is used for the spindle speed and depth respectively, $\omega_n = 5793\, rad/s$, $\zeta = 0.011$, $m_m = 0.03993\, kg$, $a_d = 1, m = 7$, $N = 75 \times z_n$ $K_{tc} = 6 \times 10^8\, N/m^2$ and $K_{nc} = 2 \times 10^8\, N/m^2$ for each flute, the pitch angles are of 90° and the helix angles are set 1°.

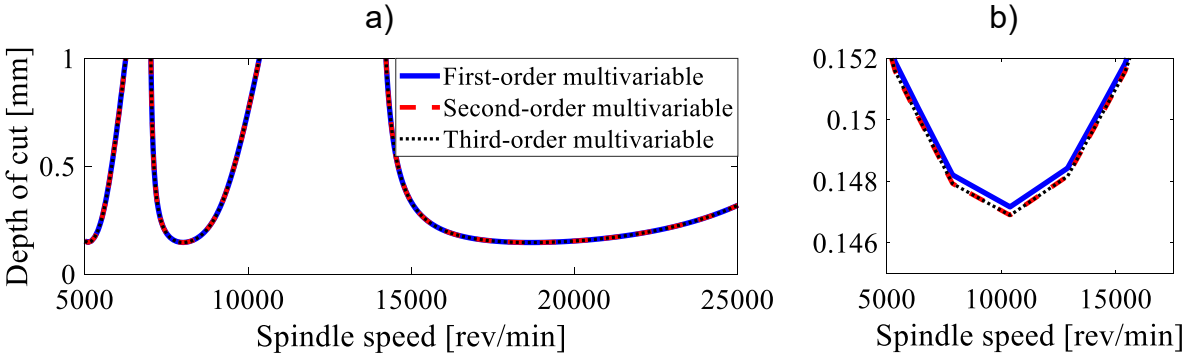

Figure 4.11 a) Stability lobes for multivariable tool in approximation of first-, second- and third-order, b) zoom in to observe the difference between methods.

If the solution is compared with the solution of the code for a regular tool, we expect to have a similar result with a slight difference attributed to the fact that the algorithm of the regular tool does not include the helix angle.

In Figure 4.11a the solutions for the first, second and third order of the multivariate algorithm are compared, it is observed that the solutions are very similar; however, in Figure 4.11b, it is observed that the second and third order solutions coincide better, as expected.

Similarly, the comparison of the solution for the third-order EMHPM for multivariable tool is carried out against the solution of the Semi-discretization method proposed by Insperger in [68], in order to validate the algorithm. Figure 4.12 presents the results with a $400x200$ mesh with $a_d = 1$ for a tool with 2 edges equally spaced, helix angles $\beta = 1°$, $m = 7$, and $N = 75 \times z_n$ used with the third-order algorithm in a down-milling operation with full immersion.

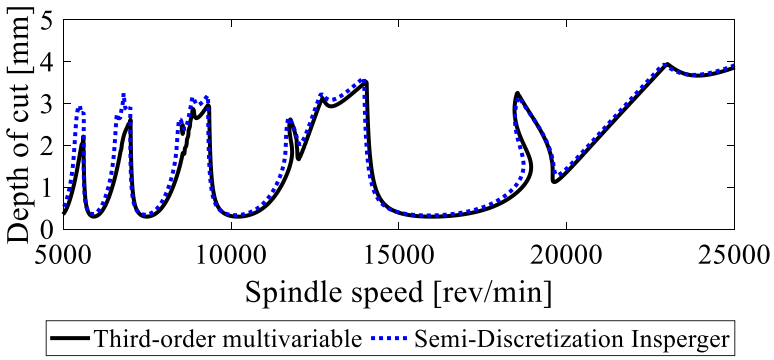

Figure 4.12 Third-order EMHPM for multivariable tool vs Semi-Discretization, $a_d = 1$, $z_n = 2$, $\beta = 1°$

Chapter 5. Validation of the milling tool

5.1 Experimental characterization of one degree of freedom milling equation and cutting force model

In the scheme showed below in Figure 5.1 is represented the methodology used to validate a multivariable milling tool using the algorithm of 3rd-order EMHPM.

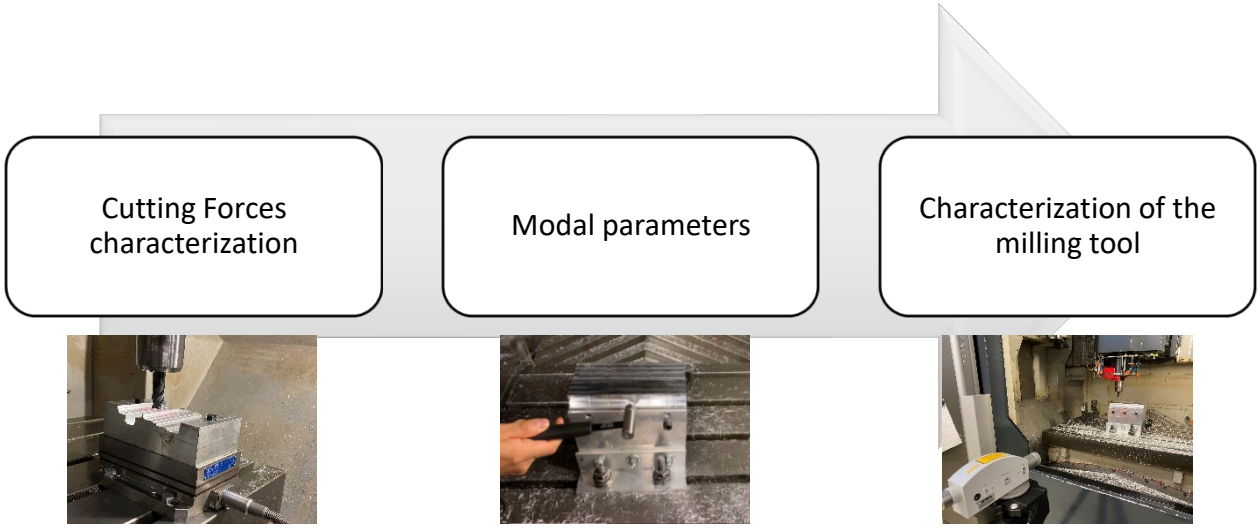

Figure 5.1 Methodology to validate a multivariable milling tool

Experimental Modal Analysis

An experimental workpiece was assembled with a 7075T6 aluminum block with dimensions of 101 mm × 172 mm supported by two thin plates (walls) with a thickness of 4.5 mm. This assembly mimics a DOF as described in Eq. (4.13). The workpiece assembly was rigidly fixed to the workbench of a Makino F3 machining center. For modal analysis, tap testing was performed using a 352C68 PCB Piezotronics accelerometer and an impact hammer model 9722A500. The signals were acquired with a Polytec VIB-E-220 data acquisition card and processed with VibSoft signal analyzer software as shown in Figure 5.2a.

Escalera in [94] obtained the modal parameters $\zeta = 0.068$, $m_m = 3.8$ kg, $f_m = 132$ Hz, and $\omega_n = 829$ rad/s for the tool described in the next section.

Experimental determination of cutting coefficients

The force model in Eq. (4.25) is used to predict the cutting force magnitude for a given depth of cut. It is based on a mechanistic approach that assumes a relationship between forces and the uncut chip thickness by means of the cutting coefficients. The cutting force model is established by introducing cutting (shearing) and edge coefficients for the tangential and normal directions of the milling tool. The characterization procedure assumes the linear relationship between the averaged experimental cutting forces $\tilde{F}$ and the feed rate f_z in x- and y- directions. This relationship is established as follows:

$$\tilde{F} = f_z \tilde{F}_c + \tilde{F}_e \tag{5.1}$$

Here, $\tilde{F}_c$ and $\tilde{F}_e$ are the cutting shear and edge components, respectively. The experimental forces at each feed rate are measured, and the cutting-edge components $\tilde{F}_c$ and $\tilde{F}_e$ are evaluated

$$K_{tc} = 4\frac{\tilde{F}_{yc}}{z_n a_p},\ K_{nc} = -4\frac{\tilde{F}_{xc}}{z_n a_p} \tag{5.2}$$

A multivariable cutter provided by a local toolmaker was characterized by using the Eq (5.2) and the experimental setup shown in Figure 5.2b. Table 5.1 summarizes the main geometric characteristics of the multivariable tool.

Table 5.1. Main geometric parameters of multivariable tool according to [94].

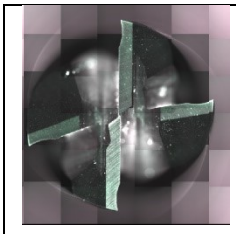	Diameter	12.7 mm
	Cutting length	25 mm
	Coating type	Uncoated
	Number of teeth	4
	Helix angles	39°, 37°, 39°, 41°
	Pitch angles	80°, 100°, 70°, 110°

a) b)

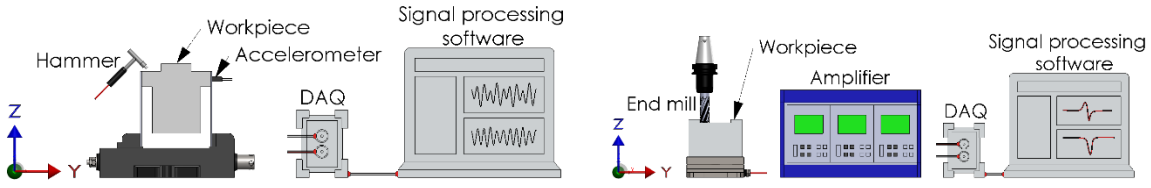

Figure 5.2 Scheme of the experimental setup for a) the modal analysis and b) cutting forces characterization.

A total of 5 cuttings were performed for full radial immersion in aluminum 7075T6 during dry machining. The forces were recorded by using a dynamometer 9257B Kistler and the spindle speed is set at 3000 rpm based on the dynamometer's natural frequency to avoid the amplification of milling forces.

The force signals were acquired using a VibSoft-20 acquisition card at a sample rate of 48 kHz and processed in a custom-made MATLAB app to remove drift and noise. Cutting forces data were collected for the axial depth of cut of 2 mm and four values of feed per tooth 0.05, 0.10, 0.15 and 0.20 mm, so the resulting cutting coefficients K_{tc} for the tooth 1, 2, 3 and 4 were 1215×10^6 N/m^2, 1369×10^6 N/m^2, 897×10^6 N/m^2 and 1799×10^6 N/m^2 respectively, while that the coefficients K_{nc} for the tooth 1, 2, 3 and 4 resulted 272×10^6 N/m^2, 520×10^6 N/m^2, 801×10^6 N/m^2 and 859×10^6 N/m^2 respectively.

Stability analysis of 1 dof milling with multivariable tool

The stability lobes computed for the multivariable tool using the third-order EMHPM with a mesh of 400×200 ($n \times a_p$) are shown in Figure 5.3 together with stability lobes for a regular tool (angles of 90° and helix angles of 30° for all flutes). An approximation of order $m = 7$ was used with N =241 and $a_d = 1$ mm. Notice from Figure 5.3 that the stable zone obtained for the multivariable tool is significantly larger, meaning that the critical depth of cut is higher in most spindle speeds, which allows having more global productivity. It is also observed in the range of spindle speed between 2,000 – 3000 rpm, a stable peninsula formed with axial depth ranging from 11 to 20 mm or higher values of critical depth of cut. For instance, for the multivariable cutter at 2500 rpm, the critical depth of cut a_p is 2.17 mm, however it becomes stable again as shown in Figure 5.3 for the interval values between 11 to 20 mm. To validate this unexpected behavior, we performed several time-domain simulations using the third-order EMHPM solution described by Eq. (4.49).

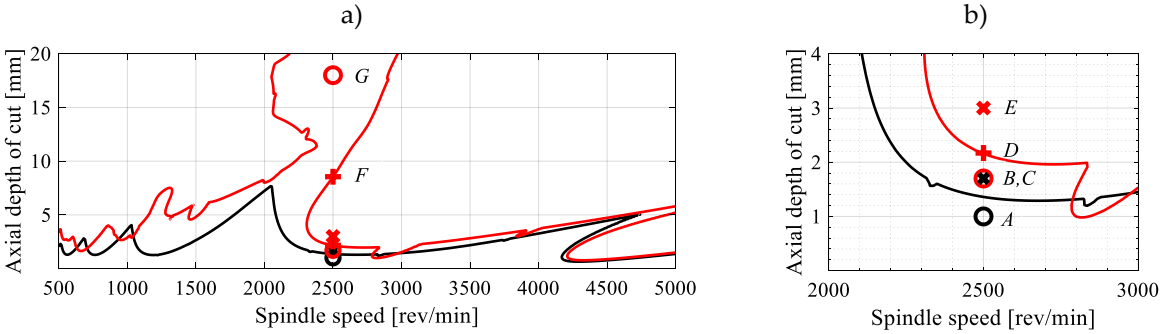

Figure 5.3 a) Comparison of stability lobes for regular (black solid line) and multivariable (red solid line) cutters by using the third-order EMHPM; b) zoom in on chosen cutting conditions for time-domain simulations. The selected points are marked as follows: unstable (cross mark), stable (circle mark), transition (plus mark) cutting conditions.

The solution obtained with the stability lobes in Figure 5.3 were also compared with the solution in time-domain using the mean of the peaks for the first 10 periods.

The surface was graphed using matlab, and contours of levels 0.0001, 0.0005, 0.001, 0.01, 0.05, 0.1, 0.5, 1 and 2 mm were explored as shown in Figure 5.4. It is observed that it gives a good approximation, but the time required to obtain the simulation is increased to many hours.

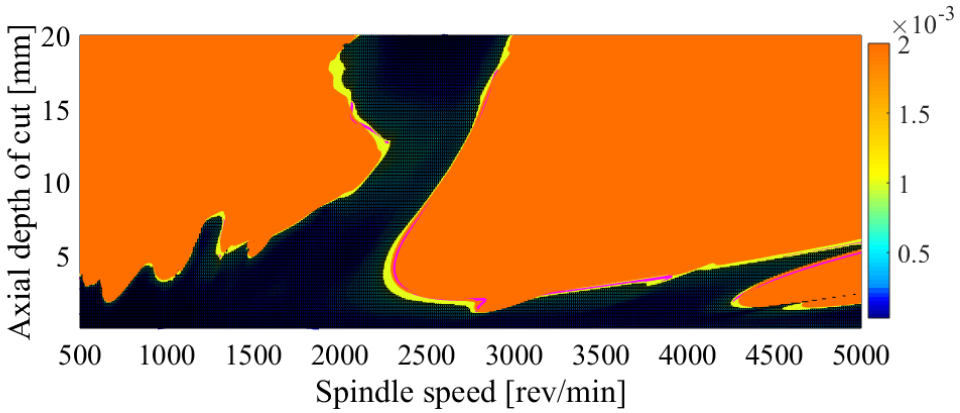

Figure 5.4 Comparison for the Floquet solution and the solution in time-domain using the mean of the peaks for the first 10 periods.

Furthermore, the simulated vibrations for the chosen cutting conditions were analyzed using the Continuous Wavelet Transform (CWT), the Power Spectral Density (PSD) and Poincaré Maps (PM). The CWT is a time-frequency representation of a signal that offers the capability to observe how frequencies evolve in time.

The scalograms display the absolute value of CWT of the simulated vibration and therefore, they are used to detect chatter phenomena that appear when milling with a multivariable tool. The PSD is based on the Fourier transform that provides the transformation from the time-domain to the frequency-domain. Also, PSD is defined as the squared value of the signal and describes the power of a signal or time series distributed over different frequencies [95]. Moreover, a PM represents points in phase space which are sampled every spindle rotation [96]. The frequencies f of the CWT and PM were normalized $f_n = f/f_h$ according to the spindle frequency f_h. When milling with a regular milling tool the excitation frequency f_e is equal to z_n times frequencies of the spindle speed f_h but in a multivariable tool, there are several excitation frequencies since the angular spacing between teeth change as a function of the axial depth of cut.

Figure 5.5 illustrates the CWT, PSD and PM for simulated vibrations using the multivariable tool with different axial depths denoted as cutting conditions A, B, and C for the axial depths of cut of 1.0, 1.7, and 1.7 mm respectively. Figure 5.5a-c refer to the vibrations of the cutting conditions A marked in Figure 5.3, using a regular tool.

The scalogram in Figure 5.5a identifies point A as a stable cutting since normalized cutting frequencies present a dominant value of f_n = 3.2 which corresponds to the natural frequency f_m = 132 Hz. This is also confirmed by the PSD analysis shown in Figure 5.5b. The PM illustrated in Figure 5.5c shows a vibration that decreases with time and sampled data concentrated in the center confirms a typical stable case. When the axial depth of cut is increased to 1.7 mm, the stability diagram predicts unstable cutting conditions according to the stability lobes for the regular tool. This case is denoted with cutting conditions B and the corresponding scalogram (shown in Figure 5.5d) illustrates how the intensity of the dominant frequency increases with time even when the excitation frequency is the same as the case in A.

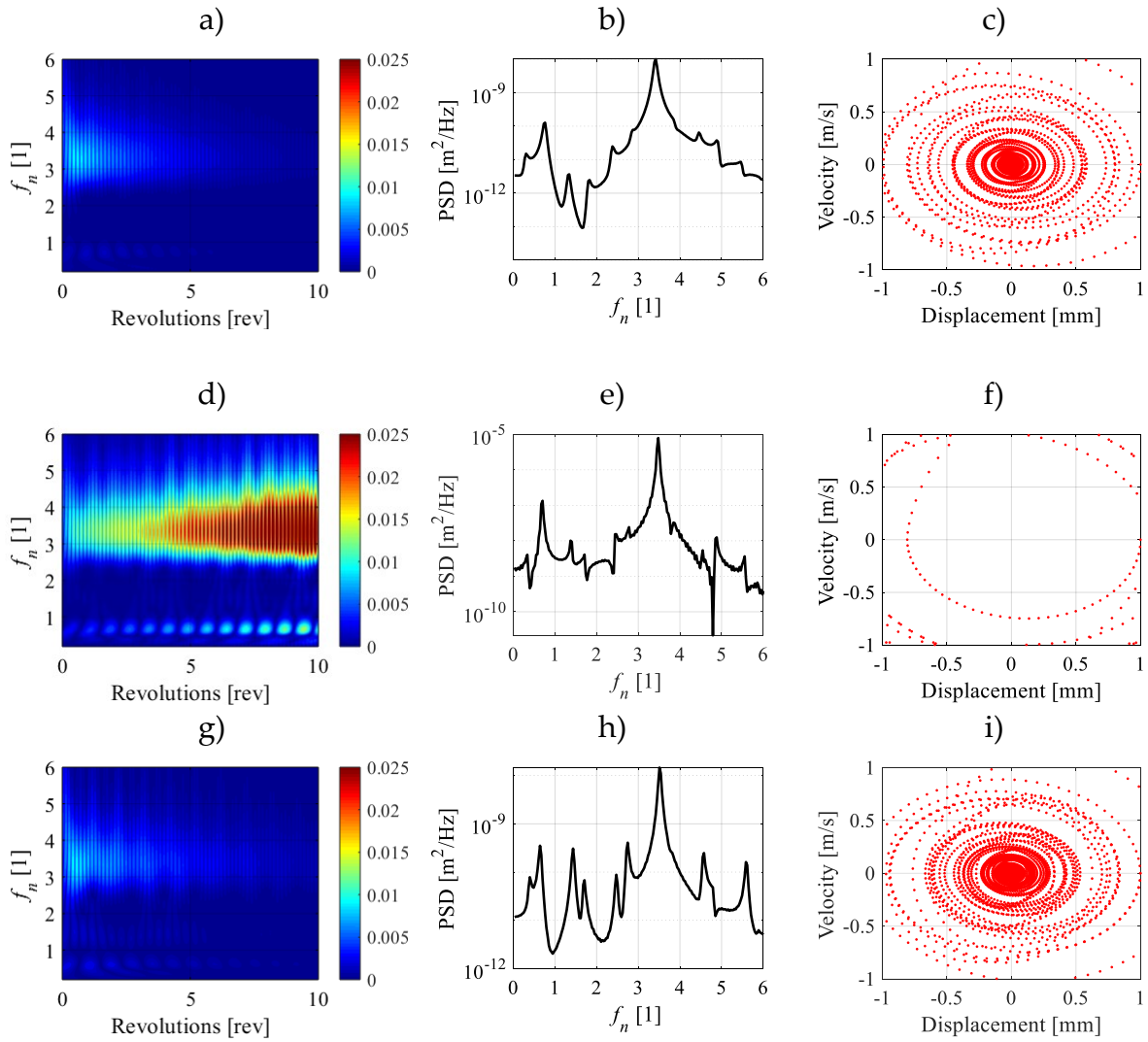

Figure 5.5 Analysis of cutting conditions A, B and C. CWT scalograms: a), d), g); PSD: b), e), h) and PM: c), f), i) corresponds to the cutting conditions A, B and C respectively.

The PM diagram shown in Figure 5.5f, exhibits a vibration far from zero. In fact, the PM diagram shows that the vibration amplitude grows exponentially because our equation of motion does not consider nonlinear effects such as those that appear when the tool loses contact with the workpiece. Both cutting conditions A and B agree with the stability boundaries in Figure 5.3. Now, the cutting conditions B are used but with a multivariable tool which is referred to as cutting conditions C. The CWT plotted in Figure 5.5g describes completely different results since there are no single dominant frequencies in comparison with cutting conditions A, but appears several frequencies around $f_n = 3.2$ and close to $f_n = 1$ that reduce in intensity with time, suggesting a stable cutting. Figure 5.5i illustrates how the vibration amplitude approaches to zero when using a multivariable tool in contrast to the PM obtained for the regular tool and exhibit in Figure 5.5f. This can be explained by observing that there are several excitation frequencies due to the irregular pitch and helix angles, that break a single excitation frequency avoiding regenerative chatter phenomena.

Figure 5.6 illustrates the CWT, PSD and PM for simulated vibrations using the multivariable tool with different axial depths denoted as cutting conditions D, E, F and G for the axial depths of cut of 2.3, 3.0, 8.55, and 18 mm respectively. Notice that a stable case C was already validated when the axial depth is 1.7 mm in Figure 5.5g-i, that corresponds to cutting conditions under the stability boundaries shown in Figure 5.3.

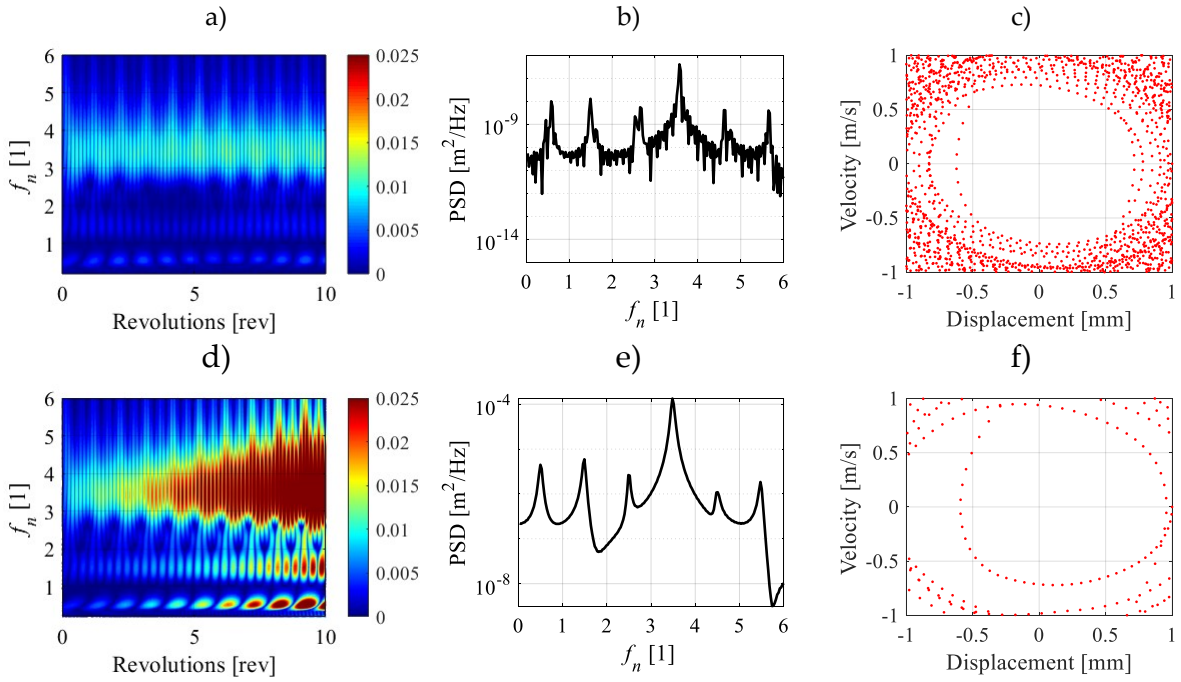

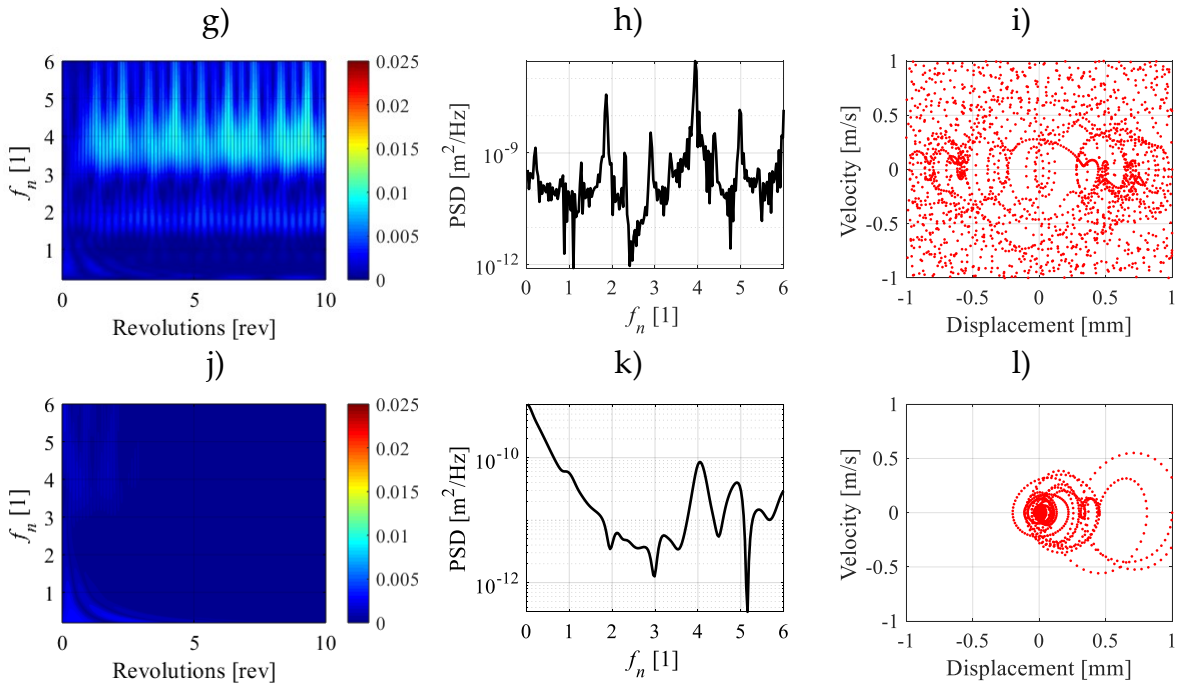

Figure 5.6 Analysis of cutting conditions D, E, F and G. CWT scalograms: a), d), g), j); PSD: b), e), h), k) and PM: c), f), i), l) corresponds to the cutting conditions D, E, F and G respectively.

For case D, a transient cutting condition was chosen very close to the critical axial depth of cut. It is interesting to point out that transition cutting conditions in the CWT scalogram shown in Figure 5.6a not only shows frequencies with higher intensity in comparison with the stable case B, but also present shifted frequencies that vary in intensity every single revolution. This shifting suggests a marginally stable cutting condition that is confirmed by the PM illustrated in Figure 5.6c, where circular trajectories are described close to the center point.

Unstable vibrations that appear for case E are because of the intensity of frequencies increase exponentially with time, see Figure 5.6d. Notice that other frequencies arise with time close to the values of f_n = 0.5 and f_n = 1.5. These frenquencies also occur for cutting conditions D which is an indication of the appearance of chatter phenomena. In contrast to Figure 5.5i for a stable case, Figure 5.6f exhibits few trajectories because the vibration amplitude is out of the range selected (± 1 mm). The qualitative and quantitative dynamic behaviour due to cutting conditions F, and illustrated in Figure 5.6g-i, were classified as transition cutting behaviour. Here, a more severe shifting in frequencies is observed in the scalogram (Figure 5.6g). From Figure 5.6g, it is seen that drastic shifting occurs in time domain in the range of normalized frequencies from 3.5 to 6. It is also evident in the PM showed in Figure 5.6i, that the amplitude of vibration remains below 1 mm during several revolutions of the tool but the amplitude of vibration never aproaches to the center point,

in contrast to the stable cutting condition C shown in Figure 5.5i in which the oscillation aplitudes aproaches fo the center.

An interesting dynamic behaviour is observed in the milling cutting process when the cutting conditions are selected in the middle of the stable peninsula, above unstable cutting conditions such as E cutting conditions. The axial depth of the cut was increased from the unstable axial depth of cut of 3 to 18 mm, 6 times higher of the stable cutting condition C, and 2 times higher than the unstable condition E. Since the vibration quickly decreases in a few revolutions no dominant frequencies appear in the CWT and PSD fails to clearly identify a dominant frequency since the vibration amplitude decreases to zero after few revolutions, as confirmed by the PM shown in Figure 5.6l.

Figure 5.7 shows the normalized excitation frequencies that the multivariable tool produces for a fixed spindle speed of 2500 rpm. The total number of disks of 50 μm of thickness was grouped in sets of each millimeter in the axial direction. The waterfall plot in Figure 5.7 explains that a stable peninsula is formed above 11 mm because the workpiece is excited with several frequencies simultaneously. For instance, for a milling operation with the axial depth of cut of 1 mm (stable cutting), 80 discrete disks were cut with four normalized excitation frequencies values (3.3, 3.6, 4.5 and 5.1). On the other hand, when milling at 18 mm (stable cutting), there are 14 normalized excitation frequencies (3.30, 3.35, 3.39, 3.44, 3.49, 3.54, 3.60, 4.55, 4.64, 4.73, 4.82, 4.92, 5.02 and 5.13), most of them with at least 115 discrete disks.

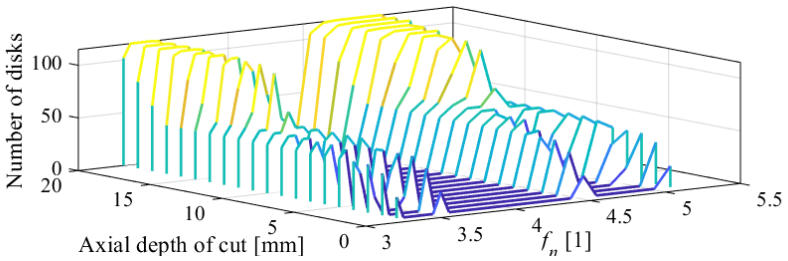

Figure 5.7 The number of discrete disks and discrete excitation frequencies as a function of axial depth of cut for the multivariable tool.

5.2 Experimental validation with new parameters of the tool

To validate the results obatined with the simulation, more experimental characterization was made. The experimental workpiece was assembled with a 7075T6 aluminum block of 101 mm × 179 mm supported by two thin plates (walls) with a thickness of 4.5 mm. The workpiece assembly was rigidly fixed to the workbench of a Makino F3 machining center.

For modal analysis, tap testing was performed using a Dytran 3035BG accelerometer with sensibility of 105.7 mV/g, and an impact hammer model 9722A500. Figure 5.8 presents the assembly arrangement and the process to obtain the modal parameters.

a) b)

Figure 5.8 a) Arrangement of the assembly and b) test to obtain the modal parameters

The signals were acquired with a Polytec VIB-E-220 data acquisition card and processed with VibSoft signal analyzer software as shown in Figure 5.2a. Using the CutPro 8 software, the modal parameters were fitted resulting the values $\zeta = 0.0423$, $m_m = 5.88$ kg, f_m = 157.5 Hz, and $\omega_n = 989.6$ rad/s before the characterization of the tool and $\zeta = 0.0328$, $m_m = 6.14$ kg, f_m = 159.3 Hz, and $\omega_n = 1000.9$ rad/s after the characterization of the tool.

Determination of cutting coefficients

A multivariable cutter provided by a local toolmaker was characterized by using the Eq. (5.2) and the experimental setup shown in Figure 5.2b.

Table 5.2 summarizes the main geometric characteristics of the multivariable tool. Notice that the parameters of Table 5.1 are different that the parameters for the tool examined at presented in Table 5.2, so although the lobes are similar, they are not equal and the simulated results obtained previously in Figure 5.5 and Figure 5.6 also differ with the results obtained with the new parameters.

A total of 4 cuttings were performed for full radial immersion in aluminum 7075T6 during dry machining. The forces were recorded by using a dynamometer 9257B Kistler and the spindle speed was set at 1500 rpm based on the dynamometer's natural frequency to avoid the amplification of milling forces. The force signals were acquired using a VibSoft-20 acquisition card at a sample rate of 48 kHz and processed in a custom-made MATLAB app to remove drift and noise.

Table 5.2. Main geometric parameters of experimental multivariable tool.

	Diameter	12.7 mm
	Cutting length	25 mm
	Coating type	Uncoated
	Number of teeth	4
	Helix angles	40.71°, 38.73°, 36.33°, 38.6°
	Pitch angles	110°, 80°, 100°, 70°

Cutting forces data were collected for the axial depth of cut of 1.5 mm and four values of feed per tooth 0.03, 0.06, 0.09 and 0.12 mm, so the resulting average cutting coefficients were $K_{tc} = 975.1517 \times 10^6$ N/m^2 and $K_{nc} = 298.7496 \times 10^6$ N/m^2; since those coefficients were the average, those values were used for each tooth. Figure 5.9 shows the workpiece assembled on the dynamometer to capture the signal of the cutting forces.

Figure 5.9 Experimental test to obtain the cutting forces

A characterization with a 25 percent of radial immersion was also performed, to analyze influence of the forces when we study it by edges. To obtain the cutting force coefficients when we have $a_d = 0.25$ Eqs. (2.12) are used, so we combine the experimental signal of the forces in X and Y and by linear regression we obtain the specific coefficients; we did not employ the equations for forces in Z since the model was considered to be in ODF.

In Figure 5.10 it is represented the scheme where we can observe the angle when the edge of the tool start to cut the workpiece and when it leaves the workpiece, when cutting with radial immersion of the tool 25 %. It is observed that for this configuration $\phi_{st} = \frac{2\pi}{3}$ and $\phi_{ex} = \pi$.

Figure 5.10 Scheme for the representation of ϕ_{st} and ϕ_{ex} for radial immersion of 25 %.

After analyzing the force signals in x-y for each tooth obtained experimentally and evaluating Eq. (2.12), we obtained the specific cutting coefficients listed in Table 5.3.

Table 5.3. Specific cutting coefficients characterized by edges with radial immersion of 25% for multivariable tool.

	K_{tc} $(\times 10^6\ N/m^2)$	K_{rc} $(\times 10^6\ N/m^2)$
Tooth 1	1596.984672	287.5141278
Tooth 2	1296.676141	487.945012
Tooth 3	2406.422162	799.772147
Tooth 4	1554.751903	529.221760

Experimental analysis of 1 dof milling with multivariable tool

The stability lobes computed for the multivariable tool before (black line) and after (blue dotted line) the characterization using the third-order EMHPM with a mesh of 200×160 $(n \times a_p)$ are shown in Figure 5.11 using the parameters of Table 5.2, and considering that in all teeth the values of K_{tc} and K_{rc} are 975.1517×10^6 N/m^2 and 298.7496×10^6 N/m^2 respectively.

The modal parameters to graph the lobes before the test, were $\zeta = 0.0423$, $m_m = 5.88$ kg, and f_m = 157.5 Hz, and after the test we obtain the parameters $\zeta = 0.0328$, $m_m =$ 6.14 kg, and f_m = 159.3 Hz. An approximation of order $m = 7$ was used with N =241 and $a_e = 3.175$ mm.

To validate the lobe, several time-domain simulations were performed using the third-order EMHPM solution described by Eq. (4.49). Experiments for n=2500 rpm, until 6000 rpm with increments of 500 rpm were developed with axial depth of 1, 2, 3, 4 and 5 mm as indicated in Figure 5.11 with a_d =25 %.

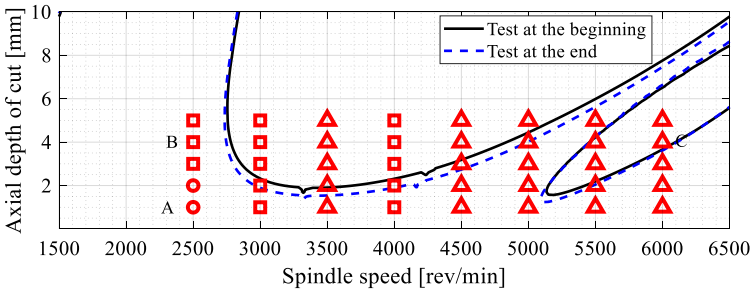

Figure 5.11 Stability lobes of multivariable tool for experimentation with $a_e = 3.175$ mm, black line represents the lobes for modal parameters at the beginning of the characterization and red lines for the end of the characterization. Circles represent stable cases; squares represent cases with hopf frequencies, and triangles cases with flip frequencies.

Also, we graphed the lobes using the modal parameters after the test, with the specific cutting coefficients presented in Table 5.3 and with the parameters of the tool presented in Table 5.2; Figure 5.12 present the lobes.

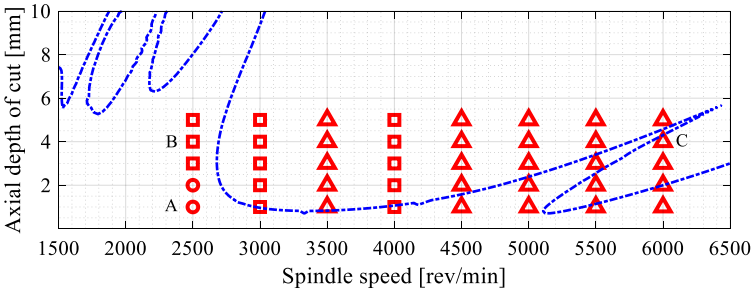

Figure 5.12 Stability lobes of multivariable tool for experimentation with $a_e = 3.175$ mm, and with specific cutting forces obtained with characterization by edges. Circles represent stable cases; squares represent cases with hopf frequencies, and triangles cases with flip frequencies.

It is clearly observed that when we characterize the forces with full immersion, and obtain the average cutting coefficients, there are a difference in the lobes if we characterize the forces by edges, however more study needs to be developed in the analysis.

Tool characterization

Figure 5.13 shows the arrangement to characterize the multivariable tool, there it is observed a laser vibrometer of doppler effect CLV-2534 employed in the test to obtain the vibrations.

Figure 5.13 Experimental arrangement to characterize the milling tool

Figure 5.14 shows by way of example the signals acquired during a series of tests with an increment of 500 rpm at a constant depth of 1 mm. Figure 5.14b shows the zoom in of the tachometer signal for the test with n=3000 rpm and a_p=1, while that Figure 5.14d shows the zoom in of the velocity signal for n=3000 rpm.

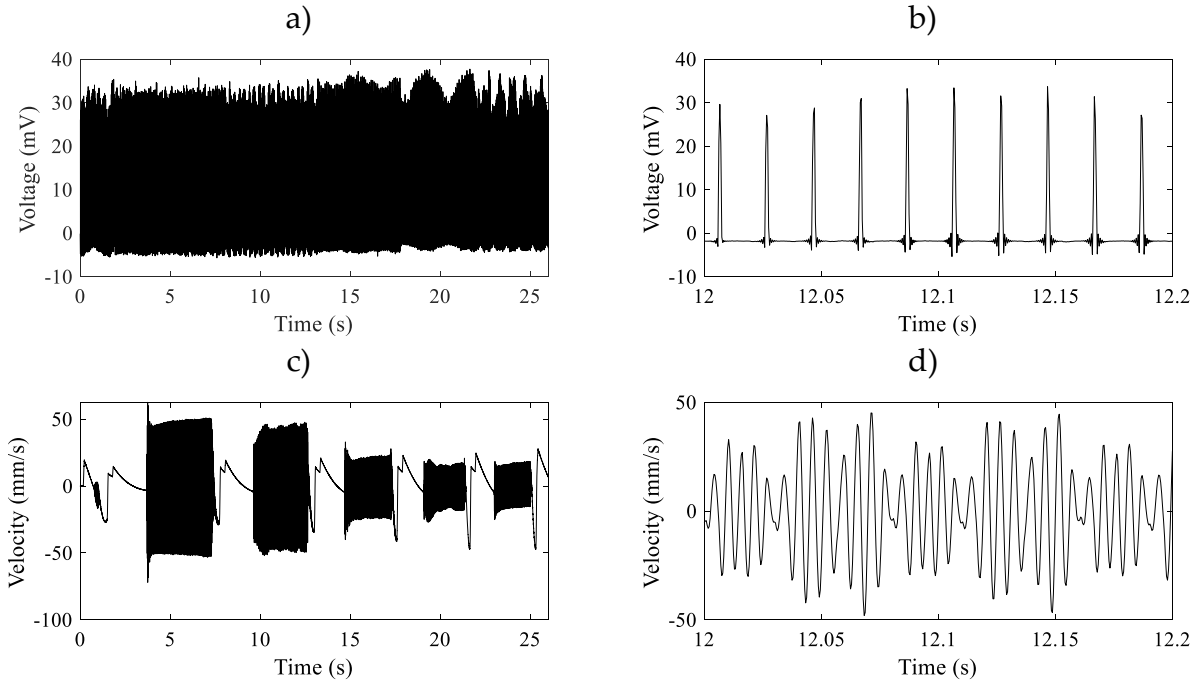

Figure 5.14 Signals obtained with n=2500, 3000, 3500, 4000, 4500 rpm, a_p=1 mm, a) tachometer signal, b) zoom in of the tachometer signal, c) velocity signal, d) zoom in of the velocity.

The simulated vibrations for the chosen cutting conditions were analyzed using the Continuous Wavelet Transform (CWT), the Power Spectral Density (PSD) and Poincaré Maps (PM). The frequencies f of the CWT and PM were normalized $f_n = f/f_h$ according to the spindle frequency f_h. Figure 5.15 illustrates the CWT, PSD and PM for simulated vibrations using the multivariable tool with different axial depths and spindle speeds.

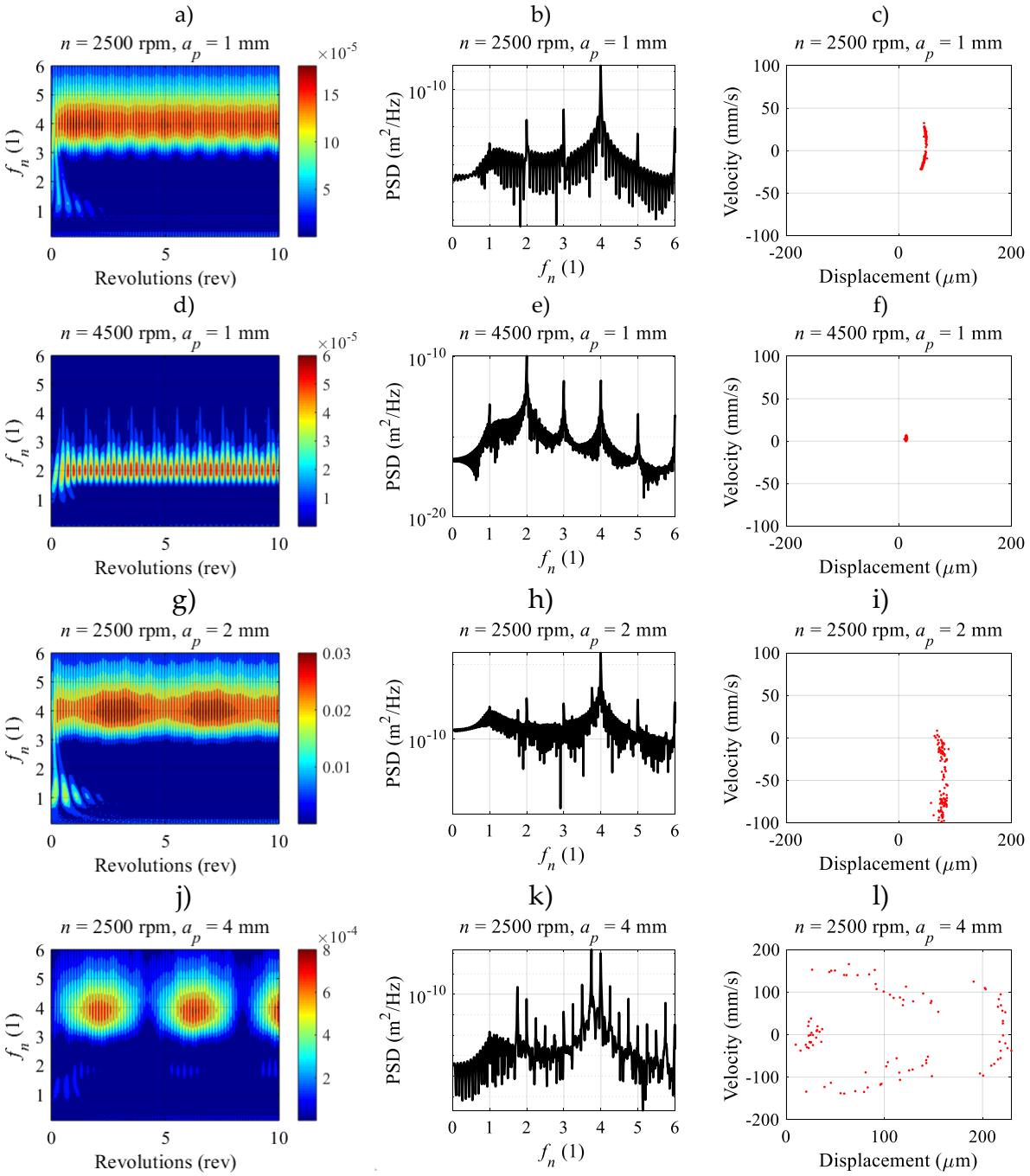

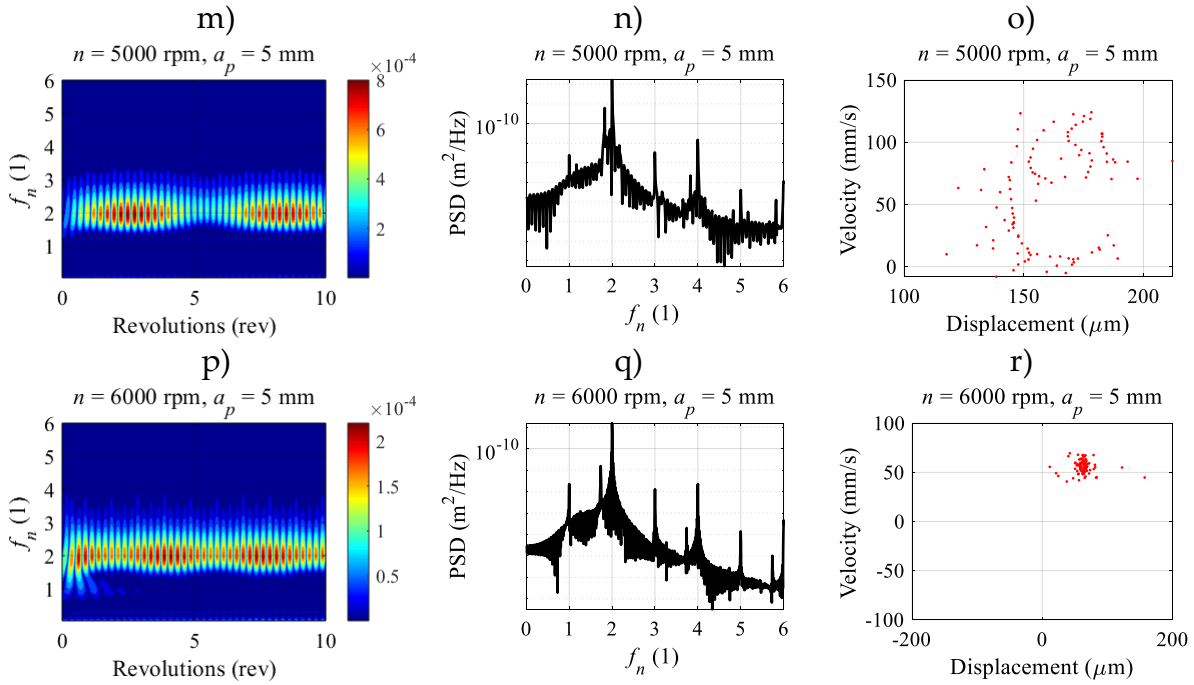

Figure 5.15 CWT, PSD and Poincaré diagrams to validate experimental tests.

The scalogram in Figure 5.15a identifies the test near to the stable cutting, but in a transition region, normalized cutting frequencies present a dominant value of f_n =4 which is almost the natural frequency f_m = 157.5 Hz. Since the dominant frequency is almost the natural frequency, the amplitude is high. This is also confirmed by the PSD analysis shown in Figure 5.15b. The PM illustrated in Figure 5.15c shows the vibration which confirms the transient zone. The scalogram in Figure 5.15d presents a case near to the stable cutting, with the normalized cutting frequency near to the natural frequency, the PSD analysis showed in Figure 5.15e also confirms it. The PM illustrated in Figure 5.15f shows a slight vibration that confirms a case approximating to a stable condition.

Figure 5.15g suggest that the lobes are crossing near to this region, the cutting frequency presented in Figure 5.15h confirms the result presented in the scalogram, and poincaré diagram in Figure 5.15i also indicates that there is a transient condition. For a_p=4 and n=2500 rpm it is observed that there is a region of instability which confirms that the stability lobes are to the left of that position, several frequencies are around the dominant.

At n=5000 rpm with a_p=5 it is observed in the Figure 5.15m-o that it is also a region unstable, but at n=6500 and a_p=5, it is observed how the vibration is reduced, showing that the stability lobes goes near to this region. Annex A present more CWT, PSD and PM for experiments with different axial depth and spindle speeds.

An exploration was realized with a depth of 15 mm, at different spindle speeds, Figure 5.16 present the results for the lobes with the multivariable tool using $\zeta = 0.0328$, m_m = 6.14 kg, f_m = 159.3 Hz, and ω_n = 1000.9 rad/s with the average cutting coefficients obtained previously in full immersion, $K_{tc} = 975.1517 \times 10^6$ N/m^2 and $K_{nc} = 298.7496 \times$

10^6 N/m^2. Notice that a lobe with the coefficients calculated by edges should be included, since the influence of the specific cutting coefficients could change the lobes significatively.

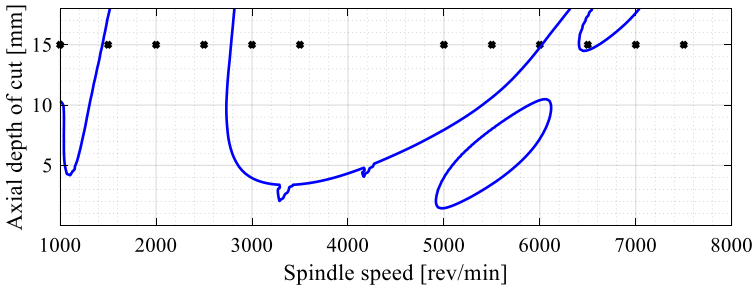

Figure 5.16 Stability lobes of multivariable tool for experimentation with $a_e = 1$ mm

Figure 5.17 illustrates the CWT, PSD and PM for simulated vibrations using the multivariable tool with different spindle speeds maintaining the axial depth to 15 mm, a_e for the essays was 1 mm.

PSD and Poincaré of Figure 5.17b,c shows a region in the stable zone, normalized cutting frequencies present a dominant value of f_n =4 which is almost the natural frequency, however, the scalogram in Figure 5.17a appears to indicate that the zone is unstable. The PM illustrated in Figure 5.17f shows clearly for n=3000 rpm an unstable condition which is confirmed by the CWT and the PSD.

The CWT in Figure 5.17j shows a dominant frequency of 2 times the spindle frequency, PSD and PM in Figure 5.17k,l shows that the tool is working in a zone that is almost stable. In Figure A.5 of the the annexes A more experiments are presented for the axial depth of 15 mm. More investigation needs to be efectuated to understant fully the behaviors that are given with multivariable tools and that present multifrequencies due to the geometry of the tool.

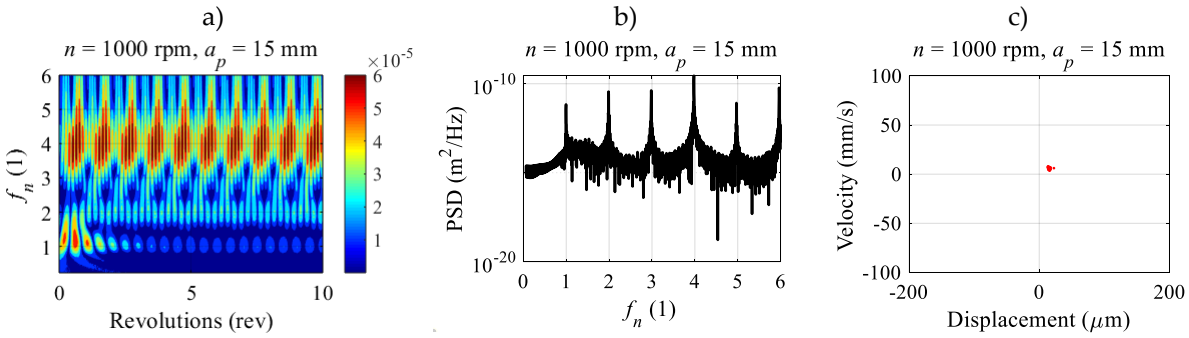

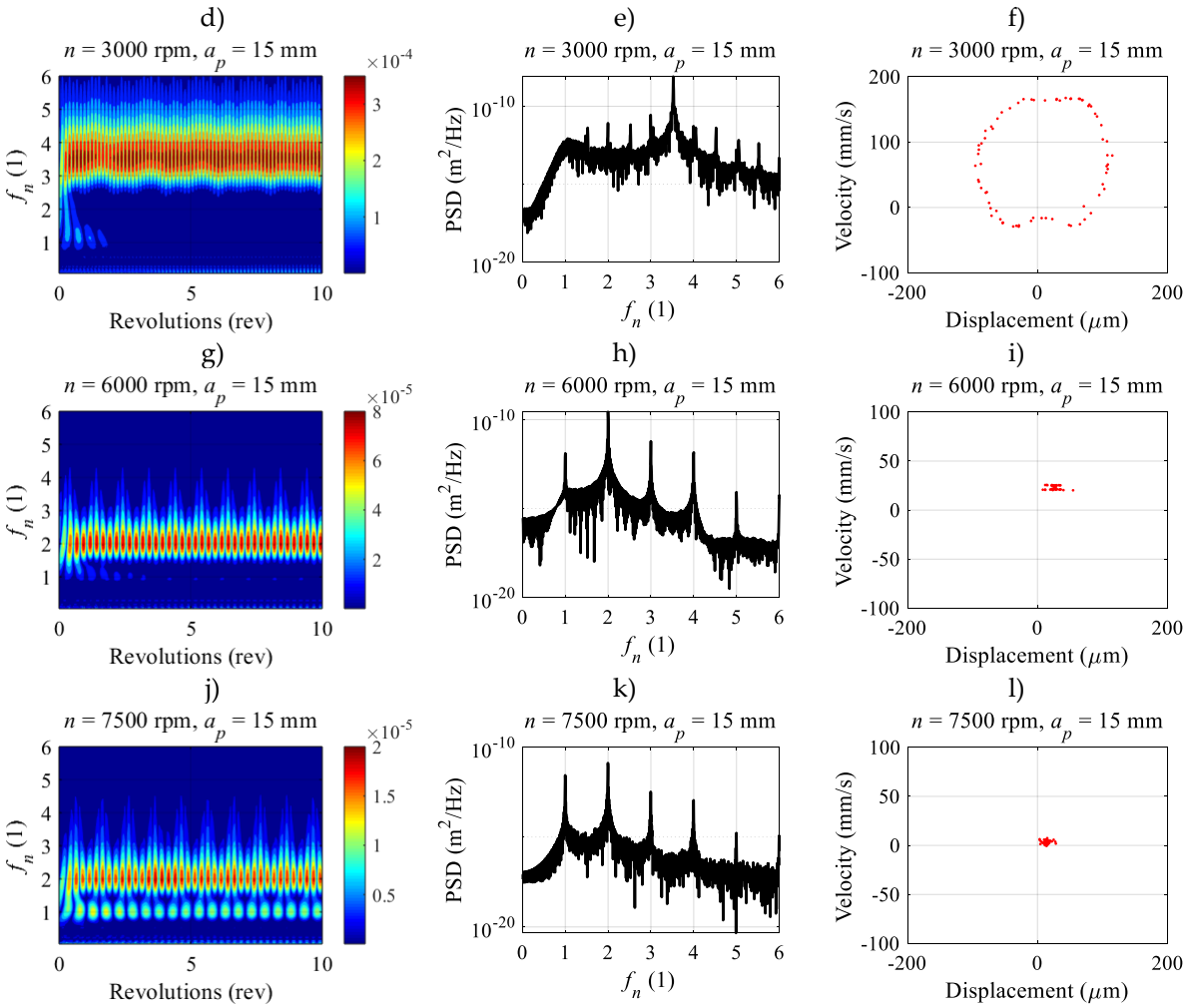

Figure 5.17 Analysis of cutting at 15 mm, with different spindle speeds.

Conclusions

In this work, quadratic and cubic polynomials were used to approximate the delayed terms of delay differential equations. Numerical simulations shown that using second- and third-order EMHPM improve convergence rate and require less computational time when compare to the first-order EMHPM, and to Semi-Discretization and Full-Discretization methods, since fewer approximations or less discrete intervals are needed to reduce the computation time.

To further assess the applicability of the proposed method, the third-order EMHPM was used for determining the stability bounds in one-degree-of-freedom milling operation with a multivariable tool, demonstrating that the stability zone is improved in comparison with a regular tool. For instance, at 2500 rpm the critical axial depth of cut is 1.3 mm using the regular milling tool. However, using the multivariable tool, the critical axial depth of cut was increased until 2.17 mm but more interesting, a stable zone appears above 8.55 mm.

The CWT scalograms, PSD charts and PM were employed to validate the stability lobes found by using the third-order EMHPM for the multivariable tool. Numerical solutions confirmed the system dynamics behavior predicted by the third-order EMHPM.

Based on the above results, this work provides evidence the third-order EMHPM can be used to study dynamic phenomena that appear at higher axial depths of cut due to the multivariable design of the tool, which breaks the excitation frequencies at lower depth of cut.

Annexes

Annex A. Characterization of the multivariable tool varying the spindle speed and the depth of cut

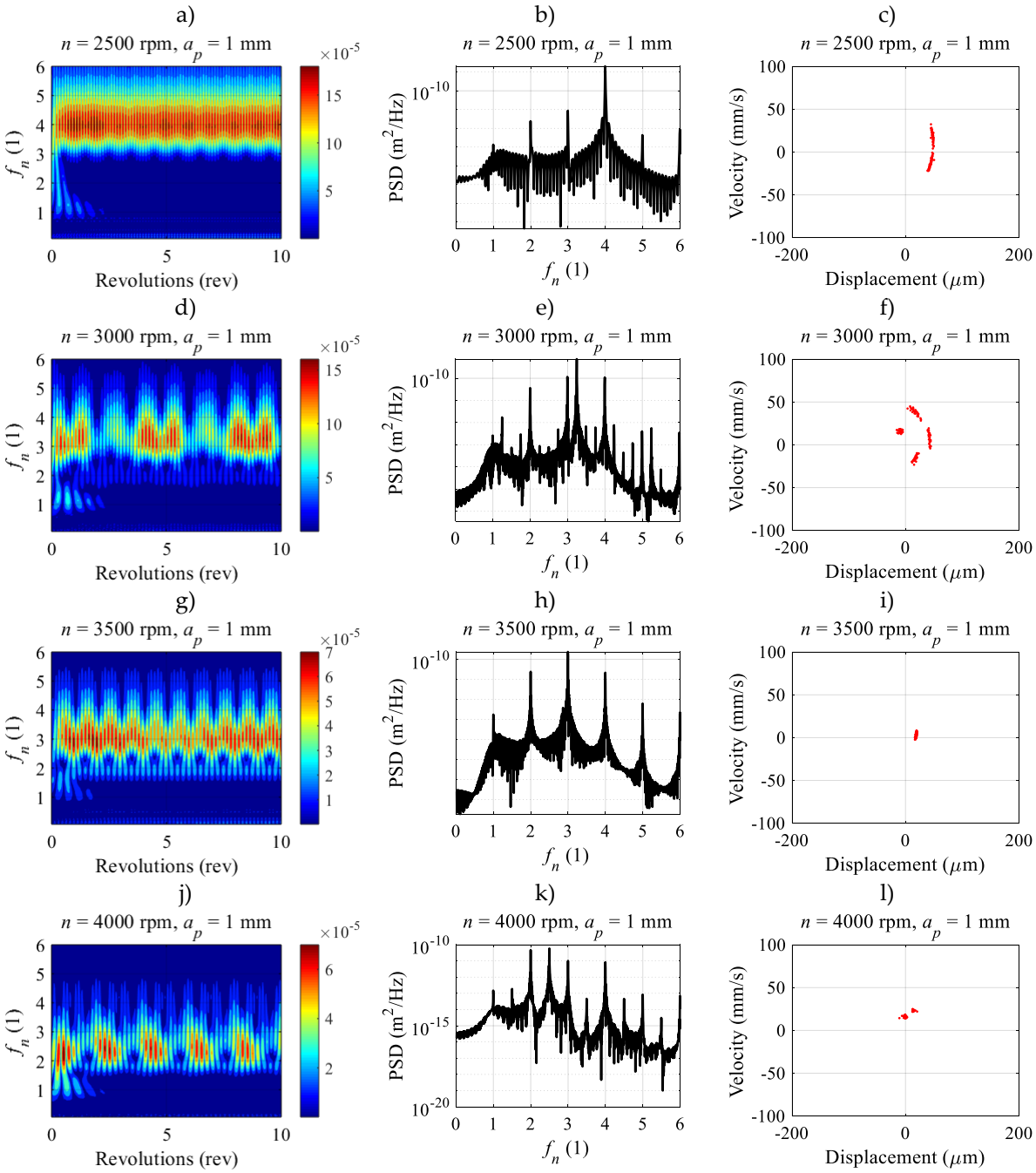

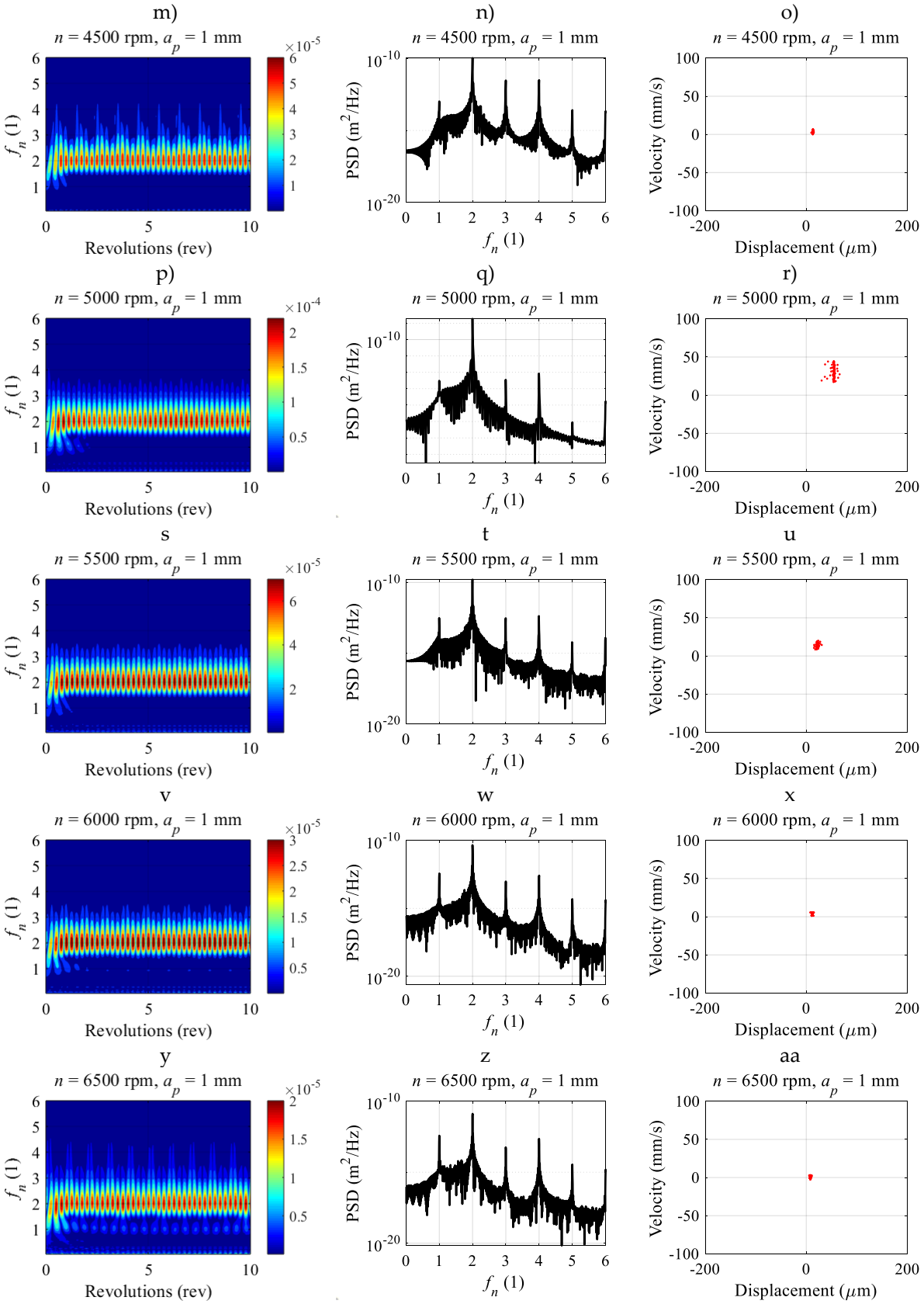
m)
n = 4500 rpm, a_p = 1 mm
f_n (1)
Revolutions (rev)
×10^-5
n)
n = 4500 rpm, a_p = 1 mm
PSD (m^2/Hz)
f_n (1)
o)
n = 4500 rpm, a_p = 1 mm
Velocity (mm/s)
Displacement (μm)
p)
n = 5000 rpm, a_p = 1 mm
×10^-4
q)
n = 5000 rpm, a_p = 1 mm
r)
n = 5000 rpm, a_p = 1 mm
s)
n = 5500 rpm, a_p = 1 mm
×10^-5
t)
n = 5500 rpm, a_p = 1 mm
u)
n = 5500 rpm, a_p = 1 mm
v)
n = 6000 rpm, a_p = 1 mm
×10^-5
w)
n = 6000 rpm, a_p = 1 mm
x)
n = 6000 rpm, a_p = 1 mm
y)
n = 6500 rpm, a_p = 1 mm
×10^-5
z)
n = 6500 rpm, a_p = 1 mm
aa)
n = 6500 rpm, a_p = 1 mm

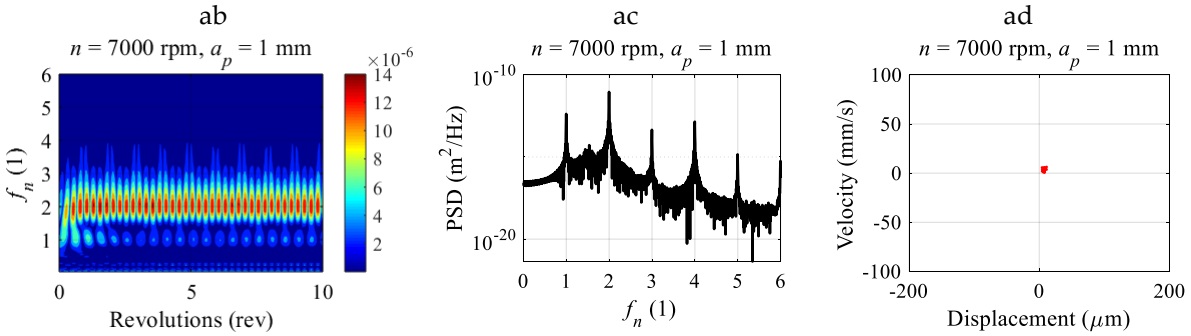

Figure A1. CWT, PSD and PM for a_p=1 mm, a_e=3.175 mm, with spindle speed from 2500-7000 rpm with increments of 500 rpm.

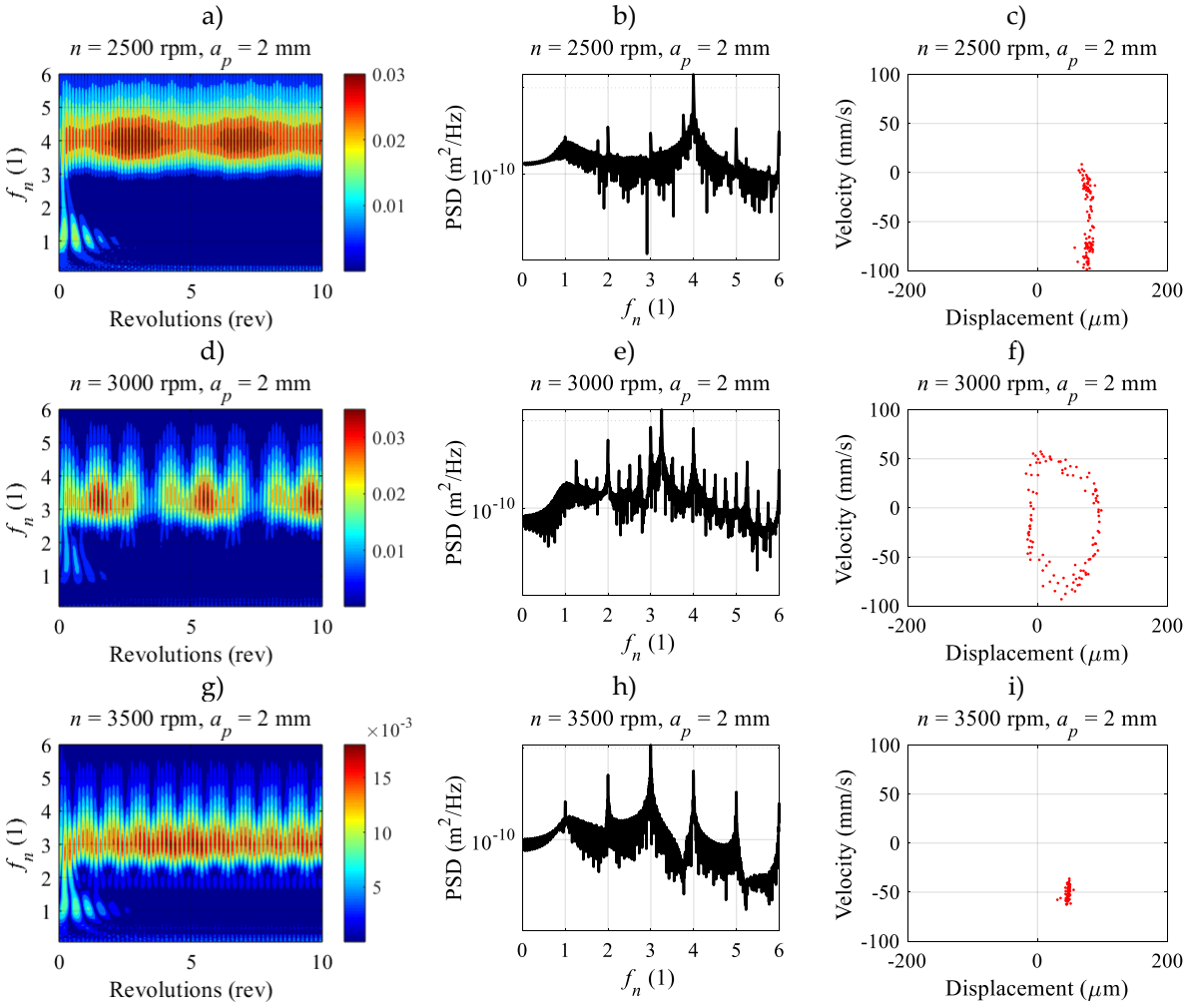

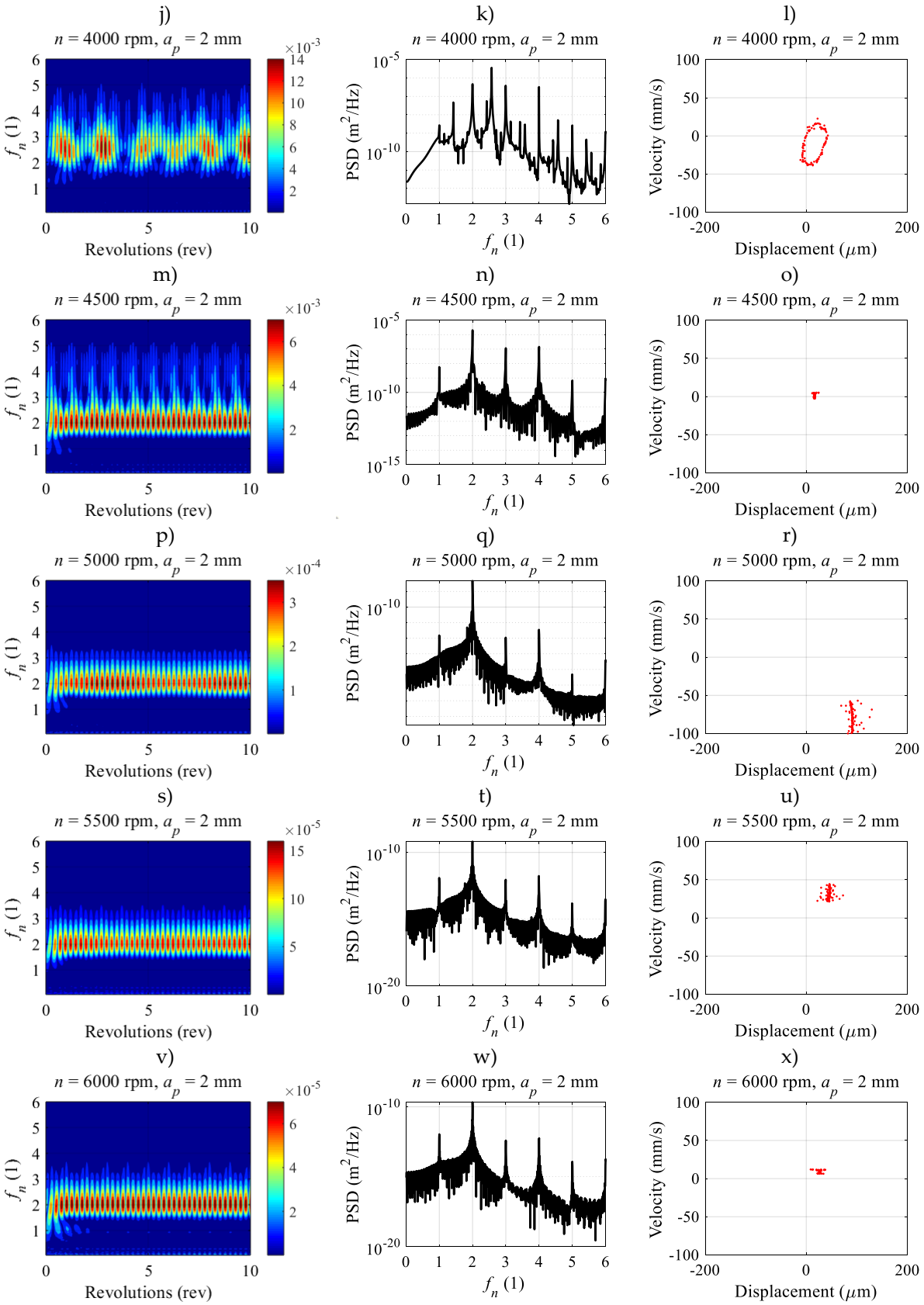
j)
n = 4000 rpm, a_p = 2 mm
f_n (1)
Revolutions (rev)
×10^-3
k)
n = 4000 rpm, a_p = 2 mm
PSD (m^2/Hz)
f_n (1)
l)
n = 4000 rpm, a_p = 2 mm
Velocity (mm/s)
Displacement (μm)
m)
n = 4500 rpm, a_p = 2 mm
f_n (1)
Revolutions (rev)
×10^-3
n)
n = 4500 rpm, a_p = 2 mm
PSD (m^2/Hz)
f_n (1)
o)
n = 4500 rpm, a_p = 2 mm
Velocity (mm/s)
Displacement (μm)
p)
n = 5000 rpm, a_p = 2 mm
f_n (1)
Revolutions (rev)
×10^-4
q)
n = 5000 rpm, a_p = 2 mm
PSD (m^2/Hz)
f_n (1)
r)
n = 5000 rpm, a_p = 2 mm
Velocity (mm/s)
Displacement (μm)
s)
n = 5500 rpm, a_p = 2 mm
f_n (1)
Revolutions (rev)
×10^-5
t)
n = 5500 rpm, a_p = 2 mm
PSD (m^2/Hz)
f_n (1)
u)
n = 5500 rpm, a_p = 2 mm
Velocity (mm/s)
Displacement (μm)
v)
n = 6000 rpm, a_p = 2 mm
f_n (1)
Revolutions (rev)
×10^-5
w)
n = 6000 rpm, a_p = 2 mm
PSD (m^2/Hz)
f_n (1)
x)
n = 6000 rpm, a_p = 2 mm
Velocity (mm/s)
Displacement (μm)

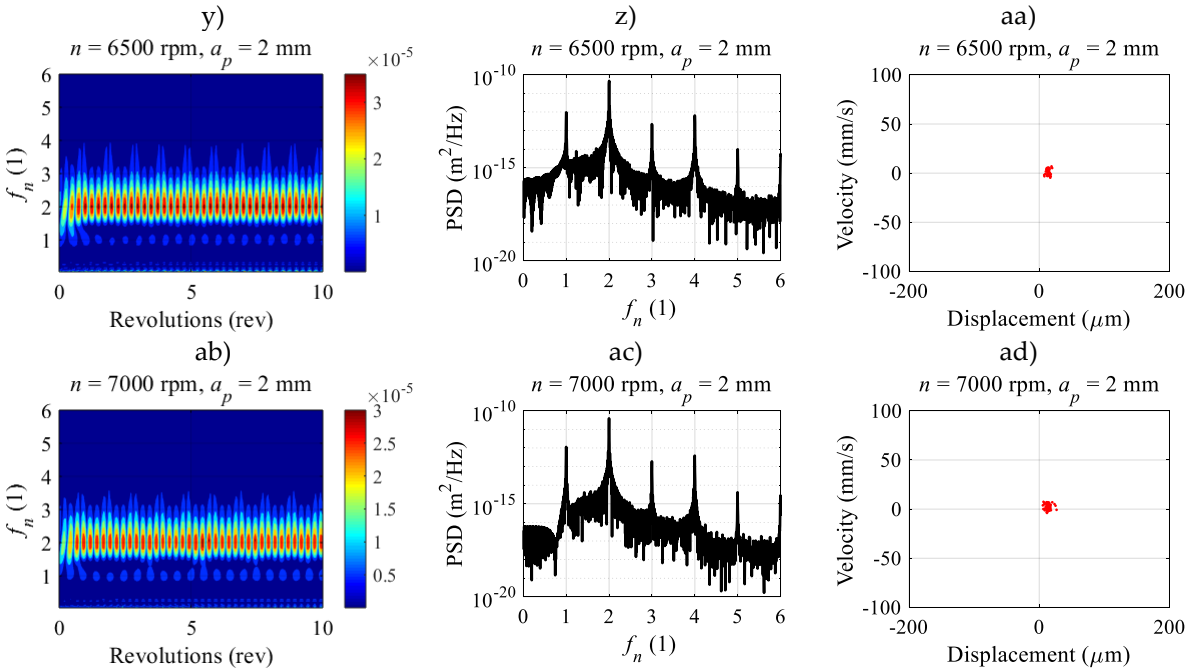

Figure A2. CWT, PSD and PM for a_p=2 mm, a_e=3.175 mm, with spindle speed from 2500-7000 rpm with increments of 500 rpm.

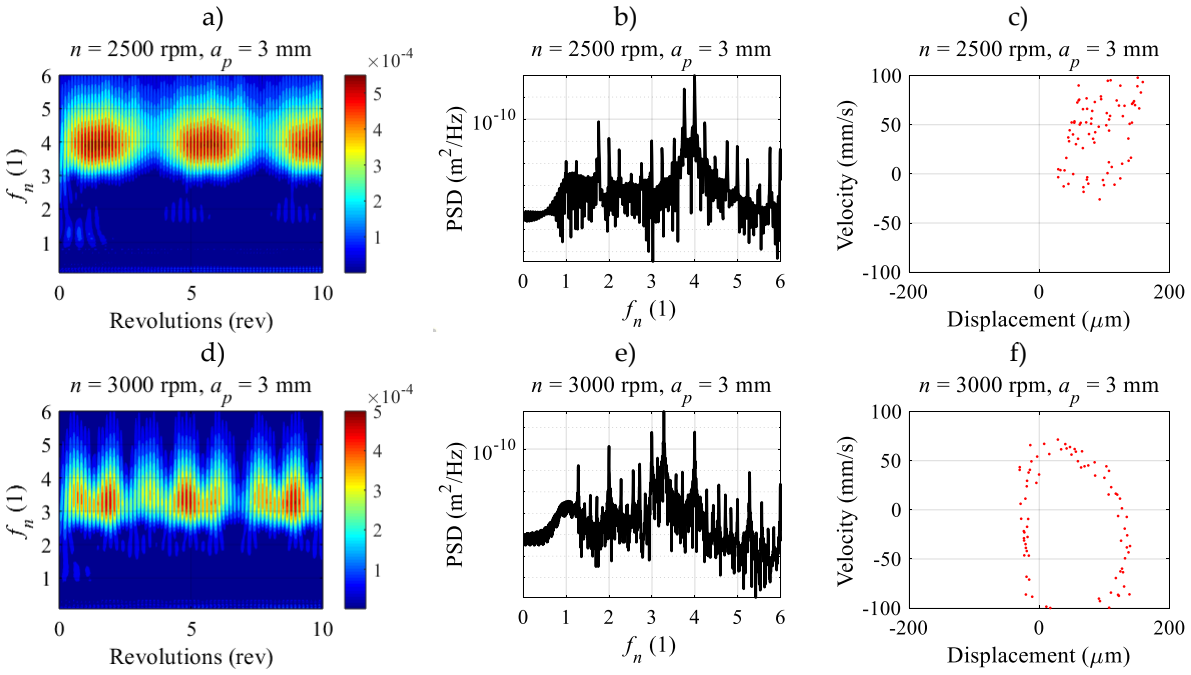

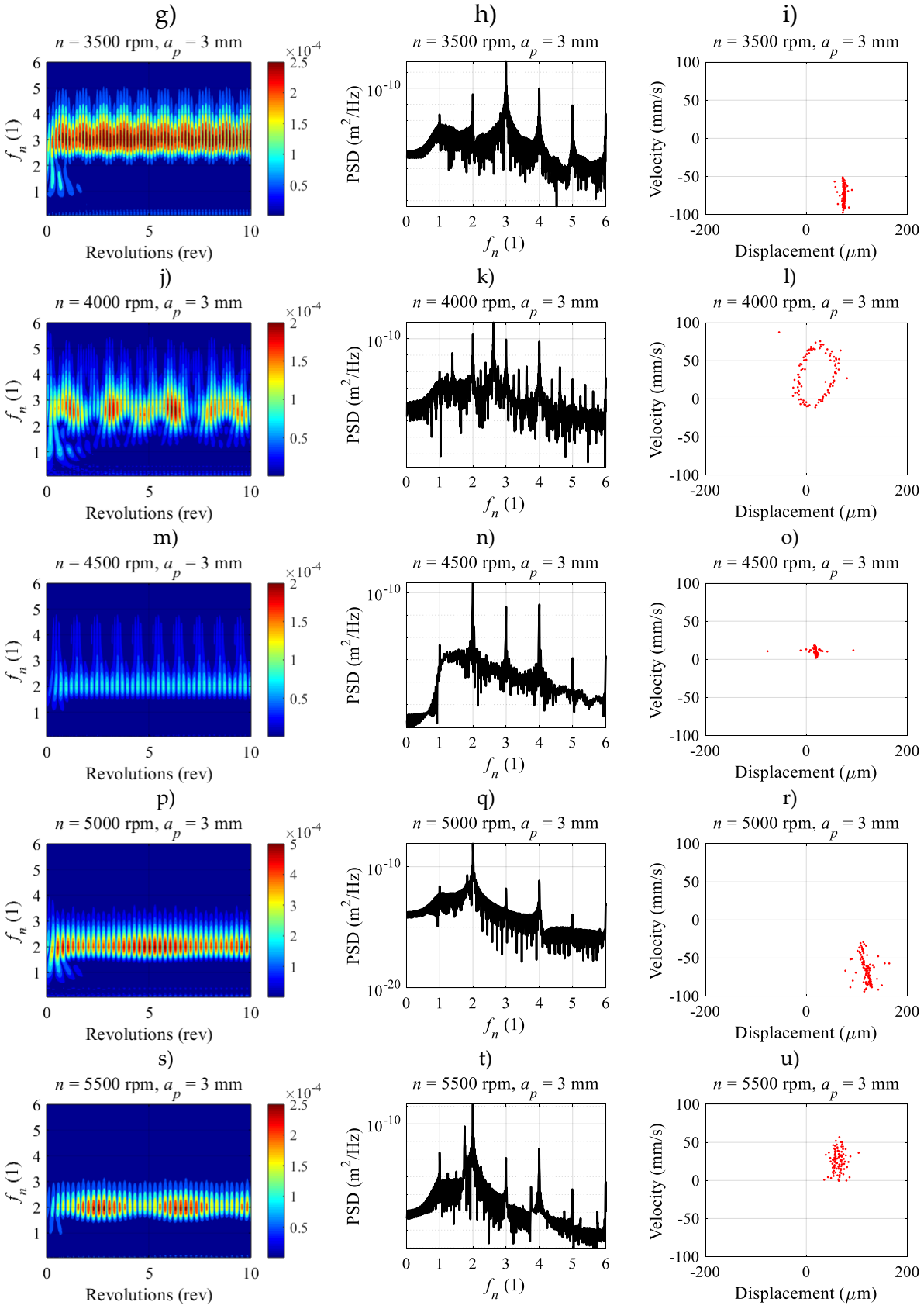
g)
n = 3500 rpm, a_p = 3 mm
f_n (1)
Revolutions (rev)
×10^-4
h)
n = 3500 rpm, a_p = 3 mm
PSD (m^2/Hz)
f_n (1)
i)
n = 3500 rpm, a_p = 3 mm
Velocity (mm/s)
Displacement (μm)
j)
n = 4000 rpm, a_p = 3 mm
k)
n = 4000 rpm, a_p = 3 mm
l)
n = 4000 rpm, a_p = 3 mm
m)
n = 4500 rpm, a_p = 3 mm
n)
n = 4500 rpm, a_p = 3 mm
o)
n = 4500 rpm, a_p = 3 mm
p)
n = 5000 rpm, a_p = 3 mm
q)
n = 5000 rpm, a_p = 3 mm
r)
n = 5000 rpm, a_p = 3 mm
s)
n = 5500 rpm, a_p = 3 mm
t)
n = 5500 rpm, a_p = 3 mm
u)
n = 5500 rpm, a_p = 3 mm

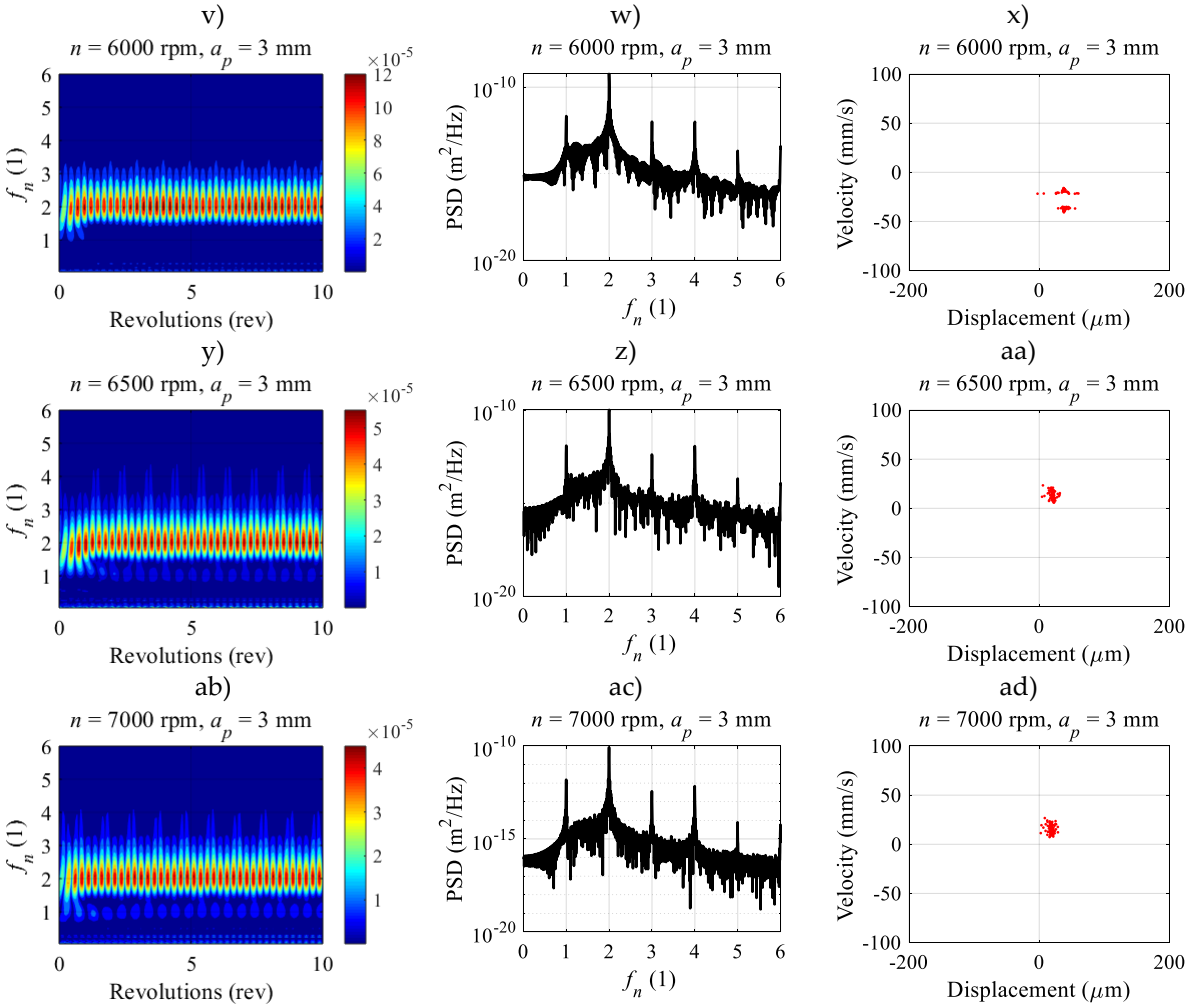

Figure A3. CWT, PSD and PM for a_p=3 mm, a_e=3.175 mm, with spindle speed from 2500-7000 rpm with increments of 500 rpm.

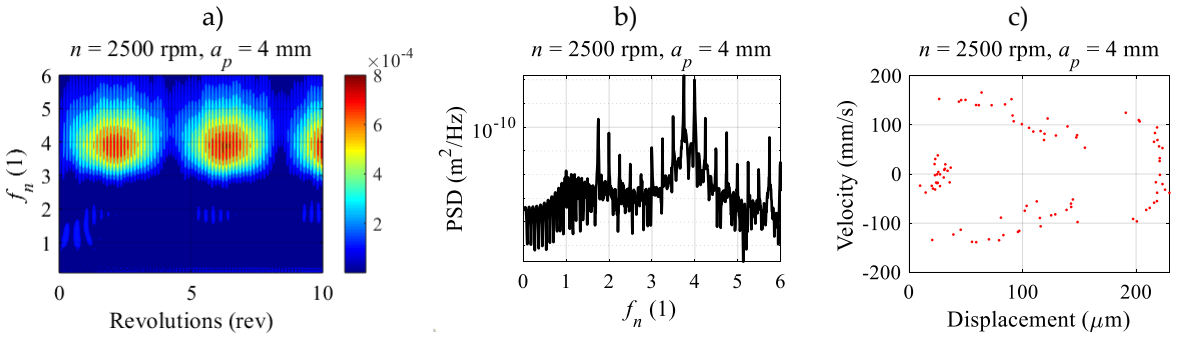

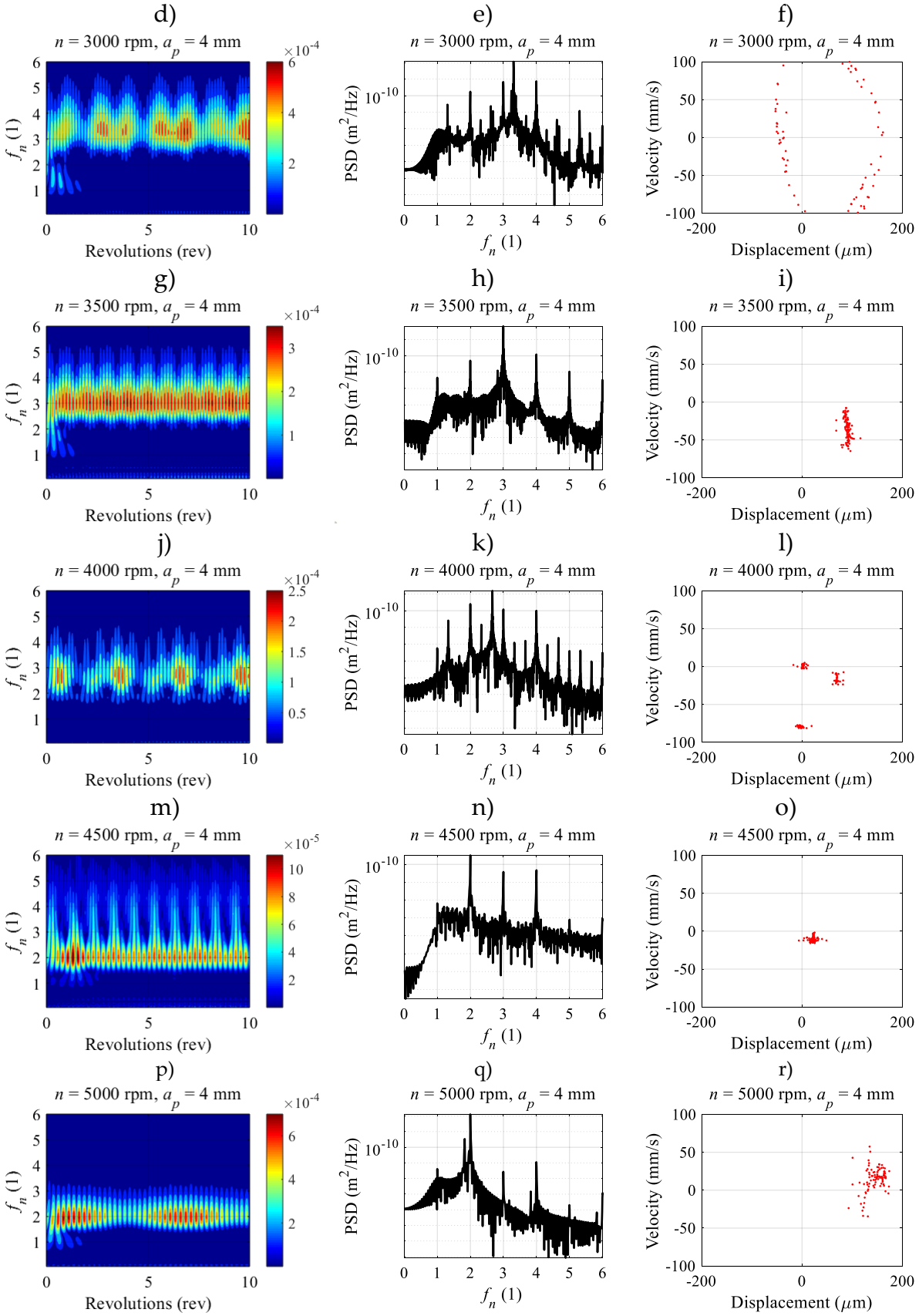
d)
n = 3000 rpm, a_p = 4 mm
f_n (1)
Revolutions (rev)
e)
n = 3000 rpm, a_p = 4 mm
PSD (m^2/Hz)
f_n (1)
f)
n = 3000 rpm, a_p = 4 mm
Velocity (mm/s)
Displacement (μm)
g)
n = 3500 rpm, a_p = 4 mm
h)
n = 3500 rpm, a_p = 4 mm
i)
n = 3500 rpm, a_p = 4 mm
j)
n = 4000 rpm, a_p = 4 mm
k)
n = 4000 rpm, a_p = 4 mm
l)
n = 4000 rpm, a_p = 4 mm
m)
n = 4500 rpm, a_p = 4 mm
n)
n = 4500 rpm, a_p = 4 mm
o)
n = 4500 rpm, a_p = 4 mm
p)
n = 5000 rpm, a_p = 4 mm
q)
n = 5000 rpm, a_p = 4 mm
r)
n = 5000 rpm, a_p = 4 mm

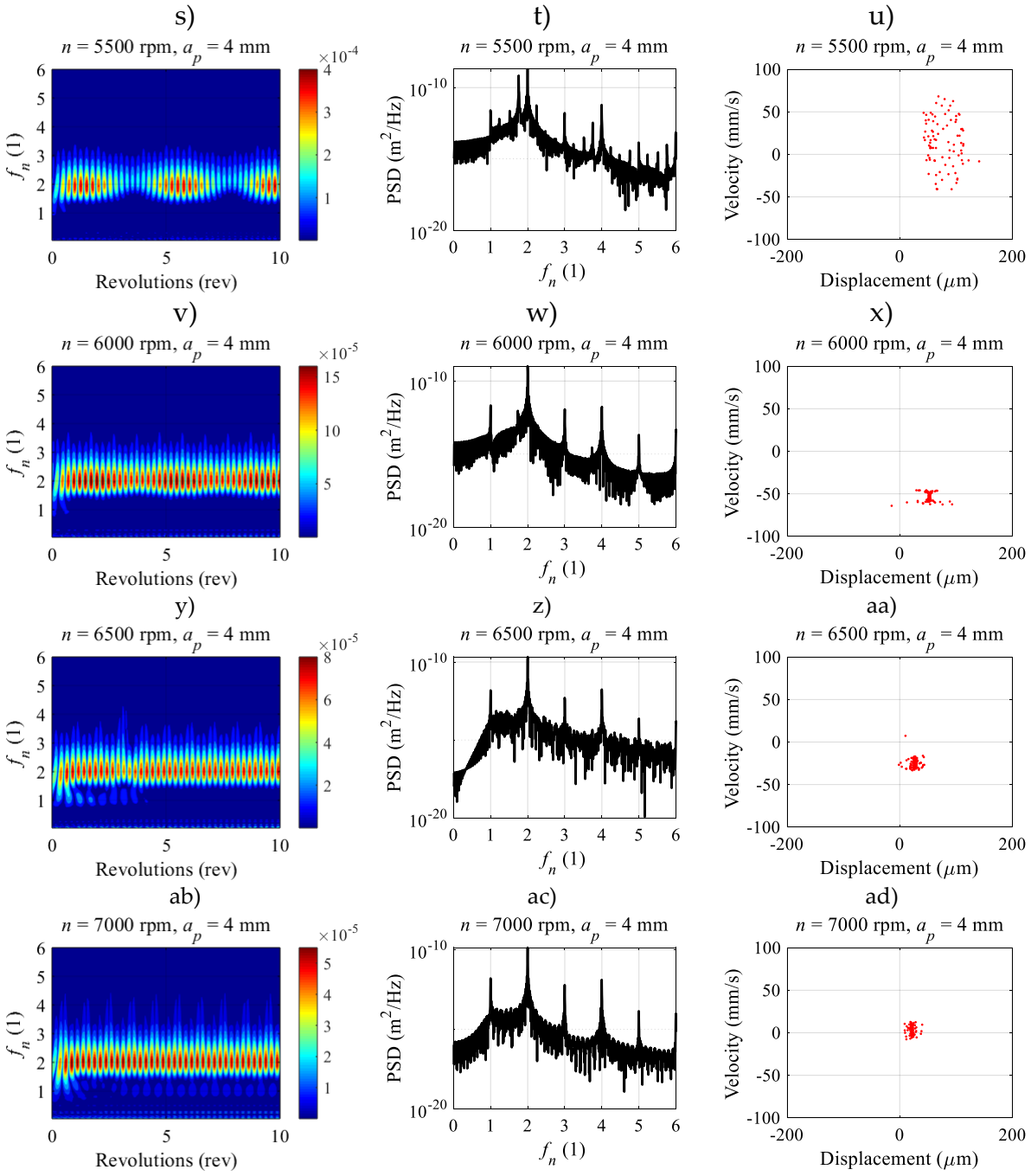

Figure A4. CWT, PSD and PM for a_p=4 mm, a_e=3.175 mm, with spindle speed from 2500-7000 rpm with increments of 500 rpm.

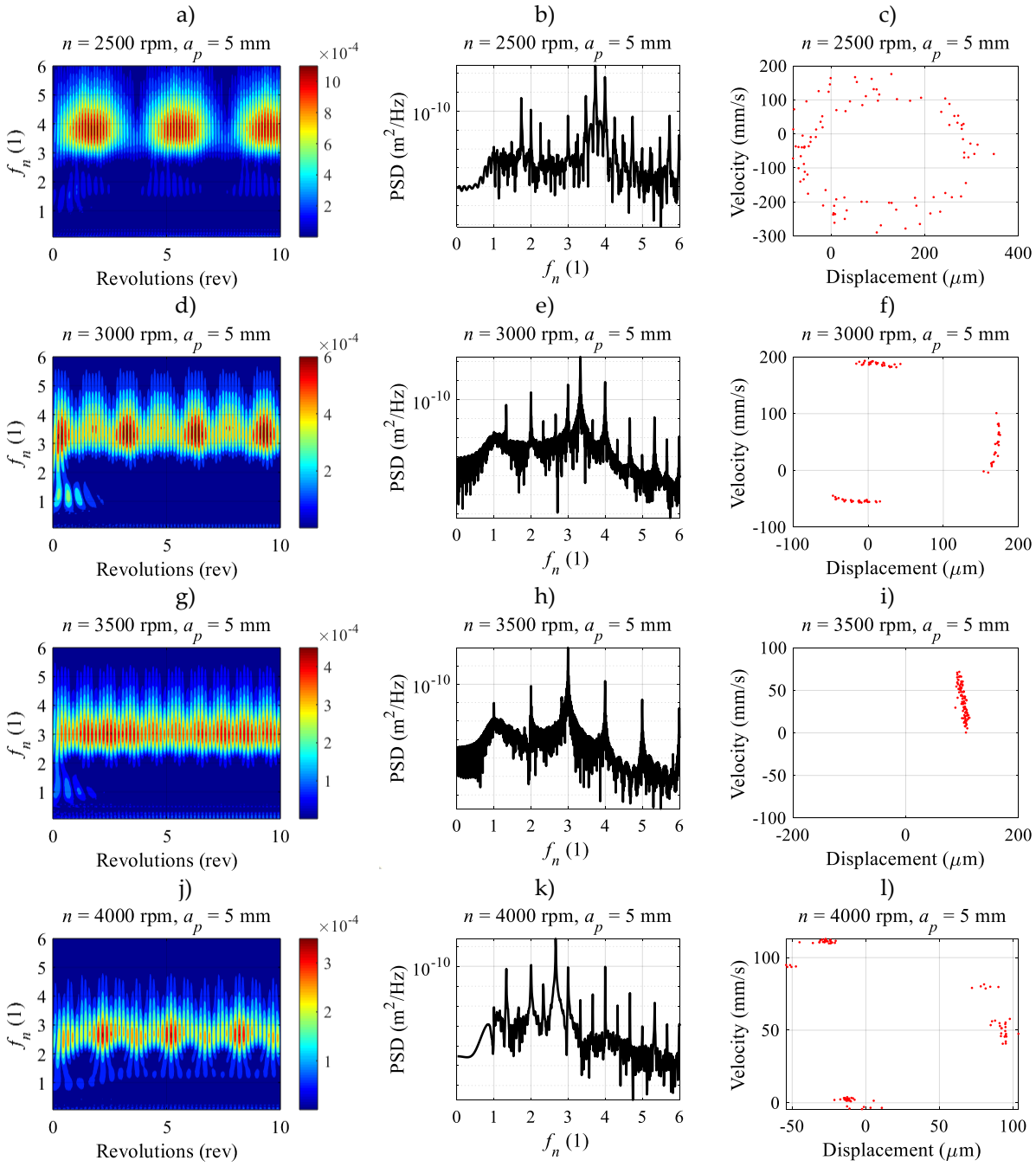
a)
n = 2500 rpm, a_p = 5 mm
f_n (1)
Revolutions (rev)
×10^-4
b)
n = 2500 rpm, a_p = 5 mm
PSD (m^2/Hz)
10^-10
f_n (1)
c)
n = 2500 rpm, a_p = 5 mm
Velocity (mm/s)
Displacement (μm)
d)
n = 3000 rpm, a_p = 5 mm
f_n (1)
Revolutions (rev)
×10^-4
e)
n = 3000 rpm, a_p = 5 mm
PSD (m^2/Hz)
10^-10
f_n (1)
f)
n = 3000 rpm, a_p = 5 mm
Velocity (mm/s)
Displacement (μm)
g)
n = 3500 rpm, a_p = 5 mm
f_n (1)
Revolutions (rev)
×10^-4
h)
n = 3500 rpm, a_p = 5 mm
PSD (m^2/Hz)
10^-10
f_n (1)
i)
n = 3500 rpm, a_p = 5 mm
Velocity (mm/s)
Displacement (μm)
j)
n = 4000 rpm, a_p = 5 mm
f_n (1)
Revolutions (rev)
×10^-4
k)
n = 4000 rpm, a_p = 5 mm
PSD (m^2/Hz)
10^-10
f_n (1)
l)
n = 4000 rpm, a_p = 5 mm
Velocity (mm/s)
Displacement (μm)

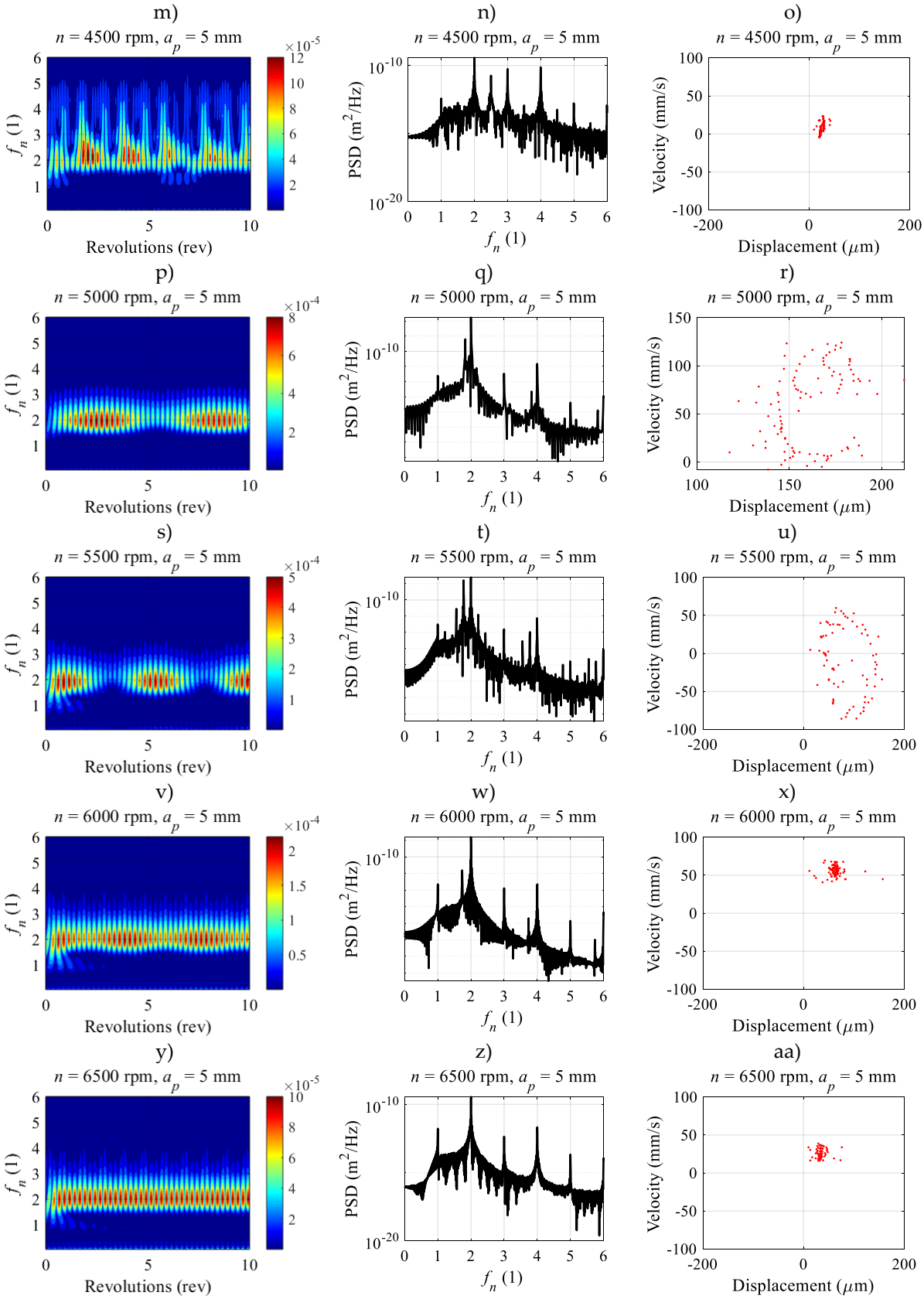
m)
n = 4500 rpm, a_p = 5 mm
f_n (1)
Revolutions (rev)
n)
n = 4500 rpm, a_p = 5 mm
PSD (m^2/Hz)
f_n (1)
o)
n = 4500 rpm, a_p = 5 mm
Velocity (mm/s)
Displacement (μm)
p)
n = 5000 rpm, a_p = 5 mm
f_n (1)
Revolutions (rev)
q)
n = 5000 rpm, a_p = 5 mm
PSD (m^2/Hz)
f_n (1)
r)
n = 5000 rpm, a_p = 5 mm
Velocity (mm/s)
Displacement (μm)
s)
n = 5500 rpm, a_p = 5 mm
f_n (1)
Revolutions (rev)
t)
n = 5500 rpm, a_p = 5 mm
PSD (m^2/Hz)
f_n (1)
u)
n = 5500 rpm, a_p = 5 mm
Velocity (mm/s)
Displacement (μm)
v)
n = 6000 rpm, a_p = 5 mm
f_n (1)
Revolutions (rev)
w)
n = 6000 rpm, a_p = 5 mm
PSD (m^2/Hz)
f_n (1)
x)
n = 6000 rpm, a_p = 5 mm
Velocity (mm/s)
Displacement (μm)
y)
n = 6500 rpm, a_p = 5 mm
f_n (1)
Revolutions (rev)
z)
n = 6500 rpm, a_p = 5 mm
PSD (m^2/Hz)
f_n (1)
aa)
n = 6500 rpm, a_p = 5 mm
Velocity (mm/s)
Displacement (μm)

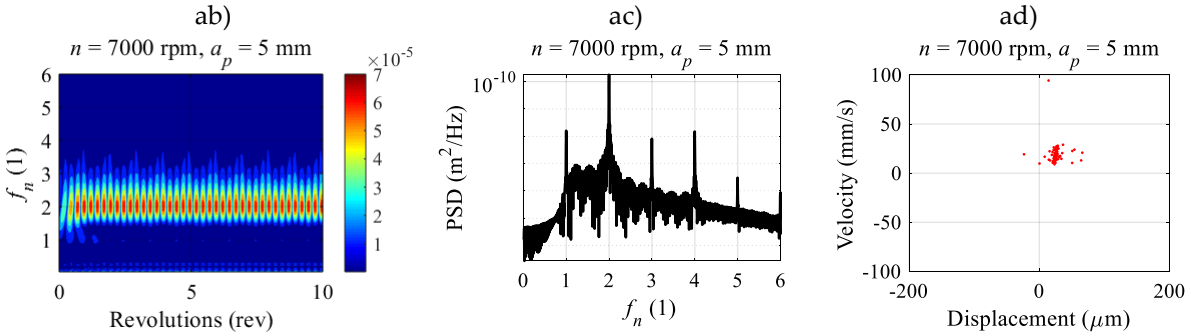

Figure A5. CWT, PSD and PM for a_p=5 mm, a_e=3.175 mm, with spindle speed from 2500-7000 rpm with increments of 500 rpm.

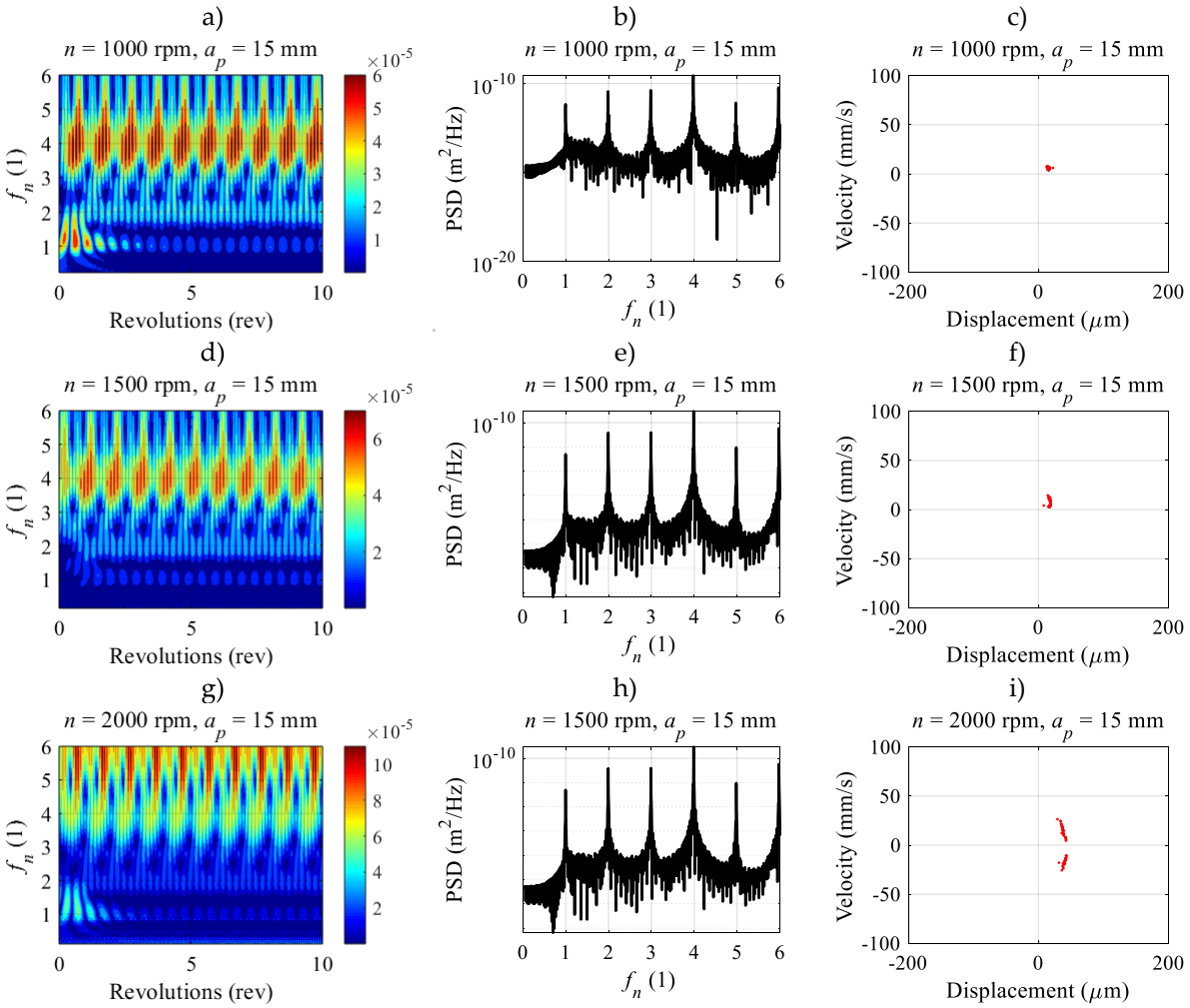

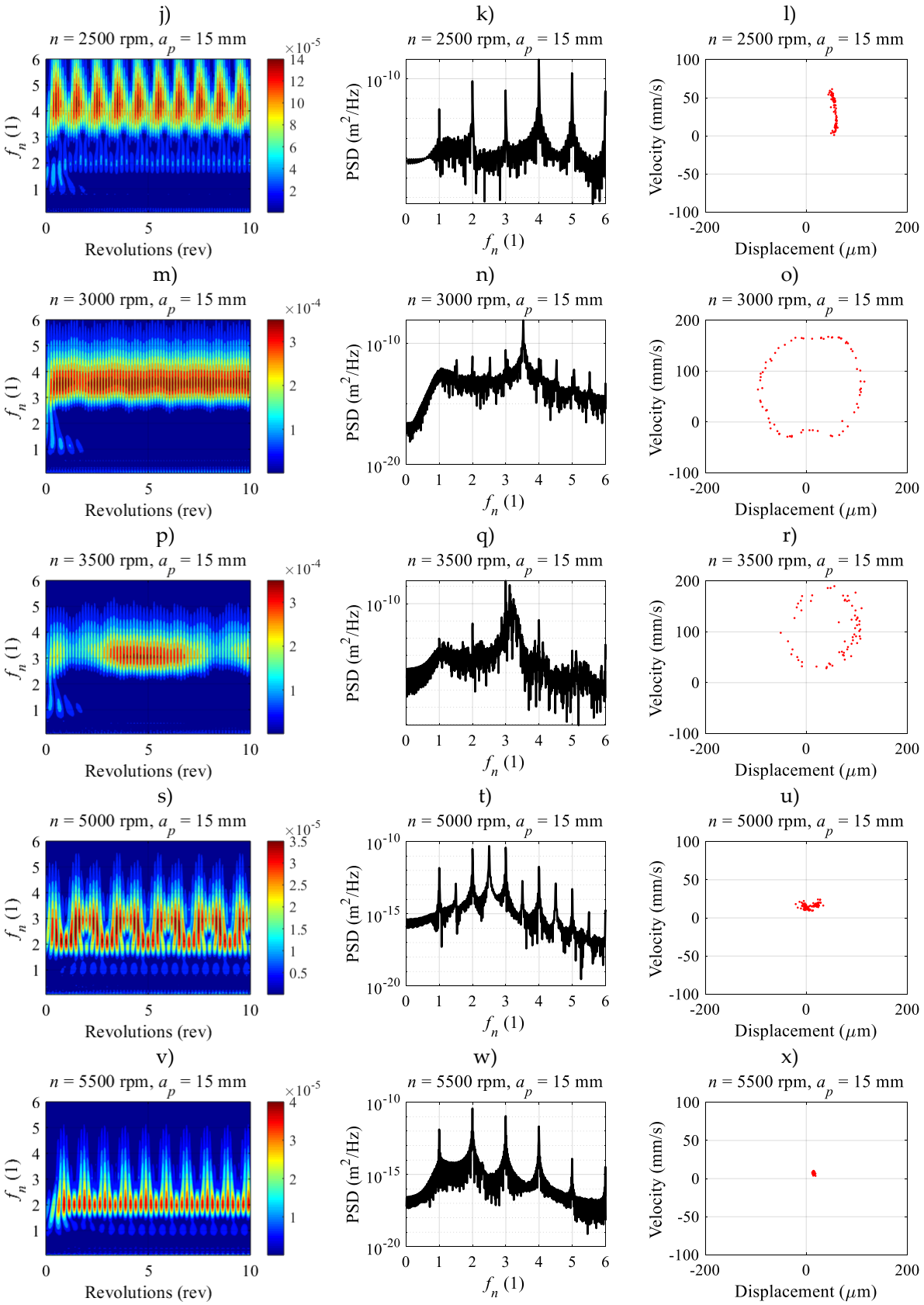
j)
n = 2500 rpm, a_p = 15 mm
f_n (1)
Revolutions (rev)
k)
n = 2500 rpm, a_p = 15 mm
PSD (m^2/Hz)
f_n (1)
l)
n = 2500 rpm, a_p = 15 mm
Velocity (mm/s)
Displacement (μm)
m)
n = 3000 rpm, a_p = 15 mm
f_n (1)
Revolutions (rev)
n)
n = 3000 rpm, a_p = 15 mm
PSD (m^2/Hz)
f_n (1)
o)
n = 3000 rpm, a_p = 15 mm
Velocity (mm/s)
Displacement (μm)
p)
n = 3500 rpm, a_p = 15 mm
f_n (1)
Revolutions (rev)
q)
n = 3500 rpm, a_p = 15 mm
PSD (m^2/Hz)
f_n (1)
r)
n = 3500 rpm, a_p = 15 mm
Velocity (mm/s)
Displacement (μm)
s)
n = 5000 rpm, a_p = 15 mm
f_n (1)
Revolutions (rev)
t)
n = 5000 rpm, a_p = 15 mm
PSD (m^2/Hz)
f_n (1)
u)
n = 5000 rpm, a_p = 15 mm
Velocity (mm/s)
Displacement (μm)
v)
n = 5500 rpm, a_p = 15 mm
f_n (1)
Revolutions (rev)
w)
n = 5500 rpm, a_p = 15 mm
PSD (m^2/Hz)
f_n (1)
x)
n = 5500 rpm, a_p = 15 mm
Velocity (mm/s)
Displacement (μm)

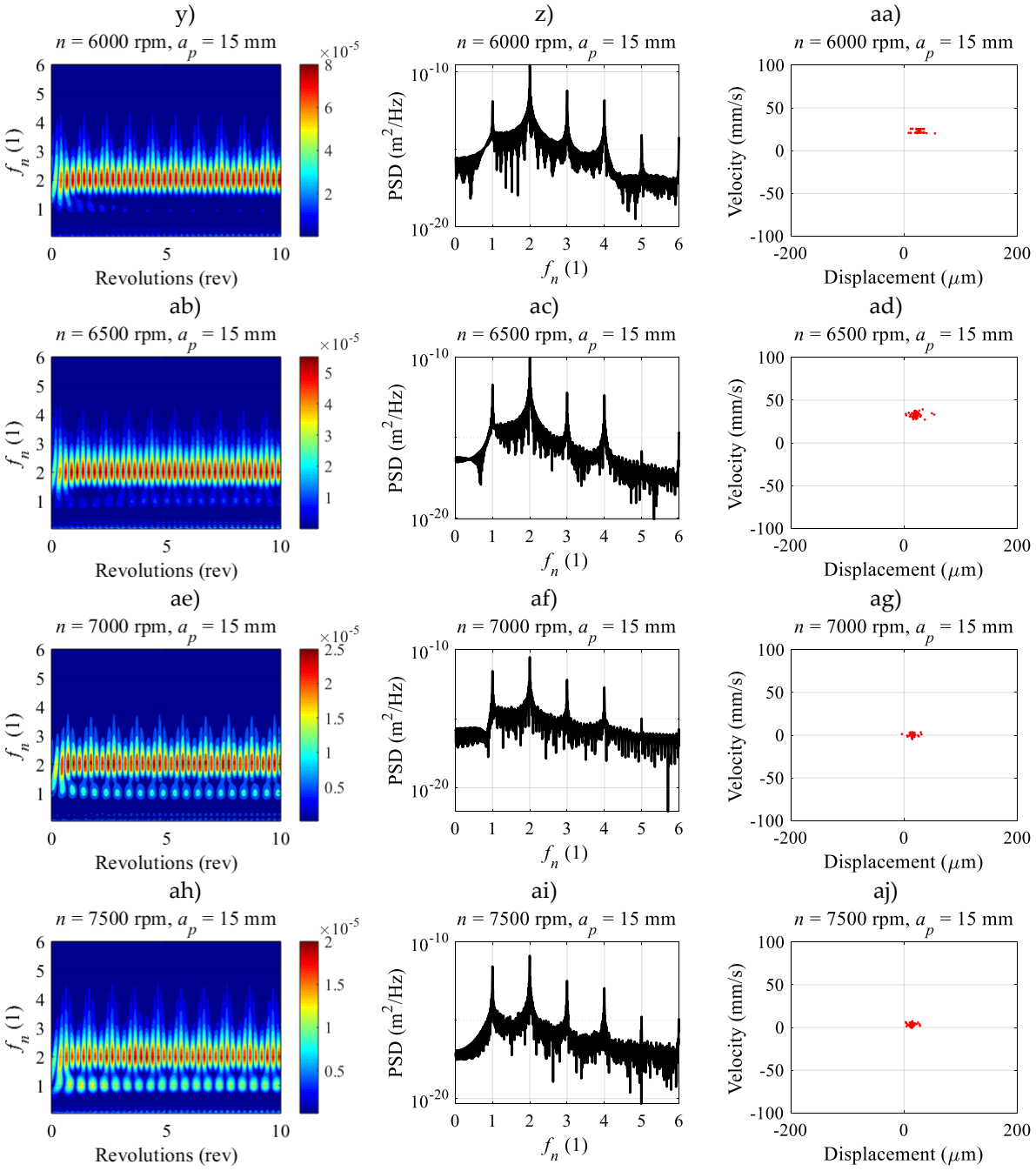

Figure A6. CWT, PSD and PM for a_p=15 mm, a_e=1 mm, with spindle speed from 2500-3500 rpm and from 5000-7000 rpm with increments of 500 rpm.

B.1 Algorithm for milling in ODF with regular tool with dde23 vs zeroth to third order EMHPM

```
function dde23_ddeEMHPM
disp('Milling equation solution')
%Modal parameters
wn=922*2*pi;amort=0.011;mm=0.03993;
%Specific cutting coefficients
Ktc=6E8;Knc=2E8;
%EMHPM parameters
N=75+1; k=7;
% Tool parameters and cutting conditions
zn=2; n=12000; ad=1;ap=0.0015; ntau=8; %number of cycles
phi_st=acos(2*ad-1);phi_ex=pi;
tau=60/(zn*n); Tincr=tau/(N-1);
tfin=ntau*tau; dsct1=N; % points in tau
tt=linspace(-tau,tfin,(dsct1-1)*(ntau+1)+1)';
tspan=[0,tfin];
tdde=linspace(0,tfin,(dsct1-1)*(ntau+1)+1);
dde=@(t,y,z)
milling_dde(t,y,z,wn,ap,amort,mm,Ktc,Knc,n,zn,phi_st,phi_ex);
sol=dde23(dde,tau,@history,tspan);
xdde=deval(sol,tdde);
%% Recursive zeroth order, initial condition c=[0.001 0]
xi_cero=zeros((dsct1-1)*(ntau+1)+1,2);
c=[0.001 0];
xi_cero(1:dsct1,[1,2])=xi_cero(1:dsct1,[1,2])+c;
for it=dsct1+1:(dsct1-1)*(ntau+1)+1
    xi_tau_N=xi_cero((it-dsct1),[1,2]);
    xi0=xi_cero((it-1),[1,2]);
    xi_cero(it,[1,2])=funcion_recursiva0(Tincr,tt(it),k,xi_tau_N,xi0,
    wn,ap,amort,mm,Ktc,Knc,n,zn,phi_st,phi_ex);
end
%% Recursive first order EMHPM
xi=zeros((dsct1-1)*(ntau+1)+1,2);
c=[0.001 0];
xi(1:dsct1,[1,2])=xi(1:dsct1,[1,2])+c;
for it=dsct1+1:(dsct1-1)*(ntau+1)+1
    xi_tau_N=xi((it-dsct1),[1,2]);
    xi_tau_N_=xi((it-dsct1+1),[1,2]);
    xi0=xi((it-1),[1,2]);
    xi(it,[1,2])=funcion_recursiva1(Tincr,tt(it),k,xi_tau_N,xi_tau_N_,
    xi0,tau,N,wn,ap,amort,mm,Ktc,Knc,n,zn,phi_st,phi_ex);
end
%% Recursive second order
xidos=zeros((dsct1-1)*(ntau+1)+1,2);
c=[0.001 0];
xidos(1:dsct1,[1,2])=xidos(1:dsct1,[1,2])+c;
```

```
for it=dsct1+1:(dsct1-1)*(ntau+1)+1
    xi_tau_N=xidos((it-dsct1),[1,2]);
    xi_tau_N_=xidos((it-dsct1+1),[1,2]);
    xi_tau_NN_=xidos((it-dsct1+2),[1,2]);
    xi0=xidos((it-1),[1,2]);
    xidos(it,[1,2])=funcion_recursiva2(Tincr,tt(it),k,xi_tau_N,
    xi_tau_N_,xi_tau_NN_,xi0,tau,N,wn,ap,amort,mm,Ktc,Knc,n,zn,phi_st,
    phi_ex);
end
%% %Recursive third order
xitres=zeros((dsct1-1)*(ntau+1)+1,2);
c=[0.001 0];
xitres(1:dsct1,[1,2])=xitres(1:dsct1,[1,2])+c;
for it=dsct1+1:(dsct1-1)*(ntau+1)+1
    xi_tau_N=xitres((it-dsct1),[1,2]);
    xi_tau_N_=xitres((it-dsct1+1),[1,2]);
    xi_tau_NN_=xitres((it-dsct1+2),[1,2]);
    xi_tau_NNN_=xitres((it-dsct1+3),[1,2]);
    xi0=xitres((it-1),[1,2]);
    xitres(it,[1,2])=funcion_recursiva3(Tincr,tt(it),k,xi_tau_N,
    xi_tau_N_,xi_tau_NN_,xi_tau_NNN_,xi0,tau,N,wn,ap,amort,mm,Ktc,Knc,
    n,zn,phi_st,phi_ex);
end
%% %Plotting
figure (2)
figure1 = figure (2);
axes1 = axes('Parent',figure1); hold(axes1,'on');
plot(tdde,xdde(1,:),'LineWidth',3,'LineStyle','-','Color',[.5 .5 .5]);
plot(tt(1:2:end)',xi_cero(1:2:end,1),'LineWidth',1.5,'Marker','none','
LineStyle',':','MarkerFaceColor',[1 0 0],'Color',[0 0 0]);
plot(tt(1:3:end)',xi((1:3:end),1),'LineWidth',1,'Marker','o',
'LineStyle','none','Color',[0 0 0]);
plot(tt(1:5:end)',xidos((1:5:end),1),'LineWidth',1,'Marker','x',
'LineStyle','none','Color',[0 0 0]);
plot(tt(1:7:end)',xitres((1:7:end),1),'LineWidth',1,'Marker',
'square','LineStyle','none','Color',[0 0 0]);
xlabel('Time (s)','FontWeight','normal','FontName','Times New
Roman','Color',[0 0 0]);
ylabel('Displacement (m)','LineWidth',1,'FontName','Times New Roman',
'Color',[0 0 0]);
legend('dde23','Zeroth-Order EMHPM','First-Order EMHPM','Second-Order
EMHPM','Third-Order EMHPM');
title('EMHPM Milling Function')
set(axes1,'FontName','Times New Roman','FontSize',22,'FontWeight',
'normal','XColor',[0 0 0],'YColor',[0 0 0],'ZColor',[0 0 0]);
legend1 = legend(axes1,'show');
set(legend1,'FontWeight','normal','Orientation','horizontal',
'NumColumns',3,'Location','southoutside');
xlim(axes1,[0 tt(end)]); box on
set(gcf,'position',[1,1, 1000 550])
fprintf('done')
end
```

```
%%
function
Xout=funcion_recursiva0(T,t,k,xi_tau_N,xi0,wn,ap,amort,mm,Ktc,Knc,n,zn
,phi_st,phi_ex)
xi=zeros(k+1,2);
xi(1,:)=xi0;
hxx=0;
for iz=1:zn
    phi_iz=mod((2*pi*n/60)*t+(2*pi*(iz-1)/zn),2*pi);
    if (phi_iz>=phi_st)&&(phi_iz<=phi_ex), gg=1;
    else, gg=0;
    end
    hxx=hxx+gg*sin(phi_iz)*(Ktc*cos(phi_iz)+Knc*sin(phi_iz));
end
for itek=2:k+1
    ik=itek-1;
    if ik==1 %(if k=1)
        g=1;
    else
        g=0;
    end
    A=[0 1; -wn^2-(ap/mm)*hxx -2*amort*wn];
    B=[0 0; (ap/mm)*hxx 0];
    xi(itek,[1,2])=((T/ik)*(A*[xi(itek-1,[1,2])']+g*B*[xi_tau_N]'))';
    xi(itek,[1,2])=((T/ik)*(A*xi(itek-1,[1,2])'+g*B*(xi_tau_N)'))';
end
Xout=sum(xi);
end
%%
function
Xout=funcion_recursiva1(T,t,k,xi_tau_N,xi_tau_N_,xi0,tau,N,wn,ap,
amort,mm,Ktc,Knc,n,zn,phi_st,phi_ex)
xia=zeros(k+1,2);
xib=zeros(k+1,2);
xia(1,:)=xi0;
hxx=0;
for iz=1:zn
    phi_iz=mod((2*pi*n/60)*t+(2*pi*(iz-1)/zn),2*pi);
    if (phi_iz>=phi_st)&&(phi_iz<=phi_ex), gg=1;
    else, gg=0;
    end
    hxx=hxx+gg*sin(phi_iz)*(Ktc*cos(phi_iz)+Knc*sin(phi_iz));
end
for itek=2:k+1
    ik=itek-1;
    if ik==1
        g=1;
    else
        g=0;
    end
    A=[0 1; -wn^2-(ap/mm)*hxx -2*amort*wn];
    B=[0 0; (ap/mm)*hxx 0];
```

```
    xia(itek,[1,2])=((T/ik)*(A*(xia(itek-1,[1,2])')+
    g*B*(xi_tau_N)'))';
    xib(itek,[1,2])=((T/itek)*((A*(xib(itek-1,[1,2])'))+
    g*((N-1)/tau)*T*((-B)*(xi_tau_N)'+B*(xi_tau_N_)')))';
end
sum(xia);
Xout=sum(xia)+sum(xib);
end
% %%
function
Xout=funcion_recursiva2(T,t,k,xi_tau_N,xi_tau_N_,xi_tau_NN_,xi0,tau,N,
wn,ap,amort,mm,Ktc,Knc,n,zn,phi_st,phi_ex)
xia=zeros(k+1,2);
xib=zeros(k+1,2);
xic=zeros(k+1,2);
xia(1,:)=xi0;
hxx=0;
for iz=1:zn
    phi_iz=mod((2*pi*n/60)*t+(2*pi*(iz-1)/zn),2*pi);
    if (phi_iz>=phi_st)&&(phi_iz<=phi_ex), gg=1;
    else, gg=0;
    end
    hxx=hxx+gg*sin(phi_iz)*(Ktc*cos(phi_iz)+Knc*sin(phi_iz));
end
for itek=2:k+1
    ik=itek-1;
    if ik==1
        g=1;
    else
        g=0;
    end
    A=[0 1; -wn^2-(ap/mm)*hxx -2*amort*wn];
    B=[0 0; (ap/mm)*hxx 0];
    xia(itek,[1,2])=((T/ik)*(A*(xia(itek-1,[1,2]))'+
    g*B*(xi_tau_N)'))';
    xib(itek,[1,2])=((T/(ik+1))*((A*(xib(itek-1,[1,2]))')+
    g*((N-1)/tau)*T*B*(-(3/2)*(xi_tau_N)'+2*(xi_tau_N_)'-
    0.5*(xi_tau_NN_)')))';
    xic(itek,[1,2])=((T/(ik+2))*((A*xic(itek-1,[1,2])')+
    g*(((N-1)/tau)^2)*((T^2)/2)*B*((xi_tau_N)'-2*(xi_tau_N_)'+
    (xi_tau_NN_)')))';
end
sum(xia);
Xout=sum(xia)+sum(xib)+sum(xic);
end
%%
function Xout=funcion_recursiva3(T,t,k,xi_tau_N,xi_tau_N_,xi_tau_NN_,
xi_tau_NNN_,xi0,tau,N,wn,ap,amort,mm,Ktc,Knc,n,zn,phi_st,phi_ex)
xia=zeros(k+1,2);
xib=zeros(k+1,2);
xic=zeros(k+1,2);
xid=zeros(k+1,2);
```

```
xia(1,:)=xi0;
hxx=0;
for iz=1:zn
    phi_iz=mod((2*pi*n/60)*t+(2*pi*(iz-1)/zn),2*pi);
    if (phi_iz>=phi_st)&&(phi_iz<=phi_ex),  gg=1;
    else, gg=0;
    end
    hxx=hxx+gg*sin(phi_iz)*(Ktc*cos(phi_iz)+Knc*sin(phi_iz));
end
for itek=2:k+1
    ik=itek-1;
    if ik==1
        g=1;
    else
        g=0;
    end
    A=[0 1; -wn^2-(ap/mm)*hxx -2*amort*wn];
    B=[0 0; (ap/mm)*hxx 0];
    xia(itek,[1,2])=((T/ik)*(A*(xia(itek-1,[1,2]))'+
    g*(B)*(xi_tau_N)'))';
    xib(itek,[1,2])=((T/(ik+1))*((A*(xib(itek-1,[1,2]))')+
    g*((N-1)/tau)*T*B*((-11/6)*(xi_tau_N)'+3*(xi_tau_N_)'-
    (3/2)*(xi_tau_NN_)'+(1/3)*(xi_tau_NNN_)')))';
    xic(itek,[1,2])=((T/(ik+2))*((A*xic(itek-1,[1,2])')+
    g*((T^2)/2)*(((N-1)/tau)^2)*B*(2*(xi_tau_N)'-
    5*(xi_tau_N_)'+4*(xi_tau_NN_)'-(xi_tau_NNN_)')))';
    xid(itek,[1,2])=((T/(ik+3))*((A*xid(itek-1,[1,2])')+
    g*((T^3)/6)*(((N-1)/tau)^3)*B*(-(xi_tau_N)'+3*(xi_tau_N_)'-
    3*(xi_tau_NN_)'+(xi_tau_NNN_)')))';
end
Xout=sum(xia)+sum(xib)+sum(xic)+sum(xid);
end
%%
%Function for dde
function dydt =
milling_dde(t,y,z,wn,ap,amort,mm,Ktc,Knc,n,zn,phi_st,phi_ex)
hxx=0;
for iz=1:zn
    phi_iz=mod((2*pi*n/60)*t+(2*pi*(iz-1)/zn),2*pi);
    if (phi_iz>=phi_st)&&(phi_iz<=phi_ex)
        gg=1;
    else
        gg=0;
    end
    hxx=hxx+gg*sin(phi_iz)*(Ktc*cos(phi_iz)+Knc*sin(phi_iz));
end
dydt = [y(2); -2*amort*wn*y(2)-wn^2*y(1)-(ap*hxx/mm)*(y(1)-z(1))];
end
%
function out=history(t)
out=[0.001+0*t 0+0*t]; %c=[0.001 0]
end
```

B.2 Algorithm for milling in ODF with multivariable tool with dde23 vs third order EMHPM

```
% Specific cutting coefficients
Ktc=[6 6]*1E8; Krc=[2 2]*1E8;
% Modal parameters
omg=922*2*pi; zta=0.011; msa=0.03993;
% Tool parameters
D=10*1E-3; %diameter of the tool
pitch=[180 180]*pi/180; %pitch angles
ang_hel=[1 1]*pi/180; %helix angles
zn=length(pitch); Ndiscos=10; n=12000; dlt_ap=(1.5e-3)/Ndiscos;
% EMHPM parameters
N=75*zn+1; k=7;
% Cutting conditions
aD=1; updw=-1; ntau=4; dsct1=N;
% Initialization
fprintf('surf: 00%%');
for itn=1:length(n)
    fprintf('\b\b\b%2d%%',floor(100*itn/length(n)));
    for it_ap=1:length(dlt_ap)
        tau=60/n(itn);
        Tincr=tau/(N-1);
        tfin=ntau*tau;
        tt=linspace(-tau,tfin,(dsct1-1)*(ntau+1)+1)';
        retraso_ang=zeros(length(zn),length(Ndiscos));
        Tau_N=retraso_ang; phi_0=retraso_ang;
%         Discretization of the tool axially
        for Ndiscos=1:Ndiscos
            for iz=1:zn
                if iz==1, iz_previous=zn;
                else,  iz_previous=iz-1;
                end
            retraso_ang(iz,Ndiscos)=pitch(iz_previous)+(Ndiscos-
            1)*dlt_ap(it_ap)*2*(tan(ang_hel(iz))-
            tan(ang_hel(iz_previous)))/D;
            Tau_N(iz,Ndiscos)=round((N-1)*retraso_ang(iz,Ndiscos)/
            (2*pi));
            % Calculation of the position angle associated with each
            cutting edge per disk
            phi_0(iz,Ndiscos)=mod(pitch(iz)-(2*tan(ang_hel(iz))/D)*
            (Ndiscos-1)*dlt_ap(it_ap)-sum(pitch(1:iz)),2*pi);
            end
        end
        %
        if updw==1, phi_st=0; phi_ex=acos(1-2*aD);
        elseif updw==-1, phi_st=acos(2*aD-1);  phi_ex=pi;
        end
        % Mechanistic model of cutting forces
        hyy=zeros(zn,Ndiscos,N-1);
```

```
    % Calculation of cutting forces on each discretization
    for iN=1:ntau*N-1
        % Searching for disks that are cutting
        phi_iN=mod(phi_0+(iN)*2*pi/(N-1),2*pi);
        hyy_cut=zeros(zn,Ndiscos);
        phi_cut=find(phi_iN>=phi_st & phi_iN<=phi_ex);
        filo_cut=mod(phi_cut,zn);
        filo_cut(filo_cut==0)=zn;
        % Calculation of cutting forces on edges that meet the
        condition
        hyy_cut(phi_cut)=sin(phi_iN(phi_cut)).*(Ktc(filo_cut)'.*cos
        (phi_iN(phi_cut))+Krc(filo_cut)'.*sin(phi_iN(phi_cut)));
        hyy(:,:,iN)=hyy_cut;
    end
     val_Nmin=min(min(Tau_N)); val_Nmax=max(max(Tau_N));
     siz=size(Tau_N);
    elements=zeros(val_Nmax-val_Nmin+1,(siz(1,1)*siz(1,2)+1));
    for i=1:(val_Nmax-val_Nmin+1)
        val=length(find(Tau_N==val_Nmin+i-1));
        elements(i,1)=val_Nmin+i-1;
        elements(i,2:val+1)=elements(i,2:val+1)+
        find(Tau_N==val_Nmin+i-1)';
    end
    iN_=(ntau*N)-1; iF_=val_Nmax-val_Nmin+1;
    Force=zeros(length(iN_),length(iF_));
    %Sum of all forces on time
    for iN=1:iN_
        hyy_iN=hyy(:,:,iN);
        for i_F=1:iF_
           Force(iN,i_F)=sum(hyy_iN(elements(i_F,2:(length(find
           (elements(i_F,2:end)))+1))));
        end
    end
    %%
    % Recursive third order multivariable
    zi_tres=zeros((dsct1-1)*(ntau+1)+1,2);
    c=[0.001 0];
    zi_tres(1:dsct1,:)=zi_tres(1:dsct1,:)+c;
    Ba_retardo=[0 0; 0 0];
    Bb_retardo=[0 0; 0 0];
    Bc_retardo=[0 0; 0 0];
    Bd_retardo=[0 0; 0 0];
    iN=0;
    for it=dsct1+1:(dsct1-1)*(ntau+1)+1
        zi0=zi_tres((it-1),:); % el anterior
        iN=iN+1;
        zi_tres(it,:)=funcion_recursiva3(Ba_retardo,Bb_retardo,
        Bc_retardo,Bd_retardo,Tincr,k,it,zi_tres,zi0,tau,N,omg,
        dlt_ap(it_ap),zta,msa,Force,val_Nmax,val_Nmin,iN);
    end
end
```

```
end
%% dde23
N=((N-1)/zn)+1; ad=aD; wn=omg; amort=zta; mm=msa;
Ktc=Ktc(1); Knc=Krc(1);
ap=dlt_ap*Ndiscos;
phi_st=acos(2*ad-1);phi_ex=pi;
tau=60/(zn*n); Tincr=tau/(N-1); ntau=ntau*2;
tfin=ntau*tau;
dsct1=N;
tspan=[0,tfin];
tdde=linspace(0,tfin,(dsct1-1)*(ntau+1)+1);
dde=@(t,y,z)
milling_dde(t,y,z,wn,ap,amort,mm,Ktc,Knc,n,zn,phi_st,phi_ex);
sol=dde23(dde,tau,@history,tspan);
xdde=deval(sol,tdde);
%%
figure (2)
figure1 = figure (2);
axes1 = axes('Parent',figure1);
hold(axes1,'on');
plot(tdde,xdde(1,:),'LineWidth',3,'LineStyle','-','Color',[.5 .5 .5]);
plot(tt(1:2:end)',zi_tres((1:2:end),1),'LineWidth',1,'Marker','x',
'LineStyle','none','Color',[0 0 0]);
xlabel('Time (s)'); ylabel('Displacement (m)');
legend('dde23','Third-Order EMHPM');
title('EMHPM Milling Function')
xlim(axes1,[0 tt(end)]); box on
set(gcf,'position',[1,1, 870 490])
fprintf('done')
%%
function
Zout=funcion_recursiva3(Ba_retardo,Bb_retardo,Bc_retardo,Bd_retardo,T,
k,it,zi,zi0,tau,N,omg,dap_xdisco,zta,msa,Force,val_Nmax,val_Nmin,iN)
zia=zeros(k+1,2);
zib=zeros(k+1,2);
zic=zeros(k+1,2);
zid=zeros(k+1,2);
zia(1,:)=zi0;
A=[0 1; -omg^2-dap_xdisco*sum(Force(iN,:))/msa -2*zta*omg];
for itek=2:k+1
    ik=itek-1;
    if ik==1
        g=1;
    else
        g=0;
    end
    for d=val_Nmin:val_Nmax
        dn=d-val_Nmin+1;
        B=[0 0; (dap_xdisco/msa)*sum(Force(iN,dn)) 0];
        Ba_retardo(:,:)=B*(zi(it-d-1))'+Ba_retardo(:,:);
         Bb_retardo(:,:)=((N-1)/tau)*T*B*(-(11/6)*zi(it-d-1)+3*zi(it-
         d)-(3/2)*zi(it-d+1)+(1/3)*zi(it-d+2))'+Bb_retardo(:,:);
```

```
        Bc_retardo(:,:)=(((N-1)/tau)^2)*((T^2)/2)*B*(2*zi(it-d-1)-
        5*zi(it-d)+4*zi(it-d+1)-zi(it-d+2))'+Bc_retardo(:,:);
        Bd_retardo(:,:)=(((N-1)/tau)^3)*((T^3)/6)*B*(-zi(it-d-
        1)+3*zi(it-d)-3*zi(it-d+1)+zi(it-d+2))'+Bd_retardo(:,:);
    end
    zia(itek,:)=((T/ik)*(A*(zia(itek-1,:))'+
    g*[0;(Ba_retardo(2,1,:))]))';
    zib(itek,:)=((T/(ik+1))*((A*(zib(itek-1,:))')+
    g*[0;(Bb_retardo(2,1,:))]))';
    zic(itek,:)=((T/(ik+2))*((A*(zic(itek-1,:)'))+
    g*[0;(Bc_retardo(2,1,:))]))';
    zid(itek,:)=((T/(ik+3))*((A*(zid(itek-1,:)'))+
    g*[0;(Bd_retardo(2,1,:))]))';
end
Zout=sum(zia)+sum(zib)+sum(zic)+sum(zid);
end
%% function for dde
function dydt =
milling_dde(t,y,z,wn,ap,amort,mm,Ktc,Knc,n,zn,phi_st,phi_ex)
hxx=0;
for iz=1:zn
    phi_iz=mod((2*pi*n/60)*t+(2*pi*(iz-1)/zn),2*pi);
    if (phi_iz>=phi_st)&&(phi_iz<=phi_ex)
        gg=1;
    else
        gg=0;
    end
    hxx=hxx+gg*sin(phi_iz)*(Ktc*cos(phi_iz)+Knc*sin(phi_iz));
end
dydt = [y(2); -2*amort*wn*y(2)-wn^2*y(1)-(ap*hxx/mm)*(y(1)-z(1))];
end
%
function out=history(t)
out=[0.001+0*t 0+0*t];
end
```

B.3 Algorithm for stability with multivariable tool using the third order EMHPM

```
function thesis_STBLBS_vHLX_vPCH
disp('Estabilidad de fresado en un grado de libertad con herramientas
multivariable, Orden 3 Jose Sosa...')
%Valores de entrada
% Parámetros del EMHPM
m_aprx=7; N=241;
% Barrido de los parámetros del sistema
n_dsk=160;
n_s=linspace(1.5E3,8E3,200); ap_s=linspace(1E-3/n_dsk,18E-3,n_dsk);
dlt_ap=(ap_s(end)-ap_s(1))/(n_dsk);
% Coeficientes de fuerza específica
Ktc=[1 1 1 1]*975.1517E6; Krc=[1 1 1 1]*298.7496E6;
```

```
% Parámetros modales
omg=158.8*2*pi; zta=3.36e-2; msa=6.13;
% Parámetros de herramienta
D=12.7E-3; %diametro
ptch=[110 80 100 70]*pi/180; %angulo entre filos
hlx=[40.71 38.73 36.33 38.6]*pi/180; %angulo entre hélices
k_bta=2*tan(hlx)/D; z_n=length(hlx); %numero filos
aD=1E-3/D; %relación de inmersión radial del corte
% Condiciones de corte
updw=-1;
if updw==1, phi_st=0; phi_ex=acos(1-2*aD);
elseif updw==-1, phi_st=acos(2*aD-1); phi_ex=pi;
end
% Inicializar variables
lambda_fEMm=zeros(length(n_s),length(ap_s));
Tau_N=zeros(z_n,n_dsk); retraso_ang=Tau_N; phi_0=Tau_N;
% Discretización de la herramienta axialmente
for i_dsk=1:n_dsk %desde el primer disco hasta el último
    for iz=1:z_n %para cada filo
        if iz==1
            iz_previous=z_n;
        else
            iz_previous=iz-1;
        end
        % Cálculo de retardo asociado con cada filo por disco
         retraso_ang(iz,i_dsk)=ptch(iz_previous)+(k_bta(iz)-
         k_bta(iz_previous))*dlt_ap*(i_dsk-1);
        Tau_N(iz,i_dsk)=round((N-1)*retraso_ang(iz,i_dsk)/(2*pi));
       % Cálculo del ángulo de posición asociado con cada filo por
       disco
       phi_0(iz,i_dsk)=mod(ptch(iz)-k_bta(iz)*(i_dsk-1)*dlt_ap-
       sum(ptch(1:iz)),2*pi);
    end
end
% Modelo mecanístico de fuerzas de corte
hyy=zeros(z_n,n_dsk,N-1);
% calculo de fuerzas de corte en cada discretizacion
for iN=1:N-1
    % Búsqueda de los discos que se encuentran cortando
    phi_iN=mod(phi_0+(iN)*2*pi/(N-1),2*pi);
    hyy_cut=zeros(z_n,n_dsk);
    phi_cut=find(phi_iN>=phi_st & phi_iN<=phi_ex);
    filo_cut=mod(phi_cut,z_n);
    filo_cut(filo_cut==0)=z_n;
    % Cálculo de las fuerzas de corte en filos que cumplen condición
    hyy_cut(phi_cut)=cos(phi_iN(phi_cut)).*(-Ktc(filo_cut)'.*
    sin(phi_iN(phi_cut))+Krc(filo_cut)'.*cos(phi_iN(phi_cut)));
    hyy(:,:,iN)=hyy_cut;
end
```

```
% Implementación del algoritmo
% Redimensionamiento al máximo retardo
N_=N; N=max(max(Tau_N))+1; %encuentra el maximo del maximo de los
vectores de retardo
% Construcción de la matriz del mapa
Di=zeros(N+1,N+1); Di(4:N+1,3:N)=eye(N-2);
Di(3,1:2)=[1 0];
% Iniciar el barrido de los parámetros del sistema
for iap=1:length(ap_s)
    for in=1:length(n_s)
        T=60/n_s(in);
        dt=T/(N_-1); D=eye(N+1);
        % Cálculo de la matriz de transición aproximada
        for iN=1:N_-1
            Di(1:2,1:N+1)=zeros(2,N+1);
            hyy_iN=hyy(:,1:iap,iN);
            ind_cut=find(hyy_iN); %encuentra elementos que no son cero
            tau_cut=unique(Tau_N(ind_cut)); %da una sola vez cada valor
            de la matriz sin repetirlo.
            % Construcción matriz A del sistema dinámico
            A=[0 1; -omg^2-dlt_ap*sum(hyy_iN(ind_cut))/msa -2*zta*omg];
            if ~isempty(tau_cut)
                % Cuando existen discos en corte
                for itau=1:length(tau_cut)
                    ind_cut_tau= find(hyy_iN~=0 &
                    Tau_N(:,1:iap)==tau_cut(itau));
                    % Construcción de las matrices B del sistema
                    B=dlt_ap*sum(hyy_iN(ind_cut_tau))/msa;
                    Q=zeros(2,4); P=eye(2); Ak=P; kt=1;
                    % Cálculo de las matrices aproximadas P, Q y R
                    for ik=1:m_aprx
                        kt=kt*dt/ik; AkBkt=Ak(:,2)*B*kt;
                        Q=[Q(:,1)+AkBkt*(dt/(ik+1))*((N_-1)/T)*
                        (1/3)+AkBkt*((dt^2/(ik+2))/(ik+1))*
                        (((N_-1)/T)^2)*(-1)+AkBkt*((dt^3/(ik+3))/
                        ((ik+2)*(ik+1)))*(((N_-1)/T)^3),
                        Q(:,2)+AkBkt*(dt/(ik+1))*((N_-1)/T)+
                        AkBkt*((dt^2/(ik+2))/(ik+1))*(((N_-1)/T)^2)*
                        (-7/2)+AkBkt*((dt^3/(ik+3))/((ik+2)*(ik+1)))*
                        (((N_-1)/T)^3)*(9/2),Q(:,3)+AkBkt*(dt/(ik+1))*
                        ((N_-1)/T),Q(:,4)+AkBkt];
                        Ak=Ak*A; P=P+Ak*kt;
                    end
                    Q(:,2)= Q(:,2)-(15/2)*Q(:,1); Q(:,3)= Q(:,3)-
                    3*Q(:,1)-2*Q(:,2); Q(:,4)= Q(:,4)-(1)*Q(:,1)-
                    (1)*Q(:,2)-(1)*Q(:,3);
                    % Construcción de la matriz del mapa i-ésimo
                    Di(1:2,1:2)=P; ind_=tau_cut(itau)+1;
                    Di(1:2,ind_-2:ind_+1)=Di(1:2,ind_-2:ind_+1)+Q;
                end
            else
```

```
                % Cuando no existen discos en corte
                P=eye(2); Ak=P; kt=1;
                for ik=1:m_aprx
                    kt=kt*dt/ik; Ak=Ak*A; P=P+Ak*kt;
                end
                Di(1:2,1:2)=P;
            end
            % Cálculo de la matriz de transición actual
            D=Di*D;
        end
        % Cálculo y almacenamiento del multiplicador de Floquet de
        mayor magnitud
        lambda_fEMm(in,iap)=max(abs(eig(D)));
    end
end
figure
contour(n_s,ap_s*1E3,lambda_fEMm',[1 1],'LineColor',[1 0 0],
'LineWidth',2); hold on
xlabel('Spindle speed [rev/min]'); ylabel('Axial depth of cut [mm]')
title(['\rm 3rd EMHPM, \itN=', num2str(N_), ', aD=', num2str(aD)])
legend('Variable tool design','Fontsize',16)
fprintf('Hecho...')
end
```

Bibliography

1. Du, J.; Zhang, H.; Geng, Y.; Ming, W.; He, W.; Ma, J.; Cao, Y.; Li, X.; Liu, K. A review on machining of carbon fiber reinforced ceramic matrix composites. *Ceram. Int.* **2019**, *45*, 18155–18166, doi:10.1016/j.ceramint.2019.06.112.
2. Kar, B.C.; Panda, A.; Kumar, R.; Sahoo, A.K.; Mishra, R.R. Research trends in high speed milling of metal alloys: A short review. *Mater. Today Proc.* **2020**, doi:10.1016/j.matpr.2020.02.559.
3. Jackson, M.J.; Ahmed, W.; Sein, H.; Phoenix, D.A.; Robinson, G.M.; Hyde, L.J.; Hassan, I.U. *Dental implants—the preparation of enamel, dentin, and bone by machining*; Elsevier Inc., 2020; ISBN 9780128197127.
4. Wu, S. xiong; Li, K. qing; Zhu, W. zhong; Wang, C. yong; Chen, W. lin *Machinability of high-speed enamel cutting with carbide bur*; Elsevier Ltd, 2020; Vol. 103; ISBN 8618925114386.
5. Gowthaman, P.S.; Jeyakumar, S.; Saravanan, B.A. Machinability and tool wear mechanism of Duplex stainless steel – A review. *Mater. Today Proc.* **2020**, doi:10.1016/j.matpr.2020.02.295.
6. Schmitz, T.L.; Smith, K.S. *Machining Dynamics: Frequency Response to Improved Productivity, Second Edition*; Springer, 2019; ISBN 9783319937069.
7. Wu, G.; Pan, W.; Wang, X.; Mo, J.; Ding, S. Chatter and deformation in machining thin-walled flexible components. *IOP Conf. Ser. Mater. Sci. Eng.* **2018**, *423*, doi:10.1088/1757-899X/423/1/012035.
8. Peng, C.; Wang, L.; Liao, T.W. A new method for the prediction of chatter stability lobes based on dynamic cutting force simulation model and support vector machine. *J. Sound Vib.* **2015**, *354*, 118–131, doi:10.1016/j.jsv.2015.06.011.
9. Moradi, H.; Nouriani, A.; Vossoughi, G. Robust control of regenerative chatter in uncertain milling process with weak nonlinear cutting forces: A comparison with linear model. *IFAC-PapersOnLine* **2019**, *52*, 1102–1107, doi:10.1016/j.ifacol.2019.11.343.
10. Sun, T.; Qin, L. fang; Fu, Y. can; Hou, J. ming Chatter stability of orthogonal turn-milling analyzed by complete discretization method. *Precis. Eng.* **2019**, *56*, 87–95, doi:10.1016/j.precisioneng.2018.10.012.
11. O. Arino; Hbid, M.L.; Dads, E.A. *Delay Differential Equations And Applications*; 2006; ISBN 9788578110796.
12. Yüzbasl, S.; Karaçaylr, M. A numerical method for solutions of Lotka-Volterra predator-prey model with time-delay. *Int. J. Biomath.* **2018**, *11*, 1–16, doi:10.1142/S1793524518500286.
13. Mi, T.; Chen, N.; Stepan, G.; Takacs, D. Energy Distribution of a Vehicle Shimmy System with the Delayed Tyre Model. *IFAC-PapersOnLine* **2018**, *51*, 7–12,

doi:10.1016/j.ifacol.2018.07.190.
14. Orosz, G.; Stépán, G. Subcritical Hopf bifurcations in a car-following model with reaction-time delay. *Proc. R. Soc. A Math. Phys. Eng. Sci.* **2006**, *462*, 2643–2670, doi:10.1098/rspa.2006.1660.
15. Hu, H.; Zaihua, W. *Dynamics of Controlled Mechanical Systems with Delayed Feedback*; Springe, Berlin, 2002; ISBN 9783642078392.
16. Altintas, Y. *Manufacturing Automation. Metal cutting mechanics, machine tool vibrations, and CNC design*; Cambridge University Press: New York, 2012;
17. Tlusty, J. Dynamics of High-Speed Milling. *J. Eng. Ind.* **1986**, 59–67.
18. Altintas, Y.; Weck, M. Chatter stability of metal cutting and grinding. *CIRP Ann. - Manuf. Technol.* **2004**, *53*, 619–642, doi:10.1016/S0007-8506(07)60032-8.
19. Stépán, G. Retarded dynamical systems: stability and characteristic functions. *Longman Sci. Tech.* **1989**.
20. Park, S.S.; Rahnama, R. Robust chatter stability in micro-milling operations. *CIRP Ann. - Manuf. Technol.* **2010**, *59*, 391–394, doi:10.1016/j.cirp.2010.03.023.
21. Urbikain, G.; Olvera, D.; de Lacalle, L.N.L.; Elías-Zúñiga, A. Stability and vibrational behaviour in turning processes with low rotational speeds. *Int. J. Adv. Manuf. Technol.* **2015**, *80*, 871–885, doi:10.1007/s00170-015-7041-2.
22. Olvera, D.; Elías-Zúñiga, A.; Martínez-Alfaro, H.; López De Lacalle, L.N.; Rodríguez, C.A.; Campa, F.J. Determination of the stability lobes in milling operations based on homotopy and simulated annealing techniques. *Mechatronics* **2014**, *24*, 177–185, doi:10.1016/j.mechatronics.2014.01.009.
23. Sosa, J. de la luz; Olvera-trejo, D.; Urbikain, G.; Martinez-romero, O. Uncharted Stable Peninsula for Multivariable Milling Tools by High-Order Homotopy Perturbation Method. **2020**, doi:10.3390/app10217869.
24. Zhu, L.; Liu, C. Recent progress of chatter prediction, detection and suppression in milling. *Mech. Syst. Signal Process.* **2020**, *143*, 106840, doi:10.1016/j.ymssp.2020.106840.
25. Al-Zubaidi, S.; Ghani, J.A.; Che Haron, C.H. Application of ANN in milling process: A review. *Model. Simul. Eng.* **2011**, *2011*, doi:10.1155/2011/696275.
26. Ghosh, S.K. *Manufacturing engineering and technology*; 1991; Vol. 25; ISBN 9780136081685.
27. Mehta, P.; Kuttolamadom, M.; Mears, L. Mechanistic force model for machining process—theory and application of Bayesian inference. *Int. J. Adv. Manuf. Technol.* **2017**, *91*, 3673–3682, doi:10.1007/s00170-017-0064-0.
28. Song, Q.; Ai, X.; Zhao, J. Design for variable pitch end mills with high milling stability. *Int. J. Adv. Manuf. Technol.* **2011**, *55*, 891–903, doi:10.1007/s00170-010-3147-8.
29. Mei, Y.; Mo, R.; Sun, H.; He, B.; Bu, K. Stability analysis of milling process with multiple delays. *Appl. Sci.* **2020**, *10*, doi:10.3390/app10103646.

30. Li, D.; Cao, H.; Chen, X. Fuzzy control of milling chatter with piezoelectric actuators embedded to the tool holder. *Mech. Syst. Signal Process.* **2021**, *148*, 107190, doi:10.1016/j.ymssp.2020.107190.
31. Wan, S.; Li, X.; Su, W.; Yuan, J.; Hong, J.; Jin, X. Active damping of milling chatter vibration via a novel spindle system with an integrated electromagnetic actuator. *Precis. Eng.* **2019**, *57*, 203–210, doi:10.1016/j.precisioneng.2019.04.007.
32. Munoa, J.; Sanz-Calle, M.; Dombovari, Z.; Iglesias, A.; Pena-Barrio, J.; Stepan, G. Tuneable clamping table for chatter avoidance in thin-walled part milling. *CIRP Ann.* **2020**, *69*, 313–316, doi:10.1016/j.cirp.2020.04.081.
33. Wang, Y.; Wang, T.; Yu, Z.; Zhang, Y.; Wang, Y.; Liu, H. Chatter prediction for variable pitch and variable helix milling. *Shock Vib.* **2015**, *2015*, doi:10.1155/2015/419172.
34. He, J.H. Homotopy perturbation technique. *Comput. Methods Appl. Mech. Eng.* **1999**, *178*, 257–262, doi:10.1016/S0045-7825(99)00018-3.
35. He, J.H. Homotopy perturbation method: A new nonlinear analytical technique. *Appl. Math. Comput.* **2003**, *135*, 73–79, doi:10.1016/S0096-3003(01)00312-5.
36. H. He, J. Recent development of the homotopy perturbation method. *J. Juliusz Schauder Cent.* **2008**, *31*, 205–209.
37. Mahmoodabadi, M.J. Epidemic model analyzed via particle swarm optimization based homotopy perturbation method. *Informatics Med. Unlocked* **2020**, *18*, 100293, doi:10.1016/j.imu.2020.100293.
38. Yusufoğlu, E. An improvement to homotopy perturbation method for solving system of linear equations. *Comput. Math. with Appl.* **2009**, *58*, 2231–2235, doi:10.1016/j.camwa.2009.03.010.
39. Wu, Y.; He, J.H. Homotopy perturbation method for nonlinear oscillators with coordinate-dependent mass. *Results Phys.* **2018**, *10*, 270–271, doi:10.1016/j.rinp.2018.06.015.
40. Jaradat, E.K.; Alomari, O.; Abudayah, M.; Al-Faqih, A.M. An approximate analytical solution of the nonlinear Schrödinger equation with harmonic oscillator using homotopy perturbation method and laplace-adomian decomposition method. *Adv. Math. Phys.* **2018**, *2018*, doi:10.1155/2018/6765021.
41. Yépez-Martínez, H.; Gómez-Aguilar, J.F. A new modified definition of Caputo–Fabrizio fractional-order derivative and their applications to the Multi Step Homotopy Analysis Method (MHAM). *J. Comput. Appl. Math.* **2019**, *346*, 247–260, doi:10.1016/j.cam.2018.07.023.
42. Ramos, J.I. Piecewise homotopy methods for nonlinear ordinary differential equations. *Appl. Math. Comput.* **2008**, *198*, 92–116, doi:10.1016/j.amc.2007.08.030.
43. Jafarimoghaddam, A. On the Homotopy Analysis Method (HAM) and Homotopy Perturbation Method (HPM) for a nonlinearly stretching sheet flow of Eyring-Powell fluids. *Eng. Sci. Technol. an Int. J.* **2019**, *22*, 439–451,

doi:10.1016/j.jestch.2018.11.001.
44. Liao, S. Comparison between the homotopy analysis method and homotopy perturbation method. *Appl. Math. Comput.* **2005**, *169*, 1186–1194, doi:10.1016/j.amc.2004.10.058.
45. Abbasbandy, S. Iterated He's homotopy perturbation method for quadratic Riccati differential equation. *Appl. Math. Comput.* **2006**, *175*, 581–589, doi:10.1016/j.amc.2005.07.035.
46. Chen, Z.; Jiang, W. Piecewise homotopy perturbation method for solving linear and nonlinear weakly singular VIE of second kind. *Appl. Math. Comput.* **2011**, *217*, 7790–7798, doi:10.1016/j.amc.2011.02.086.
47. Hendi, F.A.; Al-Qarni, M.M. An accelerated homotopy perturbation method for solving nonlinear two-dimensional Volterra-Fredholm integrodifferential equations. *Adv. Math. Phys.* **2017**, *2017*, doi:10.1155/2017/9385040.
48. Bashiri, T.; Vaezpour, S.M.; Nieto, J.J. Approximating Solution of Fabrizio-Caputo Volterra's Model for Population Growth in a Closed System by Homotopy Analysis Method. *J. Funct. Spaces* **2018**, *2018*, doi:10.1155/2018/3152502.
49. Biazar, J.; Montazeri, R. Optimal Homotopy Asymptotic and Multistage Optimal Homotopy Asymptotic Methods for Solving System of Volterra Integral Equations of the Second Kind. *J. Appl. Math.* **2019**, *2019*, doi:10.1155/2019/3037273.
50. Hosein Nia, S.H.; Ranjbar, A.N.; Ganji, D.D.; Soltani, H.; Ghasemi, J. Maintaining the stability of nonlinear differential equations by the enhancement of HPM. *Phys. Lett. Sect. A Gen. At. Solid State Phys.* **2008**, *372*, 2855–2861, doi:10.1016/j.physleta.2007.12.054.
51. Odibat, Z.M. A new modification of the homotopy perturbation method for linear and nonlinear operators. *Appl. Math. Comput.* **2007**, *189*, 746–753, doi:10.1016/j.amc.2006.11.188.
52. Hashim, I.; Chowdhury, M.S.H. Adaptation of homotopy-perturbation method for numeric-analytic solution of system of ODEs. *Phys. Lett. Sect. A Gen. At. Solid State Phys.* **2008**, *372*, 470–481, doi:10.1016/j.physleta.2007.07.067.
53. Hashim, I.; Chowdhury, M.S.H.; Mawa, S. On multistage homotopy-perturbation method applied to nonlinear biochemical reaction model. *Chaos, Solitons and Fractals* **2008**, *36*, 823–827, doi:10.1016/j.chaos.2007.09.009.
54. Chowdhury, M.S.H.; Hashim, I. Application of multistage homotopy-perturbation method for the solutions of the Chen system. *Nonlinear Anal. Real World Appl.* **2009**, *10*, 381–391, doi:10.1016/j.nonrwa.2007.09.014.
55. Chowdhury, M.S.H.; Hashim, I.; Momani, S. The multistage homotopy-perturbation method: A powerful scheme for handling the Lorenz system. *Chaos, Solitons and Fractals* **2009**, *40*, 1929–1937, doi:10.1016/j.chaos.2007.09.073.
56. Öziş, T.; Yildirim, A. Comparison between Adomian's method and He's homotopy perturbation method. *Comput. Math. with Appl.* **2008**, *56*, 1216–1224,

doi:10.1016/j.camwa.2008.02.023.
57. Olvera, D.; Elías-Zúñiga, A. Enhanced multistage homotopy perturbation method: Approximate solutions of nonlinear dynamic systems. *Abstr. Appl. Anal.* **2014**, *2014*, doi:10.1155/2014/486509.
58. Akin, J.E. *Application and implementation of finite element methods.*; 1982; ISBN 0120476509.
59. Hsu, T.-R. *The Finite Element Method in Thermomechanics*; 1986;
60. Chen, S. *Computational Geomechanics and Hydraulic Structures*; 2019; ISBN 978-981-10-8134-7.
61. Shakeri, F.; Dehghan, M. Solution of delay differential equations via a homotopy perturbation method. *Math. Comput. Model.* **2008**, *48*, 486–498, doi:10.1016/j.mcm.2007.09.016.
62. Wu, Z. ku Solution of the ENSO Delayed Oscillator with Homotopy Analysis Method. *J. Hydrodyn.* **2009**, *21*, 131–135, doi:10.1016/S1001-6058(08)60128-6.
63. Sedaghat, S.; Ordokhani, Y.; Dehghan, M. Numerical solution of the delay differential equations of pantograph type via Chebyshev polynomials. *Commun. Nonlinear Sci. Numer. Simul.* **2012**, *17*, 4815–4830, doi:10.1016/j.cnsns.2012.05.009.
64. Abolhasani, M.; Ghaneai, H.; Heydari, M. Modified homotopy perturbation method for solving delay differential equations. *Appl. Sci. Reports* **2016**, *16*, 14–17, doi:10.15192/pscp.asr.2016.16.2.8992.
65. El-Dib, Y.O. Stability approach for periodic delay Mathieu equation by the He-multiple-scales method. *Alexandria Eng. J.* **2018**, *57*, 4009–4020, doi:10.1016/j.aej.2018.01.021.
66. Shampine, L.F.; Thompson, S. Solving DDEs in MATLAB. *Appl. Numer. Math.* **2001**, *37*, 441–458, doi:10.1016/S0168-9274(00)00055-6.
67. Olvera, D.; Elías-Zúñiga, A.; López De Lacalle, L.N.; Rodríguez, C.A. Approximate solutions of delay differential equations with constant and variable coefficients by the enhanced multistage homotopy perturbation method. *Abstr. Appl. Anal. 2015*, 1–12, doi:10.1155/2015/382475.
68. Insperger, T.; Stépán, G. Updated semi-discretization method for periodic delay-differential equations with discrete delay. *Int. J. Numer. Methods Eng.* **2004**, *61*, 117–141, doi:10.1002/nme.1061.
69. Bayly, P. V.; Halley, J.E.; Mann, B.P.; Davies, M.A. Stability of interrupted cutting by temporal finite element analysis. *J. Manuf. Sci. Eng. Trans. ASME* **2003**, *125*, 220–225, doi:10.1115/1.1556860.
70. Totis, G. RCPM-A new method for robust chatter prediction in milling. *Int. J. Mach. Tools Manuf.* **2009**, *49*, 273–284, doi:10.1016/j.ijmachtools.2008.10.008.
71. Pérez-Canales, D.; Vela-Martínez, L.; Carlos Jáuregui-Correa, J.; Alvarez-Ramirez, J. Analysis of the entropy randomness index for machining chatter detection. *Int. J. Mach. Tools Manuf.* **2012**, *62*, 39–45, doi:10.1016/j.ijmachtools.2012.06.007.

72. Altintaş, Y.; Budak, E. Analytical Prediction of Stability Lobes in Milling. *CIRP Ann. - Manuf. Technol.* **1995**, *44*, 357–362, doi:10.1016/S0007-8506(07)62342-7.
73. Davies, M.A.; Pratt, J.R.; Dutterer, B.; Burns, T.J. Stability prediction for low radial immersion milling. *J. Manuf. Sci. Eng. Trans. ASME* **2002**, *124*, 217–225, doi:10.1115/1.1455030.
74. Insperger, T.; Stépán, G. Semi-discretization method for delayed systems. *Int. J. Numer. Methods Eng.* **2002**, *55*, 503–518, doi:10.1002/nme.505.
75. Insperger, T.; Stepan, G.; Turi, J. Comparison of zeroth- And first-order semi-discretizations for the delayed Mathieu equation. *Proc. IEEE Conf. Decis. Control* **2004**, *3*, 2625–2629, doi:10.1109/cdc.2004.1428855.
76. Insperger, T.; Stépán, G.; Turi, J. On the higher-order semi-discretizations for periodic delayed systems. *J. Sound Vib.* **2008**, *313*, 334–341, doi:10.1016/j.jsv.2007.11.040.
77. Butcher, E.A.; Nindujarla, P.; Bueler, E. DETC2005-84880. **2005**, 1–10.
78. Ding, Y.; Zhu, L.M.; Zhang, X.J.; Ding, H. A full-discretization method for prediction of milling stability. *Int. J. Mach. Tools Manuf.* **2010**, *50*, 502–509, doi:10.1016/j.ijmachtools.2010.01.003.
79. Insperger, T. Full-discretization and semi-discretization for milling stability prediction: Some comments. *Int. J. Mach. Tools Manuf.* **2010**, *50*, 658–662, doi:10.1016/j.ijmachtools.2010.03.010.
80. Ding, Y.; Zhu, L.; Zhang, X.; Ding, H. Second-order full-discretization method for milling stability prediction. *Int. J. Mach. Tools Manuf.* **2010**, *50*, 926–932, doi:10.1016/j.ijmachtools.2010.05.005.
81. Ding, Y.; Zhu, L.; Zhang, X.; Ding, H. Numerical integration method for prediction of milling stability. *J. Manuf. Sci. Eng. Trans. ASME* **2011**, *133*, doi:10.1115/1.4004136.
82. Bayly, P. V.; Mann, B.P.; Schmitz, T.L.; Peters, D.A.; Stepan, G.; Insperger, T. Effects of radial immersion and cutting direction on chatter instability in end-milling. *ASME Int. Mech. Eng. Congr. Expo. Proc.* **2002**, 351–363, doi:10.1115/IMECE2002-39116.
83. Sinha, S.C.; Wu, D.H. An efficient computational scheme for the analysis of periodic systems. *J. Sound Vib.* **1991**, *151*, 91–117, doi:10.1016/0022-460X(91)90654-3.
84. Butcher, E.A.; Bobrenkov, O.A.; Bueler, E.; Nindujarla, P. Analysis of milling stability by the chebyshev collocation method: algorithm and optimal stable immersion levels. *J. Comput. Nonlinear Dyn.* **2009**, *4*, 1–12, doi:10.1115/1.3124088.
85. Compeán, F.I.; Olvera, D.; Campa, F.J.; López De Lacalle, L.N.; Elías-Zúñiga, A.; Rodríguez, C.A. Characterization and stability analysis of a multivariable milling tool by the enhanced multistage homotopy perturbation method. *Int. J. Mach. Tools Manuf.* **2012**, *57*, 27–33, doi:10.1016/j.ijmachtools.2012.01.010.
86. Altintas, Y.; Engin, S.; Budak, E. Analytical stability prediction and design of variable pitch cutters. *J. Manuf. Sci. Eng. Trans. ASME* **1999**, *121*, 173–178,

doi:10.1115/1.2831201.

87. Sims, N.D.; Mann, B.; Huyanan, S. Analytical prediction of chatter stability for variable pitch and variable helix milling tools. *J. Sound Vib.* **2008**, *317*, 664–686, doi:10.1016/j.jsv.2008.03.045.
88. Wan, M.; Zhang, W.H.; Dang, J.W.; Yang, Y. A unified stability prediction method for milling process with multiple delays. *Int. J. Mach. Tools Manuf.* **2010**, *50*, 29–41, doi:10.1016/j.ijmachtools.2009.09.009.
89. Comak, A.; Budak, E. Modeling dynamics and stability of variable pitch and helix milling tools for development of a design method to maximize chatter stability. *Precis. Eng.* **2017**, *47*, 459–468, doi:10.1016/j.precisioneng.2016.09.021.
90. Niu, J.; Ding, Y.; Zhu, L.M.; Ding, H. Mechanics and multi-regenerative stability of variable pitch and variable helix milling tools considering runout. *Int. J. Mach. Tools Manuf.* **2017**, *123*, 129–145, doi:10.1016/j.ijmachtools.2017.08.006.
91. Jin, G.; Qi, H.; Li, Z.; Han, J. Dynamic modeling and stability analysis for the combined milling system with variable pitch cutter and spindle speed variation. *Commun. Nonlinear Sci. Numer. Simul.* **2018**, *63*, 38–56, doi:10.1016/j.cnsns.2018.03.004.
92. Ureña, L.; Ozturk, E.; Sims, N. Stability of variable helix milling: Model validation using scaled experiments. *Procedia CIRP* **2018**, *77*, 449–452, doi:10.1016/j.procir.2018.08.277.
93. Jiang, S.; Sun, Y. A multi-order method for predicting stability of a multi-delay milling system considering helix angle and run-out effects. *Chinese J. Aeronaut.* **2018**, *31*, 1375–1387, doi:10.1016/j.cja.2017.08.005.
94. Escalera Rodríguez, O.J. Optimización del diseño de herramienta multivariable para fresado de alto rendimiento, Tecnologico de Monterrey, 2018.
95. Lee, E.T.; Eun, H.C. Structural Damage Detection by Power Spectral Density Estimation Using Output-Only Measurement. *Shock Vib.* **2016**, *2016*, doi:10.1155/2016/8761249.
96. Fries, R.H. *Fundamentals of vibrations*; 2000; ISBN 9781482270372.

Published papers

Sosa, J. de la luz; Olvera-trejo, D.; Urbikain, G.; Martinez-romero, O. Uncharted Stable Peninsula for Multivariable Milling Tools by High-Order Homotopy Perturbation Method. **2020**, doi:10.3390/app10217869